DEVELOPMENT OF ION MOBILITY AND MASS SPECTROMETRY STRATEGIES IN SUPPORT OF INTEGRATED OMICS AND SYSTEMS BIOLOGY

By

Nichole M. Lareau

Dissertation

Submitted to the Faculty of the

Graduate School of Vanderbilt University

in partial fulfillment of the requirements

for the degree of

DOCTOR OF PHILOSOPHY

in

Chemistry

May 2016

Nashville, Tennessee

Approved:

John A. McLean, Ph.D.

David E. Cliffel, Ph.D.

Ned A. Porter, Ph.D.

John P. Wikswo, Ph.D.

To my parents,

for their constant support and encouragement.

ACKNOWLEDGEMENTS

I would like to thank my family and friends for their support and encouragement throughout my time as a graduate student. Thank you to my parents for their continuous support while I've been far from home. To my dad, it's been great to have your advice and compare the process that hasn't changed much in 30 years. To my mom, thank you for always sending pictures of Bentley and your continuous encouragement; it has made the hardest days much easier. You're both an example of success as a result of hard work and determination. Thanks for always being there for me. Thank you to my brother, Justin, for being my eyes and ears back home. Your support and constant updates made me feel closer to home. To my Aunt Anita and Uncle Robert, thank you for the care packages I looked forward to so much. I want to thank my closest friends Khristie Caola, Kelsey VanGelder, Tamra Wroblesky and Megan Reesbeck for answering my calls at any hour. You have been an amazing support system I am so grateful. To my friends here in Nashville, you have made my time here some of the best years of my life. Finally, thank you Dr. Joseph Zackular for being my best friend, sounding board, editor, alarm clock, confidence booster, and so much more. I could not ask for a better partner and appreciate all your advice throughout process.   I am forever thankful for all the love and support you, Beaker, and Erlenmeyer bring me.

TABLE OF CONTENTS

Chapters

LIST OF TABLES

LIST OF FIGURES

LIST OF ABBREVIATIONS

Ω	Collision cross section
μs	Microsecond
2D	Two-dimensional
ACN	Acetonitrile
ATD	Arrival Time Distribution
CCS	Collision cross section
CE	Capillary electrophoresis
CID	Collision induced dissociation
COM	Center of mass
Da	Dalton
DT	Drift time
DTIM	Drift tube ion mobility
ESI	Electrospray ionization
ETD	Electron transfer dissociation
EtOH	Ethanol
eV	Electron volt
Fuc	Fucose
Gal	Galatose
GalNAc	N-acetylgalactosamine
GC	Gas chromatography
GlcCer	Glycosphingolipid

Glu	Glucose
GlcNAc	N-acetylglucosamine
Hex	Hexose
HexNAc	N-acetylated hexosamine
HILIC	Hydrophilic interaction chromatography
HPLC	High performance liquid chromatography
IM	Ion mobility
IMS	Imaging mass spectrometry
IM-MS	Ion mobility-mass spectrometry
IM-MS/MS	Ion mobility-tandem mass spectrometry
LC	Liquid chromatography
LC-MS	Liquid chromatography-mass spectrometry
MALDI	Matrix-assisted laser desorption/ionization
Man	Mannose
MD	Molecular dynamics
MeOH	Methanol
ms	Millisecond
MS	Mass spectrometry
MS/MS	Tandem mass spectrometry
m/z	Mass-to-charge ratio
NCE	New chemical entities
NP	Normal phase
NeuAc	N-acetylneuraminic acid

PC	Phosphatidylcholine
PE	Phosphatidylethanolamine
ppm	Parts-per-million
PS	Phosphatidylserine
PTM	Post-translational modificationz
RP	Reverse phase
STP	Standard temperature and pressure
SM	Sphingomyelin
S/N	Signal-to-noise
Q-TOF	Quadrupole time-of-flight
TAA	Tetraalkyl ammonium salts
T_d	Drift time
TOF	Time-of-flight
TWIM	Traveling wave ion mobility
UPLC	Ultra-performance liquid chromatography

CHAPTER 1

STRUCTURAL SEPARATIONS BY ION MOBILITY-MASS SPECTROMETRY:

FUNDAMENTAL THEORY TO EMERGING APPLICATIONS

1.1. *Introduction*

Emerging techniques in mass spectrometry (MS) have found great utility in many

applications ranging from nanotechnology to the life sciences, including natural product

discovery. The rapid nature of MS analysis, which occurs on the order of microseconds

(μs), makes it one of the first choices for studies requiring large sample sets where high-

throughput is necessary. MS is often the preferred technique where sample volumes are

limited, as only femtomole quantities may be required due to its high sensitivity. The

wide-spread acceptance of MS has led to a growing number of database and informatic

tools to facilitate identification of molecular species. For fields driven to obtain

biologically significant data from complex samples, such as those in the life sciences, the

availability of these tools is highly promising. However, limitations of MS arise in the

form of same mass, termed isobaric, species that contribute to chemical noise. To

distinguish species of similar mass, enhanced selectivity can be accomplished by pairing

MS with additional separations.

Pre-ionization separation techniques, such as high performance liquid

chromatography (HPLC) or gas chromatography (GC) for condensed- and gas-phase

separations, respectively, are commonly interfaced with MS. The pairing of MS with

chromatographic separations has led to measurable benefits for fields such as proteomics

and metabolomics, in terms of extended sensitivity as well as enhanced informatics to

handle multidimensional data sets that are often encountered in natural product discovery endeavors. The fundamental theory described here is framed to support these natural product discovery efforts. LC-MS and LC-MS/MS have become the primary analytical platform for the analysis of serum, plasma, and additional complex biological matrices for metabolites and proteins of biological relevance.[4-7] Quantitative measurements of fluxes in metabolite levels of microorganisms and cells are routinely performed by GC-MS.[8,9] An alternative to chromatographic partitioning techniques is gas-phase ion mobility (IM) separation, a type of electrophoretic separation, which is substantially more rapid (μs-ms vs. min-hrs) than bi-phasic partitioning techniques. Separations by IM are performed by the differential diffusion of ions on the basis of their structures, and provide molecular information orthogonal to that obtained from chromatographic separation strategies. Pre-ionization separations can be integrated with IM-MS for further gains in data dimensionality, as IM is a post-ionization separation.

A number of outstanding monographs are available for those seeking a more detailed discussion of IM-MS fundamentals, instrumentation, and applications.[10-15] This chapter aims to highlight the utility and progress of IM-MS for the identification and interrogation of natural products, specifically secondary metabolites. Section 1.1.1. provides a historical perspective of MS and IM-MS, and introduces the reasoning for coupling IM and MS and the fundamentals for obtaining structural information from IM-MS data. Section 1.1.2 describes leveraging conformation space analysis for rapid characterization of biomolecular species with particular emphasis on primary and secondary metabolites. An outlook on the future directions of secondary metabolite discovery and characterization by IM-MS is provided in Section 1.3.

1.1.1. *Historical Perspective on Ion Mobility and Mass Spectrometry*

The discovery of X-rays by Röntgen and first studies of ion movement in the gas phase by Rutherford and Zeleny in the late 1890s mark the earliest fundamental explorations of the techniques later to be known as MS and ion mobility spectrometry (IMS) (Figure 1.1).[16-18] Despite the proximity in time of their foundational experiments, development of IM and MS did not occur in synchrony. MS has benefitted from relatively consistent expansion since the first mass spectrometer was developed in the 1910s, which has resulted in a number of diverse techniques for mass analysis. Predating many other mass analyzers, the description of the Kingdon trap was first published in the 1920s and has since been recognized as the precursor of orbitrap mass analyzers for high-resolution MS.[19,20] Now a work-horse instrument in many mass spectrometry labs, the time-of-flight (TOF) mass analyzer has its roots in the early 1940s when Stephens first published the concept of mass analysis based on a fundamental equation of physics.[21] Years later, in the mid-1960s, Mamyrin updated the TOF to include a focusing reflectron to improve the resolution of the mass analyzer.[22-24] The establishment of both matrix-assisted laser desorption/ionization (MALDI) and electrospray ionization (ESI) in the late 1980s, with reports of intact proteins of 100kDa and greater mass ionized by MALDI- and ESI-MS, furthered the utility of MS for life sciences applications.[25-27]

The foundations of contemporary IM lie in the fundamental studies of ion motion in the gas-phase conducted in the late 1890s to mid-1920s. It was Zeleny in 1898 to whom development of the first IM spectrometer is attributed. Using an electric field and several gases, his IM spectrometer measured the ratio of velocities of negative and
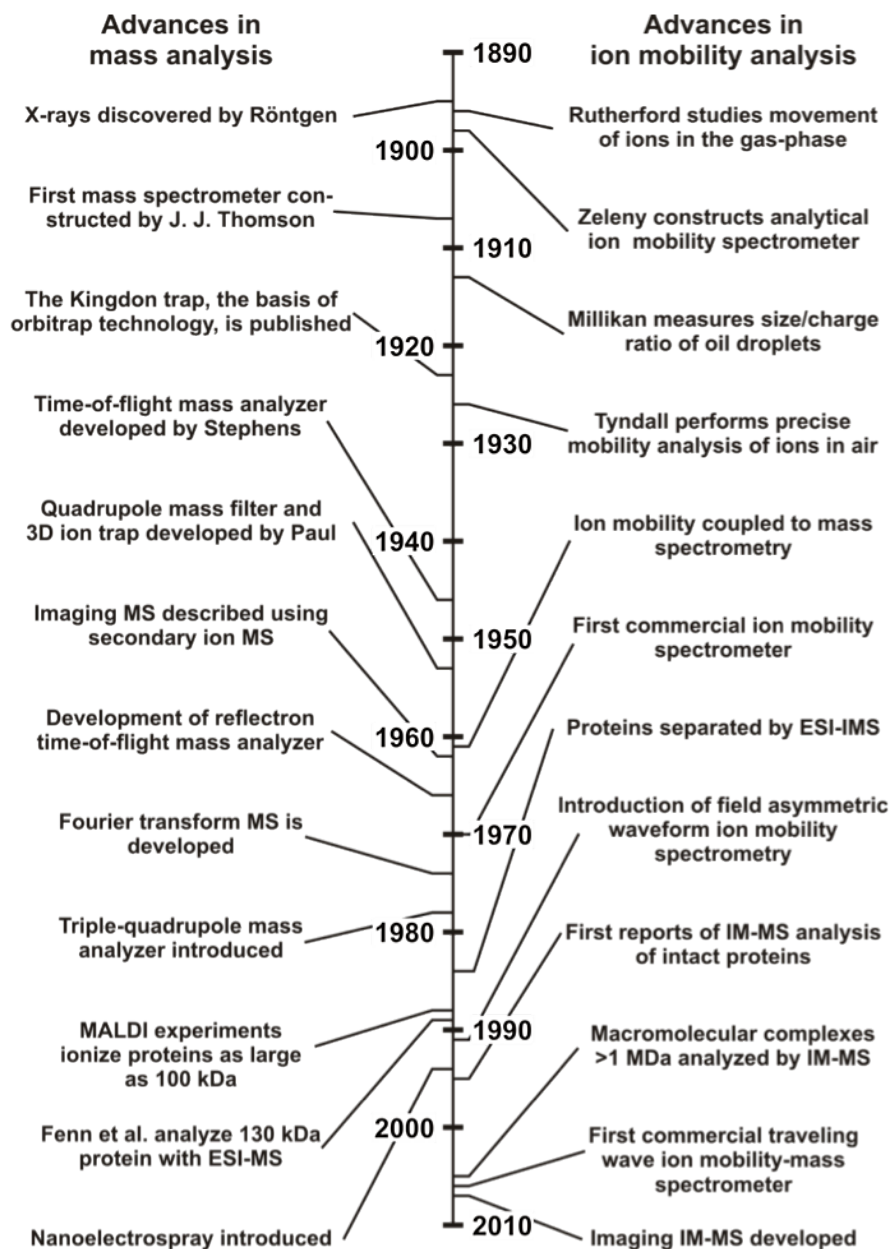
Figure 1.1. A timeline highlighting selected significant advances in the developments of MS (left) and IM (right) from their foundations in the 1890s to more contemporary achievements. (Adapted with permission from Hines, K. M.; Enders, J. R.; McLean, J. A., Multidimensional Separations by Ion Mobility-Mass Spectrometry. In *Encyclopedia of Analytical Chemistry*, Myers, R. A., Ed. John Wiley & Sons: 2012. Copyright 2012, John Wiley & Sons.)

positive ions.[18] In the mid-1920s, Tyndall performed mobility measurements on the ions in air with great attention to experimental conditions.[28-32] While these early studies were monumental in the development of IM, further progress focused on fundamental reaction parameters in astrophysics over the next thirty years.

Progress in IM research accelerated in the 1960s, when McDaniel, Edelson and colleagues first published work detailing IM and MS analyses performed in tandem.[33, 34] Within the following decade, the first commercially developed IM spectrometer was available and referred to as plasma chromatography at the time of its release.[35] The primary market for IM spectrometers was for the detection of illicit drugs and explosives for security applications.[36-38]

The 1980s generally saw a rapid growth in the application of analytical tools to life science research, and not unlike MS, the utility of IM to the biological sciences was explored. The first reports of IM separation of multiply charged proteins was published by Dole and colleagues in the mid-1980s using an ESI-IM spectrometer.[39] Bowers and colleagues published the first works on the IM-MS separation of peptides in the 1990s,[40,41] while Jarrold, Clemmer, and colleagues used IM-MS to probe the gas-phase conformations of intact proteins.[42,43] It was these studies and others, which revealed the potential of IM-MS as an analytical tool for interrogating biologically-relevant queries such as the gas-phase structures of peptides, proteins, and other biomolecules.

Research in the field of IM greatly accelerated through the late 1990s to the present (Figure 1.2). In large part this acceleration is attributed to the first commercial offerings of integrated IM-MS instruments in the early 2000s rather than standalone IMS devices (Figure 1.2, top). Likewise, exponential growth has been observed in the

5
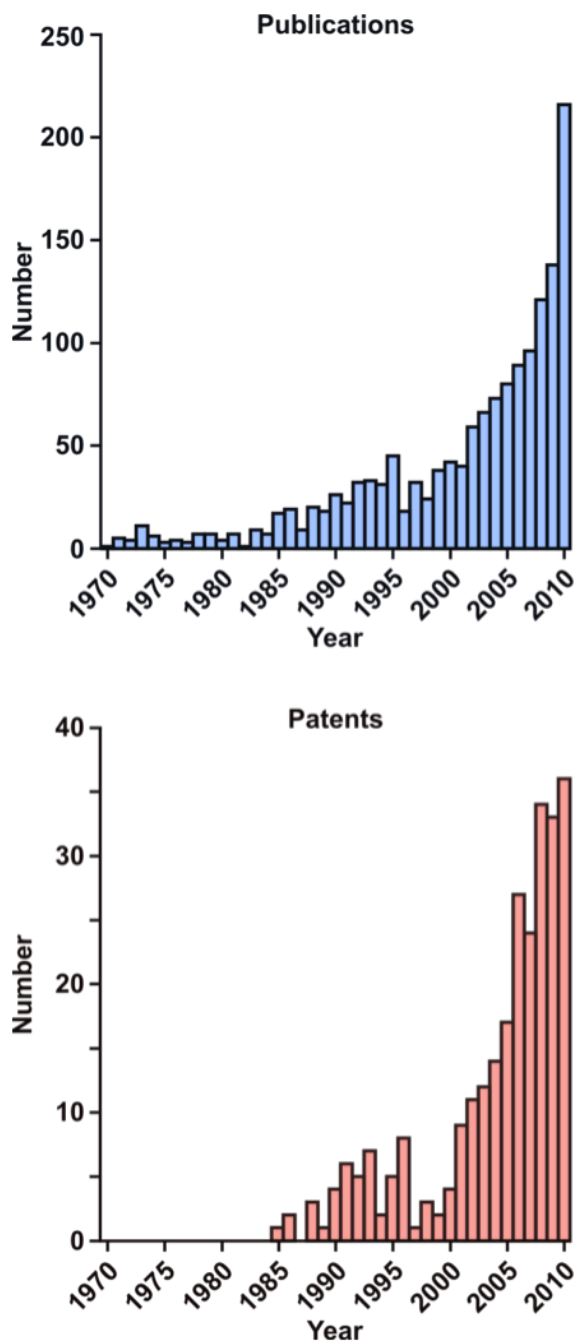
Figure 1.2. Histograms illustrating the number of publications (top) and patents (bottom) using IM-MS from 1970-2010. A search of the phrase "ion mobility with MS" was entered into SciFinder to obtain the data presented above. (Adapted with permission from Hines, K. M.; Enders, J. R.; McLean, J. A., Multidimensional Separations by Ion Mobility-Mass Spectrometry. In *Encyclopedia of Analytical Chemistry*, Myers, R. A., Ed. John Wiley & Sons: 2012. Copyright 2012, John Wiley & Sons.)

6

development of new IM and IM-MS instrumentation and technology as indicated by the number of patents (Figure 1.2, bottom). This growth is expected to continue due to additional commercial offerings and their wider acceptance in fields such as imaging [44] and macromolecular complex characterization.[45]

1.1.2. Ion Mobility-Mass Spectrometry: Correlation of Two Dimensions

Integration of IM and MS provides analyte information of two types: (i) from the IM dimension, structural information in the form of the ion-neutral collision cross section, and (ii) from the MS dimension, mass information in the form of a mass-to-charge ratio (*m/z*). A typical representation of IM-MS data is presented in Figure 1.3, which was acquired from an extract of an actinomycete collected from the Blue Springs cave.[46] The plot of drift time (ms) versus mass-to-charge (*m/z*) shown as panel (A) is referred to as conformation space.[47] In this instance, signal intensities are indicated in the form of a grey scale, where lightest grey represents low intensity signals and black represents high intensity signals. Integration over all mobility space in the 2D plot (A) produces a mass spectrum (B) comparable to the output of an MS-only analysis. In contrast, integration of the 2D plot (A) across all *m/z* space produces an IM drift time profile (C) comparable to the output of an IM-only analysis. The tricyclic antibiotic siamycin II, produced by a streptomycete within the actinomycete class, is highlighted by the black rectangle in (A). For this particular signal (multiply charged analyte with *m/z* 601.391), the integration can be performed about a defined area of conformation space, as indicated by the black rectangle. Performing the described integration yields the drift

time profile (E) and *m/z* spectrum (C) for siamycin II isolated from other components of the actinomycete extract.

As illustrated in Figure 1.3. signals are correlated between overall structure and mass, which is related to density. This correlation arises because biomolecules are typically comprised of only a few atoms (C, H, O, N, P and S) and their masses scale as volume, or length cubed. Collision cross-sections (CCSs) are effectively a measure of surface area, and therefore scale as length squared. Given the limited set of building blocks for biomolecules, they generally exist within a narrow range of densities. For example, peptides are comprised of amino acids, glycans consist of sugar moieties, and lipids are constructed of one or more fatty acid tails with discrete head groups. The practical implication is that the IM and MS dimensions of each biomolecular class are highly correlated as both measurements scale by length. Correlation between two dimensions of separation can be both advantageous and challenging compared to more orthogonal multidimensional separations.[48] In terms of complex sample analysis, this can be advantageous as each class of biomolecule (*e.g.* peptides, carbohydrates, lipids, etc.) exists with a unique average density or packing efficiency in the gas phase, which translates into a particular correlation in IM-MS spectra containing such species (Figure 1.4). The more challenging aspect of highly correlated separation dimensions is decreased peak capacity relative to more orthogonal techniques. For example, peak capacity is on the order of 10^7-10^8 for LC-Fourier Transform-MS (LC-FT-MS), while it is approximately 10^3-10^4 for IM-MS.[47,49-51] The deficit in IM-MS peak capacity is mitigated by its extraordinarily high peak capacity production rate of approximately $10^6 \, s^{-1}$ in contrast to $10^4 \, s^{-1}$ for LC-FT-MS.[47] This is generally attributed to the decreased
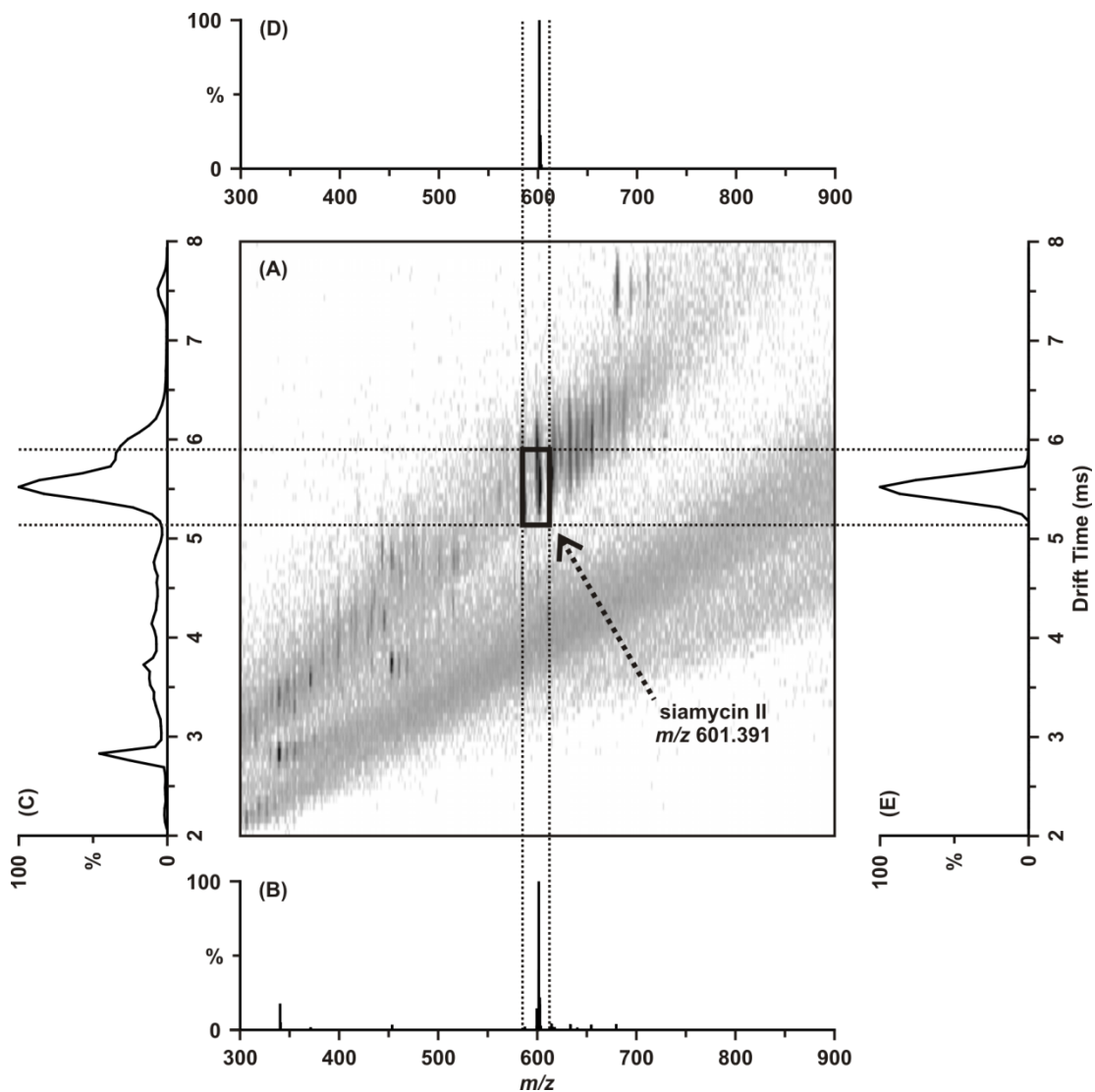
Figure 1.3. (A) A 2D ESI-IM-MS plot of conformation space for an extract of an actinomycete collected from the Blue Springs cave. (B) An integrated mass spectrum across all mobility space. (C) An integrated IM drift time profile across all *m/z* space. For the multiply charged signal *m/z* 601.391 corresponding to the tricyclic antibiotic siamycin II, integrating the defined region of drift time-*m/z* space (highlighted black rectangle in (A)) yields the extracted *m/z* (D) and drift time (E) profiles corresponding to the signal of siamycin II in the absence of chemical noise. This figure was reproduced with permissions from an invited book chapter for the Natural Product Analysis: Instrumentation, Methods, and Applications: "Structural Separations for Natural Product Characterization by Ion Mobility-Mass Spectrometry: Fundamental Theory to Emerging Applications," by Sarah M. Stow, Nichole M. Lareau, Kelly M. Hines, C. Ruth McNees, Cody R. Goodwin, Brian O. Bachmann, and John A. McLean. Vladimir Havliček and Jaroslav Splžek, Eds. John Wiley & Sons, 2014.

separation time of the gas-phase electrophoresis relative to bi-phasic partitioning techniques such as GC or LC.[51]

1.1.2.1. Complex Sample Analysis by IM-MS

Complex biological sample analysis in contemporary omics typically encompasses the measurement of a single molecular class. For example, preparation of samples for MS analyses typically requires enrichment of one particular type of biomolecule, such as proteins for proteomic experiments, where information for all other biomolecules is lost. Among the primary reasons for depleting biological samples for particular molecular classes are: (i) to remove undesired endogenous species which contribute to the chemical noise; (ii) to remove highly abundant endogenous species, such as lipids, which have ion suppressive effects and consequently limit dynamic range; and (iii) to simplify mass spectra for greater confidence in subsequent identification or quantitation. Thus, IM provides similar advantages to LC and GC separations to mitigate sample complexity issues; however, the separation times in IM are nearly 4-5 orders of magnitude faster than LC or GC.

The correlation of *m/z* and collision cross section by length has advantageous implications for complex sample analysis. The different classes of biomolecules separate in the order of increasing gas-phase packing efficiencies or densities: lipids < peptides/proteins < carbohydrates < oligonucleotides.[52-56] This trend is visible in 2D IM-MS plots in the form of unique regions of CCS-*m/z* correlation for each class of biomolecule, as depicted in Figure 1.4. This general order is highly conserved regardless of the particular parameters of the analysis, which allows for predictive power in the

assignment of unknown species based on their location in conformation space. Additional

discussions of these trends are reported at length in Chapter II. In addition to broad

assignment of biomolecular classes, more fine-grained structural information can be

resolved within the correlation region of a particular biomolecular class. For example,

this enables discrimination of cyclic peptides from linear peptides, or phosphorylated

peptides from their unmodified counterparts.[46, 56]

Relative to MS-only methods, there are several practical benefits of the structural

separation of biomolecular classes observed in IM-MS analyses. For analysis of bacterial

extracts by IM-MS like the one shown in Figure 1.3, peptide species can be isolated from

non-peptide interferences by extracting the region of 2D conformation space containing

peptides. This not only improves confidence in identifications, but also effectively

increases the dynamic range.[47] While they would be challenging to detect by MS-only,

IM structural separations can readily resolve isobaric species resulting from

conformational isomers or alterations in amino acid sequence based on differences in

their preferred conformations.[55,57-60]

1.1.2.2. Configurations of IM and MS Dimensions

Because both IM and MS separations occur in the gas phase, IM-MS allows for

some versatility in the ordering and arrangements of the IM and MS separations due to

their correlation. Depending on the particular experimental goals, a number of

configurations are possible. A box diagram representing a typical IM-MS instrument is

shown in Figure 1.5(A, left). The ion mobility drift cell is positioned between the ion

source and the mass analyzer. The choice of ion source and mass analyzer can be tailored
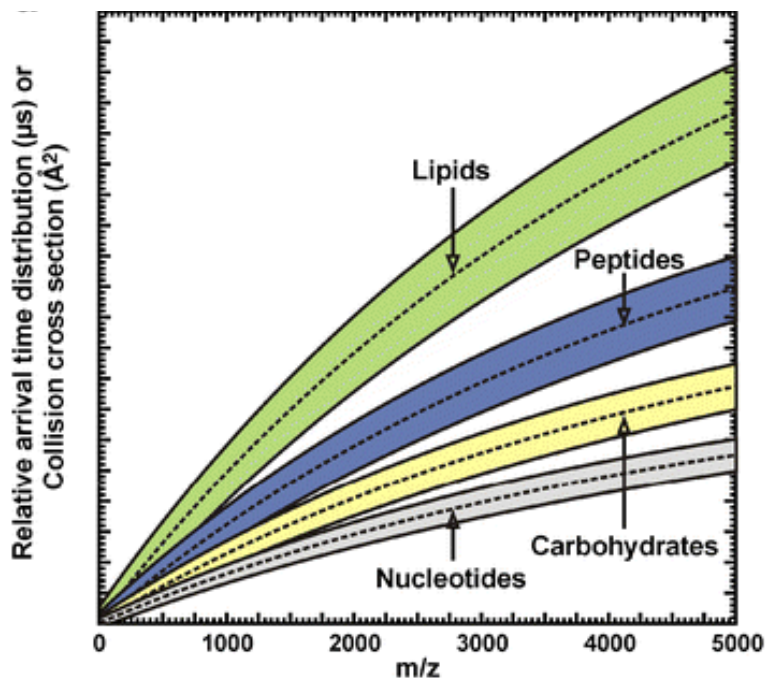
Figure 1.4. A hypothetical depiction of conformation space occupied by different classes of biomolecules. At a given mass, lipids exhibit the least average density, while nucleotides exhibit the highest average density. (Adapted with permission from Fenn, L. S.; McLean, J. A., Biomolecular structural separations by ion mobility-mass spectrometry. *Analytical and Bioanalytical Chemistry* **2008,** *391* (3), 905-909. Copyright 2008, Springer)

to the information desired; however, MALDI and ESI ion sources are most common for life science applications. Most conventional arrangements utilize an orthogonal TOFMS for full MS analysis of mobility dispersed ions, while quadrupole MS is better suited for the transmission of a single *m/z*. A typical ESI-IM-TOFMS spectrum is shown in Figure 1.5(A, right).

Two arrangements for performing IM-MS/MS are possible depending on the location of the ion activation. The first, termed pre-mobility fragmentation, is shown in Figure 1.5(B). In this arrangement, an ion activation region precedes the IM and mobility measurements are acquired for each fragment ion and any unfragmented precursor species. A collision cell may also be placed after the IM region, as shown in Figure 1.5(C). This post-mobility fragmentation arrangement provides temporal separation of precursor species by IM resulting in fragment ions correlated to the precursor by the IM drift time. This arrangement allows for multiplexed MS/MS experiments in which fragmentation is performed on nearly all ions.[61] In contrast to scanning MS/MS methods, pre-fragmentation mass selection is not necessary in these configurations as the fragment ions are dispersed in the mobility cell prior to mass analysis, but a quadrupole may be included for mass filtering if desired. Additional dimensions of MS/MS, MS, IM or IM/IM can be incorporated to suit particular experimental needs. If greater peak capacity is required, pre-ionization separations such as LC, GC or capillary electrophoresis (CE) can be interfaced with the IM-MS as well (Figure 1.5 D).[47, 50, 51, 62]
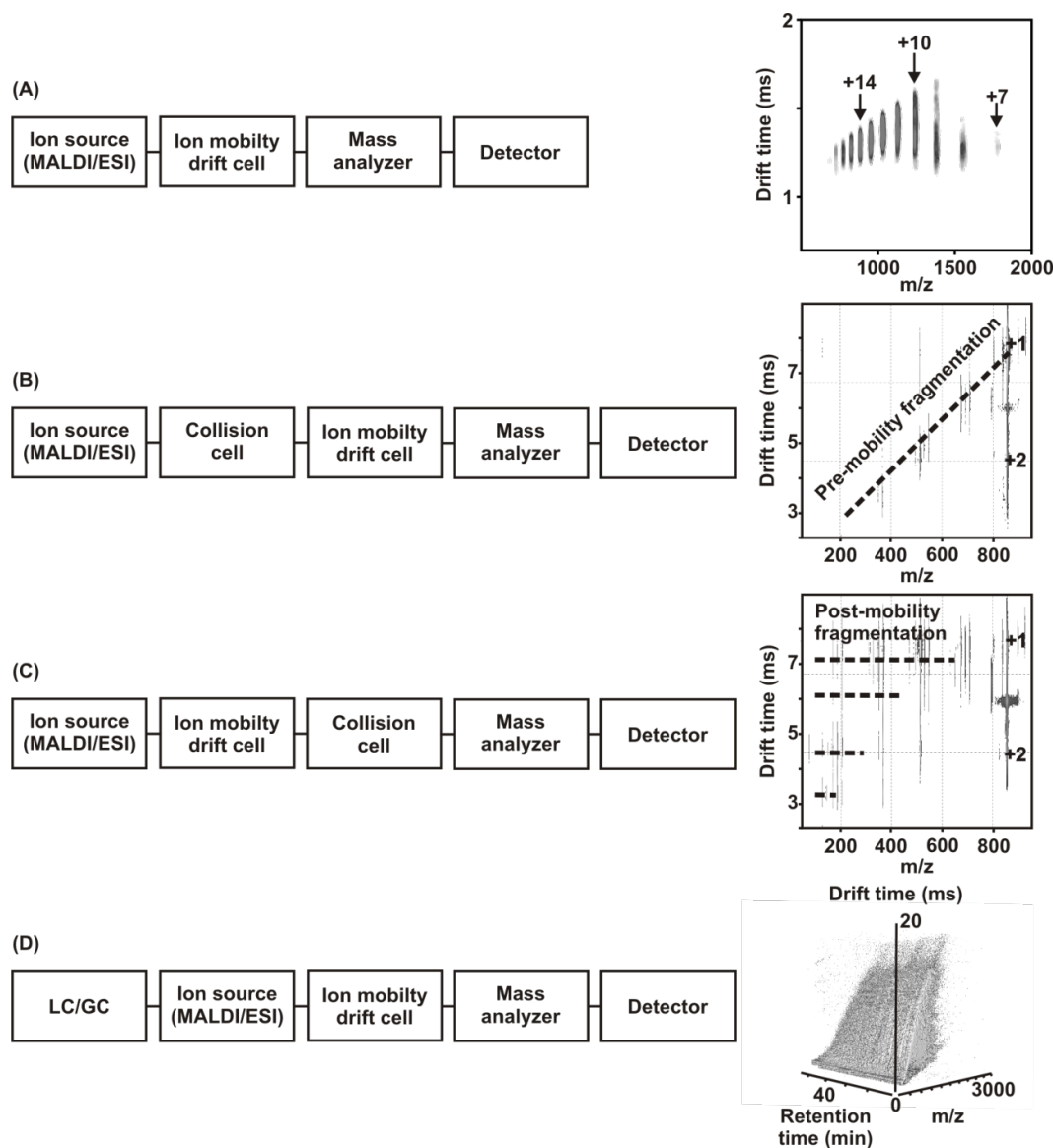
Figure 1.5 (left) Flow charts depicting different IM and MS experimental arrangements. (right) Data representative of information obtained from the corresponding experimental arrangement. (A) The most common arrangement of IM-MS consists of an ion source interfaced with an IM region, followed by a mass analyzer and detector. (B) An arrangement for IM-MS/MS in which the collision cell precedes the IM region. This provides mobility information about the resulting fragment ions and is referred to as pre-mobility fragmentation. (C) An arrangement for IM-MS/MS in which the collision cell is placed after the IM separation. This post-mobility fragmentation arrangement provides fragment ions correlated to their precursor by a common IM drift time. (D) Pre-ionization separations such as HPLC or GC can be integrated with IM-MS for enhancement of data dimensionality. (Adapted with permission from Hines, K. M.; Enders, J. R.; McLean, J. A., Multidimensional Separations by Ion Mobility-Mass Spectrometry. In *Encyclopedia of Analytical Chemistry*, Myers, R. A., Ed. John Wiley & Sons: 2012. Copyright 2012, John Wiley & Sons.)

1.1.3. *Deriving Structural Information from IM-MS Measurements*

The motivations for utilizing IM separations are two-fold: (i) to disperse ions in time to reduce sample complexity, and (ii) to obtain coarse-grained structural information in the form of collision cross sections, which can be refined by molecular modeling techniques. Several platforms for performing IM separations exist and are categorized based on the nature of the IM electric field, *i.e.* electrostatic or electrodynamic. Electrostatic, or uniform-field, IM separations can be described by the principles of the kinetic theory of gases, and therefore provide absolute structural information. Alternatively, electrodynamic IM separations cannot presently be described by this theory, and therefore provide relative structural information when compared to structural standards. The derivation of absolute structural information from electrostatic field IM separations is discussed below, and is followed by a brief discussion of complementary molecular simulation strategies for interpreting absolute or relative structural information.

1.1.3.1. *Transforming Drift Times to Collision Cross Sections*

In an ion mobility experiment, separation occurs as ions traverse the electric field and collide with neutral gas molecules based on the prevailing physical properties of ion charge state and ion surface area. The number of collisions with neutral gas molecules is proportional to the rotationally-averaged ion surface area ($Å^2$), which is directly related to the ion's structure and termed the ion-neutral CCS. Under the assumptions that these ion-neutral collisions are brief and elastic, the kinetic theory of gases can be used to derive an equation relating the IM measurement and separation parameters to CCS.

The drift velocity (v_d) of an ion through the drift cell is defined by the length of the drift cell (L) and the drift time (t_d) of the ion. Under the condition that the

electrostratic field is weak, the ion velocity through the neutral gas can also be defined in terms of the ion's mobility constant (K) and the electrostatic field strength (E):

$$v_d = \frac{L}{t_d} = KE \tag{1}$$

When the electrostatic field is sufficiently weak (*i.e.* low-field conditions) and a Maxwell distribution can be used to describe the thermodynamic equilibrium of ion velocities, the mean thermal velocity is:

$$v_{mean} = \left(\frac{8k_BT}{\pi M_r}\right)^{\frac{1}{2}} \tag{2}$$

where k_b is the Boltzmann constant, T is the temperature of the gas in Kelvins, and M_r is the molar mass of the drift gas. The remainder of the ion velocity is accounted for by a minimal component of velocity in the direction of the electrostatic field. Thus, IM is typically considered directed diffusion. It is convention to normalize K to standard temperature and pressure (STP) conditions of 0°C and 760 Torr, referred to as the reduced mobility, (K_0):

$$K_0 = K \frac{p}{760} \frac{273}{T} \tag{3}$$

The low-field condition is important as K is not constant at high field conditions. When K is constant, the ion-neutral collision cross section (Ω) and K_0 are inversely related through the following expression:

$$K_0 = \frac{(18\pi)^{1/2}}{16} \frac{ze}{(k_BT)^{1/2}} \left[\frac{1}{m_i} + \frac{1}{m_n}\right]^{1/2} \frac{760}{p} \frac{T}{273} \frac{1}{N_0} \frac{1}{\Omega} \tag{4}$$

where N_0 is the number density of the drift gas and at STP, m_i and m_n are the masses of the ion and neutral gas, respectively, in the form of the ion-neutral collision pair's reduced mass, and ze is the ion's charge.

To calculate Ω from the empirical measurement of an IM separation, Eqns. (1) and (3) are substituted for K_0 to incorporate t_d and Eqn. (4) is rearranged into the form commonly referred to as the Mason-Schamp equation:

$$\Omega = \frac{(18\pi)^{1/2}}{16} \frac{ze}{(k_BT)^{1/2}} \left[\frac{1}{m_i} + \frac{1}{m_n}\right]^{1/2} \frac{t_dE}{L} \frac{760}{p} \frac{T}{273} \frac{1}{N_0} \tag{5}$$

Equation 5 holds under the assumption that the total translational energy does not change upon ion-neutral collisions in the IM drift cell, but there are limits to this approximation.[63-66] Nevertheless, Eqn. (5) is generally accepted as that used for reporting CCSs in uniform field experiments unless otherwise noted by the particular study.

1.1.3.2. Computational Approaches for Collision Cross Sections

The CCS term derived from experimental IM-MS measurements provides a rotationally-averaged surface area of the analyte ion. However, this descriptor of ion size is relatively broad and does not offer detailed structural information. In order to obtain more detailed structural information consistent with the surface area that is measured, computational modeling methods are often used.

These computational modeling methods consist of generating a statistical ensemble of three-dimensional conformations of the ion, followed by an *in silico* IM experiment to determine the corresponding CCS of each ion conformation. Although quantum mechanics (QM) can be used for small molecules, typically molecular dynamic (MD) calculations are used to rapidly generate possible ion conformations. A common MD protocol consists of a temperature program to allow the molecular structure to sample the conformation space at high temperatures and then cool randomly selected structures slowly. These protocols are often termed simulated annealing or elevated

temperature MD. The success of a MD calculation relies on selecting a force field that is parameterized for the molecules of interest and an appropriate temperature that imparts sufficient energy for conformational diversity.[67-69] Force field selection is further complicated in that secondary metabolites typically encompass moieties of multiple biomolecular classes and/or contain difficult to parameterize elements such as transition metals. Because force fields are utilized in MD to model molecular movement and therefore imprecision in dynamics could result in erroneous structure, force field selection is critical.

An alternative approach to requiring parameterized force fields is distance geometry.[70] Distance geometry generates conformations based on sampling inter-atomic distances between the atoms in the molecule. With appropriate distance parameters, it is possible to sample all conformational space, avoiding potential energy minima that can be encountered in molecular dynamics. Once these initial conformations are generated, they must undergo a short energy minimization, introduction of an ion, and then a subsequent energy minimization to represent possible ion conformations. Effectively, distance geometry treats molecular structure as a geometry problem rather than a chemical one. Chemistry is reintroduced as the final step in energy minimization of the resulting structures. The energy minimization calculations can be performed with the Merck Molecular Force Field 94x (MMFF94x) in the Molecular Operating Environment (MOE) Software from the Chemical Computing Group.[71] Note that force fields in this context are only used to relax the resulting structures rather than explore conformational space as in MD simulations. The Merck force field is parameterized for drug like molecules, which should be an accurate description of many secondary metabolites.

Subsequently, each final structure is subjected to *in silico* IM using MOBCAL initially developed by Jarrold and coworkers,[63,64,72,73] or Sigma developed by Bowers and Wyttenbach.[65,66,74]

1.2. Utilization of Conformation Space for Exploration of Primary and Secondary Metabolites

It is becoming increasingly difficult to isolate new natural products using conventional separation methods and analytical techniques. The search for natural products with biological relevance has been a focus of many research laboratories since the isolation and identification of penicillin in the 1940s.[1,2] Due to the extensive search for new chemical entities (NCEs), many easily isolated compounds have already been identified, leaving more difficult to isolate molecules uncharacterized. However, based on genomic sequencing analysis of producers of clinically relevant natural products, it is estimated that a vast majority of secondary metabolic compounds have not been isolated.[3] Beyond the fundamental problem of gene transcription, new paradigms in separation strategies targeting orthogonal properties should greatly expand the scope of natural product discovery.

A comparison across multiple classes of primary and secondary metabolites indicates differences in molecular weight, degree of oxidation, cyclization, and atom type, among others. For example, the antibiotic vancomycin has multiple oxidations, cyclizations, and halogen atoms, creating a conformation distinct from non-secondary metabolic species in that molecular weight regime. These chemical modifications are distinct from primary metabolites, which impact the overall structural conformation that

the molecule adopts. In turn, these secondary metabolite structural differences result in altered molecular densities ultimately manifested by the occupation of different regions within conformation space, as discussed in Section 1.1.2.

Contemporary efforts are underway to construct an atlas of conformation space to direct the rapid identification of molecules from complex biological matrices based on prevailing molecular density preferences.[56,75] There are few compendiums summarizing the conformation space in which different molecular species are predicted to occur. The largest data sets are centered on linear peptides and proteins, as described elsewhere.[76-79] More modest data sets were recently generated for other primary metabolites such as carbohydrates, lipids, and oligonucleotides.[55] While each class of primary metabolites is composed of largely conserved chemical moieties, secondary metabolites can incorporate multiple chemical features from the primary metabolic classes (*e.g.* lipopeptides, glycosylation, aminoglycosides, etc.), as well as unique structural and chemical functionality (*e.g.* cyclization, oxidation, halogenation, etc.). Sections 1.2.1 and 1.2.2 address leveraging conformation space to differentiate primary and secondary metabolites based on their chemical and structural differences.

1.2.1. *Leveraging Conformation Space for Primary Metabolites*

Metabolic studies have proven difficult due to the size and complexity of the metabolome, which is comprised of thousands of metabolites having varied functional groups and chemical properties. A complicating factor for metabolite analysis by MS strategies is that they generally occur over a limited mass range (*ca.* 100-1000 Da) and thus the predicted frequency of nominally isobaric, but distinct, species can be quite high

and difficult to distinguish without additional separation. The integration of IM with MS allows the separation of isobaric species, which is helpful in metabolic profiling within dense regions of conformation space occupied by multiple subclasses of metabolites. Table 1.1 lists a number of metabolomics studies which demonstrate the advantages of IM-MS for structurally diverse metabolite species. Profiling studies of blood, liver, lymph, and urinary metabolomes with IM-MS illustrate the separation of chemical noise while simultaneously monitoring metabolic changes.[80-83] Studies utilizing IM-MS have also focused on metabolomics of prostate, skin, and colon cancer cell lines with the goal of identifying new diagnostic metabolic markers.[84,85] Real-time temporal metabolic monitoring of Jurkat cells by IM-MS has been demonstrated.[86] Targeted pharmacokinetic analyses have benefitted significantly from IM-MS in the characterization of drugs and their metabolites.[87-92] By including IM separations, Trim *et al.* demonstrated improved separation of isobaric MALDI matrix interferences from metabolites in whole body tissue sections,[89] while others have utilized IM-MS to study common microorganisms such as *Aspergillus fumigatu*, *Candida* species, and *E. coli*.[93-95] Collectively, these general metabolic studies have demonstrated great utility in the combination of IM with MS. Complimentary with these general metabolic studies are targeted analyses for sub-classes of primary metabolic species including those focused on carbohydrates and lipids.

1.2.1.1. Carbohydrates and Glycomics

Carbohydrates are ubiquitous metabolites and occur as one of the most common, and least studied, posttranslational modifications. In contrast with fields such as MS-based proteomics, glycomics faces several challenges such as the natural low abundance and

heterogeneity of isobaric structural and positional isomers.[96,97] Structurally-based separations afforded by IM-MS are well suited to probe the complex spectrum of carbohydrates. Several selected studies of carbohydrates with IM-MS are listed in Table 1.2. Standards and references have been widely used to benchmark the benefits of IM-MS for carbohydrate analysis, such as the ability to deconvolute structural and positional carbohydrate isomers.[54,55,93,98-109] The added dimension of IM can enhance carbohydrate ion signal-to-noise by the separation of chemical noise, which assists in the analysis of low abundant analytes in complex samples.[110-115] These advantages were demonstrated for carbohydrate signatures of diseases such as liver cancer.[110,111]

1.2.1.2. Lipids and Lipidomics

It is becoming increasingly recognized that lipid structure plays an important role in ultimate function, which is largely dictated by the variety of fatty acids and head group moieties (*e.g.* phosphatidylcholine, phosphatidylserine, sphingomyelin, etc.) from which they are composed.[116,117] Complications arise in MS analyses due to the limited mass range that lipids occupy, generally from 500 to 1200 Da, and the high number of isobaric species resulting from differences in double bond position and geometric isomerism of the fatty acyl tails. Selected examples of IM-MS studies centered on lipid analyses are listed in Table 1.3. Importantly, IM-MS allows separation of subclasses of lipid references and standards based on structural characteristics within these subcategories, and is capable of distinguishing sn-1 and sn-2 lipids when combined with ion activation and fragmentation strategies.[53-55,118-120] The analysis of lipids in complex biological

22

Table 1.1. Selected Studies of Metabolites Using Low Field Ion Mobility-Mass Spectrometry

Model System	Type of Study	References
Clinical		
Urine	Characterization	80
Lymph	Metabolic Changes	81
Blood	Metabolic Profiling	82
HepG2 Cells	Role of Nonoxidative Metabolites	83
Colon Cancer	Detect and Analyze	84
Prostate Cancer	Detection and Metabolomics	85
Jurkat Cells	Changes in Metabolite Levels	86
Pharmaceutical		
Opiates	Identify and Separation	87
Cocaine	Structure and Mobility in Different Gases	88
Vinblastine	Separation	89
Leflunomide and Acetominophen	Metabolic Changes	90
Carbamazepine	Structural Identification and Isomers	91
Cocaine	Metabolic Profiling	92
Microorganisms		
E. coli	Metabolic Profiling	93,94
Asperigilus fumigatus and *Candida*	Detection and Profiling	95

23

samples has been demonstrated by IM-MS, characterizing systems from brain tissue to *E. coli* lysates.[44,93,121-127]

1.2.2. *Leveraging Conformation Space for Secondary Metabolites*

In comparison to the characterization of primary metabolites, there are relatively few studies examining the utility of IM-MS for the discovery of secondary metabolites. The present discussion centers on the discovery of secondary metabolites rather than broad scale metabolic profiling. Despite the long medicinal history of secondary metabolites, IM-MS for secondary metabolite discovery is an emerging technology. Sun *et al.* used UPLC-IM-MS to structurally characterize indole alkaloids in yohimbe bark, which are utilized in dietary supplements.[128] In this study, structural separations facilitated the identification of structural isomers of the indole alkaloids when no standard reference compounds were available for product quality control. Dorrestein and coworkers demonstrated the efficacy of IM-MS data dimensionality for secondary metabolite discovery, specifically from cyanobacteria as illustrated in Figure 1.6.[129] The 2D conformation space plot is annotated with regions describing where molecules possessing halogenation and/or cyclization were identified. Corresponding mobility selected mass spectra labeled T1-4 depict the enhanced signal-to-noise obtained over MS-only analyses. Significantly, this represents one of the emerging directions for using conformation space in IM-MS for the discovery of secondary metabolites possessing differences in cyclization and atom type on the basis of structure. The conformational consequence of peptide cyclization was explored by Goodwin *et al.* to distinguish cyclic peptide conformation space from that predicted for linear peptides.[46]

Table 1.2. Selected Studies of Carbohydrates Using Low Field Ion Mobility-Mass Spectrometry

Model System	Type of Study	References
Standards and Reference		
N-link Glycan	Structural Separations	54,103,105
Carbohydrate Mixtures	Biological Class Separations	55
Carbohydrate, Hydrophilic	Identification	93
Raffinose, Melezitose, and Cyclodextrins	Structural Separations	98
Di- and Trisaccharides	Structural Separations	99
Melibose and Raffinose	Identification and Characterization	100
Glycosides and Non-complex Sugars	Structural Separations	101
Carbohydrate and Boronic Acid	Identification and Characterization	102
Carbohydrate Mixtures	Structural Separations	104, 107
Mono- and Disaccharides	Carbohydrate Signal Enhancement	106
Raffinose and Maltotriose	Structural Separations	108
Carbohydrate Mixture	Library Screening	109
Complex Biological		
Serum	Disease State Detection, Characterization, and Statistical Analysis	110,111
Urine	Identification	112,113
Antibody Glycosylation	Identification and Characterization	114
Corn Stover Hydrolyzate	Characterization	115

25

In this work, absolute CCS values were reported for a large suite of cyclized species, which demonstrated that they adopt more dense structures than their linear counterparts. This can direct secondary metabolite discovery when signals arise in regions mapped to secondary rather than primary metabolic species. This work also underscores the value of using computational approaches for interpreting structural consequences of secondary metabolic attributes (e.g. cyclization, oxidation, halogenation, etc.). Building on this approach, Derewacz *et al.* identified a series of NCEs termed mutaxanthenes from actinomycetes, in part by conformational analyses with IM-MS.[130]

1.3.   *Emerging Application of Ion Mobility Separations to Secondary Metabolite Discovery*

The addition of IM to conventional complex extract screening protocols provides distinct advantages over MS alone, though there remain a few challenges. One potential consideration for the integration of IM separations is that depending on the experimental arrangement, scattering losses can result in a modest reduction in sensitivity. However, secondary metabolite discovery workflows typically involve comparatively high concentrations of analyte for purification and structural determination predominantly through follow-up NMR methodologies, which requires significantly more sample than MS or IM-MS (ca. fmol). The measurement of positive and negative ions of unknown secondary metabolites is desirable as foreknowledge of ionizability and adduct formation is usually not available. Although in principle there is no limitation to performing polarity switching to measure both positive and negative ions such as performed on triple quadrupole instruments (< sec.), polarity switching on most contemporary IM-MS

Table 1.3. Selected Studies of Lipids Using Low Field Ion Mobility-Mass Spectrometry

Model System	Type of Study	References
Standards and Reference		
Glycerophospholipids and Sphingolipids	Biological Class Separations	53, 54, 55
Glycerophospholipids and Sphingolipids	Structural Separation and Characterization	118, 119
Fatty Acids and Phospholipids	Determination of sn-1 vs. sn-2	120
Complex Biological		
Brain, Phospholipids	Structural Separations, Imaging Mass Spectrometry	44
E. coli	Metabolic Profiling	93
Brain, Phospholipids	Structural Separations, Imaging Mass Spectrometry	121,122
Brain, Cerebrosides	Structural Separations, Signal Enhancement	123
Brain, Phospholipids	Detection, Identifications, Structural	124
Glycerophospholipids and Sphingolipids	Tissue Profiling	125
V-type ATPase Bound Lipids	Structural Separations, Binding	126
Brain, Phospholipids	Structural Separations	127

platforms are presently performed on timescales (min.) not amendable to chromatographic separations. These potential limitations are mitigated by the increased peak capacity afforded through the addition of IM, which can serve to decrease chromatographic analysis time. Herein, we describe three emerging directions in secondary metabolite discovery that are directly facilitated by IM-MS, namely: (i) conformation-based prioritization of secondary metabolites, (ii) untargeted IM-MS-based secondary metabolite workflows, and (iii) imaging IM-MS for spatial characterization of secondary metabolite distributions.

1.3.1. Prioritization and Dereplication of Secondary Metabolites

As discussed in Sections 1.1.2 and 1.2, IM has demonstrated the ability to perform biomolecular class separation based upon prevailing intramolecular forces that dominate and the subunits that are assembled to create biomolecules (*e.g.* amino acids to form peptides, sugars to form glycans, etc.).[56] These inherent properties give rise to mobility-mass correlations, also commonly referred to in the literature as "trendlines." Several of these mobility-mass correlations are well-established, as illustrated in Figure 1.4. As a result, deviations from the predicted mobility-mass correlation may be exploited for secondary metabolite isolation-lead compound prioritization purposes. For example, comparison of the mobility-mass values of peptidic secondary metabolites as they relate to the linear peptide mobility-mass correlation has demonstrated the value of IM-MS in a secondary metabolite discovery workflow.[46] In this study, peptidic secondary metabolites with differential cyclization, atom substitution (e.g. halogenation), and glycosylation were analyzed using IM-MS and compared to linear analogues. The chemical and
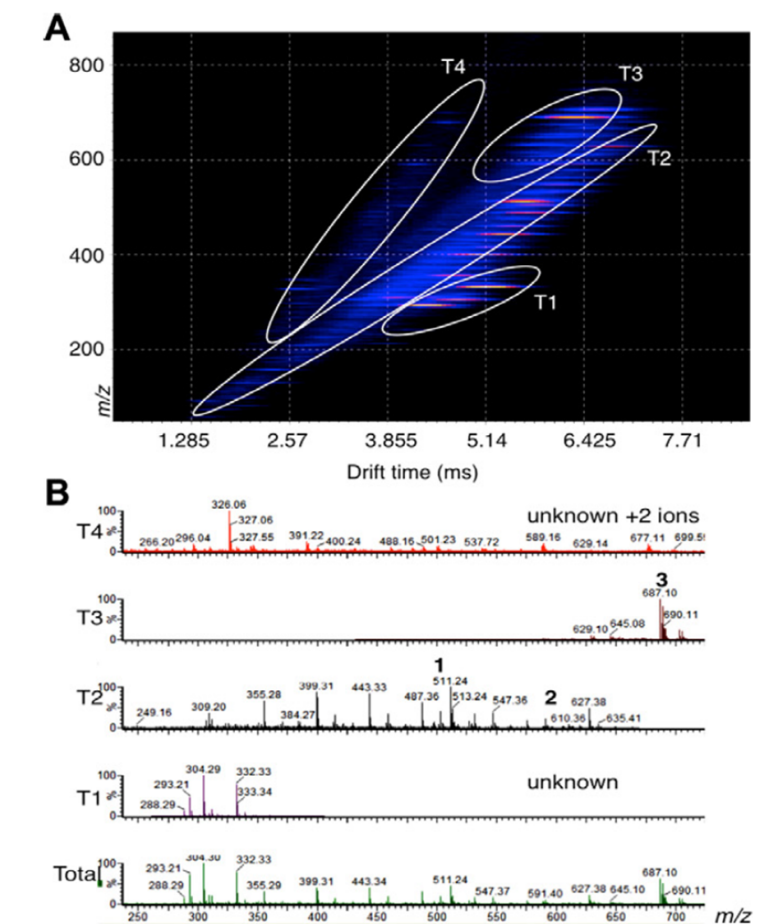
Figure 1.6. A 2D conformation space plot and corresponding mass spectra in the analysis of cyanobacteria metabolite production. Note, the axes in (A) are inverted relative to that elsewhere in this chapter. (A) Conformation space plot with selected regions of interest where particular molecules were identified as: (T1) singly-charged hydrocarbons incorporating nitrogen, (T2) singly-charged linear halogenated natural products, (T3) doubly-charged cyclic halogenated natural products, and (T4) doubly-charged species. (B) Mass spectra corresponding to those integrated over the annotated regions in (A). (Adapted with permission from Esquenazi, E., Daly, M., Bahrainwala, T., Gerwick, W. H., Dorrestein, P. C., *Bioorg. Med. Chem*. **2011**, 19, (22), 6639-6644.)

structural properties of these species resulted in the average gas-phase conformational density of peptidic secondary metabolites to be greater than linear peptides of the same *m/z* (Figure 1.7). This general motif was used to prioritize the tricyclic peptide siamycin II from a crude extract, demonstrating the application of an IM-MS driven prioritization method. It can be envisioned that the mobility-mass correlation can be extended to other secondary metabolite classes, and a more general approach to extract prioritization may follow. It should be noted that the structural and chemical properties of secondary metabolites transcend conventional biomolecular classes, and a more generalized approach to applying IM for predictive power may be applicable.

A critical and sometimes rate limiting step in secondary metabolite discovery is the process of unknown compound "dereplication," which is defined as determining if an unknown compound of interest has been previously isolated and structurally elucidated. Through coupling IM-MS with pre-ionization separations, such as LC, the resulting increased peak capacity provides a means to perform untargeted fragmentation for dereplication purposes. This has been utilized to provide in-depth, single-pass analysis of crude extracts, and is exceedingly valuable for lead compound dereplication, in addition to untargeted microbial metabolomics. In general, this method typically operates under the principle of acquiring both low- and high-energy mobility-separated evaluation, with high-energy fragmentation occurring post-mobility separation (see Section 1.1.2.1). As a result, for a given scan, an intact mobility separated spectrum and a mobility separated fragmentation spectrum exist. When considering utilizing high-resolution TOFMS data, intact spectra are necessary for accurate mass and isotopic distribution data for candidate
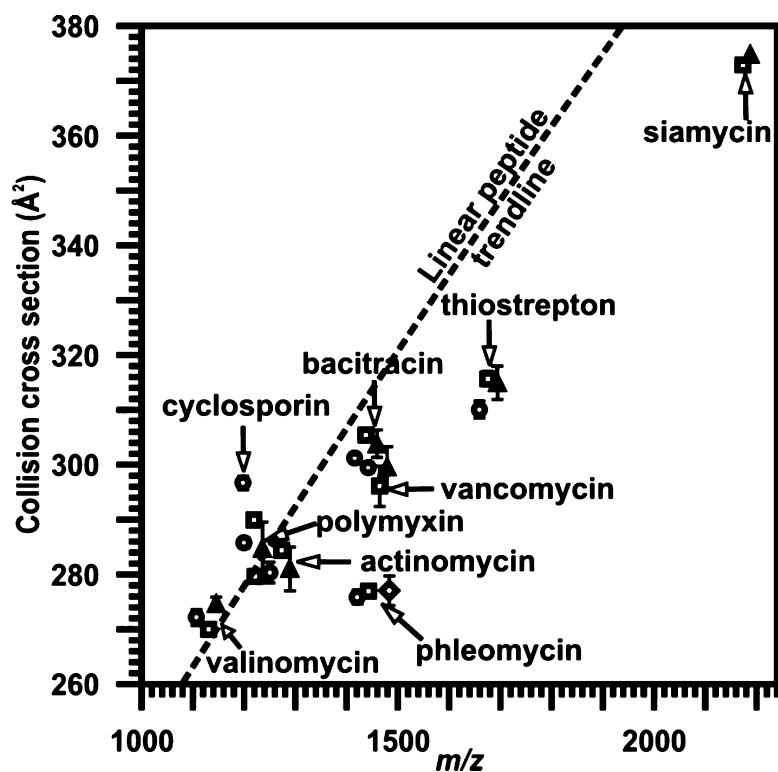
Figure 1.7. Conformation space plot depicting the relative increased gas-phase density of peptidic natural products when compared to linear peptides. IM-MS plot comparison of the collision cross sections of cyclic peptides compared to a trendline best representative of linear peptides for the mass range of 1100-2300 Da. Though deviations vary considerably, on average the peptidic natural products analyzed adopted denser gas phase conformations. Symbols are as follows: ●-$[M+H]^+$; ■-$[M+Na]^+$; ▲-$[M+K]^+$; and ♦-$[M+Cu]^+$. (Adapted with permission from Goodwin, C. R.; Fenn, L. S.; Derewacz, D. K.; Bachmann, B. O.; McLean, J. A., Structural Mass Spectrometry: Rapid Methods for Separation and Analysis of Peptide Natural Products. *Journal of Natural Products* **2012,** *75* (1), 48-53.)

chemical formula determination. These data, in addition to spectrophotometric information, are integral to initial dereplication of unknown compounds. The acquisition of untargeted high-energy data provides the ability to unambiguously dereplicate lead compounds based upon database matching using known chemical information (*i.e.* accurate mass, UV-Vis absorbance, chemical formula), and comparing matching structures with observed fragmentation data. Since fragmentation occurs post-mobility separation, product ions can be correlated to precursor species based upon the retained mobility values. In other words, a product ion will share the same mobility as the precursor, as shown in Figure 1.5(C). In this manner, fragmentation spectra for many ions are observed simultaneously with no loss of duty cycle. These mobility-separated high-energy spectra can then be exported for *in silico* fragmentation comparison to congruent database matches using any number of available software packages (*e.g.* MetFrag, Mass Spectrum Interpreter) or for *in silico* interpretation using Sirius.[131] This provides a rapid method of dereplicating lead compounds from a single analysis of a crude extract. A powerful addition to dereplication and prediction procedures would be the addition of CCS values to database entries. As CCS values are intrinsic properties, they may be used to confidently assign identity to an unknown, when complimenting additional chemical information.

1.4.   Conclusions

Secondary metabolite discovery is often challenged by the lack of analytical techniques that can properly separate these species from their complex biological matrices. In contrast with genomics, transcriptomics, and proteomics, the molecular

diversity of metabolomics is so broad that there is no "one-size-fits-all" separation technique to reduce sample complexity to the molecular class of interest. Many contemporary metabolomics studies utilize a range of separation strategies prior to identification, including LC, GC, and CE among others. In all of these cases, there is bias in the class of molecules that are preferentially analyzed based on the physiochemical properties of the separation technique. For example, LC is biased in the differential hydropathy of the analytes to be separated, GC is biased towards the volatility of the species, and CE is biased towards analyte electrophoretic physical constraints. Gas phase electrophoresis on the basis of structural conformation and mass by IM-MS is well suited for secondary metabolite discovery as these species often contain uncommon structural characteristics. Ongoing research in IM-MS is currently creating molecular atlases suitable for mapping conformation space of different molecular classes including secondary metabolites to drive discovery of NCEs. Recent studies have demonstrated great potential utility for secondary metabolite discovery. Emerging application areas utilizing untargeted molecular characterization and improved dereplication will aid in lead compound prioritization. These will invariably include imaging IM-MS to consider spatial distribution of secondary metabolites from microorganism interactions among other allied areas as forefront research directions in drug discovery.

1.5. Objectives of Dissertation Research

Ion mobility and mass spectrometry techniques play a key role the advancement of biological sample analysis. The added dimension of IM to MS allows for rapid IM separations (ms) prior to the MS analysis (μs). Combined, IM-MS allows for the

simultaneous analysis of multiple classes of biological molecules as different classes of molecules are separated due to their gas phase packing efficiency. My dissertation research has focused on the development of methodologies utilizing the unique capabilities of ion mobility-mass spectrometry. Chapter II describes these capabilities and evaluates figures of merit for a commercial high resolution IM-MS instrument. Considerations for different drift gas experiments are also described. Regions occupied by lipids, peptides, carbohydrates and alkyl ammonium salts are described as well. This is the first extensive multi-class nitrogen CCS study reported.

With these correlation regions define, Chapter III focuses on the IM-MS separations of carbohydrates and peptides. A simple LC-IM-MS method for carbohydrates is reported. The method supports both glycomic and a proteomic analysis, as it is amenable to proteomics LC platforms. The method was demonstrated on a series of maltose standards and branched glycans released from bovine fetuine. To obtain finer structural detail of carbohydrates, proteins and glycoproteins, a multimodal fragmentation method was developed. Using a combinatorial fragmentation approach in which ions are exposed to electron transfer dissociation (ETD) and subsequently collision induced dissociation (CID), a more comprehensive sequencing results. As ETD and CID are commentary techniques, different fragmentation information is acquired at each stage. Key to these experiments is the use of IM between the two stages of fragmentation. This allows for the deconvolution of spectra such that both modes can be utilized during the same experiment. This was demonstrated on a protein, ubiquitin, and a glycosylated carcinoembryonic ntigen 2 (CGM2).

Chapters II and III developed methods for multiclass CCS measurements, LC separations of carbohydrates and peptides, and comprehensive fragmentation techniques for proteins, glycopeptides, and carbohydrates. With methodology in place for carbohydrate and peptides, Chapter IV focuses on techniques for the analysis of small molecules. In particular, the methods were developed to support natural product discovery in search of novel metabolites. Potential metabolite candidates are structurally unique and typically contained peptidic and carbohydrate motifs. The methods of Chapters II and III have the potential to assist in the structural separation and elucidation of molecules with these motifs. Specific to small molecule analysis, Chapter IV describes a chip-based LC-IM-MS method. Small molecules are separated on a column embedded in a polyacrylamide chip. The addition of IM to traditional LC-MS metabolomics methods brings a dimension of separation with potential for use in dereplication. Chapter IV describes these separations and theoretical modeling to support the experimental CCS measurements. Methods presented here have the potential to aid in glycomic, proteomic and metabolomics research. A key focus of each chapter is the importance of IM-MS for the analysis of biological samples. Lastly, Chapter V summarizes the dissertation and discusses future directions of each project.

1.6. *Acknowledgements*

This chapter contains the invited book chapter for the Natural Product Analysis: Instrumentation, Methods, and Applications: "Structural Separations for Natural Product Characterization by Ion Mobility-Mass Spectrometry: Fundamental Theory to Emerging Applications," by Sarah M. Stow, Nichole M. Lareau, Kelly M. Hines, C. Ruth McNees,

Cody R. Goodwin, Brian O. Bachmann, and John A. McLean. Vladimir Havliček and Jaroslav Splžek, Eds. John Wiley & Sons, 2014.

1.7.   References

1.   Chain, E.; Florey, H. W.; Hardner, A. D.; Heatley, N. G.; Jennings, M. A.; Orr-Ewing, J.; Sanders, A. G., Penicillin as a chemotherapeutic agent. *Lancet* **1940,** *239*, 226-228.

2.   Fleming, A., On the antibacterial action of cultures of a penicillium, with special reference to their use in the isolation of B. influenzae. *British journal of experimental pathology* **1979,** *60* (1), 3.

3.   Challis, G. L., Genome mining for novel natural product discovery. *ChemInform* **2008,** *39* (29).

4.   Qian, W. J.; Jacobs, J. M.; Liu, T.; Camp, D. G.; Smith, R. D., Advances and challenges in liquid chromatography-mass spectrometry-based proteomics profiling for clinical applications. *Molecular & Cellular Proteomics* **2006,** *5* (10), 1727-1744.

5.   Metz, T. O.; Zhang, Q.; Page, J. S.; Shen, Y.; Callister, S. J.; Jacobs, J. M.; Smith, R. D., Future of liquid chromatography-mass spectrometry in metabolic profiling and metabolomic studies for biomarker discovery. *Biomarkers in Medicine* **2007,** *1* (1), 159-185.

6.   Lu, X.; Zhao, X.; Bai, C.; Zhao, C.; Lu, G.; Xu, G., LC-MS-based metabonomics analysis. *Journal of Chromatography B-Analytical Technologies in the Biomedical and Life Sciences* **2008,** *866* (1-2), 64-76.

7. Griffiths, W. J.; Wang, Y., Mass spectrometry: from proteomics to metabolomics and lipidomics. *Chemical Society Reviews* **2009,** *38* (7), 1882-1896.

8. Sauer, U., High-throughput phenomics: experimental methods for mapping fluxomes. *Current Opinion in Biotechnology* **2004,** *15* (1), 58-63.

9. Tang, Y. J.; Martin, H. G.; Myers, S.; Rodriguez, S.; Baidoo, E. E. K.; Keasling, J. D., Advances in analysis of microbial metabolic fluxes via (13)C isotopic labeling. *Mass Spectrometry Reviews* **2009,** *28* (2), 362-375.

10. McDaniel, E. W., *Collision Phenomena in Ionized Gases*. Wiley: New York, 1964.

11. McDaniel, E. W.; Mason, E. A., *The Mobility and Diffusion of Ions in Gases*. John Wiley & Sons: New York, 1973.

12. Mason, E. A.; McDaniel, E. W., *Transport Properties of Ions in Gases*. John Wiley & Sons: New York, 1988.

13. Eiceman, G. A.; Karpas, Z., *Ion Mobility Spectrometry*. 2nd ed.; CRC Press: Boca Raton, FL, 2005.

14. Wilkins, C. L.; Trimpin, S., *Ion Mobility Spectrometry-Mass Spectrometry:Theory and Applications*. CRC Press: Boca Raton, FL, 2011.

15. Hines, K. M.; Enders, J. R.; McLean, J. A., Multidimensional Separations by Ion Mobility-Mass Spectrometry. In *Encyclopedia of Analytical Chemistry*, Myers, R. A., Ed. John Wiley & Sons: 2012.

16. Rontgen, W. C., On a new kind of rays. *Science* **1896,** *3* (59), 227-31.

17. Thomson, J. J.; Rutherford, E., On the passage of electricity through gases exposed to Rontgen rays. *Philos. Mag. (1798-1977)* **1896,** *42* (5), 392.

18. Zeleny, J., VI. On the ratio of the velocities of the two ions produced in gases by Röntgen radiation; and on some related phenomena. *Philosophical Magazine Series 5* **1898,** *46* (278), 120-154.

19. Kingdon, K. H., A Method for the Neutralization of Electron Space Charge by Positive Ionization at Very Low Gas Pressures. *Physical Review* **1923,** *21* (4), 408-418.

20. Makarov, A., Electrostatic Axially Harmonic Orbital Trapping: A High-Performance Technique of Mass Analysis. *Anal. Chem.* **2000,** *72* (6), 1156-1162.

21. Stephens, W. E., A pulsed mass spectrometer with time dispersion. *Phys. Rev.* **1946,** *69*, 691.

22.   Mamyrin, B. A., Russian Patent No. 198034. 1966.

23.   Karataev, V. I.; Mamyrin, B. A.; Shmikk, D. A., New principle of the focusing of ion packets in time-of-flight mass spectrometers. *Zh. Tekh. Fiz.* **1971,** *41* (7), 1498-501.

24.   Mamyrin, B. A.; Karataev, V. I.; Shmikk, D. V.; Zagulin, V. A., Mass reflectron. New nonmagnetic time-of-flight high-resolution mass spectrometer. *Zh. Eksp. Teor. Fiz.* **1973,** *64* (1), 82-9.

25.   Karas, M.; Hillenkamp, F., Laser desorption ionization of proteins with molecular masses exceeding 10,000 daltons. *Anal. Chem.* **1988,** *60* (20), 2299-301.

26.   Tanaka, K.; Waki, H.; Ido, Y.; Akita, S.; Yoshida, Y.; Yohida, T., Protein and polymer analyses up to m/z 100,000 by laser ionization time-of-flight mass spectrometry. *Rapid Communications in Mass Spectrometry* **1988,** *2* (8), 151-3.

27.   Fenn, J. B.; Mann, M.; Meng, C. K.; Wong, S. F.; Whitehouse, C. M., Electrospray ionization for mass-spectrometry of large biomolecules. *Science* **1989,** *246* (4926), 64-71.

28.   Tyndall, A. M.; Grindley, G. C., Mobility of ions in air. I. Negative ions in moist air. *Proc. R. Soc. London, Ser. A* **1926,** *110*, 341-58.

29.   Tyndall, A. M.; Grindley, G. C., Mobility of ions in air. II. Positive ions of short age. *Proc. R. Soc. London, Ser. A* **1926,** *110*, 358-64.

30.   Tyndall, A. M.; Phillips, L. R., Mobility of ions in air. III. Air containing organic vapors. *Proc. R. Soc. London, Ser. A* **1926,** *111*, 577-91.

31.   Tyndall, A. M.; Grindley, G. C.; Sheppard, P. A., Mobility of ions in air.V. Transformation of positive ions at short ages. *Proc. R. Soc. London, Ser. A* **1928,** *121*, 185-94.

32.   Tyndall, A. M.; Starr, L. H.; Powell, C. F., Mobility of ions in air. IV. Investigations by two new methods. *Proc. R. Soc. London, Ser. A* **1928,** *121*, 172-84.

33.   Barnes, W. S.; Martin, D. W.; McDaniel, E. W., Mass spectrographic identification of the ion observed in hydrogen mobility experiments. *Phys. Rev. Lett.* **1961,** *6*, 110-11.

34.   McAfee, K. B., Jr.; Edelson, D., Identification and mobility of ions in a Townsend discharge by time-resolved mass spectrometry. *Proc. Phys. Soc., London* **1963,** *81* (520), 382-4.

35.   Cohen, M. J.; Karasek, F. W., Plasma chromatography TM--new dimension for gas chromatography and mass spectrometry. *J. Chromatogr. Sci.* **1970,** *8* (6), 330-7.

36.   Karasek, F. W., Plasma chromatography of the polychlorinated biphenyls. *Anal Chem* **1971,** *43* (14), 1982-6.

37.   Karasek, F. W., Trace analysis and fundamental studies by plasma chromatography. *Int J Environ Anal Chem* **1972,** *2* (2), 157-66.

38.   Karasek, F. W.; Denney, D. W., Evaluation of the plasma chromatograph as a qualitative detector for liquid chromatography. *Anal. Lett.* **1973,** *6* (11), 993-1004.

39.   Gieniec, J.; Mack, L. L.; Nakamae, K.; Gupta, C.; Kumar, V.; Dole, M., Electrospray mass spectroscopy of macromolecules: application of an ion-drift spectrometer. *Biomed. Mass Spectrom.* **1984,** *11* (6), 259-68.

40.   von Helden, G.; Wyttenbach, T.; Bowers, M. T., Conformation of macromolecules in the gas-phase - use of matrix-assisted laser-desorption methods in ion chromatography. *Science* **1995,** *267* (5203), 1483-1485.

41.   Wyttenbach, T.; von Helden, G.; Bowers, M. T., Gas-phase conformation of biological molecules: Bradykinin. *Journal of the American Chemical Society* **1996,** *118* (35), 8355-8364.

42.   Clemmer, D. E.; Hudgins, R. R.; Jarrold, M. F., Naked protein conformations - Cytochrome c in the gas-phase. *Journal of the American Chemical Society* **1995,** *117* (40), 10141-10142.

43.   Shelimov, K. B.; Clemmer, D. E.; Hudgins, R. R.; Jarrold, M. F., Protein structure *in vacuo*: Gas-phase conformations of BPTI and cytochrome c. *Journal of the American Chemical Society* **1997,** *119* (9), 2240-2248.

44.   McLean, J. A.; Ridenour, W. B.; Caprioli, R. M., Profiling and imaging of tissues by imaging ion mobility-mass spectrometry. *Journal of Mass Spectrometry* **2007,** *42* (8), 1099-1105.

45.   Ruotolo, B. T.; Giles, K.; Campuzano, I.; Sandercock, A. M.; Bateman, R. H.; Robinson, C. V., Evidence for macromolecular protein rings in the absence of bulk water. *Science* **2005,** *310* (5754), 1658-1661.

46.   Goodwin, C. R.; Fenn, L. S.; Derewacz, D. K.; Bachmann, B. O.; McLean, J. A., Structural Mass Spectrometry: Rapid Methods for Separation and Analysis of Peptide Natural Products. *Journal of natural products* **2012,** *75* (1), 48-53.

47.   McLean, J. A.; Ruotolo, B. T.; Gillig, K. J.; Russell, D. H., Ion mobility–mass spectrometry: a new paradigm for proteomics. *International Journal of Mass Spectrometry* **2005,** *240* (3), 301-315.

48. Giddings, J. C., Two-dimensional separations - concept and promise. *Analytical Chemistry* **1984,** *56* (12), 1258-1270.

49. Shen, Y. F.; Tolic, N.; Zhao, R.; Pasa-Tolic, L.; Li, L. J.; Berger, S. J.; Harkewicz, R.; Anderson, G. A.; Belov, M. E.; Smith, R. D., High-throughput proteomics using high efficiency multiple-capillary liquid chromatography with on-line high-performance ESI FTICR mass spectrometry. *Analytical Chemistry* **2001,** *73* (13), 3011-3021.

50. Ruotolo, B. T.; Gillig, K. J.; Stone, E. G.; Russell, D. H., Peak capacity of ion mobility mass spectrometry: Separation of peptides in helium buffer gas. *Journal of Chromatography B-Analytical Technologies in the Biomedical and Life Sciences* **2002,** *782* (1-2), 385-392.

51. Ruotolo, B. T.; McLean, J. A.; Gillig, K. J.; Russell, D. H., Peak capacity of ion mobility mass spectrometry: the utility of varying drift gas polarizability for the separation of tryptic peptides. *Journal of Mass Spectrometry* **2004,** *39* (4), 361-367.

52. Koomen, J. M.; Ruotolo, B. T.; Gillig, K. J.; McLean, J. A.; Russell, D. H.; Kang, M. J.; Dunbar, K. R.; Fuhrer, K.; Gonin, M.; Schultz, J. A., Oligonucleotide analysis with MALDI-ion-mobility-TOFMS. *Analytical and Bioanalytical Chemistry* **2002,** *373* (7), 612-617.

53. Woods, A. S.; Ugarov, M.; Egan, T.; Koomen, J.; Gillig, K. J.; Fuhrer, K.; Gonin, M.; Schultz, J. A., Lipid/peptide/nucleotide separation with MALDI-ion mobility-TOF MS. *Analytical Chemistry* **2004,** *76* (8), 2187-2195.

54. Fenn, L. S.; McLean, J. A., Biomolecular structural separations by ion mobility-mass spectrometry. *Analytical and Bioanalytical Chemistry* **2008,** *391* (3), 905-909.

55. Fenn, L. S.; Kliman, M.; Mahsut, A.; Zhao, S. R.; McLean, J. A., Characterizing ion mobility-mass spectrometry conformation space for the analysis of complex biological samples. *Analytical and Bioanalytical Chemistry* **2009,** *394* (1), 235-244.

56. McLean, J. A., The Mass-Mobility Correlation Redux: The Conformational Landscape of Anhydrous Biomolecules. *Journal of the American Society for Mass Spectrometry* **2009,** *20* (10), 1775-1781.

57. Hudgins, R. R.; Ratner, M. A.; Jarrold, M. F., Design of helices that are stable in vacuo. *Journal of the American Chemical Society* **1998,** *120* (49), 12974-12975.

58. Ruotolo, B. T.; Verbeck, G. F.; Thomson, L. M.; Gillig, K. J.; Russell, D. H., Observation of conserved solution-phase secondary structure in gas-phase tryptic peptides. *Journal of the American Chemical Society* **2002,** *124* (16), 4214-4215.

59. Counterman, A. E.; Clemmer, D. E., Cis-trans signatures of proline-containing tryptic peptides in the gas phase. *Analytical Chemistry* **2002,** *74* (9), 1946-1951.

60. Ruotolo, B. T.; Russell, D. H., Gas-phase conformations of proteolytically derived protein fragments: Influence of solvent on peptide conformation. *Journal of Physical Chemistry B* **2004,** *108* (39), 15321-15331.

61. Hoaglund-Hyzer, C. S.; Li, J. W.; Clemmer, D. E., Mobility labeling for parallel CID of ion mixtures. *Analytical Chemistry* **2000,** *72* (13), 2737-2740.

62. Valentine, S. J.; Kulchania, M.; Barnes, C. A. S.; Clemmer, D. E., Multidimensional separations of complex peptide mixtures: a combined high-performance liquid chromatography/ion mobility/time-of-flight mass spectrometry approach. *International Journal of Mass Spectrometry* **2001,** *212* (1-3), 97-109.

63. Mesleh, M. F.; Hunter, J. M.; Shvartsburg, A. A.; Schatz, G. C.; Jarrold, M. F., Structural information from ion mobility measurements: Effects of the long-range potential. *Journal of Physical Chemistry* **1996,** *100* (40), 16082-16086.

64. Shvartsburg, A. A.; Jarrold, M. F., An exact hard-spheres scattering model for the mobilities of polyatomic ions. *Chemical Physics Letters* **1996,** *261* (1-2), 86-91.

65. Wyttenbach, T.; von Helden, G.; Batka, J. J.; Carlat, D.; Bowers, M. T., Effect of the long-range potential on ion mobility measurements. *Journal of the American Society for Mass Spectrometry* **1997,** *8* (3), 275-282.

66. Wyttenbach, T.; Witt, M.; Bowers, M. T., On the stability of amino acid zwitterions in the gas phase: The influence of derivatization, proton affinity, and alkali ion addition. *Journal of the American Chemical Society* **2000,** *122* (14), 3458-3464.

67. Shvartsburg, A. A.; Schatz, G. C.; Jarrold, M. F., Mobilities of carbon cluster ions: Critical importance of the molecular attractive potential. *Journal of Chemical Physics* **1998,** *108* (6), 2416-2423.

68. Hudgins, R. R.; Jarrold, M. F., Conformations of unsolvated glycine-based peptides. *Journal of Physical Chemistry B* **2000,** *104* (9), 2154-2158.

69. Bernstein, S. L.; Wyttenbach, T.; Baumketner, A.; Shea, J. E.; Bitan, G.; Teplow, D. B.; Bowers, M. T., Amyloid beta-protein: monomer structure and early aggregation states of Abeta42 and its Pro19 alloform. *J Am Chem Soc* **2005,** *127* (7), 2075-84.

70. Havel, T. F., Distance geometry: Theory, algorithms, and chemical applications. *Encyclopedia of Computational Chemistry* **1998,** *120*.

71.   *Molecular Operating Environment (MOE)*, 2012.10; Chemical Computing Group Inc.: 1010 Sherbooke St. West, Suite #910, Montreal, QC, Canada, H3A 2R7, 2012.

72.   Shvartsburg, A. A.; Mashkevich, S. V.; Baker, E. S.; Smith, R. D., Optimization of algorithms for ion mobility calculations. *Journal of Physical Chemistry A* **2007,** *111* (10).

73.   Campuzano, I.; Bush, M. F.; Robinson, C. V.; Beaumont, C.; Richardson, K.; Kim, H.; Kim, H. I., Structural characterization of drug-like compounds by ion mobility mass spectrometry: comparison of theoretical and experimentally derived nitrogen collision cross sections. *Analytical chemistry* **2011,** *84* (2), 1026-1033.

74.   von Helden, G.; Hsu, M. T.; Gotts, N.; Bowers, M. T., Carbon cluster cations with up to 84 atoms: structures, formation mechanism, and reactivity. *The Journal of Physical Chemistry* **1993,** *97* (31), 8182-8192.

75.   Fenn, L. S.; Kliman, M.; Mahsut, A.; Zhao, S. R.; McLean, J. A., Characterizing ion mobility-mass spectrometry conformation space for the analysis of complex biological samples. *Anal. Bioanal. Chem.* **2009,** *394* (1), 235-244.

76.   Valentine, S. J.; Counterman, A. E.; Clemmer, D. E., A database of 660 peptide ion cross sections: Use of intrinsic size parameters for bona fide predictions of cross sections. *Journal of the American Society for Mass Spectrometry* **1999,** *10* (11), 1188-1211.

77.   Tao, L.; McLean, J. R.; McLean, J. A.; Russell, D. H., A collision cross-section database of singly-charged peptide ions. *Journal of the American Society for Mass Spectrometry* **2007,** *18* (7), 1232-1238.

78.   Shah, A. R.; Agarwal, K.; Baker, E. S.; Singhal, M.; Mayampurath, A. M.; Ibrahim, Y. M.; Kangas, L. J.; Monroe, M. E.; Zhao, R.; Belov, M. E.; Anderson, G. A.; Smith, R. D., Machine learning based prediction for peptide drift times in ion mobility spectrometry. *Bioinformatics* **2010,** *26* (13), 1601-1607.

79.   Enders, J. R.; Kliman, M.; Sundarapandian, S.; McLean, J. A., Peptide and Protein Analysis Using Ion Mobility–Mass Spectrometry. *Protein and Peptide Mass Spectrometry in Drug Discovery*, 139-174.

80.   Harry, E. L.; Weston, D. J.; Bristow, A. W. T.; Wilson, I. D.; Creaser, C. S., An approach to enhancing coverage of the urinary metabonome using liquid chromatography-ion mobility-mass spectrometry. *J. Chromatogr., B: Anal. Technol. Biomed. Life Sci.* **2008,** *871* (2), 357-361.

81.   Kaplan, K.; Dwivedi, P.; Davidson, S.; Yang, Q.; Tso, P.; Siems, W.; Hill, H. H., Monitoring Dynamic Changes in Lymph Metabolome of Fasting and Fed Rats by

Electrospray Ionization-Ion Mobility Mass Spectrometry (ESI-IMMS). *Analytical Chemistry* **2009,** *81* (19), 7944-7953.

82.   Dwivedi, P.; Schultz, A. J.; Hill, H. H., Metabolic profiling of human blood by high-resolution ion mobility mass spectrometry (IM-MS). *International Journal of Mass Spectrometry* **2010,** *298* (1-3), 78-90.

83.   Castaneda, F.; Zimmermann, D.; Nolte, J.; Baumbach, J. I., Role of undecan-2-one on ethanol-induced apoptosis in HepG2 cells. *Cell Biol. Toxicol.* **2007,** *23* (6), 477-485.

84.   Zimmermann, D.; Hartmann, M.; Nolte, J.; Baumbach, J. I., First detection of metabolites of the colon cancer cell line SW 480 using MCC/IMS and GC/MS. *Int. J. Ion Mobility Spectrom.* **2005,** *8* (2), 3-6.

85.   Kaplan, K.; Liu, X.; Fu, Y.-M.; Lin, H.; Meadows, G. G.; Siems, W.; Hill, H. H., Jr., Metabolic differences among melanoma and two prostate cancer cell lines by electrospray ion mobility mass spectrometry. *Int. J. Ion Mobility Spectrom.* **2011,** *14* (4), 151-158.

86.   Enders, J. R.; Marasco, C. C.; Kole, A.; Nguyen, B.; Sevugarajan, S.; Seale, K. T.; Wikswo, J. P.; McLean, J. A., Towards monitoring real-time cellular response using an integrated microfluidics-matrix assisted laser desorption ionisation/nanoelectrospray ionisation-ion mobility-mass spectrometry platform. *Iet Systems Biology* **2010,** *4* (6), 416-427.

87.   Matz, L. M.; Hill Jr, H. H., Evaluation of opiate separation by high-resolution electrospray ionization-ion mobility spectrometry/mass spectrometry. *Analytical chemistry* **2001,** *73* (8), 1664-1669.

88.   Matz, L. M.; Hill, H. H.; Beegle, L. W.; Kanik, I., Investigation of drift gas selectivity in high resolution ion mobility spectrometry with mass spectrometry detection. *Journal of the American Society for Mass Spectrometry* **2002,** *13* (4), 300-307.

89.   Trim, P. J.; Henson, C. M.; Avery, J. L.; McEwen, A.; Snel, M. F.; Claude, E.; Marshall, P. S.; West, A.; Princivalle, A. P.; Clench, M. R., Matrix-assisted laser desorption/ionization-ion mobility separation-mass spectrometry imaging of vinblastine in whole body tissue sections. *Analytical chemistry* **2008,** *80* (22), 8628-8634.

90.   Chan, E. C. Y.; New, L. S.; Yap, C. W.; Goh, L. T., Pharmaceutical metabolite profiling using quadrupole/ion mobility spectrometry/time-of-flight mass spectrometry. *Rapid Commun. Mass Spectrom.* **2009,** *23* (3), 384-394.

91.   Cuyckens, F.; Wassvik, C.; Mortishire-Smith, R. J.; Tresadern, G.; Campuzano, I.; Claereboudt, J., Product ion mobility as a promising tool for assignment of

positional isomers of drug metabolites. *Rapid Commun. Mass Spectrom.* **2011,** *25* (23), 3497-3503.

92.   Kaplan, K. A.; Chiu, V. M.; Lukus, P. A.; Zhang, X.; Siems, W. F.; Schenk, J. O.; Hill, H. H., Jr., Neuronal metabolomics by ion mobility mass spectrometry: cocaine effects on glucose and selected biogenic amine metabolites in the frontal cortex, striatum, and thalamus of the rat. *Anal Bioanal Chem* **2013**.

93.   Dwivedi, P.; Wu, P.; Klopsch, S. J.; Puzon, G. J.; Xun, L.; Hill, H. H., Jr., Metabolic profiling by ion mobility mass spectrometry (IMMS). *Metabolomics* **2008,** *4* (1), 63-80.

94.   Dwivedi, P.; Puzon, G.; Tam, M.; Langlais, D.; Jackson, S.; Kaplan, K.; Siems, W. F.; Schultz, A. J.; Xun, L. Y.; Woodsd, A.; Hill, H. H., Metabolic profiling of Escherichia coli by ion mobility-mass spectrometry with MALDI ion source. *Journal of Mass Spectrometry* **2010,** *45* (12), 1383-1393.

95.   Perl, T.; Juenger, M.; Vautz, W.; Nolte, J.; Kuhns, M.; Borg-von, Z. M.; Quintel, M., Detection of characteristic metabolites of Aspergillus fumigatus and Candida species using ion mobility spectrometry - metabolic profiling by volatile organic compounds. *Mycoses* **2011,** *54* (6), e828-e837.

96.   Varki, A., Biological roles of oligosaccharides - all of the theories are correct. *Glycobiology* **1993,** *3* (2), 97-130.

97.   Gorelik, E.; Galili, U.; Raz, A., On the role of cell surface carbohydrates and their binding proteins (lectins) in tumor metastasis. *Cancer and Metastasis Reviews* **2001,** *20* (3-4), 245-277.

98.   Liu, Y. S.; Clemmer, D. E., Characterizing oligosaccharides using injected-ion mobility mass spectrometry. *Analytical Chemistry* **1997,** *69* (13), 2504-2509.

99.   Clowers, B. H.; Dwivedi, P.; Steiner, W. E.; Hill, H. H.; Bendiak, B., Separation of sodiated isobaric disaccharides and trisaccharides using electrospray ionization-atmospheric pressure ion mobility-time of flight mass spectrometry. *Journal of the American Society for Mass Spectrometry* **2005,** *16* (5), 660-669.

100.   Clowers, B. H.; Hill, H. H., Mass analysis of mobility-selected ion populations using dual gate, ion mobility, quadrupole ion trap mass spectrometry. *Analytical Chemistry* **2005,** *77* (18), 5877-5885.

101.   Dwivedi, P.; Bendiak, B.; Clowers, B. H.; Hill, H. H., Rapid Resolution of Carbohydrate Isomers by Electrospray Ionization Ambient Pressure Ion Mobility Spectrometry-Time-of-Flight Mass Spectrometry (ESI-APIMS-TOFMS). *J. Am. Soc. Mass Spectrom.* **2007,** *18* (7), 1163-1175.

102. Fenn, L. S.; McLean, J. A., Enhanced carbohydrate structural selectivity in ion mobility-mass spectrometry analyses by boronic acid derivatization. *Chem. Commun. (Cambridge, U. K.)* **2008,** (43), 5505-5507.

103. Plasencia, M. D.; Isailovic, D.; Merenbloom, S. I.; Mechref, Y.; Clemmer, D. E., Resolving and assigning N-linked glycan structural isomers from ovalbumin by IMS-MS. *Journal of the American Society for Mass Spectrometry* **2008,** *19* (11), 1706-1715.

104. Zhu, M. L.; Bendiak, B.; Clowers, B.; Hill, H. H., Ion mobility-mass spectrometry analysis of isomeric carbohydrate precursor ions. *Analytical and Bioanalytical Chemistry* **2009,** *394* (7), 1853-1867.

105. Williams, J. P.; Grabenauer, M.; Holland, R. J.; Carpenter, C. J.; Wormald, M. R.; Giles, K.; Harvey, D. J.; Bateman, R. H.; Scrivens, J. H.; Bowers, M. T., Characterization of simple isomeric oligosaccharides and the rapid separation of glycan mixtures by ion mobility mass spectrometry. *International Journal of Mass Spectrometry* **2010,** *298* (1-3), 119-127.

106. Bohrer, B. C.; Clemmer, D. E., Biologically-inspired peptide reagents for enhancing IMS-MS analysis of carbohydrates. *J. Am. Soc. Mass Spectrom.* **2011,** *22* (9), 1602-1609.

107. Fenn, L. S.; McLean, J. A., Structural resolution of carbohydrate positional and structural isomers based on gas-phase ion mobility-mass spectrometry. *Physical Chemistry Chemical Physics* **2011,** *13* (6), 2196-2205.

108. Zekavat, B.; Solouki, T., Chemometric Data Analysis for Deconvolution of Overlapped Ion Mobility Profiles. *J. Am. Soc. Mass Spectrom.* **2012,** *23* (11), 1873-1884.

109. El-Hawiet, A.; Shoemaker, G. K.; Daneshfar, R.; Kitova, E. N.; Klassen, J. S., Applications of a Catch and Release Electrospray Ionization Mass Spectrometry Assay for Carbohydrate Library Screening. *Anal. Chem. (Washington, DC, U. S.)* **2012,** *84* (1), 50-58.

110. Isailovic, D.; Kurulugama, R. T.; Plasencia, M. D.; Stokes, S. T.; Kyselova, Z.; Goldman, R.; Mechref, Y.; Novotny, M. V.; Clemmer, D. E., Profiling of human serum glycans associated with liver cancer and cirrhosis by IMS-MS. *Journal of Proteome Research* **2008,** *7* (3), 1109-1117.

111. Isailovic, D.; Plasencia, M. D.; Gaye, M. M.; Stokes, S. T.; Kurulugama, R. T.; Pungpapong, V.; Zhang, M.; Kyselova, Z.; Goldman, R.; Mechref, Y.; Novotny, M. V.; Clemmer, D. E., Delineating Diseases by IMS-MS Profiling of Serum N-linked Glycans. *J. Proteome Res.* **2012,** *11* (2), 576-585.

112. Vakhrushev, S. Y.; Langridge, J.; Campuzano, I.; Hughes, C.; Peter-Katalinic, J., Identification of Monosialylated N-glycoforms in the CDG Urinome by Ion

Mobility Tandem Mass Spectrometry: The Potential for Clinical Applications. *Clin. Proteomics* **2008,** *4* (1-2), 47-57.

113.   Vakhrushev, S. Y.; Langridge, J.; Campuzano, I.; Hughes, C.; Peter-Katalinic, J., Ion Mobility Mass Spectrometry Analysis of Human Glycourinome. *Anal. Chem. (Washington, DC, U. S.)* **2008,** *80* (7), 2506-2513.

114.   Damen, C. W. N.; Chen, W.; Chakraborty, A. B.; van Oosterhout, M.; Mazzeo, J. R.; Gebler, J. C.; Schellens, J. H. M.; Rosing, H.; Beijnen, J. H., Electrospray ionization quadrupole ion-mobility time-of-flight mass spectrometry as a tool to distinguish the lot-to-lot heterogeneity in N-glycosylation profile of the therapeutic monoclonal antibody trastuzumab. *Journal of the American Society for Mass Spectrometry* **2009,** *20* (11), 2021-2033.

115.   Munisamy, S. M.; Chambliss, C. K.; Becker, C., Direct Infusion Electrospray Ionization - Ion Mobility - High Resolution Mass Spectrometry (DIESI-IM-HRMS) for Rapid Characterization of Potential Bioprocess Streams. *J. Am. Soc. Mass Spectrom.* **2012,** *23* (7), 1250-1259.

116.   Janmey, P. A.; Kinnunen, P. K. J., Biophysical properties of lipids and dynamic membranes. *Trends in Cell Biology* **2006,** *16* (10), 538-546.

117.   Wymann, M. P.; Schneiter, R., Lipid signalling in disease. *Nature Reviews Molecular Cell Biology* **2008,** *9* (2), 162-176.

118.   Jackson, S. N.; Ugarov, M.; Post, J. D.; Egan, T.; Langlais, D.; Schultz, J. A.; Woods, A. S., A study of phospholipids by ion mobility TOFMS. *Journal of the American Society for Mass Spectrometry* **2008,** *19* (11), 1655-1662.

119.   Kim, H. I.; Kim, H.; Pang, E. S.; Ryu, E. K.; Beegle, L. W.; Loo, J. A.; Goddard, W. A.; Kanik, I., Structural Characterization of Unsaturated Phosphatidylcholines Using Traveling Wave Ion Mobility Spectrometry. *Analytical Chemistry* **2009,** *81* (20), 8289-8297.

120.   Trimpin, S.; Tan, B.; Bohrer, B. C.; O'Dell, D. K.; Merenbloom, S. I.; Pazos, M. X.; Clemmer, D. E.; Walker, J. M., Profiling of phospholipids and related lipid structures using multidimensional ion mobility spectrometry-mass spectrometry. *International Journal of Mass Spectrometry* **2009,** *287* (1-3), 58-69.

121.   Jackson, S. N.; Wang, H. Y. J.; Woods, A. S.; Ugarov, M.; Egan, T.; Schultz, J. A., Direct tissue analysis of phospholipids in rat brain using MALDI-TOFMS and MALDI-ion mobility-TOFMS. *Journal of the American Society for Mass Spectrometry* **2005,** *16* (2), 133-138.

122.   Jackson, S. N.; Wang, H. Y. J.; Woods, A. S., In situ structural characterization of phosphatidylcholines in brain tissue using MALDI-MS/MS. *Journal of the American Society for Mass Spectrometry* **2005,** *16* (12), 2052-2056.

123. Jackson, S. N.; Ugarov, M.; Egan, T.; Post, J. D.; Langlais, D.; Schultz, J. A.; Woods, A. S., MALDI-ion mobility-TOFMS imaging of lipids in rat brain tissue. *Journal of Mass Spectrometry* **2007,** *42* (8), 1093-1098.

124. Kliman, M.; Vijayakrishnan, N.; Wang, L.; Tapp, J. T.; Broadie, K.; McLean, J. A., Structural mass spectrometry analysis of lipid changes in a Drosophila epilepsy model brain. *Molecular Biosystems* **2010,** *6* (6), 958-966.

125. Woods, A. S.; Jackson, S. N., The application and potential of ion mobility mass spectrometry in imaging MS with a focus on lipids. *Methods Mol. Biol. (N. Y., NY, U. S.)* **2010,** *656* (Mass Spectrometry Imaging), 99-111.

126. Zhou, M.; Morgner, N.; Barrera, N. P.; Politis, A.; Isaacson, S. C.; Matak-Vinković, D.; Murata, T.; Bernal, R. A.; Stock, D.; Robinson, C. V., Mass spectrometry of intact V-type ATPases reveals bound lipids and the effects of nucleotide binding. *Science* **2011,** *334* (6054), 380-385.

127. Ridenour, W. B.; Kliman, M.; McLean, J. A.; Caprioli, R. M., Structural Characterization of Phospholipids and Peptides Directly from Tissue Sections by MALDI Traveling-Wave Ion Mobility-Mass Spectrometry. *Analytical Chemistry* **2010,** *82* (5), 1881-1889.

128. Sun, J.; Baker, A.; Chen, P., Profiling the indole alkaloids in yohimbe bark with ultra-performance liquid chromatography coupled with ion mobility quadrupole time-of-flight mass spectrometry. *Rapid Commun. Mass Spectrom.* **2011,** *25* (18), 2591-2602.

129. Esquenazi, E.; Daly, M.; Bahrainwala, T.; Gerwick, W. H.; Dorrestein, P. C., Ion mobility mass spectrometry enables the efficient detection and identification of halogenated natural products from cyanobacteria with minimal sample preparation. *Bioorganic & Medicinal Chemistry* **2011,** *19* (22), 6639-6644.

130. Derewacz, D. K.; Goodwin, C. R.; McNees, C. R.; McLean, J. A.; Bachmann, B. O., Antimicrobial drug resistance affects broad changes in metabolomic phenotype in addition to secondary metabolism. *Proceedings of the National Academy of Sciences* **2013,** *110* (6), 2336-2341.

131. Böcker, S.; Letzel, M. C.; Lipták, Z.; Pervukhin, A., SIRIUS: decomposing isotope patterns for metabolite identification. *Bioinformatics* **2009,** *25* (2), 218-224.

CHAPTER 2

CONFORMATIONAL ORDERING OF BIOMOLECULES IN THE GAS PHASE BY

HIGH RESOLUTION DRIFT TUBE ION MOBILITY-MASS SPECTROMETRY

2.1. Introduction

With the rising demand for high-throughput analyses of increasingly complex samples, ion mobility-mass spectrometry (IM-MS) has found broad application in the analysis of biological systems, as this rapid 2D separation (ms and μs, respectively) provides comprehensive molecular information regarding analyte size, mass, and relative abundance. In ion mobility, separation is achieved by low-energy interactions of charged analytes with an inert buffer gas (conventionally helium or nitrogen), where analyte size-to-charge ratio is measured as a function of the time required to traverse the mobility region.[1] As a means of comparison with other laboratory measurements, drift time values are either normalized to standard temperature and pressure as a reduced mobility (K_0) or converted to a collision cross-section (CCS) value, the latter of which is a size parameter related to the averaged momentum transfer impact area of the molecule.[2] Structural information in the form of CCS values assists in the characterization of analytes by biomolecular class, as these classes are known to separate in IM-MS space and adopt conformational correlations due to prevailing class-specific structural folding in the gas-phase.[3, 4] These class-specific mobility-mass correlations can be used as a predictor for molecule class, demonstrating the potential value of IM-MS structural separations for life sciences research which seek systems biology level information. Expanding upon this

concept, CCS-based molecular prediction has previously been explored for peptides, utilizing intrinsic size parameter calculations[5, 6] and machine learning algorithms[7] for sequence prediction, but no detailed study of other biochemical classes has yet been undertaken.

The separation and characterization of biological samples by IM-MS has been achieved using both commercial and laboratory built instrumentation. Virtually all contemporary commercial IM-MS instruments utilize nitrogen as the buffer gas for IM separations, motivated by practical considerations of cost, availability, and technical considerations for pumping requirements and electrical discharge. The most common commercial IM-MS platform utilizes an electrodynamic field (*i.e.*, a traveling wave potential) for mobility separation,[8] and drift time measurements must be calibrated against electrostatic drift tube data in order to convert these measurements to CCS values.[9, 10] Conversely, many independently constructed instruments incorporate uniform electrostatic field mobility regions utilizing helium as the buffer gas. Uniform field measurements serve as the benchmark for electrodynamic CCS value determination, as the CCS obtained from a uniform field drift tube can be determined empirically through kinetic theory.[11-13]

One common practice among researchers utilizing IM-MS is calibration of nitrogen-based traveling wave ion mobility measurements against helium-based CCS values reported in the literature.[13, 14] The use of helium-based CCS values to calibrate nitrogen-based drift time measurements results in calibrated "helium-equivalent" CCS values, which can be useful for comparing with literature values and correlating measurements to theory.[15, 16,19] There is, however, concern that this practice introduces

added experimental error, as nitrogen vs. helium mobility measurements differ substantially in magnitude, and the success of calibration strategies relies heavily on careful selection of calibrants that accurately describe the sample conditions, charge state, mass range and chemical class of the system of interest.[9, 14, 17] Differences in CCS values in helium versus nitrogen arise due to several factors including intrinsic size differences between the buffer gases, mass effects which factor into the momentum transfer cross-section (the experimental CCS), and the over 8 fold difference in gas polarizability between helium and nitrogen (0.21 x 10^{-24} and 1.74 x 10^{-24} cm^3, respectively).[12, 18, 23]

Recently, a prototype IM-MS instrument utilizing nitrogen drift gas was developed (Agilent Technologies, Santa Clara, CA). This instrument incorporates a uniform electrostatic field ion mobility separator bracketed by electrodynamic focusing devices (ion funnels), which allows for high sensitivity and direct measurements of CCS values in nitrogen.[7, 19] Presented in this report is an extensive and diverse database of empirically-derived nitrogen CCS measurements (594 values), which comprises four molecular classes and expands upon several previous databases for the structural characterization of biological molecules.[5, 7, 9, 20-23] This affords the opportunity to explore the fundamental considerations of buffer gas composition and the subsequent effects on ion mobility parameters (reduced mobility and CCS) across different molecular classes.

2.2. Experimental Methods

2.2.1. Preparation of Standards

Lipids. All solvents and buffers were purchased as HPLC grade from Sigma-Aldrich (St. Louis, MO, USA). Dry lipid extracts were purchased from Avanti Lipids

(Birmingham, AL, USA) and constituted in chloroform prior to analysis. Lipid extracts include sphingomyelins (SM, porcine brain), glycosphingolipids (GlcCer, porcine brain), phosphatidylcholines (PC, chicken egg), phosphatidylserines (PS, porcine brain), and phosphatidylethanolamines (PE, chicken egg). For analysis, lipid standards were diluted in 90% chloroform/10% methanol (v/v) with 10 mM sodium acetate to a final concentration of 10 μg/mL. Putative identification of lipids was performed using the exact mass measurement through the Lipid Metabolites and Pathways Strategy (LIPID MAPS) Structural Database (LMSD).[24] A full list of identified lipids can be found in the supporting information.

Carbohydrates. Carbohydrate dextrins (linear and cyclic) and sugar alcohol standards were purchased from Sigma-Aldrich. Lacto-N-difucohexaose I and II and lacto-N-fucopentaose I and II were purchased from Dextra Laboratories (Reading, UK). All carbohydrate standards were prepared as received and reconstituted in water with 10 mM ammonium acetate to final concentrations of 10 μg/mL. For cationization, 10 mM NaCl, 10 mM LiCl, 10 mM CsCl, 10 mM KCl, and 10 mM RbCl solutions were prepared in water to a final concentration of *ca.* 10 μM. A full list of identified carbohydrates can be found in the supporting information.

Peptides. Predigested peptide standards (MassPREP) were purchased from Waters (Milford, MA, USA). Peptide standards (SDGRG and GRGDS) were purchased from Sigma-Aldrich. All peptide standards were received as a lyophilized powder and reconstituted in 10 mM ammonium acetate in water to a final concentration of 10 μg/mL. The MassPREP digestion standard mix contained approximately equimolar concentrations of four tryptically digested proteins: Alcohol Dehydrogenase (ADH,

yeast), Serum Albumin (BSA, bovine), Phosphorylase B (PHOSPH, Rabbit) and Enolase (ENOLASE, yeast). Peptide identifications were assigned based on exact mass of all possible tryptic peptides (no missed cleavages) produced by the Expert Protein Analysis System (ExPASy) PeptideMass proteomics tool[25] (Swiss Institute of Bioinformatics, Lausanne, Switzerland) using the SWISS-PROT database entry number for each intact protein (P00330, P02769, P00924 and P00489, respectively). A full list of identified peptides can be found in the supporting information.

Quaternary Ammonium Salts. Tetraalkylammonium (TAA) salts with alkyl chain lengths between 1 and 18 carbons (TAA1 to TAA18) were purchased from the following sources: TAA2, TAA4, TAA6, TAA7, TAA10, TAA12, and TAA16 from Sigma-Aldrich; TAA1, TAA3, TAA5, and TAA8 from Acros Organics; and TAA18 from Alfa Aesar. All TAA salts were supplied with a stated purity of greater than 98% and were prepared as received. TAA1 to TAA8 were prepared in 50% methanol/50% water, while TAA10, TAA12, TAA16 and TAA18 were prepared in 50% methanol/50% isopropanol. Final concentrations were *ca.* 1 μg/mL. A full list of primary TAA salt standards and concomitant ions identified in the samples can be found in the supporting information.

2.2.2. Instrumentation

A schematic of the instrumentation used to obtain the cross-section measurements is shown in Figure 2.1. The instrument used in this work is a commercial prototype IM-MS which incorporates a drift tube coupled to a quadrupole time-of-flight mass spectrometer (IM-Q-TOFMS, Agilent Technologies, Santa Clara, CA). For this work, an orthogonal electrospray ionization (ESI) source (Agilent Jet Stream) was utilized which

incorporates a heated sheath gas nebulizer to aerodynamically focus and desolvate ions prior to introduction into the vacuum system. Ions from the ESI are introduced to a single-bore glass capillary tube which is resistively coated across its length, allowing the nebulizer to be maintained at ground potential, while the exit end of the capillary can be biased to around 2100 V.[26] Ions exiting the capillary are introduced into a tandem ion funnel interface consisting of a high-pressure transmission ion funnel in the first stage,[27] followed by a second stage trapping ion funnel which incorporates a dual-grid ion gate.[28] The second stage ion funnel trap operates as an ion focusing and accumulation region whereby temporally narrow (typically 100 to 150 μs) ion pulses are gated into the IM spectrometer.

Mobility separation occurs in a 78 cm uniform field drift tube comprised of a series (*ca.* 150) of 50 mm internal diameter gold-plated ring electrodes. The buffer gas is high purity nitrogen. Ions traverse the drift tube under the influence of a weak electric field (10 to 20 V·cm^{-1}) and consequently drift under low-field conditions. The combination of extended drift length, precision electronics, and high drift voltages enables high resolution ion mobility separations in excess of 60 resolving power (t/Δt, observed for a +1 ion, m/z 294). Resolving power values can vary, and do not depend on the class of molecules being investigated. Ions exiting the drift region are refocused axially using an ion funnel and traverse a differential pressure interface region by means of a resistively-coated hexapole ion guide. Following the hexapole, ions are introduced into a modified Q-TOFMS (Agilent 6550), which incorporates a quadrupole mass filter
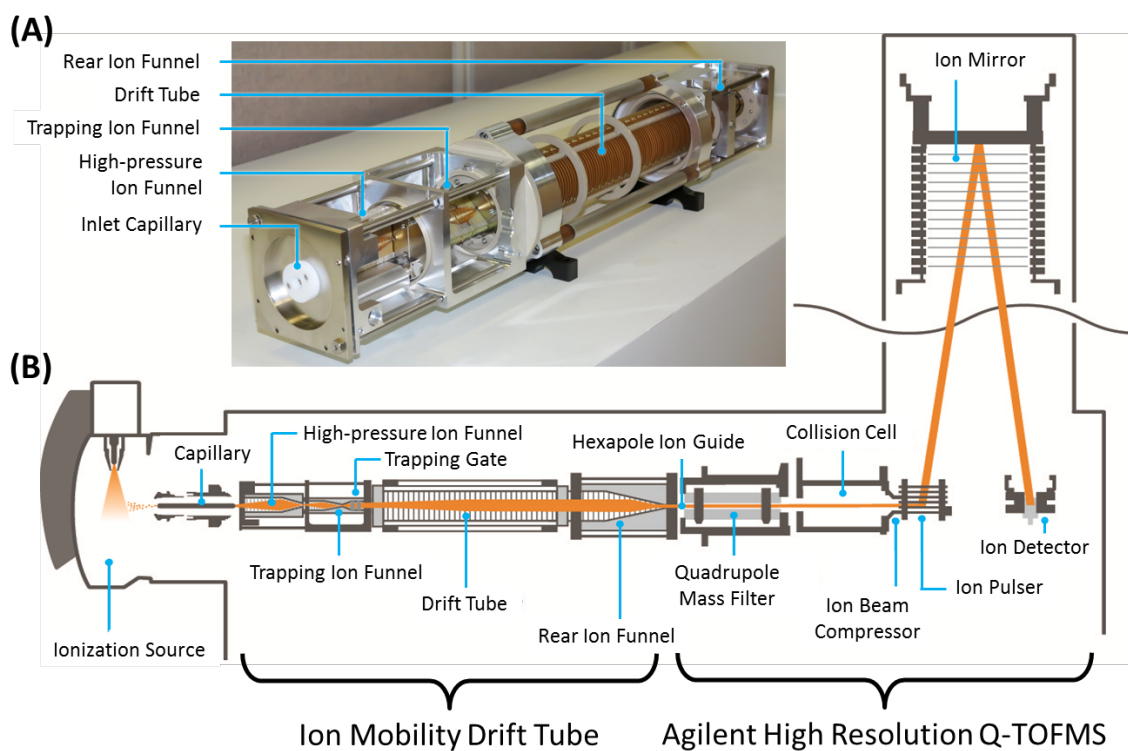
Figure 2.1. Details of the prototype IM-MS instrumentation used in this study. (A) A picture of the ion optical elements of the ion mobility component. (B) A representative schematic of the instrumentation used with significant components annotated.

and collision cell to enable mass-selective ion fragmentation experiments. The TOFMS is capable of greater than 40,000 mass resolving power and can acquire MS spectra at a rate of up to 8.3 kHz (120 μs transients at m/z 1700). Additional instrumentation details are provided in Figure 2.1.

2.2.3. Experimental Parameters

All 2D IM-MS spectra were acquired via direct infusion using positive mode electrospray ionization (Agilent Jet Stream Source) with a flow rate of *ca.* 10 μL/min. The Jet Stream source was operated with a nitrogen sheath gas temperature between 400 and 600 K (solvent dependent) at a flow rate of 12 L/min. Nitrogen drying gas applied at the source entrance was heated to *ca.* 570 K at a flow rate of 10 L/min. The source was operated in positive mode with the following voltages: ground potential emitter, -4.5 kV capillary entrance, and -1.8 kV nozzle. The three ion funnels were operated as follows: high-pressure funnel RF 100 Vpp (peak-to-peak) at 1.5MHz, 150 V DC; trapping funnel RF 100 Vpp at 1.2 MHz, 180 V DC; rear funnel RF 100 Vpp at 1.2 MHz, 200 V DC. The IM drift gas pressure (nitrogen) was maintained at *ca.* 4 Torr and *ca.* 300 K, while the drift potential varied from 750 V to 1450 V, which represents an E/N ratio of 7 to 15 Td. In this E/N range, the mobility operates under low field conditions as all analytes investigated exhibited a linear change in drift times with respect to the electric field. Data was acquired with a modified version of the MassHunter software (Agilent Technologies). The mass measurement was calibrated externally using a series of homogeneously-substituted fluorinated triazatriphosphorines (Agilent tuning mixture, *ca.* 100 to 3000 m/z), which are characterized as being amphoteric and nonreactive.

Additionally, a mixture of tetraalkylammonium salts (TAA3 to TAA18) was added to all samples as an internal mass and mobility calibration standard for positive mode analysis.

2.2.4. Collision Cross-Section Calculations

Uncorrected drift times are extracted as centroid values using a beta version of the IM-MS Browser (Agilent Technologies). This uncorrected drift time represents the total transit time of the ions, including the mobility drift time and the flight time through the interfacing IM-MS ion optics and MS. Because the non-mobility flight time component (the transit time of ions outside the drift region) is independent of the drift voltage, this value can be determined from a plot of the measured drift time versus the inverse drift voltage,[23, 29] where a linear fit to the data will indicate the non-mobility time component (y-intercept) in the limit of infinite electric field (1/V of zero). Time measurements are obtained from a minimum of six different drift voltages, ranging from 750 V to 1450 V. The determined non-mobility time is subtracted from the uncorrected drift times in order to obtain the corrected ion mobility drift time. Corrected drift times are used to determine the gas-phase momentum transfer collision cross-section (CCS) using the Mason-Schamp relationship,[30] incorporating the scaling terms for standard temperature and pressure. Based on a propagation-of-error analysis incorporating the limits of precision for individual experimental parameters, we estimate the accuracy of all CCS values to be better than 2% (see supporting information).

Table 2.1. A summary of statistics related to the CCS database.

| | **Collision Cross-Section Statistics** | | | | | | **Fits to Empirical Data** | | |
	Number of CCS Values	Mass Range [Da]	CCS Range [Å^2]	Average CCS Pre-cision[1]	Average N for Each Value	Fit Equation Coefficients ($y = Ax^B$)	Coefficient of Determination[2]	Amount of Data Included Within ±5% of Fit[3]
Peptides	92	430 –1760	200 –450	0.2% (±0.1%)	7 (±2)	A= 6.8440 B= 0.5547	R^2= 0.975	91%
Carbohydrates	125	190 –2150	140 –410	0.3% (±0.1%)	12 (±3)	A= 11.553 B= 0.4656	R^2= 0.983	89%
Lipids	314	500 –1600	220 –460	0.2% (±0.1%)	10 (±2)	A= 5.2469 B= 0.6000	R^2= 0.949	96%
Tetraalkyl-ammonium Salts	63	130 –1030	140 –400	0.4% (±0.1%)	18 (±8)	A= 8.2631 B= 0.5561	R^2= 0.991	98%

1. The precision reported here represents the reproducibility across replicate measurements. The total precision due to propagation of uncertainty in experimental parameters is estimated to be less than 2%.
2. The observed R^2 value for the nonlinear power fit.
3. The data inclusion band chosen is based on the smallest sized band, which incorporates the most amount of data (refer to Figure 2.1 B, inset).

2.3. Results and Discussion

2.3.1. Database Description and General Cross-Section Trends in Nitrogen

A total of 594 nitrogen collision cross-section values were measured empirically in this study, representing three biomolecular classes (lipids, carbohydrates, and peptides), and TAA salts. This includes 92 peptides, 125 carbohydrates, 314 lipids, and 63 TAA salts and TAA salt derivatives. All CCS values were measured in positive ion mode and all represent singly-charged analytes, of which 63 are molecular ions, 111 are protonated species, 273 are sodiated, 124 are potassiated, and the remaining representing other cations (lithium, rubidium, and cesium). The range of CCS values measured spans from 140-460 $Å^2$, covering a mass range of 130-2150 Da. Summary statistics regarding the CCS database are provided in Table 2.1. The average RSD of all database values was 0.3% (±0.1%), with each CCS value representing an average of 11 (±4) measurements. A complete list of all analytes and respective CCS measurements is provided as supplemental material.

TAA salts ranging from tetrapropylammonium (TAA3) to tetraoctadecylammonium (TAA18) were analyzed and a subset of these measured CCS values were compared with literature values in order to estimate the CCS measurement accuracy.[16] Results of this comparison are summarized in Table 2.2. Where CCS literature values existed for nitrogen, the absolute differences were found to be less than 1% and, in most cases, less than 0.5% deviation was observed. All TAA salts investigated exhibited excellent CCS measurement reproducibility (less than 0.5% RSD).

A scatter plot of CCS versus *m/z* for all database values is presented in Figure 2.1A, separated into chemical classes. We refer to this type of 2D IM-MS projection as

Table 2.2. Measured CCS values for the TAA salts compared with literature values.

Name		Exact Mass [Da]	CCS (This Work)[1] [Å²]	CCS (Literature)[2] [Å²]	Abs. Percent Difference[3] [%]
Tetramethylammonium	TAA1	74.14	-	107.40	-
Tetraethylammonium	TAA2	130.25	-	122.20	-
Tetrapropylammonium	TAA3	186.36	144.1 ± 0.7 (23)	143.80	0.22%
Tetrabutylammonium	TAA4	242.46	166.6 ± 0.9 (16)	166.00	0.36%
Tetrapentylammonium	TAA5	298.57	190.1 ± 1.0 (28)	190.10	0.02%
Tetrahexylammonium	TAA6	354.68	213.5 ± 1.0 (31)	214.00	0.23%
Tetraheptylammonium	TAA7	410.78	236.4 ± 0.4 (31)	236.80	0.17%
Tetraoctylammonium	TAA8	466.54	256.6 ± 0.7 (31)	258.30	0.64%
Tetradecylammonium	TAA10	579.11	293.5 ± 0.7 (24)	-	-
Tetradodecylammonium	TAA12	691.32	319.0 ± 0.9 (24)	-	-
Tetrahexadecylammonium	TAA16	915.04	361.5 ± 0.9 (24)	-	-
Tetraoctadecylammonium	TAA18	1027.16	379.0 ± 1.7 (21)	-	-

1. Number of measurements are reported in parenthesis. The error due to experimental uncertainty is reported next to each value and is less than 0.5% for all measurements. The total error based on propagating the limits of precision in experimental parameters is estimated to be less than 2%.
2. Literature values from: Campuzano *et al.* Analytical Chemistry **2011**, *84*, 1026-1033.
3. The absolute percent difference is the difference in CCS compared to the average of both values.

conformational space analysis,[4, 31] as the differential scaling of mass (m/z) and size (CCS) between molecular classes is indicative of differences in gas-phase packing efficiency.[20]

2.3.2. Description of the Fits to the Empirical Data

Several different equation functional forms were evaluated in order to determine which expression best described molecular class correlations between CCS and m/z values, and, it was found that the datasets were adequately described by a power-law relationship ($y=Ax^B$), based upon the coefficient of determination (R^2). Conceptually, power-law equations are descriptors for several phenomena related to mass-size scaling, including allometric scaling laws in biology,[32] stellar velocity dispersion relative to black hole mass (M-sigma relation),[33] and the well-known square-cube law, first described by Galileo,[34] which universally relates any shape's increase in volume relative to its surface area. Additionally, power-law relationships are scale-invariant such that different power-law functions can be related by a simple scaling factor, which has implications for describing universal relationships independent of the specific details of the measurement.

The resulting power-law fits to the empirical data are presented in Figure 2.2B. Coefficients and associated R^2 values are summarized in Table 2.1. The data inclusion bands projected in Figure 2.2B representing ±5% deviation from the line of best fit. Other inclusion band sizes are summarized in Figure 2.2B, inset, averaged across the four datasets. For all datasets, a ±5% inclusion band incorporated an average of 94% (±4%) of data. Decreasing the band to ±4% results in an average of 86% (±3%) of data being included (a decrease of *ca.* 8% data inclusion), whereas increasing the band to ±6% only incorporated an additional 3% (±2%) of data on average. Thus, the ±5% data inclusion

band represents an optimal balance between specificity and data incorporation. Interestingly, the ±5% band describes all datasets similarly, regardless of chemical class. Several observations can be made from the data contained in Figure 2.2. The TAA salts were found to exhibit the highest CCS values relative to m/z, and were located in a region of 2D IM-MS space, which was disparate from the biomolecules. Previously, TAA salts were recommended as an ion mobility calibrant due to their low propensity for forming clusters, which otherwise complicates the interpretation of mobility data.[35] Here, it is found that in addition to the lack of clustering, the TAA salts are useful mobility-mass calibrants as the complete series (1 to 18 carbons) span a wide range of CCS values (107 to 400 Å^2), m/z values (75 to 1027 Da), and occupy a region of 2D IM-MS space where biomolecules are not predicted to occur. Carbohydrates were observed to have the lowest CCS values relative to their mass, while peptides and lipids occupy similar regions of conformational space. In general, all of the biochemical classes surveyed were readily separated above a mass of *ca.* 1200 Da, indicating that differences in relative gas-phase packing scale with molecular size and mass.

2.3.3. *Extraction of Sub-Trend Information from the Data*

From a cursory analysis of the CCS database described in this report, it is evident that the general chemical class information is retained through the specific mobility-mass correlation trends in the 2D IM-MS projection. While class separations are unambiguous at the higher m/z values (beyond *ca.* 1200), class-specific trend information is still largely retained within the regions of overlap. For example, within the intermediate region where the majority of signals occur (m/z 700 to 1000), the class-specific mobility-mass
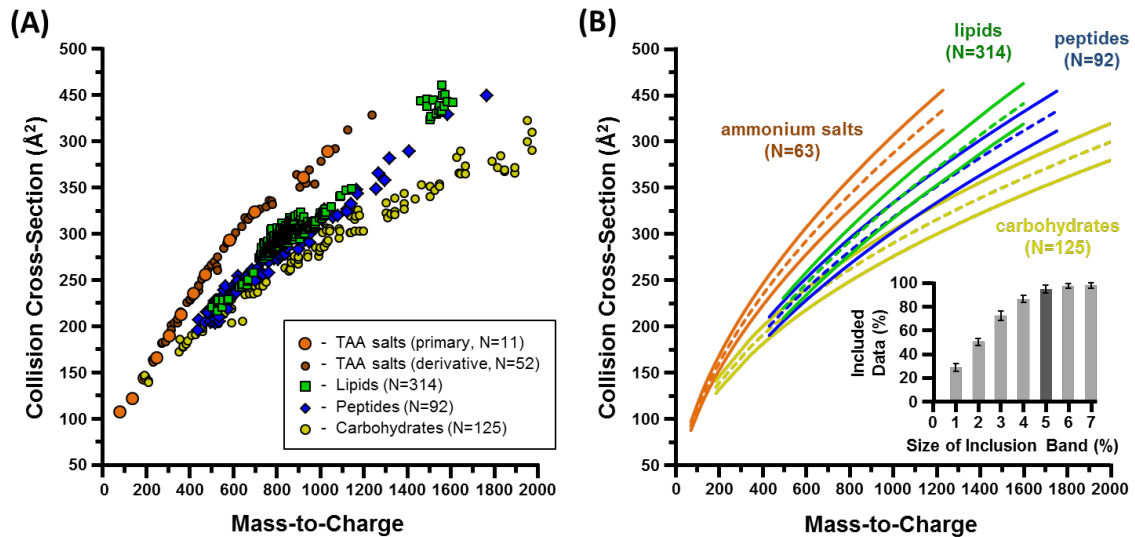
Figure 2.2. (A) A scatter plot of the CCS values measured in this study, separated by chemical class. (B) Best fit lines of the data, separated into class and fit to a power-law function. Also shown are data inclusion bands representing ±5% deviation from the best fit line. The inset bar graph represents the amount of data included within different sized inclusion bands. Fit equations and their corresponding coefficients of determination (R^2) can be found in Table 2.1.

correlations partition into distinct bands which can be subjected to a probability distribution analysis for molecular class information (see, for example, Figure B2). The molecular information derived from such trends hold promise for conducting comprehensive omics experiments whereby unknown analytes originating from a complex sample (*e.g.*, blood, tissue, whole cell lysate) can be prioritized based upon their likely chemical class. This biomolecular filtering would allow for the sorting of unknown analytes into distinct identification workflows, as lipid, peptide, metabolite, and glycan identification methods often warrant searching of specific databases. In order to determine the detail of class-specific information obtained from the conformational space analysis, select coarse biomolecular classes were further categorized into finer specific sub-classes. Figure 2.3. contains a detailed analysis of carbohydrates, which were further delineated into glycans (human milk oligosaccharides), cyclic dextrins (cyclodextrins), and linear dextrins (maltose polysaccharides). Figure 2.3. A and B illustrates the relative location of each carbohydrate sub-class in conformational space, while Figure 2.3. C describes the data as a histogram relative to the best fit line.

In general, there is no strong correlation between the carbohydrate sub-classes, with all signals distributed in relatively the same locations with respect to the power-law fit. This suggests that the carbohydrates surveyed do not adopt strong structural differences, which can be easily differentiated in the 2D analysis. On the other hand, the sub-classes chosen here represent broad descriptors for carbohydrate structure, and as such are not structurally-descriptive sub-classifications. For example, glycans can represent both linear and branched oligosaccharides and thus occupy a broad region of the total carbohydrate conformational trend. Interestingly, the cyclization of sugars

63
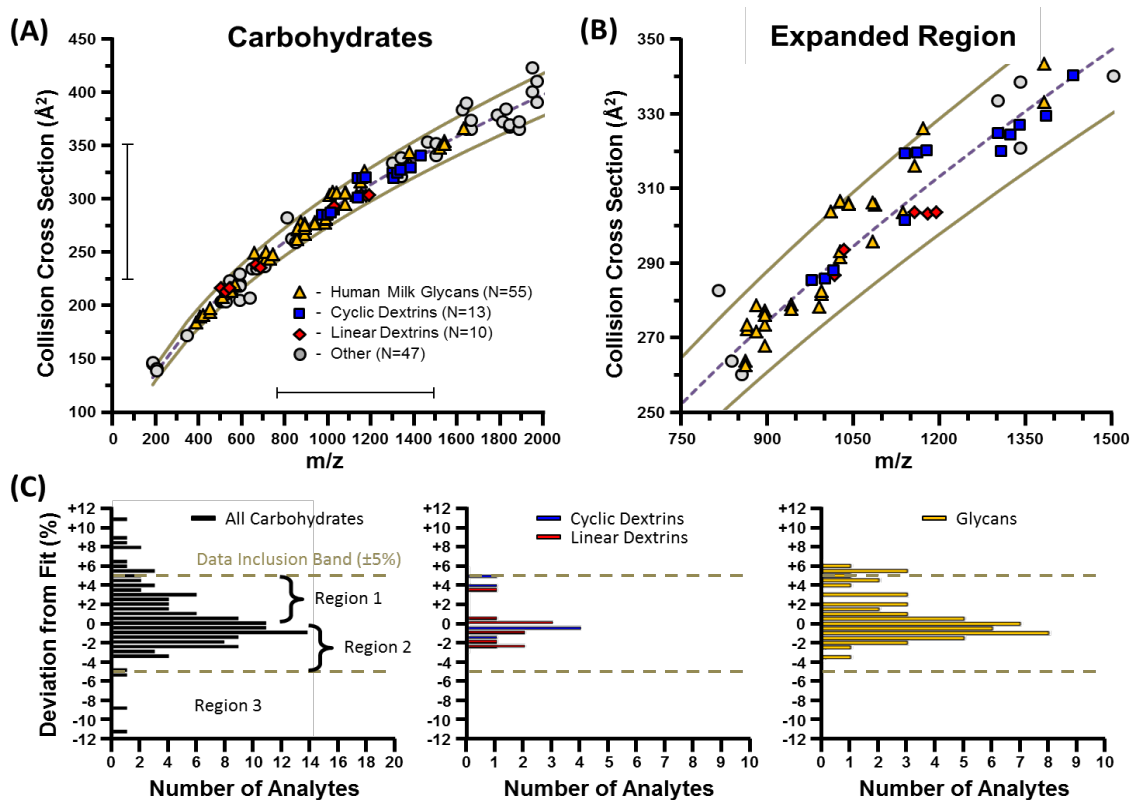
Figure 2.3. A sub-class analysis of carbohydrates, with sub-classes comprised of human milk derived glycans, cyclic, and linear dextrins. (A) A scatter plot of the relative location of carbohydrate sub-classes in 2D IM-MS conformational space. (B) An expanded region of the scatter plot where all three sub-classes of carbohydrates are observed. (C) A histogram analysis of carbohydrate sub-class deviation in 2D IM-MS space relative to the best fit line. In general, the carbohydrate sub-classes do not differentiate into distinct regions of conformational space.

(cyclodextrins) does not seem to enhance gas-phase packing efficiency as compared with their linear analogues. A more comprehensive carbohydrate dataset may engender sub-class differentiation, or differences may bear out for more limited situations such as positional and structural isomers or various metal-coordinated species.[36] It should also be noted that the data projected in Figure 2.2. includes various alkali cationized species. While previous work has indicated that carbohydrate gas-phase ion structure is strongly influenced by the cation,[37] it is difficult to draw any definitive cation-specific effects in this work due to the structurally-diverse nature of the analytes (the cation-specific carbohydrate analysis is provided in Appendix B, Figure B.1.).

Application of a similar sub-class analysis to the lipid dataset is illustrated in Figure 2.4. In this case, the lipid dataset is substantially larger than the carbohydrate dataset (N=314 *vs.* N=125, respectively), and measurements were obtained from five distinct lipid structural classes. These lipid sub-classes can be broadly categorized into two structural classes as sphingolipids (SM, GlcCer) and glycerophospholipids (PE, PC, PS). It is qualitatively evident in Figure 2.4. A and B that each class of lipid exists in a distinct region of conformational space. The histogram distribution analysis in Figure 2.4. C (right panel) indicates that sphingolipids fall predominantly above the best fit line (97% in region 1), whereas glycerophospholipids (Figure 2.4. C, middle panel) are more broadly dispersed around the mobility-mass correlation (33% in region 1, 65% in region 2), and adopt denser gas phase conformations than sphingolipids. These results suggest that, with proper structural sub-class descriptors, conformational space analysis is capable of differentiating finer structural detail beyond general biomolecular class.
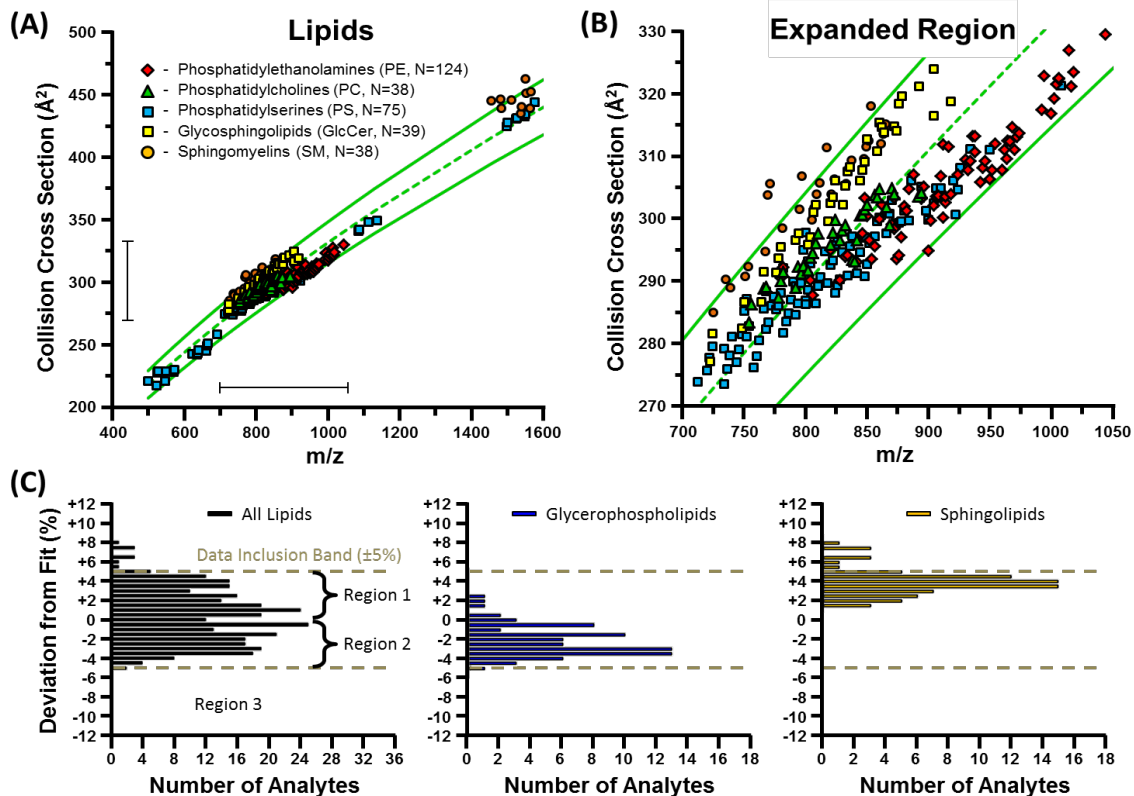
Figure 2.4. A sub-class analysis of lipids comprised of PE, PC, PS, GlcCer, and SM lipids. These lipids are further categorized into two general structural groups: glycerophospholipids (PE, PC, PS) and sphingolipids (GlcCer, SM). (A) A scatter plot of the conformational ordering of each sub-class of lipid. (B) An expanded region of the scatter plot detailing a preferentially ordering of the different lipid sub-classes in conformational space. (C) A histogram analysis and locations of general lipid structural groups relative to the best fit line. Unlike carbohydrates, individual lipid sub-classes partition into distinct regions of 2D IM-MS space, allowing for finer structural information to be extracted from the conformational space analysis.

2.3.4. Comparisons between Helium and Nitrogen CCS Values

The diverse compilation of CCS values described in this report allows for direct comparisons against helium-derived CCS values reported in the literature. Of the over 3000 singly-charged helium CCS values surveyed from the literature, overlapping measurements exist for 119 nitrogen CCS values in the current database (8 TAA salts, 49 lipids, 38 peptides, and 24 carbohydrates; refer to supporting information). Differences between helium and nitrogen-derived CCS measurements have been previously noted for atomic species,[38] small molecules and peptides,[39] and, more recently, proteins and large protein complexes.[9, 23] Here, we add the differences observed for TAA salts, lipids, and carbohydrates, in addition to corroborating previous peptide observations.

A scatter plot of the overlapping helium and nitrogen CCS values is provided in Figure 2.5. A. Vertical error bars representing ±2% are also included, although this error is sufficiently small such that most of the error bars are obscured within the scale of individual data points. Figure 2.5. B contains the power fits to the data, which are useful in visualizing differences between datasets. In general, gross separation trends between chemical classes are retained within the helium and nitrogen-based datasets, with qualitatively similar conformational space ordering being exhibited regardless of the drift gas (*i.e.* carbohydrate density > peptide density > lipid density > TAA salt density). Figure 2.5. C contains the same overlap data as projected on a plot of nitrogen versus helium CCS values. In Figure 2.5. C, all of the class-specific data reside within the same region of the projection, indicating that overall differences between helium and nitrogen CCS are systematic within this range, and thus can be accounted for to allow conversion of one dataset to another, with some loss in precision associated with error propagation.
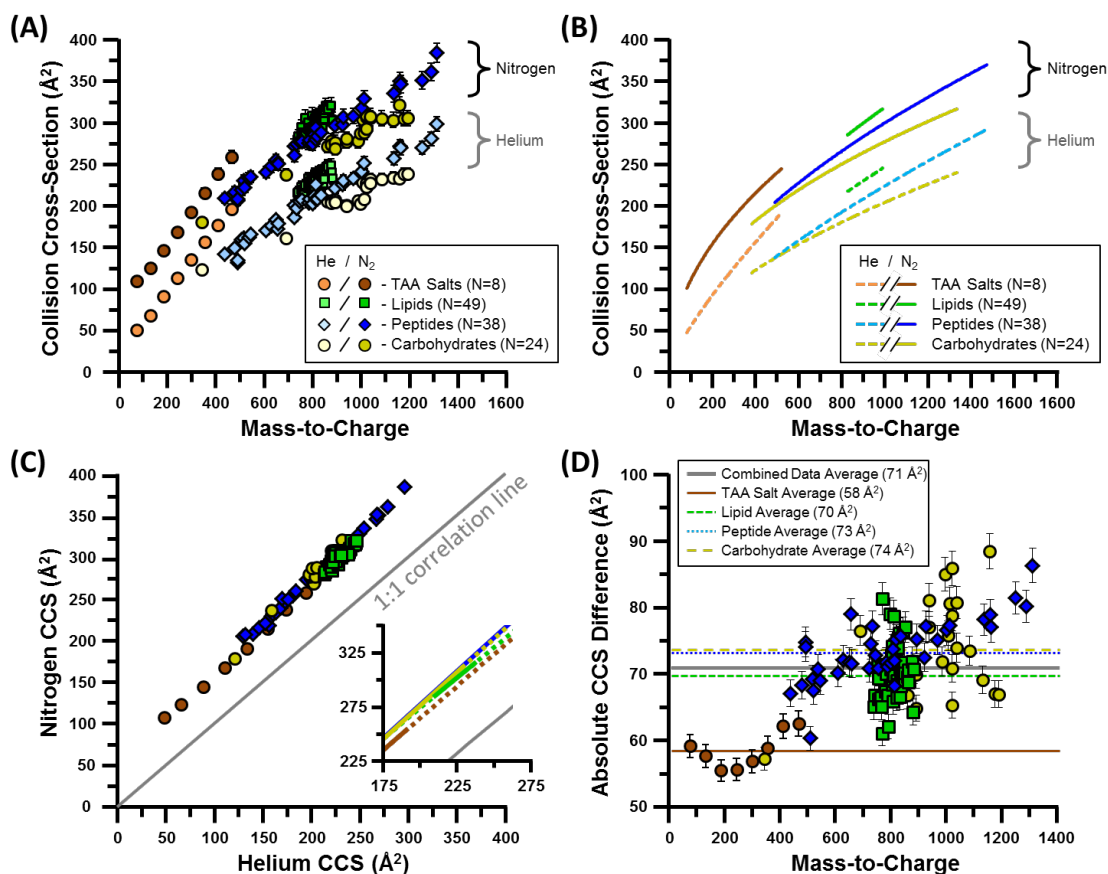
Figure 2.5. Comparisons between helium and nitrogen-derived CCS values. (A) A scatter plot of class-specific subsets of CCS data measured in both helium and nitrogen. (B) Power fits to the data projected in panel A. (C) Correlation plot of helium vs. nitrogen CCS values. (D) Absolute differences in CCS between helium and nitrogen measurements, plotted as a function of mass-to-charge. In general, nitrogen CCS values are significantly larger than helium, with subtle differences being observed between different chemical classes.

68

This possibility of generating effective helium-based CCS values from nitrogen measurements was previously noted by Bush *et al.* for peptides and proteins.[9, 11, 22] Recently, Pagel and Harvey noted good correlation (less than 1.5% error) between helium and nitrogen CCS measurements for singly-charged carbohydrates, though significant error was introduced when multiply-charged values were incorporated into the calibration.[17] Here we confirm a strong correlation between singly-charged helium and nitrogen CCS values for lipids, peptides, carbohydrates and TAA salts. It should be cautioned, however, that the relationship between helium and nitrogen-based CCS values are both charge-state and mass-dependent,[40] and it is expected that any correlation between the two measurements would deviate at the extremes of low and high mass. In fact, Bush *et al.* previously noted that cross-calibration error from nitrogen to helium CCS is higher at lower masses (up to 15% error) where the magnitude of the CCS value is small, while at higher masses, the error can be reduced to as low as 2.2% for predicting helium CCS from nitrogen measurements.[9]

It was also noted in this study and elsewhere that calibration across different chemical classes (*e.g.*, using literature peptide values to calibrate lipids[14]) introduces additional and significant error (*ca.* 7%), further underscoring the importance of compiling a chemically diverse set of empirical drift tube CCS values. Figure 2.5. C, inset contains the linear best fits to the data, with the axes rescaled to a region where data exists for all four chemical classes. Linear fits are extrapolated (dotted lines) for visualization purposes. Here, the small but notable differences between chemical classes can be observed as offset correlation lines, which corroborate with the absolute CCS differences between helium and nitrogen noted previously for each chemical class.

Specifically, peptides, carbohydrates, and lipids fall along a similar helium-nitrogen CCS correlation trend, while the TAA salts exhibit a slightly lower correlation. Interestingly, all class correlations exhibit similar slopes (*ca.* 1), suggesting that the factors which give rise to the cross-sectional differences between helium and nitrogen (buffer gas size, mass and polarizability) affect different chemical classes in a similar manner across a broad range of both size and mass.

Absolute CCS differences between the helium and nitrogen datasets are plotted as a function of mass in Figure 2.5D, with error bars representing ±2% CCS uncertainty. Average absolute CCS differences are projected as a horizontal line through each class distribution, with the following values: TAA salts, 58 (±3) Å^2; lipids, 70 (±4) Å^2; carbohydrates, 74 (±8) Å^2; and peptides, 73 (±5) Å^2. Cross-sectional differences are lowest for the TAA salts, while lipids, carbohydrates and peptides differ by approximately the same amount. Overall, there is a small but notable increase in the helium-nitrogen CCS difference with increasing mass for all classes except lipids where a limited mass range is surveyed. This suggests that the nitrogen and helium CCS are not increasing at the same rate relative to the mass of the analyte, with the greater CCS increase occurring in nitrogen. Wyttenbach *et al.* recently noted that ion systems up to *ca.* 760 Da (sodiated PEG_{17}) still exhibit strong contributions from the ion-neutral interaction potential in their measured CCS.[41] From their atomic superposition argument, it would be expected that with nitrogen buffer gas, the combined effect of each atomic potential for large polyatomic systems would give rise to a steeper increase in CCS than with helium buffer gas, since the atom-nitrogen interaction potential is stronger than the atom-helium interaction potential. In other words, the stronger interaction potential of nitrogen would

be expected to scale with the number of atoms in the ionic system being measured, at least to a first approximation. Ion systems with different heteroatom compositions (*e.g.*, lipids *vs.* peptides) would also be expected to exhibit different scaling of mass to CCS between helium and nitrogen; this effect cannot be definitively observed in the relatively narrow mass range surveyed in this work, though cursory effects of gas polarization seem to be present in the enhanced high-mass separation of lipids and peptides in nitrogen vs. helium. A discussion of the polarization effects specific to carbohydrates and applications to alternate instrument platforms is reported in Appendix B. Such class-specific CCS differences may bear out as more overlapping measurements are obtained in future studies.

2.4. Conclusions

The large database of nitrogen-derived CCS values presented here offers a glimpse at the intrinsic intermolecular packing forces of four chemically-different molecular classes across a relatively wide range of both size (*ca.* 150 to 450 Å^2) and mass (*ca.* 150 to 2200 Da). Four molecular classes were investigated in this study, with relative gas-phase densities observed as follows, from least to most efficient packing: TAA salts, lipids, peptides and carbohydrates. The biopolymers (carbohydrates and peptides) demonstrated the highest efficiency for gas-phase packing, and among these, carbohydrates tend to adopt the most compact gas-phase CCS values. This observation is somewhat intuitive in that carbohydrates have considerable degrees of freedom and can adopt both linear and branched primary structures. In contrast, lipids exhibit the largest CCS values among the biomolecules investigated, and this observation appears to be intrinsic to the inability of lipids for forming compact, self-solvated structures in the gas-

phase. Noteworthy among these findings is that despite the significant differences between helium and nitrogen in terms of mass, degrees-of-freedom (atomic *vs.* diatomic) and polarization, the biomolecular class trends observed here for the nitrogen-based ion mobility are qualitatively the same as those previously observed in helium.[3, 20] We do observe evidence that these qualitative trends between the two drift gases are not retained at low mass, and a more detailed investigation of helium and nitrogen-based ion mobility studies for low mass analytes (less than 200 Da) will be the subject of future studies.

We emphasize that these studies are only possible by the remarkable advances made over the past decade in the development of biological IM-MS instrumentation. The IM-MS described in this report can achieve high resolving powers with high sensitivity, making it possible to observe and characterize low abundance isomeric species in highly complex samples with unprecedented scale and throughput. While we have purposely chosen to report only the highest abundant species, we note that the observation of multiple ion mobility peak features *(i.e.,* mass isomers) is routine with this instrumentation. As the analytical capabilities of distinguishing low-abundance isomeric species become widely accessible, we begin to move towards a new paradigm whereby it no longer becomes the question of if a particular isomer exists, but rather how much if it is present and in what context.

2.5. Associated Content

A brief description of drift gas considerations for carbohydrates and applications for alternative instrumentation are reported (Figure B.1., B.2., B.3., and Table B.1.). Empirically measured transport properties for the analytes evaluated in this work (Tables

B2, B3, B4, & B5). A summary of the overlapping helium and nitrogen CCS measurements compared in this study (Table B6). This material is available in Appendix B.

2.6. Acknowledgements

2.7. References

1. McDaniel, E. W., Collision phenomena in ionized gases. Wiley: New York, **1964**; Vol. 1.

2. McDaniel, E. W.; Mason, E. A., Mobility and diffusion of ions in gases. John Wiley and Sons, Inc., New York: **1973**.

3. Fenn, L.; McLean, J., Biomolecular structural separations by ion mobility-mass spectrometry. Analytical and Bioanalytical Chemistry **2008**, 391 (3), 905-909.

4. McLean, J. A., The Mass-Mobility Correlation Redux: The Conformational Landscape of Anhydrous Biomolecules. Journal of the American Society for Mass Spectrometry **2009**, 20 (10), 1775-1781.

5. Valentine, S. J.; Counterman, A. E.; Clemmer, D. E., A database of 660 peptide ion cross sections: Use of intrinsic size parameters for bona fide predictions of cross sections. Journal of the American Society for Mass Spectrometry 1999, 10 (11), 1188-1211.; Valentine, S. J.; Counterman, A. E.; Hoaglund-Hyzer, C. S.; Clemmer, D. E., Intrinsic Amino Acid Size Parameters from a Series of 113 Lysine-Terminated Tryptic Digest Peptide Ions. Journal of Physical Chemistry B. **1999**, 103 (8), 1203-1207.

6. Shvartsburg, A. A.; Siu, K. W. M.; Clemmer, D. E., Prediction of peptide ion mobilities via a priori calculations from intrinsic size parameters of amino acid residues. *Journal of the American Society for Mass Spectrometry* **2001**, 12 (8), 885-888.

7. Shah, A. R.; Agarwal, K.; Baker, E. S.; Singhal, M.; Mayampurath, A. M.; Ibrahim, Y. M.; Kangas, L. J.; Monroe, M. E.; Zhao, R.; Belov, M. E.; Anderson, G. A.; Smith, R. D., Machine learning based prediction for peptide drift times in ion mobility spectrometry. *Bioinformatics* **2010**, 26 (13), 1601-1607.

8. Giles, K.; Pringle, S. D.; Worthington, K. R.; Little, D.; Wildgoose, J. L.; Bateman, R. H., Applications of a travelling wave-based radio-frequency-only stacked ring ion guide.. *Rapid Communications in Mass Spectrometry* **2004**, 18 (20), 2401-2414; Pringle, S. D.; Giles, K.; Wildgoose, J. L.; Williams, J. P.; Slade, S. E.; Thalassinos, K.; Bateman, R. H.; Bowers, M. T.; Scrivens, J. H., An investigation of the mobility separation of some peptide and protein ions using a new hybrid quadrupole/travelling wave IMS/oa-ToF instrument. *International Journal of Mass Spectrometry* **2007**, 261 (1), 1-12.

9. Bush, M. F.; Hall, Z.; Giles, K.; Hoyes, J.; Robinson, C. V.; Ruotolo, B. T., Collision cross sections of proteins and their complexes: a calibration framework and database for gas-phase structural biology. *Analytical Chemistry* **2010**, 82 (22), 9557-9565.

10. Williams, J. P.; Grabenauer, M.; Holland, R. J.; Carpenter, C. J.; Wormald, M. R.; Giles, K.; Harvey, D. J.; Bateman, R. H.; Scrivens, J. H.; Bowers, M. T., Characterization of simple isomeric oligosaccharides and the rapid separation of glycan mixtures by ion mobility mass spectrometry. *International Journal of Mass Spectrometry* **2010,** *298* (1-3), 119-127.

11. Revercomb, H. E.; Mason, E. A., Theory of plasma chromatography/gaseous electrophoresis. *Analytical Chemistry* **1975**, 47 (7), 970-983.

12. Mason, E. A.; McDaniel, E. W., Transport Properties of Ions in Gases. John Wiley & Sons: New York, **1988**; p 560.

13. Ruotolo, B. T.; Giles, K.; Campuzano, I.; Sandercock, A. M.; Bateman, R. H.; Robinson, C. V., Evidence for macromolecular protein rings in the absence of bulk water. *Science* **2005**, 310 (5754), 1658-1661; Ruotolo, B. T.; Benesch, J. L. P.; Sandercock, A. M.; Hyung, S.-J.; Robinson, C. V., Ion mobility-mass spectrometry analysis of large protein complexes. *Nature Protocols* **2008**, 3 (7), 1139-1152; Knapman, T. W.; Berryman, J. T.; Campuzano, I.; Harris, S. A.; Ashcroft, A. E., Considerations in experimental and theoretical collision cross-section measurements of small molecules using travelling wave ion mobility spectrometry-mass spectrometry. *International Journal of Mass Spectrometry.* **2010**, 298 (1–3), 17-23.

14. Ridenour, W. B.; Kliman, M.; McLean, J. A.; Caprioli, R. M., Structural Characterization of Phospholipids and Peptides Directly from Tissue Sections by MALDI Traveling-Wave Ion Mobility-Mass Spectrometry. *Analytical Chemistry* **2010,** *82* (5), 1881-1889.

15. Shvartsburg, A. A.; Mashkevich, S. V.; Siu, K. W. M., Incorporation of thermal rotation of drifting ions into mobility calculations: drastic effects for heavier buffer gases. The *Journal of Physical Chemistry A.* **2000**, 104 (42), 9448-9453; Shvartsburg, A. A.; Hudgins, R. R.; Dugourd, P.; Jarrold, M. F., Structural information from ion mobility measurements: applications to semiconductor clusters *Chemical Society Reviews* **2001**, 30 (1), 26-35; Larriba, C.; Hogan, C. J., J Ion Mobilities in Diatomic Gases: Measurement versus Prediction with Non-Specular Scattering Models The Journal of *Physical Chemistry A* **2013**, 117 (19), 3887-3901.

16. Campuzano, I.; Bush, M. F.; Robinson, C. V.; Beaumont, C.; Richardson, K.; Kim, H.; Kim, H. I., Structural characterization of drug-like compounds by ion mobility mass spectrometry: comparison of theoretical and experimentally derived nitrogen collision cross sections. *Analytical chemistry* **2011,** *84* (2), 1026-1033.

17. Ion Mobility–Mass Spectrometry of Complex Carbohydrates: Collision Cross Sections of Sodiated N-linked Glycans, *Analytical Chemistry.* **2013**, *85* (10), 5138-5145.

18. Haynes, W. M.; Lide, D. R.; Bruno, T. J., CRC Handbook of Chemistry and Physics 2012-2013. 93 ed.; CRC press: 2012.

19. Baker, E. S.; Clowers, B. H.; Li, F.; Tang, K.; Tolmachev, A. V.; Prior, D. C.; Belov, M. E.; Smith, R. D., Ion mobility spectrometry-mass spectrometry performance using electrodynamic ion funnels and elevated drift gas pressures. *Journal of the American Society for Mass Spectrometry* **2007**, 18 (7), 1176-1187.

20. Fenn, L. S.; Kliman, M.; Mahsut, A.; Zhao, S. R.; McLean, J. A., Characterizing ion mobility-mass spectrometry conformation space for the analysis of complex biological samples. *Analytical Bioanalytical Chemistry* **2009,** *394* (1), 235-244.

21. Tao, L.; McLean, J. R.; McLean, J. A.; Russell, D. H., A collision cross-section database of singly-charged peptide ions. *Journal of the American Society for Mass Spectrometry* **2007,** *18* (7), 1232-1238.

22. Bush, M. F.; Campuzano, I. D. G.; Robinson, C. V., Ion mobility mass spectrometry of peptide ions: effects of drift gas and calibration strategies. *Analytical Chemistry* **2012**, 84 (16), 7124-7130.

23. Salbo, R.; Bush, M. F.; Naver, H.; Campuzano, I.; Robinson, C. V.; Pettersson, I.; Jørgensen, T. J. D.; Haselmann, K. F., Traveling-wave ion mobility mass spectrometry of protein complexes: accurate calibrated collision cross-sections of human insulin oligomers. *Rapid Communications in Mass Spectrometry* **2012**, 26 (10), 1181-1193.

24. Sud, M.; Fahy, E.; Cotter, D.; Brown, A.; Dennis, E. A.; Glass, C. K.; Merrill, A. H.; Murphy, R. C.; Raetz, C. R. H.; Russell, D. W.; Subramaniam, S., LMSD: LIPID MAPS structure database. *Nucleic Acids Research* **2007**, 35 (suppl 1), D527-D532.

25. Wilkins, M. R.; Lindskog, I.; Gasteiger, E.; Bairoch, A.; Sanchez, J.-C.; Hochstrasser, D. F.; Appel, R. D., Detailed peptide characterization using PEPTIDEMASS--a World-Wide-Web-accessible tool. *Electrophoresis* **1997,** 18 (3-4), 403-408.

26. Fenn, J. B.; Mann, M.; Meng, C. K.; Wong, S. F.; Whitehouse, C. M., Electrospray ionization for mass-spectrometry of large biomolecules. *Science* **1989,** *246* (4926), 64-71.

27. Ibrahim, Y.; Tang, K.; Tolmachev, A. V.; Shvartsburg, A. A.; Smith, R. D., Improving mass spectrometer sensitivity using a high-pressure electrodynamic ion funnel interface. *Journal of the American Society of Mass Spectrometry.* **2006**, 17 (9), 1299-1305.

28. Ibrahim, Y.; Belov, M. E.; Tolmachev, A. V.; Prior, D. C.; Smith, R. D., Ion funnel trap interface for orthogonal time-of-flight mass spectrometry. *Analytical Chemistry* **2007**, 79 (20), 7845-7852.

29.   Kemper, P. R.; Bowers, M. T., A hybrid double-focusing mass spectrometer—high-pressure drift reaction cell to study thermal energy reactions of mass-selected ions. *Journal of the American Society of Mass Spectrometry* **1990**, 1 (3), 197-207; von Helden, G.; Hsu, M.-T.; Kemper, P. R.; Bowers, M. T., Structures of carbon cluster ions from 3 to 60 atoms: Linears to rings to fullerenes, *The Journal of Chemical Physics* **1991**, 95 (5), 3835-3837.

30.   Mason, E. A.; Schamp, H. W., Mobility of gaseous Ions in weak electric fields *Annals of Physics* **1958**, 4 (3), 233-270.

31.   McLean, J. A.; Ruotolo, B. T.; Gillig, K. J.; Russell, D. H., Ion mobility–mass spectrometry: a new paradigm for proteomics. *International Journal of Mass Spectrometry* **2005,** *240* (3), 301-315.

32.   West, G. B.; Brown, J. H.; Enquist, B. J., A general model for the origin of allometric scaling laws in biology. *Science* **1997**, 276 (5309), 122-126.

33.   Shen, Y.; Greene, J. E.; Strauss, M. A.; Richards, G. T.; Schneider, D. P., Biases in Virial Black Hole Masses: An SDSS Perspective. *The Astrophysical Journal* **2008**, 680 (1), 169.

34.   Galilei, G., Leiden (**1638**) 1638.

35.   Viidanoja, J.; Sysoev, A.; Adamov, A.; Kotiaho, T., Tetraalkylammonium halides as chemical standards for positive electrospray ionization with ion mobility spectrometry/mass spectrometry. *Rapid Communications in Mass Spectrometry*, **2005**, *19* (21), 3051-3055.

36.   Fenn, L. S.; McLean, J. A., Structural resolution of carbohydrate positional and structural isomers based on gas-phase ion mobility-mass spectrometry. *Physical Chemistry Chemical Physics* **2011,** *13* (6), 2196-2205.

37.   Huang, Y.; Dodds, E. D., Ion mobility studies of carbohydrates as group I adducts: isomer specific collisional cross section dependence on metal ion radius. *Analytical Chemistry,* **2013**, *85* (20), 9728-9735.

38.   Ellis, H. W.; Pai, R. Y.; McDaniel, E. W.; Mason, E. A.; Viehland, L. A., Transport properties of gaseous ions over a wide energy range. *Atomic Data and Nuclear Data Tables*, **1976**, *17* (3), 177-210; Ellis, H. W.; McDaniel, E. W.; Albritton, D. L.; Viehland, L. A.; Lin, S. L.; Mason, E. A., Transport properties of gaseous ions over a wide energy range, II. *Atomic Data and Nuclear Data Tables* 1978, 22 (3), 179-217; Ellis, H. W.; Thackston, M. G.; McDaniel, E. W.; Mason, E. A., Transport properties of gaseous ions over a wide energy range, III, *Atomic Data and Nuclear Data Tables* 1984, 31 (1), 113-151; Viehland, L. A.; Mason, E. A., Transport properties of gaseous ions over a wide energy range, IV. *Atomic Data and Nuclear Data Tables* **1995**, *60* (1), 37-95.

39.   Matz, L. M.; Hill, H. H.; Beegle, L. W.; Kanik, I., Investigation of drift gas selectivity in high resolution ion mobility spectrometry with mass spectrometry

detection. *Journal of the American Society for Mass Spectrometry* **2002,** *13* (4), 300-307

40. Berant, Z.; Karpas, Z., Mass-mobility correlation of ions in view of new mobility data. *Journal of the American Chemical Society*. **1989**, *111* (11), 3819-3824.

41. Wyttenbach, T.; Bleiholder, C.; Bowers, M. T., Factors contributing to the collision cross section of polyatomic ions in the kilodalton to gigadalton range: application to ion mobility measurements. *Analytical Chemistry,* **2013**, *85* (4), 2191-2199; von Helden, G.; Wyttenbach, T.; Bowers, M. T., Conformation of macromolecules in the gas-phase - use of matrix-assisted laser-desorption methods in ion chromatography. *Science* **1995,** *267* (5203), 1483-1485.

CHAPTER 3

APPROACHES FOR SEPARATION AND CHARACTERIZATION OF GLYCANS

AND GLYCOCONJUGATES BY RAPID CHROMATOGRAPHY, ION MOBILITY-

MASS SPECTROMETRY, AND MULTIMODAL SEQUENCING TECHNIQUES

3.1. Introduction

Systems biology greatly enhances the study of complex biological processes by expanding on traditional reductionist approaches, where individual components are targeted (i.e. glycomics). Systems biology strategies allow for the comprehensive analysis of biological samples as a whole. To support these systems analyses strategies, we have developed ion mobility-mass spectrometry (IM-MS) techniques to study biological systems in the gas phase through class specific structural separations. Proteins, lipids, and carbohydrates, which exhibit overlapping signals in a 1-D mass spectrum, are separated in IM-MS because each biomolecular class occupies a unique region of conformational space.[1-4] Thus, IM-MS analysis is able to differentiate molecules present in complex biological samples with minimal sample purification, which greatly improves upon current methodologies. IM-MS provides broad scale biological structural descriptors, which can be further honed to describe class and subclass descriptors.[5-7]

Glycoproteins are highly implicated in protein stability, cellular signaling and other key biological functions. Glycosylation is one of the most common and least studied post translational modifications (PTMs) due to complexity and corresponding

separation challenges.[8-10] Traditional mass spectrometry (MS) techniques often require extensive treatment prior to analysis. Ion mobility –mass spectrometry (IM-MS) addresses several of these analytical challenges as molecules are separated by structure (IM) and mass (MS).[2, 11-12]

3.1.1. *LC-IM-MS Glycan Analysis*

Structural analysis of N-linked glycan and glycan conjugates is challenging due to the high level of heterogeneity of glycan isomers and the corresponding difficulty of separation.[13] The study of non-derivatized (native) glycans poses additional challenges due to their low abundance and the inherent preference of sodium-coordinated glycans in endogenous biological matrices containing salts which partitions analyte signal into multiple ion channels and contributes to interfering chemical noise. Liquid chromatography (LC) and mass spectrometry (MS) techniques are frequently used for rapid characterization of carbohydrate samples, but commonly require extensive sample preparation and purification as well as multi-stage fragmentation analysis (tandem MS) in order to gleam structural information.[13-21]

Ion mobility-mass spectrometry (IM-MS) addresses several analytical challenges related to the complex heterogeneity of glycans through rapid gas-phase separations based on structurally selective IM, which is complementary to MS.[22-25] The IM-MS separation improves analytical sensitivity by partitioning signals of interest from endogenous or exogenous chemical noise. Furthermore, structural information can be derived from mobility measurements that are specific to isomeric species. The methodologies described in sections 3.1.1., 3.2.1.-4., 3.2.6., 3.3.1., and 3.4.1. have been developed for the analysis of native or non-derivatized glycan using LC-IM-MS. With

minimal sample preparation and no prior purification necessary, this robust methodology can be applied to various complex glycan samples.

Initial motivation for this study was to develop methodologies for integrating multiple omics workflows (glycomics and proteomics) towards a comprehensive IM-MS-based structural analysis of glycoproteins.[22] To minimize time and cost, a single stage of liquid chromatography was utilized, and a method was optimized wherein both proteins and non-derivatized glycans could be fractionated on the same reverse-phase (RP) column. Typical glycoproteomics workflows target either peptides or glycans, but rarely both in the same experiment. For many research facilities that address a wide spectrum of samples (e.g., omics cores and systems-based centers) it would be advantageous in terms of cost, time, sample comparability, and consumption to conduct proteomic, glycomic and glycoproteomic studies on the same LC-MS platform. The ability to utilize the same RP column for both analyses results from adjusting solvent gradients such that glycan studies are carried out under normal phase solvent conditions. This combination of a RP column with a normal phase gradient allows for the stabilization of non-derivatized glycans and produces primarily protonated and minor sodium coordinated glycan signals. This results in the observance of predominately protonated carbohydrate ions within the IM-MS spectra. While this convention is not necessary in some cases, many studies benefit from native glycan analysis. Three different approaches for glycan analysis by MS methods are described in Figure 3.1.

The traditional biochemistry approach for glycoprotein analysis by MS is described in Figure 3.1. Scheme 1 in which glycoproteins are denatured, reduced, and alkylated followed by digestion with trypsin. Samples are separated such that proteomic

81

analysis is carried out independently of glycomics analysis.[13, 26, 27] Enzymes such as PNGaseF are utilized to cleave glycans from the peptide backbone. In this context, glycans are typically derivatized, commonly by permethylation, or fluorescently tagged, to affect glycan separation and/or enhance detection. Although the separation and detection capacity of the presently reported strategy may be reduced over those of labeling, labeling methodologies require extensive separation and purification in addition to alteration of the free glycan structure through derivatization. The present methodology obviates the need for and attendant challenges of labeling including perturbation and potential contamination of the sample and increases throughput by not requiring different LC column technologies between proteomics and glycomics.[28-32] Fenn et al. published a simultaneous glycoproteomics protocol in which glycoprotein samples are sequentially processed with trypsin and PNGase F in the same vial which simplifies purification requirements while eliminating the sample fractionation step.[22] IM-MS was then utilized to simultaneously acquire both proteomic and glycomic information from the same sample. These analyses were carried out using either matrix assisted laser desorption/ionization (MALDI) or direct infusion electrospray ionization (ESI) sources. In order to batch process samples with ESI and obtain an additional dimension of pre-ionization separation through LC, the techniques originally developed by Fenn and co-workers were further optimized for the studies presented here using bovine fetuin as a biological standard.

Scheme 1

Glycoprotein

↓

Denature, reduce, alkylate

↓

Digest with trypsin

↓

Purification and separation

↙ ↘

Peptide analysis by MS   N-Linked glycan release by PNGase F

↓

Derivatization (permethylation)

↓

Derivatized glycan analysis by MS

Current proteomic/ glycomic approach

Scheme 2

Glycoprotein

↓

Denature, reduce, alkylate

↓

Digest with trypsin

↓

N-Linked glycan release by PNGase F

↓

Simultaneous analysis of peptides and glycans by IM-MS

Simultaneous *omics* aproach using IM-MS

Scheme 3

Glycoprotein

↓

Denature, reduce, alkylate

↓

N-Linked glycan release by PNGase F

↓

Analysis of glycans by IM-MS

Glycomic specific approach using IM-MS

Figure 3.1. (Scheme 1) A standard protocol for glycoprotein analysis. Purification and derivatization (permethylation) methods are commonly necessary to increase analytical sensitivity, resulting in a time consuming and complex procedure.[26] (Scheme 2) Previously reported protocol for the simultaneous omics approach using IM-MS.[22] This protocol allows both peptides and N-linked glycans to be simultaneously analyzed with minimal sample preparation. Sensitivity gains are afforded by the use of IM-MS. (Scheme 3) The protocol describes the separation and analysis of carbohydrates without modification by IM-MS. In this scheme, glycoproteins are subjected to denaturing by heat followed by PNGase F enzyme incubation prior to analysis. This procedure simplifies the interpretation of carbohydrates without derivatization or further purification

3.1.2. *Multimodal Fragmentation of Glycopeptides*

Glycomic and glycoproteomic studies are often challenging due to the biological complexity and corresponding difficulty of separation. MS techniques play a critical role in the analysis of carbohydrates and PTMs of proteins such as glycosylation.[33] One promising approach is sequencing by tandem mass spectrometry. Novel sequencing workflows were developed that utilize fragmentation techniques to obtain finer structural detail of glycoconjugate and glycoprotein complexes. Although common to proteomics, vibrational activated collision induced dissociation (CID) does not retain glycosylation PTMs. Electron transfer dissociation (ETD), however, is a radical driven fragmentation technique which preserves PTMs in a manner complementary to CID.[34-39] Further supporting the utility within glycoproteomic applications, the capabilities of ETD has been extended to the structural sequencing of carbohydrates.[40-41] While ETD is a more comprehensive technique for glycoprotein analysis, data analysis can be difficult due to interfering background signals. The addition of IM separations to ETD-MS analysis assists in fragmentation analysis as interfering signals may be deconvoluted.[42-45]

The IM-MS configuration allows for radical driven fragmentation by ETD and subsequent vibrational activated CID fragmentation as complementary techniques in support of structural assignment. Several studies have utilized a combinatorial fragmentation approach incorporating both collision-based and radical-based fragmentation modes.[46-50] Donohoe et al. demonstrated a IM-CID method with subsequent ETD fragmentation.[51] Williams and coworkers described a two-stage fragmentation method separated by IM.[52-53] Katzenmeyer et al. utilize this workflow for

cationized polyesters.[54] Methods proposed here utilize the mobility separation between fragmentation stages to assist in the deconvolution of the complementary techniques.

Presented here is an application of these techniques using the IM separation for data deconvolution, resulting in both ETD and CID fragmentation spectra obtained in one experiment. Methodologies for characterizing proteins and glycoproteins by ETD-IM-CID-MS show promise as a more comprehensive sequencing strategy. The workflow was benchmarked using a protein standard, ubiquitin, and subsequently applied to a glycopeptide, carcinoembryonic antigen (CGM2). Research recently described the significance of glycan profiling of CGM2 from human tumor tissue for improved tumor diagnosis and treatment.[55] The analysis of a CGM2 standard validates the methodology for glycopeptide studies. Combining broad and fine structural studies in this manner creates a toolbox for extensive analysis of proteomics, glycomics, and more generally, integrated omics at large.

3.2. Experimental Details

3.2.1. Sample Preparation for LC Glycan Analysis

A 1 mg mL^{-1} sample of bovine fetuin (Sigma Aldrich) was prepared in 10 mM sodium phosphate buffer solution to a final volume of 100 μL. To denature the protein, the sample was heated to 90°C for 10 minutes and subsequently cooled to room temperature. While alkylation and reduction is recommended, it was not necessary as sufficient cleavage of the glycan was achieved for this experiment with only denaturing by heat. The sample was then treated with 10 μL of 500 units/mL PNGaseF (Sigma Aldrich) followed by incubation at 37 °C for 24 hours. To quench PNGaseF activity, the

sample was heated to 90°C for 5 minutes followed by 15 minutes in the -20°C freezer. The sample was dried down by a vacuum concentrator (speedvac) and reconstituted in approximately 250 μL of 100% ACN with 0.1% TFA and remaining protein content was precipitated by centrifugation. The glycan containing solvent (~150-200 μL) was transferred to an LC maximum recovery vial. It should be noted that removal of protein content is an optional step for IM-MS analysis as the protein will not occupy the same region of conformational space as the glycans.

3.2.2. *Sample Preparation for Multimodal Sequencing*

Glycopeptide samples were purchased from Protea Biosciences Inc (Morgantown, WV, U.S.A.). Glycosylated Carcinoembryonic Antigen (CGM2) was prepared according to the manufacture's product information protocol. Briefly, CGM2 was reconstituted in 500 μL Optima LC/MS grade water with 0.1% Formic Acid (Fisher Scientific, Ottawa, Ontario, Canada) for a final concentration of 1 pmol/μL. The sample was then vortexed, sonicated, and transferred to a 1.5 mL Eppendorf tube. Ubiquitin from bovine erythrocytes and substance P standards were purchased from Sigma Aldrich (St. Louis, MO, U.S.A.) and reconstituted in LC/MS grade water and methanol (1:1, v/v) to a final concentrations ranging from 10 pg/mL to 10 μg/mL. Both 1,3-dicyanobenzene and nitrosylbenzene ETD reagents were purchased as part of the MS ETD Reagent Kit from Waters Inc. (Milford, MA, U.S.A.).

3.2.3. Liquid Chromatography Conditions

Fetuin samples were analyzed using an Acquity UPLC system (Waters, Milford, MA) coupled to the ESI source of a Synapt G2 HDMS instrument using a Waters HSS C18 column (1.8 μm, 1.0 x 100 mm) stored at 40°C. Samples are loaded into an autosampler which is held at 4°C. The LC solvents are prepared such that solvent A consists of 100% H_2O with 0.1% TFA and solvent B consists of 100% ACN with 0.1% TFA. Alternately, buffered solvents can be used to make this method compatible with the analysis of less stable samples. The maltose sample contained 10μg mL^{-1} of each M1, M3-M7 in 10 mM ammonium acetate with 0.1% formic acid. The chromatographic separation used 100% H_2O with 0.1% formic acid and 100% ACN with 0.1% formic acid as solvents A and B, respectively. Sample can also be spiked with small amounts of NaI or NaCl to induce ionization preference of the sodiated species. The 20 minute method starts with 100% solvent B and linearly transitions to 100% solvent A over the course of 12 minutes and held for 3 minutes for at 60 μL min^{-1} with an injection volume of 5 μL. The flow is then reversed to initial conditions for the remainder of the experiment. This is summarized in Table 3.1.

3.2.4. Ion Mobility- Mass Spectrometry Conditions for LC Glycan Analysis

IM-MS data is collected in positive resolution mode over a mass range of 100-4000 Da using the following instrument conditions; 3.5 kV capillary, 80°C source temperature, 40 V sampling cone, 2 V extraction cone, and 150 °C desolvation

Table 3.1. LC Method Details

Time (min)	Flow rate (µL min^{-1})	% Solvent A (Water)	% Solvent B (ACN)	Curve
1. Initial	60.000	0.0	100.0	
2. 1.00	60.000	0.0	100.0	6
3. 12.00	60.000	100.0	0.0	6
4. 15.00	60.000	100.0	0.0	6
5. 15.10	60.000	0.0	100.0	6

temperature. The traveling wave velocity was set to 650 m s^{-1} and wave height to 40 V for mobility separation. Fragmentation data was collected post-mobility in the transfer region with a collision energy ramp from 5-30 eV in a MS^E experiment. The incorporation of MS/MS to this method allows for the potential of carbohydrate identification by fragmentation. When this capability is employed in a secondary function during the LC run, fragmentation spectra is automatically acquired and can be customized using a targeted precursor mass lists or various CID voltage ramps dependent on the type of analysis required. A key advantage to fragmentation post-mobility is related to the alignment of fragment peaks as they retain the mobility of their respective precursor.[56, 57] Lock mass correction was applied using Leucine-enkephalin to maintain high mass accuracy.

3.2.5. *Instrument Conditions for Multimodal Sequencing Analysis*

All experiments utilized a Waters Synapt G2-S HDMS instrument fitted with an ETD upgrade kit. Samples were directly infused at a rate of 10 μl/min using either the Synapt built in fluidics or a Harvard Apparatus (Holliston, MA U.S.A.) syringe pump for limited sample volumes. All data was acquired in positive resolution mode. The following source conditions were used: a capillary and sample cone voltages of 2.2 kV and 0 kV, respectively, a source temperature of 100 °C, a source offset of 60, a desolvation temperature of 250 °C and desolvation gas flow rate of 100 L/hr, cone gas flow of 25 L/hr, and a nebulizer gas flow of 6 bar. The ETD reagent was introduced through the ETD reagent chamber. ETD reagent ionization was adjusted in negative ion mode to determine optimized makeup gas flows for 25 L/hr, a discharge voltage of 0.9

kV, and a current of 20 μA. Trap settings were amended for ETD experiments as follows: a trap DC entrance and bias of 0 and 35 V, respectively, a trap gate of -2 V, a trap DC and DC exit of -3V, a trap wave velocity of 300 m/s and height of 0.3 V, a trap pressure of 5.9×10^{-2} mbar, a trap gas flow of 14 mL/min, a collision energy of 4 eV and a mobility delay after trap release of 1000 μs. ETD refill functions were set the ETD refill mass to the mass of the reagent ion, refill scan interval time of 1 s and a 0.1 s refill scan time.

Mobility settings varied to accommodate a both larger mass precursor ions and smaller mass fragment ions. However, the mobility settings generally utilized a gas flow of 40 mL/min and IMS pressure of 3.56, a helium cell gas flow of 150 mL/min and pressure of 2.47×10^{1}, an IMS DC entrance and exit of 10 and 0 V, helium cell DC and exit of 35 and -20 V, an IMS wave velocity of 300 m/s and height of 25 V, an optional variable wave velocity from 300 to 1000 m/s linearly. Transfer settings without CID fragmentation post mobility were a transfer gas flow of 0.8 mL/min, a transfer DC entrance and exit voltages of 5 and 15 V, respectively, a transfer wave velocity of 300 m/s and height of 3.1 V, a transfer region pressure of 1.6×10^{-2} and a collision energy of 0 to 0.5 eV. Transfer settings with CID fragmentation retain the same settings as previously mentioned with the exception of the collision energy that ranges from 5 to 50 eV and can be optionally ramped. Quadrupole selection was used prior to ETD fragmentation with a scan time of 1 s and interscan time of 0.015 s.

3.2.6. *Data Analysis of LC-IM-MS Glycan Separations*

Data is processed off line with Driftscope software v2.5 (Waters, Milford, MA), which allows mobility selection of regions of the IM-MS data that pertain to

carbohydrate signals. Liquid chromatography data is analyzed through MassLynx (Waters, Milford MA). Both drift time selection and liquid chromatography selection precedes the generation of mass spectra in MassLynx.

3.2.7. *Data Analysis of Multimodal Sequencing*

Data was analyzed manually with the assistance of predicted fragment ions using ProSight PTM Ion Predictor (The Kelleher Group, Northwestern University, Chicago, IL, U.S.A.) to predict c/z and b/y ions given then protein or peptide sequence. CGM2 ions were predicted by adding a custom mass shift modification on the asparagine corresponding to the mass shift of the GlcNAc attached. Additionally, ChemBio Draw v12 (PerkinElmer Inc., Waltham, MA) assisted in visual manual interpretation of fragmentation data. All mobility data was accessed using Driftscope v2.5. Subsequently, raw and drift time filtered mass spectra were analyzed in MassLynx.

3.3. Results and Discussion

3.3.1. Results of LC-IM-MS Analysis of Glycans

Non-derivatized free glycans elute with the initial aqueous solvent plug in typical RP-LC separations, thus optimization focused on procedures amenable to the separation of free glycans with a RP column. By running a normal phase gradient (organic to aqueous) over a RP C-18 column, separation conditions are created which extends the retention time of carbohydrates disparate from the initial solvent plug as observed in Figures 3.2. (b) and (d). In this mode, non-derivatized glycans are retained by the column and elute at approximately 6 minutes into the 20 minute chromatographic run. While the

chromatographic separation observed is not as well separated as in other methods (such as hydrophilic interaction LC (HILIC)), the addition of LC to previously reported IM-MS based glycoproteomics protocols further increases peak capacity and allows separation of non-derivatized glycans on a RP column.

This is demonstrated in Figures 3.2. (a) and (c) as a series of maltose standards elute in the solvent plug of a reverse phase gradient resulting in lower ion intensity when compared to (b) and (d) which were separated by a normal phase gradient on the same column. Impurities in the sample (such as the presences of maltooctaose (M8)) appear in (b) and (d), illustrating the increased sensitivity of the chromatographic separation for higher mass carbohydrates. Additionally, the lower abundance of signal in (c) in comparison to (d) supports this claim. This allows glycan analysis to be conducted on a standard MS instrument platform fitted with an RP column, such that both glycomic- and proteomic-based samples can be prepared and batch processed with the auto-sampler and conventional RP column of the LC system.

Another consequence of this approach is that glycans are predominately ionized as protonated glycans (M+H) in contrast to MALDI and direct infusion ESI where glycans are predominately ionized as alkali metal-coordinated (M+Na or M+K) species. It should be noted that this LC-IM-MS analysis of non-derivatized glycans with a RP column also creates alkali metal-coordinated ions as minor products (Figure C.1.) which can be utilized to compare previously published glycan MS results, where these species are more typical. As MALDI-MS is considered a gold standard due to high sensitivity for carbohydrate analysis,[26, 27, 58] LC-IM-MS data obtained in this study were evaluated with
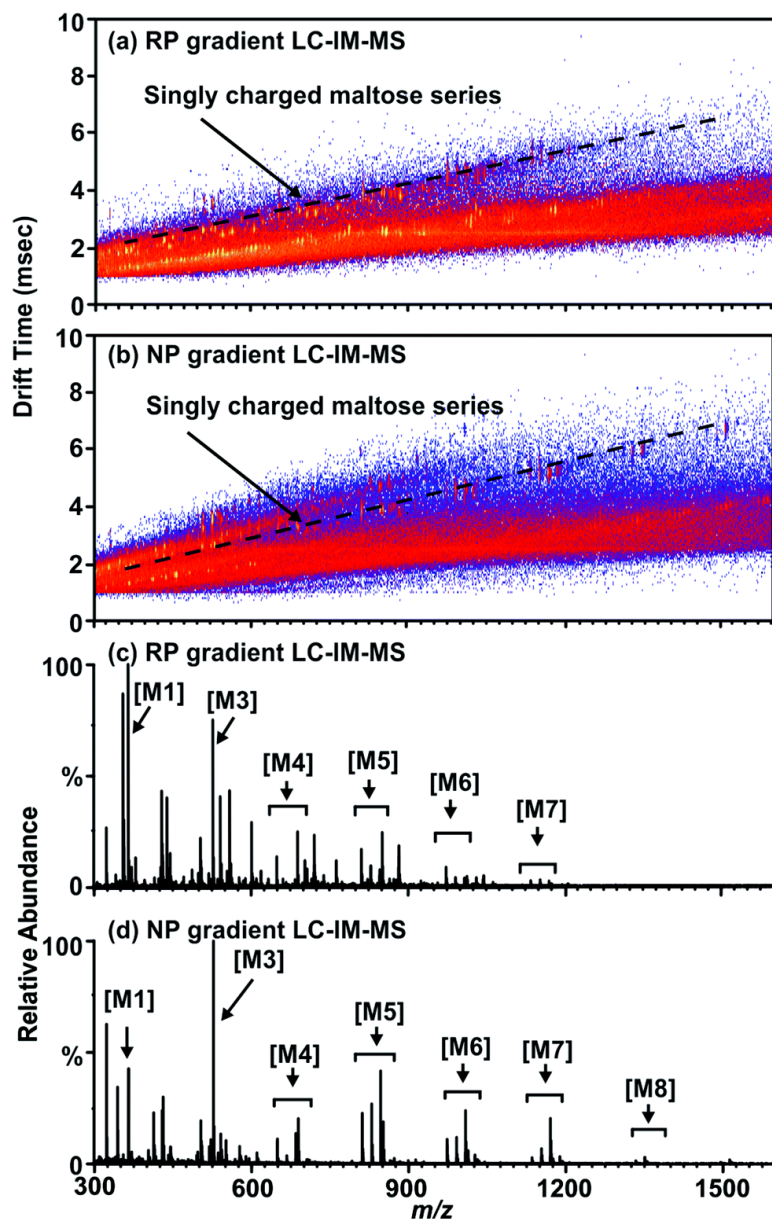
Figure 3.2. (a) A 2D LC-ESI-IM-MS plot of a mixture of maltose standards separated using a reverse phase gradient on a C18 column. A region of singly charged ions corresponding to the maltose series is annotated by a dashed line. (b) A 2D LC-ESI-IM-MS plot of the same maltose standard mixture using the same column as in figure (a) with a normal phase gradient (organic to aqueous). (c) A mobility selected mass spectrum illustrating the carbohydrate series peaks as annotated by a dashed line in (a) where the base peak intensity is 2.93×10^4. (d) The mobility-selected area occupied by the maltose ion series as noted by a dashed line in (b) where the base peak intensity is 3.78×10^4. Maltose abbreviations are as follows: maltose (M1), maltotriose (M3), Maltotetraose (M4), maltopentaose (M5), maltohexaose (M6), maltoheptaose (M7), maltooctaose (M8).

respect to data obtained by MALDI-IM-MS by the previously published methodology described in Figure 3.1., Scheme 2 in further detail in the supplementary information.[22]

The utility of IM-MS separations for glycan analysis is further illustrated by Figure 3.3. The integrated mass spectrum (panel b) represents the data as would be obtained by conventional ESI-MS analysis alone. A region of mobility space occupied by fetuin carbohydrate species is selected (annotated in Figure 3.3. (a)). Thus, subsequent data-analysis discrimination of the chemical and chemical noise produces an enhanced mass spectrum representative of the doubly charged, non-derivatized glycan species (Figure 3.3. (c)).

It should be noted that signal abundances in Figure 3.2. and 3.3. describe peak intensities relative to the base peak with 100% intensity. Figure 3.2. (c) and (d) display relative ion abundances from 300-1600 *m/z* such that the base peak of the spectrum represents a relative abundance of 100%. The relative abundance of the base peak in 3.2. (c) was 2.93×10^4 and in 3.2(d) 3.78×10^4. Figure 3.3. (b) and (c) display relative ion abundances from 950-1650 *m/z* such that the base peak of the spectrum represents a relative abundance of 100%. The relative abundance of the base peak in 3.3(b) was 1.15×10^4 and 6.57×10^3 in 3.3(c).

3.3.2 Results of Multimodal Sequencing

3.3.2.1 Mobility Assisted Electron Transfer Dissociation of a Protein Standard

To benchmark electron transfer dissociation-ion mobility-mass spectrometry (ETD-IM-MS) experiments, a well-studied 76 amino acid protein, ubiquitin, was analyzed by both ETD-MS and ETD-IM-MS workflows. The $[M+6H]^{+6}$ ion with a *m/z* of 1427.61 was
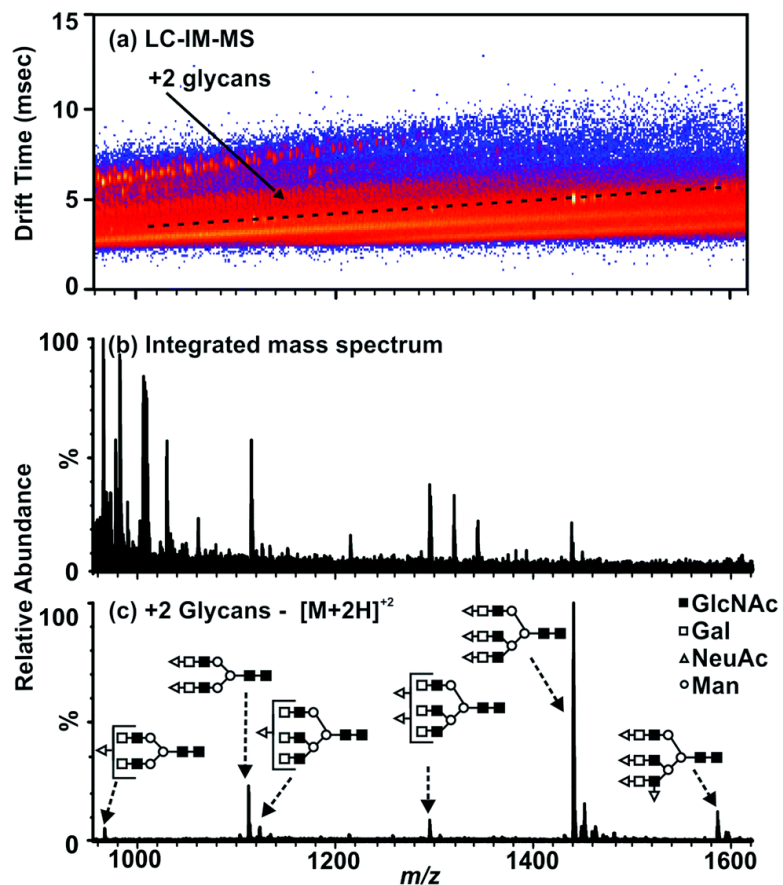
Figure 3.3. LC-ESI-IM-MS plot and extracted mass spectra from bovine fetuin deglycosylated using PNGase F (protocol from Scheme 3, Figure 3.1). (a) A 2-D IM-MS spectrum corresponding to the analysis of carbohydrates from a model glycoprotein (fetuin). Selected region for +2 glycans represent the extracted mass spectrum (c). (b) An integrated mass spectrum illustrating the chemical and chemical noise which would be present without the use of the mobility separation where the base peak intensity is 1.15×10^4. (c) Extracted mass spectrum of free N-linked glycans from fetuin where the base peak intensity is 6.57×10^3. Carbohydrate structures are represented here and elsewhere by the annotations in (c) as follows: ○ -mannose, Δ -sialic acid, ■ -N-acetylglucosamine, and □ -galactose. LC separations are performed on a RP column under normal-phase gradient conditions which give rise to an ionization preference for protonated carbohydrate ions.

selected as the precursor ion of interest by the quadrupole prior to ETD fragmentation in the trap region. Figure 3.4. (a) describes a 2D IM-MS plot of ubiquitin with emphasis on resulting ETD fragment c and z ions and side product charge reduction. Panel b illustrates a mass spectrum resulting without mobility (ETD-MS) where charge reduction products are more predominant than the minor c and z ion fragment products. These findings are described previously in the literature on this instrument system.[59] Utilizing the mobility selection post analysis, it is possible to remove background signals to enhance areas of interest annotated in the 2D IM-MS plot of Figure 3.4. (a). Figures 3.4. (b) and (c) further illustrate the ability to enhance signals of interest as the predominant ions in spectra 2.4. (b) correspond to c and z ions as ETD fragmentation products of the $[M+6H]^{+6}$ precursor ion. Figure 3.4. (c) contains mobility-selected spectra of the charge-reduced species. Both mass spectra and drift time values can be analyzed after mobility selection to obtain conformational information in the form of a collision cross section supported by theoretical computational modeling.[60-63] Mobility separation after ETD fragmentation enhances the fragmentation spectra through the reduction of interfering chemical background such as charge-reduced species, thus enhancing the signal-to-noise ratio of the fragment ions. Further, previous studies have demonstrated separation of c and z ion types.[52] Spectra obtained in this manner allows for a simpler assignment of sequence annotation, thus reducing the time require for data analysis.
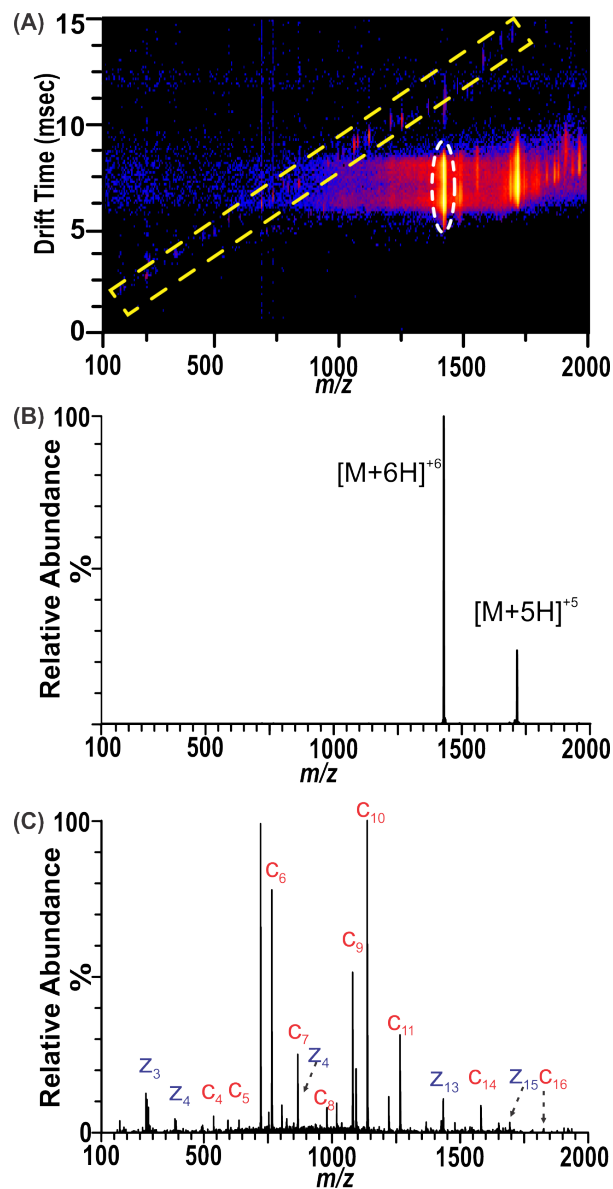
Figure 3.4. Electron transfer dissociation of ubiquitin. A. The 2D IM-MS plot of ubiquitin after initial mass selection for the +6 charge state ion. The regions correlating to ETD product ions and charge-reduced product ions are annotated by yellow dashed box. B. An ETD-MS only spectrum. This mass spectrum illustrates the relative low abundance of ETD fragments in relation to endogenous chemical noise (charge reduced species). C. An IM-MS selected mass spectrum from the region annotated in yellow in Figure 1.A. ETD fragments of the +6 ubiquitin ion are annotated as c and z ions in the spectra.

3.3.2.2. *Comprehensive Sequence Analysis by Multimodal ETD and CID fragmentation*

Further optimization of mobility-assisted fragmentation techniques takes advantage of complementary fragmentation techniques. To best utilize the combination of ETD and CID fragmentation, ion mobility is used to deconvolute multimodal spectra. ETD fragmentation occurs prior to mobility analysis in the trap region of the instrument. Consequently, c and z fragments resulting from ETD are analyzed in the IM region. After mobility, CID fragmentation occurs in the transfer region. Fragments produced after the IM analysis retains the mobility information of the precursor ion. This results in aligned fragmentation spectra where all fragments appear in a horizontal alignment in 2D IM-MS space. Mobility selection of the data assists the deconvolution of the ETD fragmentation spectra as described previously from the CID post-mobility aligned spectra. The complexity of overlapping multimodal fragmentation spectra is reduced through the mobility selection process, enhancing feature assignments in both complementary fragmentation experiments.

Figure 3.5 illustrates this mobility enhanced multimodal fragmentation methodology for ubiquitin. The [M+6H]+6 ion with a *m/z* of 1427.61 was mass selected in the quadrupole prior to ETD fragmentation in the transfer region under the same conditions as described for ETD-IM-MS previously. After mobility analysis, ions are fragmented in the transfer region by collision-induced dissociation with argon gas at various voltages relative to the approximate size of the precursor ion of interest. Figure 3.5. A depicts the 2D IM-MS plot with regions corresponding to ETD fragments and CID fragments annotated by a
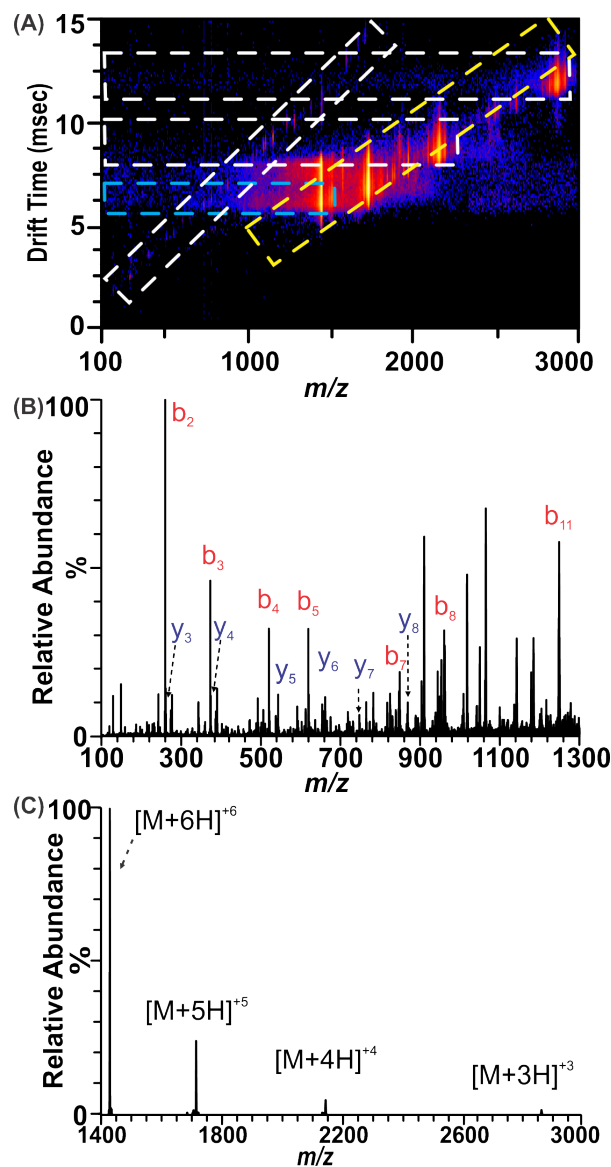
Figure 3.5. The ETD-IM-CID-MS analysis of ubiquitin. A. An IM-MS plot of the mass selected +6 ubiquitin ion analyzed by multimodal fragmentation. ETD product ions are annotated with a white dashed box position on a diagonal. CID post mobility product ions are annotated by blue, and white boxes. B. An IM-MS selected region, annotated by the blue dashed box in Figure 3.5. A, correlating to the CID fragmentation of ubiquitin. The b and y ions produced by the CID fragmentation retain the mobility of the precursor ion and are aligned in the 2D IM-MS plot (Figure 3.5. A). This allows for easier data analysis and deconvolution of the spectra by mobility selection. C. An IM-MS selected mass spectrum from the yellow dashed box annotated in Figure 3.5. A representing the charge-reduced species of the ETD reaction.

diagonal line and horizontal lines, respectively. Figure 3.5. B describes the mass spectra obtained without mobility selection. Spectra without mobility selection represents the data complexity from ETD-CID-MS experiments in contrast to ETD-IM-CID-MS. Figure 3.5. C is the mobility selected CID spectra aligned to the precursor $[M+6H]^{+6}$ ion. This spectra illustrates the spectral deconvolution gained with the addition of ion mobility. Specifically, the placement of an IM cell between two regions of fragmentation assists in the selection of correlation regions as depicted in Figure 3.5. A. Spectra can be obtained from both modes of fragmentation simultaneously in one experiment allowing for a comprehensive multimodal fragmentation and thus sequencing of a protein.

3.3.2.3. Comprehensive Sequencing of a Glycopeptide by ETD-IM-CID-MS

To evaluate the utility of this methodology for posttranslational modification sequencing, in particular glycosylation, a glycopeptide was subjected to the same workflow as the benchmarking protein, ubiquitin. The carcinoembryonic antigen 2 (CGM2) glycopeptide was selected as it contains 10 amino acids with an N-linked GlcNAc. This simple system allows for the sequencing of the amino acids as well as the position of the site of glycosylation. Fragmentation by ETD in the first stage retains the PTM modification, GlcNAc, at the 8 position. The amino acid sequence can be determine by the c and z fragment ion spectra. After mobility analysis, an ETD fragment serves as the precursor ion of CID in the secondary stage of fragmentation. Figure 3.6. A depicts a 2D IM-MS plot of the CGM2 glycopeptide with regions corresponding to ETD fragments, CID fragments, and charge reduced side products of the ETD fragmentation.
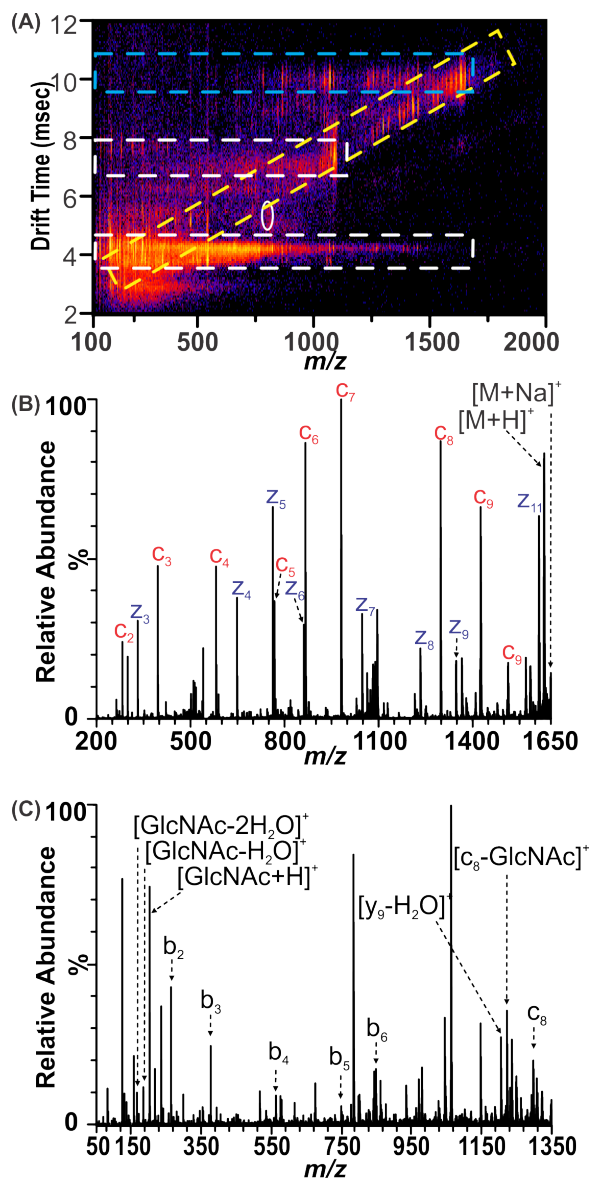
Figure 3.6. The multimodal fragmentation and comprehensive sequencing of the CGM2 glycopeptide. A. The IM-MS plot of the ETD-IM-CID-MS analysis of the mass selected doubly-charged CGM2 glycopeptide ion. ETD fragment ions are annotated by a yellow box. CID fragment ions are annotated by blue and white boxes. B. The ETD fragmentation spectrum produced by selecting the region annotated by the yellow box in Figure 3.6. A. This spectrum illustrates the c and z ions produced aiding in the sequencing of the glycopeptide while retaining PTM (glycosylation at the asparagine reside). C. The post-mobility CID fragmentation spectrum obtained by IM-MS selection of the blue box in Figure 3.6A. The spectrum depicts the loss of the N-linked glycan from the c_9 ETD fragment as a result of the CID fragmentation. Additionally, ETD fragment ions which did not disassociate prior to mobility are disassociated in the post-mobility fragmentation region as a result of collision energy. This process produces c and z ions aligned in the 2D IM-MS plot. Note the alignment of fragments as CID occurs after the mobility analysis, assisting in the deconvolution of multimodal fragmentation.

Figure 3.6. B and 3.6. C illustrate the ETD and CID fragmentation spectra, respectively. Figure 3.6. describes the ETD fragments along the sequence of the CGM2 peptide, which retain the carbohydrate PTM. This allows for mapping of the sites of glycosylation and illustrates the PTM retention during this fragmentation mechanism. Secondary fragmentation by CID then cleaves the carbohydrate from the peptide as described in figure 3.6. The loss of 203 Da corresponds to the loss of a GlcNAc.

A full workflow of the ETD-IM-CID-MS technique for glycopeptides is described in Figure 3.7. This multimodal fragmentation allows for the comprehensive sequencing of both the amino acid sequence of the peptide as well as the sites of glycosylation. The addition of ion mobility between the two complementary stages of fragmentation supports deconvolution of the spectra. This produces simplified spectra for annotation and assists in data analysis as both ETD and CID are run simultaneously.

3.4. Conclusions

3.4.1. Conclusions for LC Glycan Analysis

The methodology described herein is readily amenable to LC systems with RP columns allowing for simultaneous omics experiments (proteomics and glycomics) to be conducted on the same analytical platform. To further confirm the effectiveness of the LC methodology for N-linked glycan analysis, studies can be optimized in a mode which obtains MS/MS spectra simultaneously. In this manner, we can begin to assemble comprehensive and multi-dimensional datasets of a suite of biomolecules obtained from minimally processed samples (See Appendix C).[56, 57]
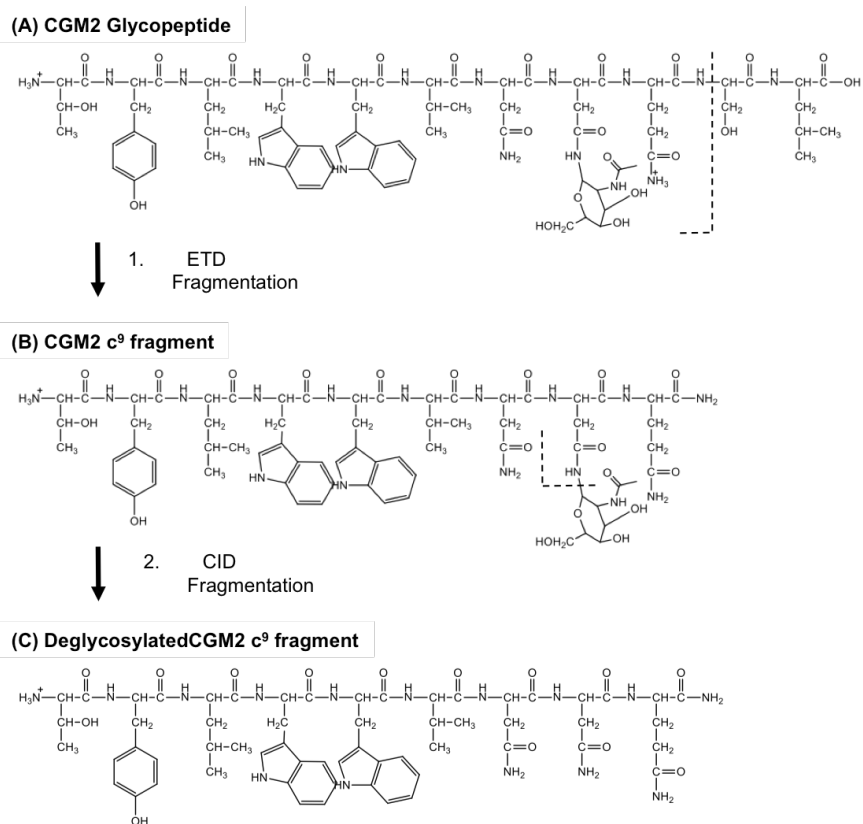
Figure 3.7. A schematical representation of the ETD-IM-CID-MS analysis of the CGM2 glycopeptide. A. The initial structure of the doubly-charged CGM2 glycopeptide ion annotated with a cleavage site for ETD fragmentation. B. The structure of the singly charged c_9 ETD product ion after fragmentation. Note the glycosylation at the asparagine side chain remains intact through the ETD fragmentation process. The glycosidic bond is annotated for cleavage by CID post-mobility. C. The subsequent CID fragmentation product ion by which the glycan has been cleaved. This deglycosylated singly charged fragment is the result of both ETD and CID complementary fragmentation techniques coupled by ion mobility.

3.4.2. Conclusions for Multimodal Sequencing

Multimodal fragmentation supported by ion mobility separation provides a comprehensive sequencing approach for glycosylated peptides and proteins. These methods can be extended to other post-translational modifications as well. This configuration supports simultaneous ETD and CID fragmentation in one experiment. After ETD fragmentation and IM, all ions can be subjected to CID producing fragment spectra that are mobility aligned. Fragmentation stages separated by ion mobility are deconvoluted in the data analysis by selecting regions of 2D IM-MS space. Mapping the amino acid sequence and the glycosylation sites can be achieved simultaneously in this workflow. Addition examples of spectral deconvolution using ion mobility-mass spectrometry in support of multimodal fragmentation can be found in Appendix C. Examples are shown for both ubiquitin and the CGM2 glycopeptide. The incorporation of multimodal fragmentation techniques with the separation capabilities of ion mobility produces a rich dataset of deconvoluted spectra. Multimodal sequencing enhances the analysis of glycaopeptides, and proteins with a more comprehensive approach supported by ion mobility separations.

3.4.3. Summary of IM-MS supported glycoproteomics

A simple method for the analysis of non-derivatized glycans using a reverse phase column on a liquid chromatography- ion mobility- mass spectrometry (LC-IM-MS) instrument was described. Methodology supports both glycomic and proteomic work flows without the necessity of switching columns. To obtain finer structural details, a

multimodal fragmentation method was developed such that ETD and CID modes were activated sequentially. The use of IM allows for the deconvolution of fragmentation modes resulting in a more comprehensive sequencing. The chromatographic and fragmentation methods are presented in this chapter as platforms enabling integrated omics research. Key to these methodologies is the unique separation capabilities of ion mobility-mass spectrometry.

3.5. Acknowledgements

3.6 Associated Content

Supporting Information. The following experimental details and figures are included in Appendix C. A 2D IM-MS plot and spectra illustrating the charged adduct distributions of carbohydrates separated by the LC-IM-MS method (**Figure C.1.**). A mobility profile describing the separation in the IM cell of branched glycans cleaved from bovine fetuin is reported. (**Figure C.2.**). Comparisions of the LC method to that of the method considered to be the gold standard for carbohydrate analysis, MALDI, is provided (**Figure C.3.**). A detailed description to the experimental methods supporting the LC-IM-MS method are reported in **Appendix C.1.1.** A comparison of LC total ion current traces are presented. (**Figure C.4.**).

3.7. References

1. Fenn, L. S.; Kliman, M.; Mahsut, A.; Zhao, S. R.; McLean, J. A., Characterizing ion mobility-mass spectrometry conformation space for the analysis of complex biological samples. *Analytical and Bioanalytical Chemistry* **2009,** *394* (1), 235-244.

2. Fenn, L. S.; McLean, J. A., Enhanced carbohydrate structural selectivity in ion mobility-mass spectrometry analyses by boronic acid derivatization. *Chemical Communications,* **2008,** (43), 5505-5507.

3. Ridenour, W. B.; Kliman, M.; McLean, J. A.; Caprioli, R. M., Structural Characterization of Phospholipids and Peptides Directly from Tissue Sections by MALDI Traveling-Wave Ion Mobility-Mass Spectrometry. *Analytical Chemistry* **2010,** *82* (5), 1881-1889.

4. Woods, A. S.; Ugarov, M.; Egan, T.; Koomen, J.; Gillig, K. J.; Fuhrer, K.; Gonin, M.; Schultz, J. A., Lipid/peptide/nucleotide separation with MALDI-ion mobility-TOF MS. *Analytical Chemistry* **2004,** *76* (8), 2187-2195.

5. May, J. C.; Goodwin, C. R.; Lareau, N. M.; Leaptrot, K. L.; Morris, C. B.; Kurulugama, R. T.; Mordehai, A.; Klein, C.; Barry, W.; Darland, E.; Overney, G.; Imatani, K.; Stafford, G. C.; Fjeldsted, J. C.; McLean, J. A., Conformational Ordering of Biomolecules in the Gas-Phase: Nitrogen Collision Cross Sections Measured on a Prototype High Resolution Drift Tube Ion Mobility-Mass Spectrometer, *Analytical Chemistry*, **2014**, 84, 2107-2016.

6.   Paglia, G.; Angel, P.; Williams, J. P.; Richardson, K.; Olivos, H. J.; Thompson, J. W.; Menikarachchi, L.; Lai, S.; Walsh, C.; Moseley, A.; Plumb, R. S.; Grant, D. F.; Palsson, B. O.; Langridge, J.; Geromanos, S.; Astarita, G., Ion mobility-derived collision cross section as an additional measure for lipid fingerprinting and identification. *Analytical Chemistry*. **2015,** *87*, 1137-1144.

7.   Williams, J. P.; Grabenauer, M.; Holland, R. J.; Carpenter, C. J.; Wormald, M. R.; Giles, K.; Harvey, D. J.; Bateman, R. H.; Scrivens, J. H.; Bowers, M. T., Characterization of simple isomeric oligosaccharides and the rapid separation of glycan mixtures by ion mobility mass spectrometry. *International Journal of Mass Spectrometry* **2010,** *298* (1-3), 119-127.

8.   Bahl, O. P., Glycoconjugates: Composition, Structure and Function. Marcel Dekker: New York, NY, 1992; pp. 1-12.

9.   Gorelik, E.; Galili, U.; Raz, A., On the role of cell surface carbohydrates and their binding proteins (lectins) in tumor metastasis. *Cancer and Metastasis Reviews* **2001,** *20* (3-4), 245-277.

10.   Monteuil, J.; Vilegenthart, J. F. G.; Schachter, H., Glycoproteins I. Elsevier Science: New York, NY, 1995; p. 644.

11.   Lareau, N. M.; May, J. C.; McLean, J. A., Non-derivatized Glycan Analysis by Reverse Phase Liquid Chromatography and Ion Mobility-Mass Spectrometry *Analyst,* **2015**, *140*, 3335-3338.

12.   Plasencia, M. D.; Isailovic, D.; Merenbloom, S. I.; Mechref, Y.; Clemmer, D. E., Resolving and assigning N-linked glycan structural isomers from ovalbumin by IMS-MS. *Journal of the American Society for Mass Spectrometry* **2008,** *19* (11), 1706-1715.

13.   Harvey, D. J. Identification of protein-bound carbohydrates by mass spectrometry. *Proteomics*, **2001**, *1*, (2) 311-328.

14.   Morelle, W.; Canis, K.; Chirat, F.; Faid, V.; Michalski, J. C.; Proteomics, 2006, 6, 3993-4015.

15.   Harvey, D. J. Proteomic analysis of glycosylation: structural determination of N- and O-linked glycans by mass spectrometry. *Expert Reviews of Proteomics*, **2005**, *2*, (1) 87-101.

16.   Wuhrer, M.; de Boer, A.R. and Deelder, A.M.; Structural glycomics using hydrophilic interaction chromatography (HILIC) with mass spectrometry. *Mass Spectrometry Reviews*, **2009**, *28*, (2), 192-206.

17.   Bones, J.; Mittermayr, S.; Donoghue, N. O.; Rudd, P. M. 2D-LC Analysis of BRP 3 Erythropoietin *N*-Glycosylation using Anion Exchange Fractionation and

Hydrophilic Interaction UPLC Reveals Long Poly-*N*-Acetyl Lactosamine Extensions, *Electrophoresis*, **2010**, *82*, 10208-10215.

18. Bones, J. Mittermayr, S. Mcloughlin, N. Hilliard, M. Wynne, K. Johnson, G. R., Grubb, J. H. Sly, W. S., Rudd, P. M. Identification of N-glycans displaying mannose-6-phosphate and their site of attachment on therapeutic enzymes for lysosomal storage disorder treatment. *Analytical Chemistry,* **2011**, *83*, 5344-5352.

19. Klapoetke, S. C. Zhang, J., Becht, S. Glycosylation characterization of Human IgA1 with differential deglycosylation by UPLC-ESI TOF MS. *Journal of Pharmaceutical and Biomedical Analsis*, **2011**, *56*, 513-520.

20. Knežević, A. Bones, J. Kračun, S. K. Gornik, O. Rudd, P. M., Lauc, G. High throughput plasma N-glycome profiling using multiplexed labelling and UPLC with fluorescence detection. *Analyst*, **2011**, *136*, 4670-4673.

21. Kurihara, T. Min J. Z., Hirata, A. Toyo'oka T., Inagaki, S. Rapid analysis of N-linked oligosaccharides in glycoproteins (ovalbumin, ribonuclease B and fetuin) by reversed-phase ultra-performance liquid chromatography with fluorescence detection and electrospray ionization time-of-flight mass spectrometry. *Biomedical Chromatography*, **2009**, *23*, 516-523.

22. Fenn, L. S., McLean, J. A. Simultaneous glycoproteomics on the basis of structure using ion mobility-mass spectrometry. *Molecular BioSystems*, **2009**, *5,* 1298-1302.

23. Damen, C. W. N.; Chen, W.; Chakraborty, A. B.; van Oosterhout, M.; Mazzeo, J. R.; Gebler, J. C.; Schellens, J. H. M.; Rosing, H.; Beijnen, J. H., Electrospray ionization quadrupole ion-mobility time-of-flight mass spectrometry as a tool to distinguish the lot-to-lot heterogeneity in N-glycosylation profile of the therapeutic monoclonal antibody trastuzumab. *Journal of the American Society for Mass Spectrometry* **2009,** *20* (11), 2021-2033.

24. Plasencia, M. D.; Isailovic, D.; Merenbloom, S. I.; Mechref, Y.; Clemmer, D. E., Resolving and assigning N-linked glycan structural isomers from ovalbumin by IMS-MS. *Journal of the American Society for Mass Spectrometry* **2008,** *19* (11), 1706-1715.

25. Fenn, L. S.; McLean, J. A., Enhanced carbohydrate structural selectivity in ion mobility-mass spectrometry analyses by boronic acid derivatization. *Chemical Communications,* **2008,** (43), 5505-5507.

26. Harvey, D. J. Matrix-assisted laser desorption/ionization mass spectrometry of carbohydrates. *Mass Spectrometry Reviews,* **1999**, *18*, (6) 349-450

27. Harvey, D. J. Analysis of carbohydrates and glycoconjugates by matrix-assisted laser desorption/ionization mass spectrometry: an update for the period 2005-2006. *Mass Spectrometry Reviews*, **2011**, *30*, (1), 1-100.

28. Alvarez-Manilla, G. Warren, N. L. Abney, T. Atwood, J. Azadi, P. York, W. S. Pierce, M., Orlando, R. Tools for glycomics: relative quantitation of glycans by isotopic permethylation using 13CH3I. *Glycobiology*, **2007**, *17*, 677-687.

29. Ciucanu, I. Per-O-methylation reaction for structural analysis of carbohydrates by mass spectrometry. *Analytical Chimica Acta***, 2006**, *576*, (2), 147-155.

30. Kang, P. Mechref, Y., Novotny, M. V. High-throughput solid-phase permethylation of glycans prior to mass spectrometry. *Rapid Communications Mass Spectrometry,* 2008, 22, 771-734.

31. Mechref, Y., Kang, P., Novotny, M. V., Methods in Molecular Biology Glycomics: Methods and Protocols, Totowa, NJ: Humana Press, 2009, 534, 53-64.

32. Price, N. P. J. Permethylation linkage analysis techniques for residual carbohydrates. *Applied Biochemistry and Biotechnology*, **2008**, *148*, (1), 271-276

33. Leymarie, N.; Zaia, J., Effective use of mass spectrometry for glycan and glycopeptide structural analysis**.** *Analytical Chemistry.* **2012,** *84*, 3040-3048.

34. Syka, J. E. P.; Coon, J. J.; Schroeder, M. J.; Shabanowitz, J.; Hunt, D. F., Peptide and protein sequence analysis by electron transfer dissociation mass spectrometry. *Proceedings of the National Academy of Science .* **2004,** *101*, 9528-9533.

35. Zhurov, K. O.; Fornelli, L.; Wodrich, M. D.; Laskay, U. A.; Tsybin, Y. O., Principles of electron capture and transfer dissociation mass spectrometry applied to peptide and protein structure analysis. *Chemical Society Reviews.* **2013,** *42*, 5014-5030.

36. Wiesner, J.; Premsler, T.; Sickmann, A., Application of electron transfer dissociation (ETD) for the analysis of posttranslational modifications**,** *Proteomics* **2015,** *8*, 4466-4483.

37. Kim, M. S.; Pandey, A., Electron transfer dissociation mass spectrometry in proteomics. *Proteomics* **2012,** *12*, 530-542.

38. Mikesh, L. M.; Ueberheide, B.; Chi, A.; Coon, J. J.; Syka, J. E.; Shabanowitz, J.; Hunt, D. F., The utility of ETD mass spectrometry in proteomic analysis. *Biochimca et Biophysica Acta.* **2006,** *1764*, 1811-1822.

39. Udeshi, N. D.; Compton, P. D.; Shabanowitz, J.; Hunt, D. F.; Rose, K. L., Methods for analyzing peptides and proteins on a chromatographic timescale by electron-transfer dissociation mass spectrometry. *Nature Protocols.* **2008,** *3*, 1709-1717.

40. Han, L.; Costello, C. E., Electron transfer dissociation of milk oligosaccharides. *Journal of the American Society for Mass Spectrometry.* **2011,** *22*, 997-1013.

41.   Yu, X.; Huang, Y.; Lin, C.; Costello, C. E., *De Novo* Sequencing of Heparan Sulfate Oligosaccharides by Electron-Activated Dissociation. *Analytical Chemistry.* **2012,** *84*, 7487-74-84.

42.   Pepin, R.; Laszlo, K. J.; Peng, B.; Marek, A.; Bush, M. F.; Tureček, F., Comprehensive Analysis of Gly-Leu-Gly-Gly-Lys Peptide Dication Structures and Cation-Radical Dissociations Following Electron Transfer: From Electron Attachment to Backbone Cleavage, Ion–Molecule Complexes, and Fragment Separation. *Journal of Physical Chemistry A.* **2014,** *118*, 308-324.

43.   Lermyte, F.; Konijnenberg, A.; Williams, J. P.; Brown, J. M.; Valkenborg, D.; Sobott, F., ETD allows for native surface mapping of a 150 kDa noncovalent complex on a commercial Q-TWIMS-TOF instrument. *Journal of the American Society for Mass Spectrometry.* **2014,** *25*, 343-350.

44.   Huang, Y.; Dodds, E. D., Discrimination of Isomeric Carbohydrates as the Electron Transfer Products of Group II Cation Adducts by Ion Mobility Spectrometry and Tandem Mass Spectrometry. *Analytical Chemistry.* **2015,** *87,* 5664-5668.

45.   Lermyte, F.; Verschueren, T.; Brown, J. M.; Williams, J. P.; Valkenborg, D.; Sobott, F., Characterization of top-down ETD in traveling-wave ion guide. *Methods* **2015,** *1,* (89), 22-29.

46.   Zhao, C.; Xie, B.; Chan, S. Y.; Costello, C. E.; O'Connor, P. B., Collisionally activated dissociation and electron capture dissociation provide complementary structural information for branched permethylated oligosaccharides. *Journal of the American Society for Mass Spectrometry* **2008,** *19*, 138-150.

47.   Gupta, K.; Kumar, M.; Chandrashekara, K.; Krishnan, K. S.; Balaram, P., Combined electron transfer dissociation-collision-induced dissociation fragmentation in the mass spectrometric distinction of leucine, isoleucine, and hydroxyproline residues in Peptide natural products. *Journal of Proteome Research.* **2012,** *11*, 515-522.

48.   Scott, N. E.; Parker, B. L.; Connolly, A. M.; Paulech, J.; Edwards, A. V.; Crossett, B.; Falconer, L.; Kolarich, D.; Djordjevic, S. P.; Hojrup, P.; Packer, N. H.; Larsen, M. R.; Cordwell, S. J., Simultaneous glycan-peptide characterization using hydrophilic interaction chromatography and parallel fragmentation by CID, higher energy collisional dissociation, and electron transfer dissociation MS applied to the N-linked glycoproteome of Campylobacter jejuni. *Molecular & Cellular Proteomics* **2011,** *10*, 1-18.

49.   Wu, S. L.; Jiang, H.; Hancock, W. S.; Karger, B. L., Identification of the unpaired cysteine status and complete mapping of the 17 disulfides of recombinant tissue plasminogen activator using LC-MS with electron transfer dissociation/collision induced dissociation.*Anal. Chem.* **2010,** *82*, (12), 5296-5303.

50. Catalina, M. I.; Koeleman, C. A.; Deelder, A. M.; Wuhrer, M., Electron transfer dissociation of N-glycopeptides: loss of the entire N-glycosylated asparagine side chain. *Rapid Communications in Mass Spectrometry.* **2007,** *21*, 1053-1061.

51. Donohoe, G. C.; Maleki, H.; Arndt, J. R.; Khakinejad, M.; Yi, J.; McBride, C.; Nurkiewicz, T. R.; Valentine, S. J., A new ion mobility-linear ion trap instrument for complex mixture analysis. *Analytical Chemistry.* **2014,** *86*, 8121-8128.

52. Williams, J. P.; Brown, J. M.; Campuzano, I.; Sadler, P. J., Identifying drug metallation sites on peptides using electron transfer dissociation (ETD), collision induced dissociation (CID) and ion mobility-mass spectrometry (IM-MS). *Chemical Communications.* **2010,** *46*, 5458-5460.

53. Williams, J. P.; Pringle, S.; Richardson, K.; Gethings, L.; Vissers, J. P.; De Cecco, M.; Houel, S.; Chakraborty, A. B.; Yu, Y. Q.; Chen, W.; Brown, J. M., Characterisation of glycoproteins using a quadrupole time-of-flight mass spectrometer configured for electron transfer dissociation. *Rapid Communications in Mass Spectrometry.* **2013,** *27*, 2383-2390.

54. Katzenmeyer, B. C.; Cool, L. R.; Williams, J. P.; Craven, K.; Brown, J. M.; Wesdemiotis, C., Tandem mass spectrometry and ion mobility mass spectrometry for the analysis of molecular sequence and architecture of hyperbranched glycopolymers *International Journal of Mass Spectrometry.* **2015,** *378*, 303–311.

55. Huang, C.; Zhan, T.; Liu, Y.; Li, Q.; Wu, H.; Ji, D.; Li, Y., Glycomic profiling of carcinoembryonic antigen isolated from human tumor tissue. *Clinical Proteomics* **2015,** *12, (*17), 1-7.

56. Hoaglund-Hyzer, C. S., Li, J., Clemmer, D. E., *Mobility labeling for parallel CID of ion mixtures. Analytical Chemistry.*, **2000**, *72*, 2737-2740.

57. Hines, K. M., Ballard, B. R., Marshall, D. R., McLean, J. A., Structural mass spectrometry of tissue extracts to distinguish cancerous and non-cancerous breast diseases. *Molecular BioSystems.*, **2014**, *10*, 2827-2837.

58. Harvey, D. J., Analysis of carbohydrates and glycoconjugates by matrix-assisted laser desorption/ionization mass spectrometry: an update for 2007-2008. *Mass Spectrometry Reviews*, **2012**, *31*, 183-311.

59. Lermyte, F.; Williams, J. P.; Brown, J. M.; Martin, E. M.; Sobott, F., Extensive Charge Reduction and Dissociation of Intact Protein Complexes Following Electron Transfer on a Quadrupole-Ion Mobility-Time-of-Flight MS. *. Journal of the American Society for Mass Spectrometry,* **2015,** *26*, 1068-1076.

60. Campuzano, I.; Bush, M. F.; Robinson, C. V.; Beaumont, C.; Richardson, K.; Kim, H.; Kim, H. I., Structural characterization of drug-like compounds by ion mobility mass spectrometry: comparison of theoretical and experimentally

derived nitrogen collision cross sections. *Analytical chemistry* **2012,** *84* (2), 1026-1033.

61. Scarff, C. A.; Thalassinos, K.; Hilton, G. R.; Scrivens, J. H., Travelling wave ion mobility mass spectrometry studies of protein structure: biological significance and comparison with X-ray crystallography and nuclear magnetic resonance spectroscopy measurements. *Rapid Communications in Mass Spectrometry.* **2008,** *22*, 3297-3304.

62. Bush, M. F.; Campuzano, I. D. G.; Robinson, C. V., Ion mobility mass spectrometry of peptide ions: effects of drift gas and calibration strategies. *Analytical Chemistry* **2012**, 84 (16), 7124-7130.

63. Ruotolo, B. T.; Benesch, J. L. P.; Sandercock, A. M.; Hyung, S.J.; Robinson, C. V., Ion mobility–mass spectrometry analysis of large protein complexes. *Nature Protocols.* **2008**, *84*, 1139-1152.

CHAPTER 4

CHIP-BASED LIQUID CHROMATOGRAPHY ION MOBILITY-MASS

SPECTROMETRY STRATEGIES IN SUPPORT OF SMALL MOLECULE

ANALYSIS

4.1. Introduction

Metabolomics is a rapidly emerging field in chemical biology due to its ability to

provide information concerning the physiological state of an organism.[1,2] Biomarker

discovery, a goal in metabolomics, is proving key to diagnosing diseases at early stages

in patients. In order to perform these studies, analytical techniques are required that can

analyze complex biological samples. While LC-MS techniques provide retention time

and mass-to-charge ratio (*m/z*) information that can be compared with databases to aid in

identification[3-8], database searching does not always yield an unambiguous metabolite

identity. Ion mobility-mass spectrometry (IM-MS) allows for the separation of ionized

molecules based on their size and shape, in addition to their *m/z*.[9] Drift time data

obtained from IM-MS can be used to determine the collision cross section (CCS) of these

ions. This additional feature of the metabolite ion allows for more accurate

identifications to be made in complex biological samples.[10-12]

Initial motivation to incorporate chip-based technology to the IM-MS platform is

two-fold. First, many metabolomics extracts are challenged with limitations of sample

size. Chip-based technology would reduce the sample volume required in many cases.

Second, the inclusion of liquid chromatography to the IM-MS platform would provide

addition dimension of separation, therefore expanding the variables comprising features.[2,13-20] Metabolomics often utilizes the separation power of LC-MS based technologies as the metrics from each provide information about polarity of the molecule, as well as the mass and charge, respectively.[6-8] The added dimension of IM introduces a size and shape descriptor to the analysis. In particular, this additional descriptor has potential for dereplication in discovery efforts. By expanding separation in four dimensions (RT, DT, *m/z*, and relative intensity), the peak capacity of the analysis is increased, thus supporting the potential to distinguish molecular features previously collapsed by signals sharing the variables of LC-MS alone.

The study reported here explores small molecules from approximately 100 Da to 900 Da across several subclasses of metabolites such as vitamins, carbohydrates, and organic acids among others. Samples were analyzed using chip-based LC technology integrated with an IM-MS instrument. To benchmark this methodology, multi-field CCS measurements were compiled in both helium and nitrogen drift gases. Single-field CCS measurements support LC as CCS values can be obtained on the LC time scale. In addition to experimental CCS values, theoretical CCS values can also be obtained by computationally sampling the conformational space of the molecule of interest. DTIM CCS measurements are obtained directly using the kinetic theory of gases and can arguably generate CCS values that show better agreement with theoretical CCS values based on current theoretical approaches.

Typically, these theoretical studies include a method for obtaining a theoretical structure by sampling the conformational space followed by an *in silico* CCS calculation for each conformation. The theoretical CCS value that most closely agrees with the

experimental value is then selected for further structural investigations. Additional approaches consider one low energy structure either from experiment (X-ray crystallography and NMR) or theoretical calculation and determine a theoretical CCS value for the individual structure. Rather than attempting to calculate a specific CCS value, we propose the generation and use of theoretical CCS ranges that result from sampling all the conformational space of the molecule. Developing a comprehensive database of these theoretical CCS ranges for typical metabolite molecules will facilitate the identification process.

While the long-term goal of this work is to aid in identification of unknown metabolites through database generation of theoretical CCS ranges, there is also an additional benefit to finding these ranges. They can serve as a guide when determining experimental CCS values for metabolite standards. Metabolites generally occupy a low-mass region of the spectra, which suffers from complexity due to noise from the sample and instrumental noise at that mass region. This makes feature selection and identification a challenge for these compounds. Benchmarking experimental CCS values against the theoretical ranges that result from sampling all conformational space of the metabolite can provide extra validation for the CCS value. The work presented here shows that good agreement can be found between experimental and theoretical CCS values for metabolite standards and serves as an early step in generating databases of theoretical CCS ranges for metabolomics research.

4.2. Experimental Methods

4.2.1. Preparation of standards

The metabolite samples, HPLC grade methanol, and tetraalkyammonium bromides (TAA 1-8) were purchased from Sigma-Aldrich (St. Louis, MO). Tune mix was provided from Agilent Technologies (Santa Clara, CA). Water with 0.1% formic acid (Optima) grade was obtained from Thermo Fisher Scientific (Waltham, MA). Metabolite samples were at a concentration of 10mmol in 1:1 methanol:water containing 0.1% formic acid. Small molecule, metabolite, and drug compound standards were purchased from Sigma Aldrich (St. Louis, MO, USA) and prepared as received in either 10mM ammonium acetate in H_2O or 10mM ammonium acetate in methanol, depending upon solubility. Final concentrations ranged from 1ng/mL to 10μg/mL. A full list of metabolites analyzed can be found in the Supporting Information (Table D3).

4.2.2. Instrumentation

Collision cross section experiments were performed on an Agilent 6560 IM-QTOF instrument equipped with a HPLC Chip Cube interface and microflow binary liquid chromatography (Agilent Technologies, Santa Clara, CA). The chip based interface utilizes an Agilent 1260 Infinity High Performance Micro Autosampler. Details of the IM-QTOF instrumentation are provided elsewhere,[21, 22] but, briefly, the IM-MS consists of a 78 cm uniform-field drift tube coupled to a high resolution QTOFMS (m/Δm 40,000). The buffer gas (helium or nitrogen) was maintained at a pressure of *ca.* 4 Torr and the drift voltages were varied in order to correct for the non-IM flight time of ions through the interfacing ion optics. The collision cross section calculator available

with the IM-MS Browser software utilizes the Mason-Schamp equation to determine experimental CCS values for the metabolites.

4.2.3. Data Acquisition Parameters

4.2.3.1. Liquid Chromatography Conditions

The binary HPLC setup was comprised of a capillary pump, a nanopump with degasser, and a microwell autosampler. Both the capillary and nano pumps infused binary solvents A and B, Optima LC grade water with 0.1% formic acid and Optima LC grade acetonitrile with 0.1% formic acid (ThermoFischer Scientific, Waltham, MA), respectively. All pumps were set to return to initial conditions at 15 minutes. LC methods were based on the ultra-high capacity chip application note.[23] Briefly, the capillary pump infused 98% solvent A at 4 μL/min with a pressure limit of 200 bar and a flow deviation limit of 3% for the duration of the chromatographic run. The nano pump was set to micro flow mode with a flow rate of 0.3 μL/min and a pressure limit of 200 bar with a flow deviation of 3%. The 15 min gradient began with 98% solvent A and lowered to 68% A over 5 minutes. The gradient was then adjusted to 20% solvent A at 8.5 minutes and held for one minute after which the initial gradient was reestablished. A timetable describing the solvent composition across the duration of the 15 minute chromatographic run is included in the Appendix D (Table D.5.). For samples injected through the microautosampler, a 2 μL injection was drawn at 20 μL/min and ejected at 40 μL/min with a wait time of 5 seconds post drawing the sample. A flush out factor of four times the injection volume (in this case 8 μL) was applied to ensure the sample was completely

transferred to the column. Gradients remained isocratic at 98% solvent A for all direct infusion experiments through the chip.

4.2.3.2. Chip Conditions

Liquid chromatography on chip utilized the ultra-high capacity (UHC) chip designed for small molecule analysis, UHC Chip (II) G4240-65010 (Agilent Technologies). The polyimide chip was etched to incorporate an enrichment and analytical column. First, the sample is loaded onto the 500 nL, 25 mm enrichment column and after flushing, the value is switched automatically to the analytical column. The analytical column consists of a 75 μm by 150 mm channel packed with a reversed phase HPLC material, Zorbax 80SB-C18 300 Å particles. Direct infusion for multi-field CCS experiments utilized a calibration chip designed for MS calibration and diagnostics, Calib-Chip (II) G4240-61010 (Agilent Technologies). The chip contained a 75 μm by 100 cm empty channel allowing for the infusion of standards for calibration and infusion of small molecules by direct infusion for multi-field CCS experiments. The maximum pressure was set to 150 bar for this chip. The flow rates from an external syringe pump were set between 0.3-0.6 μL/min.

4.2.3.3. Source Conditions

The chip cube source conditions utilized a zero air generator (Parker Hannifin, Haverhill, MA) supplying between approximately 5 L/min mixed with ultra-high purity nitrogen gas for a final gas flow between 10-13 L/min at a temperature of 250 °C. The capillary voltage was set between 1650 V to 2100 V depending on chip, solvent, and

analytes of interest. The fragmenter was set to 175 V, skimmer at -30 V, and octopole RF at 400.

4.2.3.4. IM-MS Parameters

The IM-MS instrument was calibrated using the phosphazine standards (Agilent tuning mixute, Agilent Technologies) over a mass range of 50-1700 Da. The mobility was tuned for sensitivity and resolution using these compounds for both helium and nitrogen drift gases for the respective drift gas experiments prior to interfacing the chip cube to the IM-QTOF. Mass calibration was performed through the direct infusion chip if needed. Acquisition parameters were as follows: front funnel pressures at ~3.8 Torr, IM drift tube at ~4 Torr; mass range from 50-1700 m/z; 18 IM transients/frame; maximum drift time of 60 ms; trap fill and release times of 20,000 μs and 150 μs, respectively; drfit tube entrance voltage at 500 V. All methods were developed for positive ion mode experiments. Multi-field helium mobility analyses typically collect mobility data at 7 different voltages for 2 minutes each with a total run time of 14 minutes. Voltages in helium were 400, 450, 500, 550, 600, 700, and 800 V with a 250 V bias resulting in a field of 1.92, 2.56, 3.21, 3.85, 4.49, 5.77, and 7.05 V/cm, respectively. Multi-field IM studies with nitrogen drift gas were run using 8 different voltages for 0.5 minutes each time point. Voltages were ramped from 800, 900, 1000, 1100, 1200, 1400, 1600, and 1800 V creating a field of 7.05, 8.33, 9.62, 10.90, 12.18, 14.74, 17.31, and 19.87 V/cm, respectively. Single field drift tube experiments were collected by direct infusing the sample of choice at one field condition in the drift tube. To obtain CCS measurements,

tune mix is applied to the chip cube wick as an standard. Additionally, tune mix is typically measured before, after, and periodically interspaced during sample queues.

4.2.4. Experimental Collision Cross-Section Calculations

4.2.4.1. Multi-field CCS Calculations

As previously mentioned, the experimental drift time values are converted to CCS in the Mass Hunter IMS Browser B 7.01 software package (Agilent Technologies) using the Mason-Schamp equation. Initially, drift times are collected at several voltages in order to plot a relationship between the drift time and the inverse of the electric field. This plot allows the user to systematically determine the dead time, or the fraction of time ions are not in the drift tube. This dead time, or T_0 is then subtracted to correct for a drift time representing only the time an ion spends in the drift tube. Immediately following this process, the software determined the mass of the ion, charge state, mass of the collision gas, pressure and temperature of the ion selected. The built in CCS calculator used this information to calculate a CCS value for each voltage frame. CCS values from at least two different days were compiled to account for possible environmental variables in the laboratory.

4.2.4.2. Single-field CCS Calculations

The tune mix was run before, after, and intermittently between samples sets at a set drift voltage. In addition, the tune mix was applied to the calibrant wick in the chip cube source housing to desorb during each run. All samples were collected using the same voltage as the tune mix. This matched voltage allowed for a correlation factor to be

determined for each voltage. These values were input to the single-field CCS calculator in the Mass Hunter IMS Browser software. With the known relationship of drift time and voltage, the software produces a CCS value for each ion selected manually, or for each feature through the molecular feature extractor (MFE). The MFE analyzed data to identify compounds with four unique descriptors, retention time, drift time, *m/z*, and relative ion intensity, or counts. The MFE function will process a feature list with both drift time and cross section if the previously mentioned correlation factors have been included. Multiple LC runs were analyzed in this manner and the resulting CCS values were averaged.

4.2.5. Theoretical Collision Cross Section Calculations

The generation of theoretical collision cross sections utilizes a distance geometry based computational as described by Stow et al.[24] Briefly, two dimensional neutral structures of each small molecule were acquired from PubMed and geometrically optimized. After initial optimization, a proton or alkali cation such as sodium or potassium were coordinated with the optimized molecule. These structures are depicted in the appendix (Figures D.2.-D.7.). The distance geometry protocol then sampled conformational space of each molecule based on the interatomic distances of the structure as to avoid selection of potentially inappropriate force fields. All structurally possible three-dimensional structures were clustered to remove analogous conformations. Clustering thresholds are described in the appendix (Figure D.8.). Conformations were then energy minimized and subjected to appropriate software to determine a theoretical

CCS value from the energy-minimized conformation. Details and parameters are further described in the appendix (Section D 1.1. and Table D.6.)

4.3. Results and Discussion

The metabolites analyzed in this study span a *m/z* range of 90.03 Da to 851.26 Da and represent different subclasses of metabolites including organic acids, nucleotides, vitamins, carbohydrates, and other classes. Samples were analyzed using both helium and nitrogen drift gases to describe the versatility of these analyses, as well as to determine practical challenges associated. LC separations and direct infusion of samples were performed on chip. Multi-field CCS measurements were obtained through direct infusion measurements to populate a basis set of experimental CCS values for small molecules in both helium and nitrogen. Single-field CCS measurements were utilized to support LC separations on chip. This allowed CCS values to be obtained continuously across the course of an LC run without requiring multiple runs are varying voltages. Data was further supported by theoretical modeling of CCS in both helium and nitrogen. Conformational space was explored such that a range of all structurally possible conformations of a molecule were subjected to modeling obtaining the resulting theoretical CCS. This provides a theoretical CCS range for each small molecule studied here. Advantages of a theoretical range include the ability to tease out possible false assignment of CCS based on structural feasibility. A CCS range mitigates challenges associated with reporting one finite structure for a particular experimental CCS value. Lastly, theoretical CCS ranges provide added confidence in experimental values.

4.3.1. Compilation of Multi-field Experimental CCS Values

Approximately 60 small molecule ions were analyzed using helium drift gas across a mass range of 122.10 Da to 851.26 Da. All data was compiled with mass (Da) and collision cross section (Å^2) in a two-dimensional conformation space plot in Figure 4.1 A. This data includes singly-charged ions with either sodium, potassium or a proton adducted. Details of these parameters are described in the Appendix D (Table D.3. and Table D.4.). To best describe the region of conformation space occupied by the small molecules studied, a power fit was applied to the data with the resulting equation $y = 4.027x^{0.5648}$ and a coefficient of determination, R^2, of 0.9476. This correlation approximation was depicted on the plot as the dashed blue line. Data was then analyzed against the % deviation from the power fit trend as plotted in the inset histogram. It was determined that a 6% deviation from the correlation approximation would best describe the data as it included 86% of the data. This 6% deviation was annotated on the conformation space plot of Figure 4.1. A as the two solid black lines.

In a similar manner as the helium CCS dataset, approximately 40 small molecule ions were measured using nitrogen drift gas. This dataset spans a mass range of 165.07 Da to 851.26 Da as depicted in Figure 4.1. B. This collection of nitrogen CCS values are best described by a power fit with the equation $y = 18.022x^{0.3951}$ and a R^2 of 0. 9468 plotted as the dotted blue line. The best fit correlation band for the nitrogen data was determined to be a deviation of 5% from the fit line. At 5% deviation from the power fit correlation line, 90% of the data points fall within the band as described in the inset histogram. It should be noted that the helium CCS values generally are smaller in magnitude for the same ion as the corresponding nitrogen CCS value. This is due to the
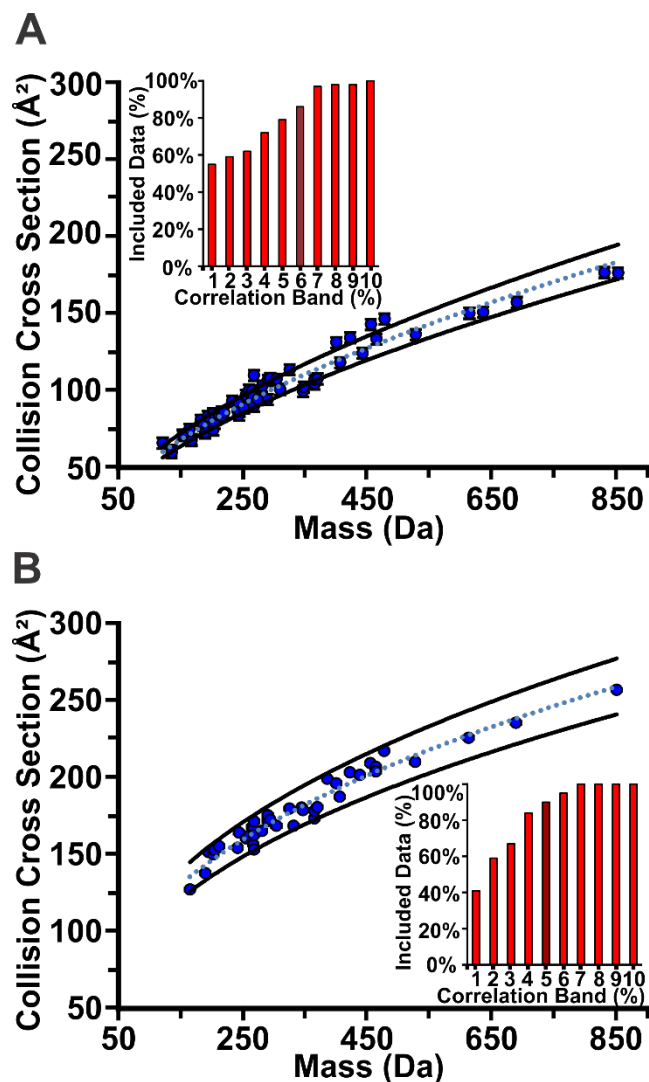
Figure 4.1. Conformational space plots summarizing small molecule descriptors of ions in both A) helium and B) nitrogen drift gases. The mass and CCS descriptors are fitted with a power fit trend, which represents the best correlation fit for the data in a blue dotted line. Data was then analyzed to determine the correlation band by the inset. The inset of A) depicts that a correlation of 6% deviation from the trend incorporated 86% of the data. The black lines represent the 6% correlation bands for helium IM-MS data. The inset of B) describes the included data within each correlation band. The 5 % correlation band is depicted as the black lines on the 2D nitrogen IM-MS plot.

interactions between the drift gas and the ion, which are described previously in the literature. These datasets provide a measure of multi-field CCS values to benchmark both single-field CCS values in support of chip based LC-IM-MS and the development of theoretical CCS ranges.

4.3.2. Development and Considerations of Chip-based LC-IM-MS

An HPLC chip cube was interfaced with a 6560 IM-QTOF for LC experiments of small molecules under helium and nitrogen drift gas conditions. In order to obtain CCS values on an LC timescale, single-field ion mobility CCS were utilized. Single-field IM analyses mitigate traditional LC-IM challenges such that a CCS for each molecular feature of interest could be produced for each individual LC run without the need of running multiple runs at varying voltages in a pseudo multi-field manner. To benchmark the utility of chip-based LC-IM-MS, a mixture of 7 small molecules at a concentration of 1ng/mL diluted in a starting mobile phase of 98% solvent A and 2% solvent B. 2 μL of the sample mixture was injected through the micro-autosampler and loaded onto the UHC Chip (II) and separated by a 15 minute gradient with subsequent helium IM separation and mass analysis described previously. An example workflow is described in Figure 4.2 such that the LC base peak chromatogram in Figure 4.1 A depicts the LC trace from the chip cube prior to IM interpretation of the data. Data can be further analyzed using the IM-MS dimensions as described in Figure 4.2. B. Figure 4. 2. B depicts the 2D IM-MS plot
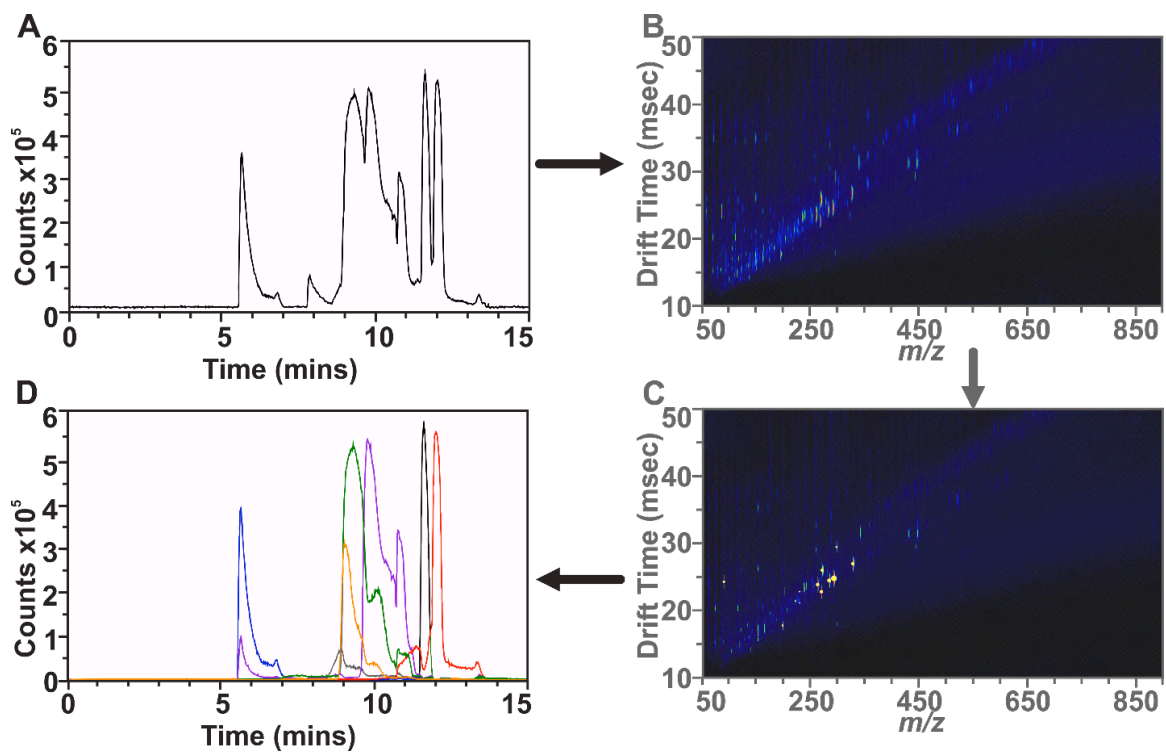
Figure 4.2. A workflow illustrating the utility of chip based-LC-IM-MS for a mixture of seven small molecules. A) A base peak chromatogram depicting a chromatogram prior to feature analysis. B) A 2D IM-MS plot illustrating the complexity of the molecular features within the LC range 5.5-12.5 minutes. C) The 2D IM-MS plot after features have been annotated by the data analysis software producing the four descriptors listed in Table 4.1. D) A feature specific chromatogram colored with overlaid ion chromatograms based on features found in C. The seven metabolites in the mixture annotated in C are atenolol (blue), caffeine (grey), quinine (orange), atropine (green), metoprolol (purple), propranolol (black), and imipramine (red).

over the chromatographic region of interest (5.5-12.5 minutes). The data analysis software assists in feature identification as shown in Figure 4.2. C. The thresholds were set to include only singly-charged ions within the chromatographic region of interest and a minimal ion intensity n the molecular feature extraction software. These thresholds were set to ensure ions in the LC region of interest were not excluded, but were set more strictly to exclude unwanted features in other cases.

The resulting features were annotated by the software as seen in Figure 4.2 C. Using the mobility single-field coefficients determined by the tune mix run under the same IM-MS conditions, the software can compile CCS values from the drift times obtained in the raw experimental data of Figure 4.2 B and 4.2 C. With the features of interest annotated, the seven metabolites were then correlated back to the LC as all variables are described in the feature finding process. The annotated feature specific chromatogram in Figure 4.2 D depicts overlaid feature specific LC traces. Each trace is distinguished by a color representing one of the seven metabolites described in more detail in Table 4.1. Table 4.1. reports the analyte with corresponding color to Figure 4.2. D, the retention time, *m/z*, drift time for the single-field LC-IM-MS experiment, CCS values and relative standard deviations (RSD) for both single- and multi-field CCS experimental measurements and the corresponding error between these, as well as the theoretical range and a representative structure in agreement with the experimental CCS value. It should be noted that there was good agreement with single and multi-field CCS experiments. With the exception of atropine, all compounds were below 0.5% error. Atropine had an increased error of 1.3%. This was likely due to the high intensity of the

Table 4.1. The 7 metabolites examined by chip-based LC-IM-MS with descriptors obtained by single-field CCS measurements.

Feature	Retention Time (min)	*m/z*	Drift Time (ms)	Single Field CCS (Å²)	CCS %RSD	Multi Field CCS (Å²)	CCS %RSD	% Error	Theoretical CCS Range (Å²)	Representative Structure in Agreement with CCS
Atenolol	5.72	267.15	22.70	95.4	0.1	95.4	0.5	0.1	96.9-117.0	
Caffeine	8.96	195.09	17.77	74.3	0.1	74.3	0.5	0.1	78.9-78.9	
Quinine	9.13	325.16	26.80	112.7	0.2	113.0	0.5	0.3	110.7-120.0	
Atropine	9.35	290.18	24.68	107.3	0.1	105.9	0.7	1.3	99.9-113.4	
Metoprolol	9.95	268.19	25.94	109.1	0.1	109.4	0.5	0.1	99.1-122.8	
Propranolol	11.64	260.14	23.80	99.9	0.1	100.1	0.5	0.1	94.6-111.8	
Imipramine	12.03	281.18	24.40	102.4	0.1	102.6	0.5	0.1	101.7-113.1	

Descriptors include chromatographic retention time, m/z, drift time and corresponding single-field CCS with % relative standard deviation (RSD), multi-field CCS measurement with %RSD, the % error comparing single and multi-field CCS values. The table also includes theoretical CCS ranges and a representative structure, which agree with the experimental CCS value.

peak, making it difficult to accurately assess the apex. Regardless, the increased error of 1.3% was below the 2% error considered to be acceptable for CCS measurements.[7] The average error for this study of small molecules in helium by single-field CCS was 0.3% (± 0.4). This table reports the extent of feature information that can be obtained in support of small molecule analysis on chip-based LC-IM-MS platforms.

Theoretical CCS ranges and a cluster representative conformation that agrees with the experimental CCS value are included in Table 4.1. These ranges give further confidence in the experimental CCS value as we see agreement for all the metabolites except caffeine and atenolol. Atenolol and caffeine are both small metabolites and although the range and experimental CCS value do not agree they are within 1.5% and 6.2%, respectively. This may suggest a lower bound m/z cutoff of approximately 200 m/z for comparison of experimental CCS values and theoretical CCS values. Further insight into deviations between experiment and theory are discussed further in Appendix D.1.3. The sample conformations give insight into the structural differences that cause separation of these species in the gas phase.

4.3.3. Theoretical CCS Values Support Experimental CCS Values

Theoretical CCS ranges were determined for the metabolites investigated experimentally in this study. Ranges for all metabolites were determined based on the most compact structure (smallest CCS) to the most elongated structure (largest CCS) generated theoretically. Although many structures are not energetically favorable, all structures chemically possible due to interatomic distance constraints were included. These structures set the bounds for the extremes of possible structural conformations.

A

B
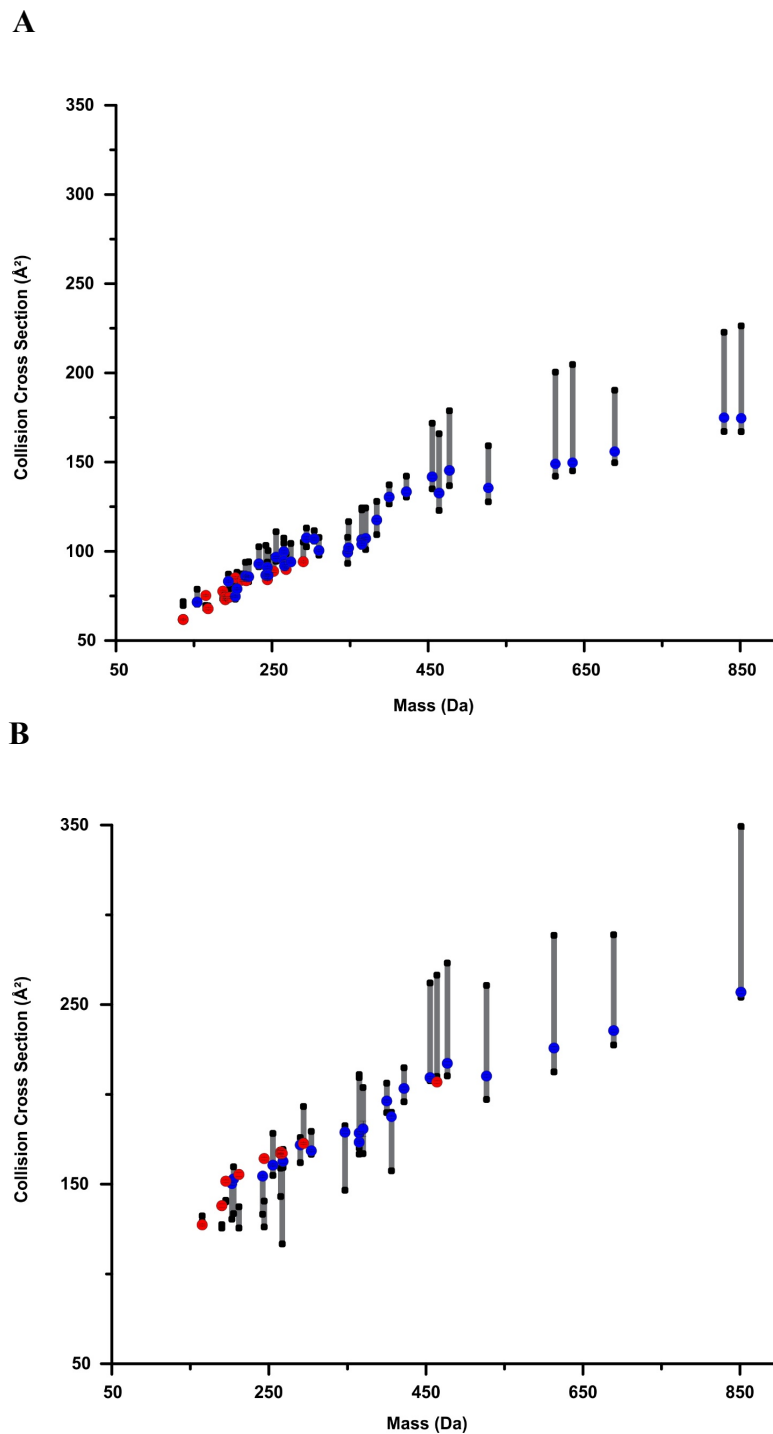
Figure 4.3. (A) Theoretical ranges helium CCS ranges for all small molecules listed in Table D.2. The experimental CCS values are overlaid as a circular marker. Experimental CCS markers are colored blue if it is in agreement with the theoretical range and red if it does not. (B) Theoretical nitrogen CCS ranges for all small molecules listed in Table D.3. The experimental CCS values are overlaid as a circular marker (blue agrees, red does not)

Theoretical ranges have been projected with overlaid experimental CCS values obtained in helium drift gas and nitrogen drift gas below in Figures 4.3 A and 4.3. B, respectively. Figure 4.3 A spans a mass range from approximately 90 Da to 850 Da and a CCS range from approximately 50 Å^2 to 225 Å^2. Experimental CCS values that were in agreement with the theoretical CCS range were projected with a blue marker. Values, which did not agree are projected with a red marker. It can be noted that experimental CCS values and theory agree well for masses approximately >200 Da in helium drift gas. Difficulties in modeling molecules less than 100 Da in helium drift gas is discussed in greater details in Appendix D (sections D 1.2-1.4.). Although there was some disagreement, the majority of experimental values agree with the theoretical CCS values ranges for helium drift gas experiments.

Nitrogen drift gas experiments produced ca. 40 CCS values supported by theoretical CCS ranges. Figure 4.3. B depicts the theoretical CCS ranges with experimental values overlaid. Similar to Figure 4.3. A, experimental values in agreement with theory were colored blue and those disagreeing with theory were colored red. A mass range of approximately 100 Da to 850 Da and a CCS range of approximately 100 Å^2 to 350 Å^2 was covered in the conformational space plot. Disagreement was observed below 300 Da and was described in Appendix D. Briefly, the computational approaches have difficulty simulating the polar interactions of the nitrogen drift gas on smaller molecules. In addition, the placement of the proton or cation to the small molecule was another concern. These issues will be address as part of the future directions for this work. Although there are limitations for some of the smaller metabolites studied, the theoretical ranges do support the majority of the experimental CCS values presented here.

The theoretical modeling adds confidence in the experimental work and has great potential for use in future metabolomics endeavors.

4.3.4. Time Advantage with the Chip-Based LC and Distance Geometry Modeling Method

One major drawback that has hindered computational modeling of large sets of molecules in support of IM-MS research is the time that is required for many of these calculations. If each metabolite requires weeks or months of computational time to produce theoretical CCS ranges, creating databases of these ranges would take much too long to prove useful. Distance geometry circumvents this issue because it generates these CCS ranges on the time scale of hours or days, not weeks or months. Similarly, the chip-based LC platform performs LC separations on the microscale. This results in chromatographic runs of 15 minutes for the small molecules examined in Figure 4.2. Minimizing the LC time required allowed samples to be batch processed in a higher throughput manner. Additionally, the support of single field CCS greatly decreases the time required for LC-IM-MS as a CCS can be obtained without running the sample under different drift voltage conditions to obtain CCS values.

The histogram in Figure 4.4 show the time required for generating the set of conformations for the metabolites used in this study in comparison to the experimental separation methods. The time required for MS (black) and IM (green) measurements is on the order of μs and ms respectively, with LC (red) methods requiring several minutes. With the time required for sampling the conformational space of metabolites ranging from minutes (cyan for small metabolites) to hours (blue for large metabolites), results in

132
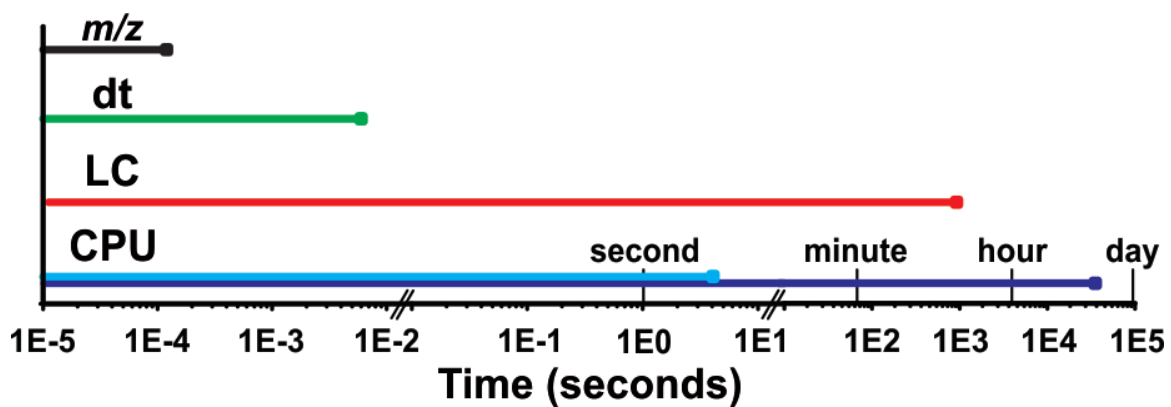
Figure 4.4. Bar graph showing the time required for the experimental separation methods (*m/z* in black, drift time in green, and chip cube liquid chromatography in red) and the distance geometry protocol used to sample the conformational space (cyan for the smallest metabolite and blue for the largest metabolite).

a more favorable time scale for the generation of theoretical CCS values. Additional time is required to obtain an initial starting structure for the distance geometry calculation and for the theoretical CCS calculation for the resulting conformation. The time requirements for various approaches are tabulated in the supplemental materials along with independent data for each of the metabolites analyzed theoretically in this study. Data for protonated species is shown in the supporting information (Figure D.9.A.) and for sodiated species (Figure D.9.B.). Calculation of the theoretical CCS depends greatly on the drift gas and the level of theory used. Although the CPU time plotted in Figure 4.5 and Figure D.9. is not fully encompassing, it more clearly reflects the time required for conformational sampling with distance geometry methods. These additional time requirements may add anywhere from two hours to two days to the calculation. While this increases the time required, initial structure parameterization and *in silico* theoretical CCS measurements are required for any conformational sampling approach in support of IM-MS measurements. Combining the capabilities of chip-based LC, single-field CCS measurements and a distance geometry theoretical CCS method greatly reduces the time required to perform LC-IM-MS with theoretical support. These time advantages reduce resources required to obtain CCS values and increased throughput.

4.4. Conclusions

The integration of a chip-based HPLC to IM-MS methodology for metabolomics analysis has been demonstrated for a series of small molecules in both helium and nitrogen drift gases. First, a database of small molecules were analyzed by direct infusion through a calibration chip prior to IM-MS analysis. These small molecules were

subjected to multi-field CCS measurements as done in traditional drift tube IM-MS CCS studies. Using these values as a basis set to benchmark single-field CCS measurements, the IM-MS experiments supported analyses on the timescale of the LC separation. Single-field CCS measurements were performed in both helium and nitrogen. Small molecules were separated using a small molecule reversed phase chip for LC separation prior to IM-MS analysis. The single-field CCS values were found to have good agreement with the multi-field values supporting this strategy of IM measurements.

The use of single-field CCS allows for the curation CCS values during the time scale of the LC run without requiring replicate analysis at additional drift voltages. With a higher throughput methodology for LC-IM-MS, these efforts may be applied to metabolomics at large. A key advantage of this technology is the additional dimensions IM offers in comparison to traditional LC-MS experiments. Combined, LC-IM-MS provides a four dimensional descriptor (RT, DT, *m/z* and relative intensity) of the features in complex samples. Expansion of peak capacity assists in the search for unique molecular features. These efforts are well suited for discovery of structurally diverse metabolites. Additional advantages of this workflow is the considerable reduction of time as the LC is performed on the order of minutes without the need for subsequent runs at varying drift voltages. The employment of single-field IM analyses reduces the number of runs required, and provides a mean for four-dimensional separations. These separations are further supported by the development of theoretical CCS ranges.

Applying the distance geometry conformational sampling protocol to metabolite compounds proves to be a time efficient method for generating accurate theoretical CCS

ranges. Future studies will aim to gain insight into incongruences between the experimental and theoretical CCS values.

4.5. Associated Content

Supporting Information. A description of the computational methods are reported in section D. 1.1. A discussion of theoretical CCS values is provided (**Sections D 1.2-1.4., Figures D. 1., Table D.1.)** List of all metabolites examined are reported (**Table D.2.**). Empirically measured experimental collision cross section values and theoretical ranges for the analytes evaluated in this work in both nitrogen and helium drift gases (**Tables D.3.-D.4.)**. Chromatographic solvent composition timetables are provided. (**Table D.5.**). Structures of metabolites with respective attached protonated species or coordinating cation species are included (**Figues D.2.-D.7.**). A figured describing the determination of RMSD cutoffs for distance geometry calculations is shown (**Figure D.8.**). Details describing initial parameterization and theoretical CCS calculations are described (**Table D.6.**). CPU time considerations for sampling conformational space are provided (**Figure D.9.**). Sample theoretical computational space plots are also reported (**Figure D.10.**).

4.6. Acknowledgements

This chapter includes the following manuscript in preparation for *Nature Molecular Phenomics*: **Nichole M. Lareau**[*], Sarah M. Stow[*], Terry P. Lybrand, and John A. McLean, " Ion Mobility-Mass Spectrometry Strategies in Support of Small Molecule Analysis: Considerations for Chip-based LC and the Development of Small Molecule

Structural Prediction," In Preparation for *Nature Molecular Phenomics*, 2015 ([*]These authors contributed to an equal extent).

4.7. References

1.   Derewacz, D. K.; Goodwin, C. R.; McNees, C. R.; McLean, J. A.; Bachmann, B. O. Antimicrobial drug resistance affects broad changes in metabolomic phenotype in addition to secondary metabolism. *Proceedings of the National Academy of Sciences* **2013**, 110 (6), 2336-2341.

2.   Dwivedi, P.; Wu, P.; Klopsch, S. J.; Puzon, G. J.; Xun, L.; Hill Jr, H. H. Metabolic profiling by ion mobility mass spectrometry (IMMS). *Metabolomic*s **2008**, 4 (1), 63-80.

3.   Guan, W.; Zhou, M.; Hampton, C. Y.; Benigno, B. B.; Walker, L. D.; Gray, A.; McDonald, J. F.; Fernández, F. M. Ovarian cancer detection from metabolomic liquid chromatography/mass spectrometry data by support vector machines. *BMC Bioinformatics* **2009**, 10 (1), 259.

4.   Bruce, S. J.; Tavazzi, I.; Parisod, V.; Rezzi, S.; Kochhar, S.; Guy, P. A. Investigation of human blood plasma sample preparation for performing metabolomics using ultrahigh performance liquid chromatography/mass spectrometry. *Analytical Chemistry* **2009**, 81 (9), 3285-3296.

5. Vuckovic, D. Current trends and challenges in sample preparation for global metabolomics using liquid chromatography–mass spectrometry. *Analytical and Bioanalytical Chemistry* **2012**, 403 (6), 1523-1548.

6. Lu, X.; Zhao, X.; Bai, C.; Zhao, C.; Lu, G.; Xu, G., LC-MS-based metabonomics analysis. -Analytical Technologies in the Biomedical and Life Sciences, *Journal of Chromatography B,* **2008**, 866 (1-2), 64-76.

7. Metz, T. O.; Zhang, Q.; Page, J. S.; Shen, Y.; Callister, S. J.; Jacobs, J. M.; Smith, R. D., Future of liquid chromatography-mass spectrometry in metabolic profiling and metabolomic studies for biomarker discovery. *Biomarkers in Medicine* **2007**, 1 (1), 159-185.

8. Zimmermann, D.; Hartmann, M.; Nolte, J.; Baumbach, J. I., First detection of metabolites of the colon cancer cell line SW 480 using MCC/IMS and GC/MS. *International Journal of Ion Mobility Spectrometry* **2005**, 8 (2), 3-6.

9. Fenn, L. S., McLean, J. A. Biomolecular Structural Separations by Ion Mobility-Mass Spectrometry. *Analytical Bioanalytical Chemistry*. **2008**, *391*(3): 905-909.

10. Fenn, L. S.; Kliman, M.; Mahsut, A.; Zhao, S. R.; McLean, J. A., Characterizing ion mobility-mass spectrometry conformation space for the analysis of complex biological samples. *Analytical Bioanalytical Chemistry* **2009**, 394 (1), 235-244.

11. Valentine, S. J.; Kulchania, M.; Barnes, C. A. S.; Clemmer, D. E., Multidimensional separations of complex peptide mixtures: a combined high-performance liquid chromatography/ion mobility/time-of-flight mass spectrometry approach. *International Journal of Mass Spectrometry* **2001**, 212 (1-3), 97-109.

12. Lareau, N. M.; May, J. C.; McLean, J. A., Non-derivatized Glycan Analysis by Reverse Phase Liquid Chromatography and Ion Mobility-Mass Spectrometry *Analyst,* **2015**, *140*, 3335-3338.

13. Harry, E. L.; Weston, D. J.; Bristow, A. W. T.; Wilson, I. D.; Creaser, C. S., An approach to enhancing coverage of the urinary metabonome using liquid chromatography-ion mobility-mass spectrometry. *Journal of Chromatography, B: Analytical Technologies in the Biomedical and Life Sciences*, **2008**, 871 (2), 357-361.

14. Sun, J.; Baker, A.; Chen, P., Profiling the indole alkaloids in yohimbe bark with ultra-performance liquid chromatography coupled with ion mobility quadrupole time-of-flight mass spectrometry. *Rapid Communications in Mass Spectrometry* **2011**, 25 (18), 2591-2602.

15. Chan, E. C. Y.; New, L. S.; Yap, C. W.; Goh, L. T., Pharmaceutical metabolite profiling using quadrupole/ion mobility spectrometry/time-of-flight mass spectrometry. *Rapid Communications in Mass Spectrometry* **2009**, 23 (3), 384-394.

16.   Cuyckens, F.; Wassvik, C.; Mortishire-Smith, R. J.; Tresadern, G.; Campuzano, I.; Claereboudt, J., Product ion mobility as a promising tool for assignment of positional isomers of drug metabolites. *Rapid Communications in Mass Spectrometry* **2011**, 25 (23), 3497-3503.

17.   Kaplan, K. A.; Chiu, V. M.; Lukus, P. A.; Zhang, X.; Siems, W. F.; Schenk, J. O.; Hill, H. H., Jr., Neuronal metabolomics by ion mobility mass spectrometry: cocaine effects on glucose and selected biogenic amine metabolites in the frontal cortex, striatum, and thalamus of the rat. *Analytical Bioanalytical Chemistry* **2013**. *405,* (6), 1959-1968.

18.   Dwivedi, P.; Puzon, G.; Tam, M.; Langlais, D.; Jackson, S.; Kaplan, K.; Siems, W. F.; Schultz, A. J.; Xun, L. Y.; Woodsd, A.; Hill, H. H., Metabolic profiling of Escherichia coli by ion mobility-mass spectrometry with MALDI ion source. *Journal of Mass Spectrometry* **2010**, 45 (12), 1383-1393.

29.   Perl, T.; Juenger, M.; Vautz, W.; Nolte, J.; Kuhns, M.; Borg-von, Z. M.; Quintel, M., Detection of characteristic metabolites of Aspergillus fumigatus and Candida species using ion mobility spectrometry - metabolic profiling by volatile organic compounds. *Mycoses* **2011**, 54 (6), e828-e837.

20.   Paglia, G.; Williams, J. P.; Menikarachchi, L.; Thompson, J. W.; Tyldesley-Worster, R.; Halldórsson, S. d.; Rolfsson, O.; Moseley, A.; Grant, D.; Langridge, J. Ion mobility derived collision cross sections to support metabolomics applications. Analytical Chemistry 2014, 86 (8), 3985-3993.

21.   Tang, K.; Shvartsburg, A. A.; Lee, H.-N.; Prior, D. C.; Buschbach, M. A.; Li, F.; Tolmachev, A. V.; Anderson, G. A.; Smith, R. D. High-sensitivity ion mobility spectrometry/mass spectrometry using electrodynamic ion funnel interfaces. *Analytical Chemistry* **2005**, 77 (10), 3330-3339.

22.   May, J. C.; Goodwin, C. R.; Lareau, N. M.; Leaptrot, K. L.; Morris, C. B.; Kurulugama, R. T.; Mordehai, A.; Klein, C.; Barry, W.; Darland, E. Conformational Ordering of Biomolecules in the Gas Phase: Nitrogen Collision Cross Sections Measured on a Prototype High Resolution Drift Tube Ion Mobility-Mass Spectrometer. *Analytical Chemistry* **2014**, 86 (4), 2107-2116.

23.   Buckenmaier, S.; Vollmer, M., Trojer, L. Ultra-high Capacity Small Molecule Chips for the Quantification of Pharmaceuticals Using Triple-quadrupole Mass Spectrometry. Agilent Application Note, publication number 5989-7967EN, **2008**, 1-8.

24.   Stow, S. M.; Goodwin, C. R.; Kliman, M.; Bachmann, B. O.; McLean, J. A.; Lybrand, T. P. Distance Geometry Protocol to Generate Conformations of Natural Products to Structurally Interpret Ion Mobility-Mass Spectrometry Collision Cross Sections. *The Journal of Physical Chemistry B* **2014**, 118 (48), 13812-13820.

CHAPTER 5

CONCLUSIONS AND FUTURE DIRECTIONS FOR ION MOBILITY AND MASS

SPECTROMETRY TECHNOLOGIES IN SUPPORT OF INTEGRATED OMICS

5.1. Summary

The emergence of the fields of integrated omics and systems biology has challenged
traditional analytical techniques, as improved throughput, separation, and sensitivity,
among others were required. Traditionally, complex sample analysis relied greatly on
class-specific methodology run in parallel. For example, proteomic and glycomic
analyses have been processed separately, as compound types vary from amino acid based
peptides to cyclic sugar residues of carbohydrates. Ion mobility and mass spectrometry
techniques challenged these traditionally approaches with an additional dimension of
separation supporting integrated omics analysis.

The separation capabilities of ion mobility combined with mass spectrometry allow
for simultaneous analysis of glycomics and proteomics samples. Compounds that would
be convoluted by potentially occupying the same regions of the mass spectrum are
separated in the IM dimension. The structural diversity that makes selection of a
traditional separation technique challenging is the basis for separation by IM-MS. During
IM-MS analysis, classes of biological molecules occupy different regions of
conformation space. Biological classes differ in their gas-phase packing efficiency and
thus traverse an ion mobility drift cell in relation to their size and charge. The gas-phase

electrophoretic separation of IM is well suited for integration with mass spectrometry as both are rapid gas phase techniques on the timescale of μs and ms, respectively.

Previous applications of IM-MS for carbohydrates, lipids, and metabolites have been described in Chapter I. Cases for incorporating multidimensional separation techniques coupled to IM-MS analysis were also explored. Specifically, multidimensional separation techniques support metabolomics analyses through dereplication in discovery efforts. Methods described in Chapters II-IV were developed to approach the challenges associated with glycomics, proteomics, metabolomics and complex sample analysis as a whole.

Investigations into the ordering of biological classes in conformational space explored peptides, lipids, carbohydrates and alkyl ammonium salts by nitrogen drift gas IM-MS were described in Chapter II. This presented the first comprehensive analysis of biomolecular separations and ordering in 2D IM-MS space for nitrogen gas experiments. As current trends in the IM-MS field are moving from helium based IM studies towards nitrogen based IM studies, this fundamental study lays the groundwork for biological separations using nitrogen. Similar to helium separations, biological classes exhibit packing efficiency trends such that lipids < peptides < carbohydrates. An extensive database of CCS values in nitrogen was presented in Appendix A and summarized in Chapter II. Descriptors of each class were reported and comparisons between drift gases are also addressed in the aforementioned sections.

With descriptors of common biological classes described in Chapter II, Chapter III focused on using the described IM-MS separation capabilities to analyze glycomic and proteomic data simultaneously. A simple liquid chromatography method was developed

for IM-MS analysis of glycans under conditions for peptide analysis. Typically, glycan based LC separations utilize a HILIC or specialized columns, and often require the derivatization of the carbohydrate. Derivatization modifies the structure of the carbohydrate and requires manipulation of the original sample as well as the removal of other biological classes prior to analysis. Similarly, traditional proteomic analyses utilize reverse phase columns, which do not retain carbohydrate as they are eluted with the solvent plug. Chapter II described a method in which a normal phase gradient is applied to a reverse phase column removing the carbohydrates from the solvent plug. IM separation post-analysis allows for the enhancement of the glycan signal by removing the chemical noise. In this manner, LC columns can be used in both glycomic and proteomic analysis, reducing waste, cost, and time required.

Expanding on separation methodology for simultaneous glycomics and proteomics, a series of multimodal fragmentation techniques to elucidate structural detail for glycoproteomics are described in Chapter III. Using the separation power of IM to deconvolute spectra, it was shown that both ETD and CID fragmentation modes could be sequentially activated within the same experiment. Combining ETD and CID allowed for a more comprehensive sequencing of glycoproteins. First, glycans were retained by radically driven ETD fragmentation providing information about the location of the glycan on the protein and peptide backbone. Following ETD fragmentation and IM separation, ions were subjected to a second stage of CID fragmentation. IM supports the deconvolution of spectra such that spectra containing ETD and CID fragments could be analyzed independently. Using this techniques, a glycosylated carcinoembryonic antigen

CGM2 was sequenced by ETD-IM-CID-MS, demonstrating the structural detail provided by from multimodal sequencing supported by IM.

Building on the techniques described in Chapters II and III, Chapter IV discussed the development of chip-based LC-IM-MS techniques for small molecules. These methodologies were designed to support natural product discovery efforts, in search of structurally unique molecules, which often contain peptidic and glycomic motifs. Methods for glycomic and proteomic analyses from previous workflows can be applied to these chip-based methods for a comprehensive analysis of small molecules with structural diversity. Chip-based LC-IM-MS was demonstrated for a series of approximately 50 small molecules. A database of experimental and theoretical CCS values was curated for IM studies in both nitrogen and helium. These descriptors along with retention time, *m/z*, and relative intensity, define each molecular feature for use in dereplication. This was the first example of a four dimensional separation of metabolites on a chip-based LC integrated with a drift tube IM-MS instrument in both nitrogen and helium drift gases. The addition of molecular modeling provided added confidence in the experimental data and presented a new method for comparing experimental and theoretical CCS values.

These workflows described in this dissertation support the separation and analysis of complex samples. In particular, the methodologies presented in this dissertation are well suited for application towards the elucidation of structurally unique small molecules decorated with glycomic and peptide motifs as part of natural product discovery initiatives.

5.2. Future Directions

5.2.1. Conformational Ordering of Biomolecules

Biomolecular class regions of correlation were described for lipids, peptides, carbohydrates and alky-ammonium salts in Chapter II. One key expansion of this research, yet to be explored, is the regions of correlations for interclass biological molecules, such as glycolipids, and peptidoglycans. Understanding the influence of one class on another could assist in prediction regions for post-translational modification work. One such example would be the influence of the addition of a carbohydrate on a peptide in terms of CCS. In order to study this effect, a broad mass range of peptides and proteins would have to be measured both glycosylated and de-glycosylated to determine if there is a statistically significant deviation due to the addition of the carbohydrate motif.

An alternative avenue of research stemming from the conformational ordering studies in Chapter II is the analysis of the coordinating ion to the CCS of the molecule. Preliminary data explored the influence of the coordinating ion on the CCS specifically for carbohydrates. These studies measured ca. 40 carbohydrates on a commercial drift tube IM-MS instrument. A combination of human milk derived glycans and common carbohydrate standards such as maltose sugars have been selected and analyzed on a commercial drift tube based IM-MS instrument. Carbohydrates were analyzed in metal complexes to gleam insight on the influence of sodium, potassium, lithium, rubidium, and cesium, on the observed IM separation. Figure 5.1. depicts the influence of the metal ion on the structure by measure of CCS. By comparing specific ion adducts to the trend of all carbohydrates, the influence can be noted by positive or negative deviation from the

correlation line. Figure 5.1. illustrates the negative deviation from the fit of the cesium-adducted ions. Conversely, lithium-adducted ions have a positive deviation from the fit. The mass of the ion is accounted for when comparing the CCS value. This indicates a trend in which the structure of the carbohydrate collapses in the presence of the cesium ion. Similar trends have been described previously, but were restricted to carbohydrates with at least five rings in a branched structure.[1-3] Here, as few as a three rings follows this trend. An expansion on this dataset with theoretical modeling support would provide a more detailed analysis of the structural impact of the alkali ion. Additional interests may lie with the presence of these alkali metals and other coordinating ions such as calcium and magnesium in relation to biological relevance.

Studies of intraclass or multi-class molecules such as glycopeptides and glycolipids, as well as the student of cation coordination effects on molecular structure are potential future directions of the research described in Chapter II. The analysis of glycopeptides and glycolipids may provide information about predicted regions of these biologically important subclasses. Additionally, the influence of a carbohydrate motif on the CCS of a peptide or protein, as seen in post-translational modifications, may suggest possible changes in the structure of the molecule. The study of the influence of alkali metals on carbohydrate CCS may also provide information structural changes in coordination events.
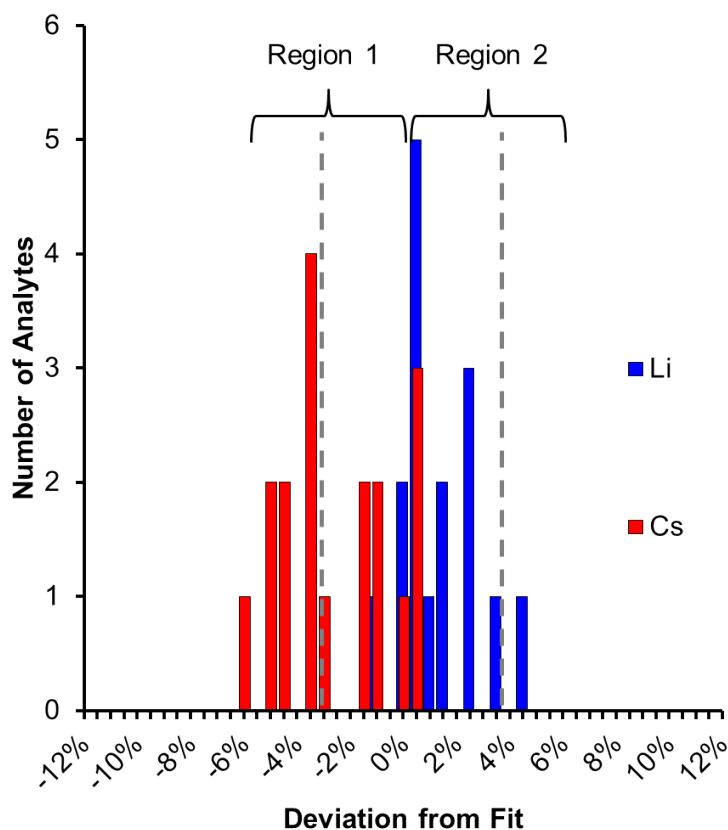
Figure 5.1. Histogram of carbohydrate CCS deviation from a the carbohydrate class fit. A series of ca. 40 carbohydrates were analyzed in six different cation forms: adducted to lithium, potassium, sodium, rubidium, and cesium as well as the protonated form. From this, all 163 ions were plotted in IM-MS space and a power fit equation was used to describe the carbohydrate trend. The histogram above illustrates the influence of the adducted ion on the CCS, accounting for mass of the ion. The cesium ion in red projects data falling in negative deviation from the fit. The lithium ion in blue exhibits positive deviation from the fit.

5.2.2. Approaches for the Separation and Characterization of Glycans

5.2.2.1. A Simple LC-IM-MS Method for the Analysis of Glycans

Methods were developed for simultaneous analysis of glycomics and proteomics by LC-IM-MS. These methods were benchmarked against a series of maltose carbohydrate standards as well as glycans cleaved from bovine fetuin. The subsequent analysis of the peptide fractions in addition to the cleaved glycans would demonstrate further the separation capabilities. Simultaneous trypsin digest to cleave the protein to peptides and treatment with PNGase F to cleave glycans from the peptide backbones would result in free peptides and glycans. The LC-IM-MS method proposed here could be implemented with subsequent fragmentation. This would exploit the separation capabilities as both classes could be analyzed and sequenced.

5.2.2.2. Multimodal Sequencing Supported by Ion Mobility

Chapter III described multimodal sequencing using both ETD and CID fragmentation stages to comprehensively sequence ubiquitin and CGM2. Expanding on these studies, a top-down multimodal sequencing of a larger protein with PTM could benefit from these methodologies. As the PTM would be retained in the ETD mode of fragmentation, the protein backbone could be sequenced. Additionally, the CID post-IM would provide drift time correlated spectra releasing the PTM. Other studies could utilize CID pre-IM to cleave the PTM with post-IM CID to sequence the released PTM molecule. In a similar manner, this workflow may have use for lipidomics in which glycolipids could be treated in a similar manner. For carbohydrate studies, the multimodal sequencing could provide information about structural isomers. ETD

fragmentation would create cross-ring cleavages while the CID fragmentation would cleave at glycosidic linkages.

5.2.4. Methodology and Theory in Support of Small Molecule Analysis

A chip-based LC-IM-MS method was developed in support of small molecule analysis with support of theoretical CCS ranges. The method was applied to curate a database of experimental and theoretical CCS values of small molcules in both helium and nitrogen drift gases. Trends in separation power between the two drift gases has yet to be explored. These molecules could aslo be run with a third drift gas, carbon dioxide, to explore the influence of a collision gas with higher polarization constants. The chip-base LC methods should be applied to samples in a complex matrix to determine the ability of the system to handle potentially dirty compounds. The in-line filter should remove larger particulates prior to the column. A complex matrix would also demonstrate the ability of the LC-IM-MS separation to assist in molecular analysis of samples with larger numbers of features. The technology has the potential to assist in system biology based experiments due to the added dimension of separation afforded by IM to a traditional LC-MS experiment.

5.3. Conclusions

Ion moblity and mass spectrometry based techniques have been explored in support of integrated omics and systems biology. The historical landscape of IM and MS was described with emphasis on figures or merit and utility to biological sample analysis. Specifically, small molecule separation and dereplication benefits from IM-MS based

methods. The ordering of biological classes in confromational space was described. A series of lipids, peptides, carbohydrates and alkyl ammonium salts were analyzed on a high resolution commerical drift tube IM-MS instrument using nitrogen drift gas. These classes were analyzed and described with correlation fits to each class. Focusing on peptides and carbohydrates, a simple LC separation method was developed to analyze carbohydrates on the same platform typically utilized for proteomics studies. In this way, both peptides and glycans can be analyzed on one platform making glycoproteomics accessable to more laboratories. To analyze glycoproteomic molecules with a focus on finer structural detail, multimodal sequencing was developed on an IM-MS platform. The addition of IM to multimodal fragmentation allowed for the deconvolution of ETD fragmentation and subsequent CID fragmentation within one experiment. The combination of techniques provides a more comprehenisve analysis of glycopeptides. Lastly, methods were developed specifically for small molcules with an emphasis on structurally unique metabolites.

The methods described in Chapters II-III focus on approached for glycans and peptides which can be applied to metabolites containing carbohydrate or peptidic motifs. The chip-based LC-IM-MS methods allow for an added dimension of separation from traditional LC-MS metabolomic methods. Using a drift tube IM-MS instrument, CCS values are acquired in both nitrogen and helium drift gases. To further support these efforts, theoretical CCS values are calculated to provide added confidence in the experimental workflow. These descriptors (retention time, drift time, *m/z,* and relative intensity) assist in the dereplication of small molecules. The workflows presented in this dissertation provide a novel mechanism by which IM mediated separation can be utilized

to enhance the analyses of complex biological samples. Combining broad and fine structural studies creates a comprehensive toolbox for the determination of class descriptors and molecular identification. The addition of IM to MS allows for the analysis of multiple classes simultaneously and has the potential to enhance the analysis of metabolomics, glycomics and more generally, complex biological samples in the future. Moreover, these methodologies can be applied to clinical applications for diagnostics and biomarker development. The broad application for these techniques exemplifies the versatility of ion mobility-mass spectrometry.

5.4   References

1.   Angyal, S. J., Complexes of carbohydrates with metals: I. Determination of the extent of complexing by NMR spectroscopy. *Austrailian Jounral of Chemistry,* **1972**, *25*, 1957-1966.

2.   Fenn, L. S.; McLean, J. A., Structural resolution of carbohydrate positional and structural isomers based on gas-phase ion mobility-mass spectrometry. *Physical Chemistry Chemical Physics* **2011,** *13* (6), 2196-2205.

3.   Zhu, F.; Glover, M. S.; Shi, H.; Trinidad, J. C.; Clemmer, D. E., Populations of metal-glycan klhjgructures influence MS fragmentation pattersn. *Journal of the American Society of Mass Spectrometry*, **2015**, *26*, (1) 25-35.

APPENDIX A

REFERENCES OF ADAPTATION FOR CHAPTERS

Chapter I.   Sarah. M. Stow, **Nichole M. Lareau**, Kelly M. Hines, C. Ruth McNees, Cody R. Goodwin, Brian O. Bachmann, John A. McLean, "Structural Separations for Natural Product Characterization by Ion Mobility-Mass Spectrometry: Fundamental Theory to Emerging Applications," Invited chapter for inclusion in "Natural Product Analysis: Instrumentation, Methods, and Applications," Vladimir Havliček and Jaroslav Splžek, Eds. *John Wiley & Sons, Ltd.* 2014.

Chapter II.   Jody C. May, Cody R. Goodwin, **Nichole M. Lareau**, Katrina L. Leaptrot, Caleb C. Morris, Ruwan T. Kurulugama, Alex Mordehai, Christian Klein, William Barry, Ed Darland, Gregor Overney, Kenneth Imatani, George C. Stafford, John C. Fjeldsted, and John A. McLean, "Conformational Ordering of Biomolecules in the Gas-Phase: Nitrogen Collision Cross Sections Measured on a Prototype High Resolution Drift Tube Ion Mobility-Mass Spectrometer," *Analytical Chemistry*, **2014**, *84*, 2107-2016.

Chapter III.   **Nichole M. Lareau**, Jody C. May, and John A. McLean, "Non-derivatized Glycan Analysis by Reverse Phase Liquid Chromatography and Ion Mobility-Mass Spectrometry," *Analyst*, **2015**, *140*, 3335-3338.

Nichole M. Lareau, and John A. McLean, "Multimodal Fragmentation Enhanced by Ion Mobility for Glycoproteomics," In Preparation for *Analytical Chemistry*, 2015.

Chapter IV.   **Nichole M. Lareau**[#], Sarah M. Stow[#], Terry P. Lybrand, and John A. McLean, " Ion Mobility-Mass Spectrometry Strategies in Support of Small Molecule Analysis: Considerations for Chip-based LC and the Development of Small Molecule Structural Prediction," In Preparation for *Nature Molecular Phenomics*, 2016. ([#] Co-first authors)

151

APPENDIX B

SUPPLEMENTARY MATERIALS FOR CHAPTER II

B.1. Supplemental Materials for Ordering of Biomolecules in the Gas Phase

B1.1. Comments Regarding Limits of Precision for the CCS Measurements Presented in this Work

The experimental uncertainty is determined from technical replicates representing a minimum of six measurements of CCS, obtained during separate instrument acquisitions. We consider a parsimonious approach essential when compiling a database, and thus individual CCS measurements which contributed to a percent relative standard deviation (RSD) beyond 0.5% were generally found to be indicative of a poor centroid fit (*i.e.,* multiple peak features or low ion counting statistics) and ultimately were not included in the datasets reported in this manuscript. While all CCS values reported are better than 0.5% in experimental uncertainty, the accuracy associated with the result is a sum of this experimental reproducibility and the uncertainty associated with measuring each experimental parameter. The CCS uncertainty for significant experimental parameters is estimated as follows for the lowest CCS value measured in this work (TAA3, 144 $Å^2$): Pressure ±0.05 Torr (±1.3%), temperature ±1 K (±0.3%), drift voltage ±2.5 V (±0.2%), and time centroid extraction ±0.1 ms (±0.6%), resulting in a total uncertainty of ±1.5%, as propagated through the Mason-Schamp equation. There is good reason to believe that the measurement precision is better than what is estimated in the above example. Thus, the accuracy of all values within the database is estimated to be better than 2%.

B.1.2. Notes on Supplemental Tables

In many cases, lower abundance concomitant species were present in the analytical standards, denoted as *derivative signal* in the tables. Analyte identities for the

derivative signals are putative and based on the mass measurement. No special considerations were made to optimize for accurate mass data, and so the measured mass and associated accuracies reported in the tables are as obtained from the production prototype instrumentation using an offline calibration. CCS and K_0 measurement precision representing experimental reproducibility error (σ) is reported along with the number of measurements (N). The total accuracy of all transport property values (CCS and K_0) is estimated to be better than 2% (refer to the above discussion).

B.1.3. Symbol Key, Definitions, and Associated Equations:

Mass Accuracy – Mass accuracy (in ppm) is calculated from the following expression:

$$Mass\ Accuracy = \frac{Exact\ Mass - Measured\ Mass}{Exact\ Mass} \cdot 10^6$$

K_0 – Reduced mobility (the mobility scaled to standard temperature and pressure), as calculated from the following equation:

$$K_0 = \frac{L^2}{V \cdot t_d}\left(\frac{273.15}{T}\right)\left(\frac{P}{760}\right)$$

Here, L is the drift length (cm), V is the drift voltage (V), t_d is the corrected drift times (s), T is the drift gas temperature (K), and P is the drift gas pressure (Torr). This gives the units of K_0 in V·cm^{-1}·s^{-1}. Reduced mobility values are classically reported for small mass ions, and provided in the following tables for convenience.

CCS – The first approximation solution of the momentum transfer collision cross-section, as calculated from the following equation (the expanded Mason-Schamp relationship, Mason & Schamp 1958):

$$CCS = \left(\frac{3 \cdot Z \cdot e_c}{16 \cdot N}\right) \cdot \left(\frac{2\pi}{k_B \cdot T}\right)^{\frac{1}{2}} \cdot \left(\frac{m_{ion} + m_{gas}}{m_{ion} \cdot m_{gas}}\right)^{\frac{1}{2}} \cdot \left(\frac{V \cdot t_d}{L^2} \cdot \frac{273.15}{T} \cdot \frac{P}{760}\right)$$

Here, Z is the integer charge state of the ion (unitless), e_c is the constant for elementary charge (1.60217657 x 10^{-19} C), N is the gas number density (determined from the ideal gas law, in units of molecules/m^3),k_B is the Boltzmann constant (1.3806488 x 10^{-23} J·K^{-1}), m_{ion} is the ion mass (Da), and m_{gas} is the neutral drift gas masses (N$_2$ in this work, Da), respectively. Other terms are as described previously.

Note that here and by convention, the CCS is reported in units of Å^2 (square angstroms). In order to obtain square angstroms directly from the above calculation, it is necessary to multiply the expression (in m^2) by 10^{-20}, with consideration given for converting the above terms to the proper units: e_c (C), N (molecules/m^3), k_B (J·K^{-1}), T (K), m_{ion} and m_{gas} (kg), V (V), td (s), L (m), and P (Torr).

The CCS expression above is considered a first approximation due to the actual dependency on the cross section on the effective ion temperature (two-temperature theory, Mason & McDaniel 1988, Chapter 6-2-C), which is the gas temperature plus the field-induced ion temperature. In the Agilent IM-MS instrument described in this manuscript, for the smallest ion investigated (TAA3, m/z 186) at the highest drift field utilized (20 V·cm^{-1} at 4 Torr, or *ca.* 15 Td) the field-induced ion temperature is *ca.* 3 K greater than the gas temperature (Wannier 1953). This affects the magnitude of the CCS by less than 0.5% for the ions investigated in this work and so only the drift gas temperature is used for all CCS calculations. For low mass ions where the CCS values are small, incorporating a higher-order (two- or three-temperature) scaling may be significant.

RSD – Relative standard deviation represents the measurement precision (reported as a unitless percentage) and is calculated as follows:

$$RSD = \frac{\sigma}{average} \cdot 100$$

Here, σ is the standard deviation from multiple measurements.

Analyte Source – Can be either from a known *analytical standard*, or as a *derivative signal* which represents a concomitant ion signal that appears in the samples, often at lower abundances than the standard. For example, the TAA salts were analyzed as received with a reported purity of 98%. The instrument sensitivity was high enough to observe additional ions representing differences of CH_2 (m/z 14), which is suggestive of low abundance impurities possessing various alkyl chain lengths. Note that for the lipid samples, the analyte sources were biological extracts purified into specific lipid classes, thus analyte identifications are putatively based on the mass measurement and the expected mobility-mass correlation trends.

B 1.4. Considerations of Fundamental Differences of CCS Measurements in He and Nitrogen Buffer Gas

Due to the commercial availability of electrodynamic IM-MS instruments, many groups currently perform mobility separations in nitrogen. The majority of previously published CCS values have been measured in helium as most homebuilt instruments utilize helium buffer gas. The use of helium based CCS values for the calibration of drift times acquired on a TWIM-MS instrument in a nitrogen buffer gas increases the error associated with the calibrated CCS values obtained.[1] This stems from the differing interaction potentials of helium and nitrogen gases. The use of helium as a buffer gas in a drift region represents the closest experimental approximation to a purely elastic

collision. This allows for the most accurate description of the molecular cross section as the collisions the analyte would experience with the buffer gas would be nearly elastic describing only the size or surface area of the analyte. Contrary to helium, buffer gases such as nitrogen deviate further form the ideal elastic collision as the size of the buffer gas has increased, and parameters such as polarization, charge density and interaction potentials are more influential in the collision.

This trend is visible in a dataset of carbohydrate signals selected across a mass range of about 300-1200 Da plotted in Figure B.1. Figure B.1. (a) depicts the shift in CCS due to the change in buffer gas from helium (yellow data series) to nitrogen (blue data series). The change in CCS as a percentage of the experimental CCS for lactose is 56.22% where as a larger carbohydrate analyte such as β-cyclodextrin deceases to 38.04%. Generally, this deviation decreases with increasing mass. Figure B.1. (b) illustrates the

Calculations were performed to determine the contribution of the size of the buffer gas in the resulting CCS. Additionally, these calculations describe the remaining influence of nitrogen as opposed to helium when accounting for size effects and are illustrated in Figure B.2. A collision cross section was corrected (CCS') by using the Van der Waal's (VDW) radius to calculate the area ($Å^2$) difference between helium and nitrogen buffer gases, where the VDW area was subtracted from the empirical CCS for the respective buffer gas. The contribution of the VDW radius to the CCS is described in Figure B.2. (b). Resulting differences in CCS' values for nitrogen and helium illustrate that the CCS measured is influenced by additional effects such as polarization, impact parameters, and charge density (see Figure B.2. (b)). The resulting difference between

156

nitrogen and helium CCS' values support the necessity of a CCS database obtained from experiments using nitrogen as the contributing parameters are not easily compensated by theoretical calculations or modeling.[2,3] Additionally, a nitrogen based set of CCS standards would improve upon calibration methods for obtaining CCS on a TWIM-MS instrument. The current methods convert drift times measured in nitrogen buffer gas to helium based CCS values. As a result of the transition between buffer gasses, additional error is introduced as the parameters associated with nitrogen are not accounted for in the calibration process.
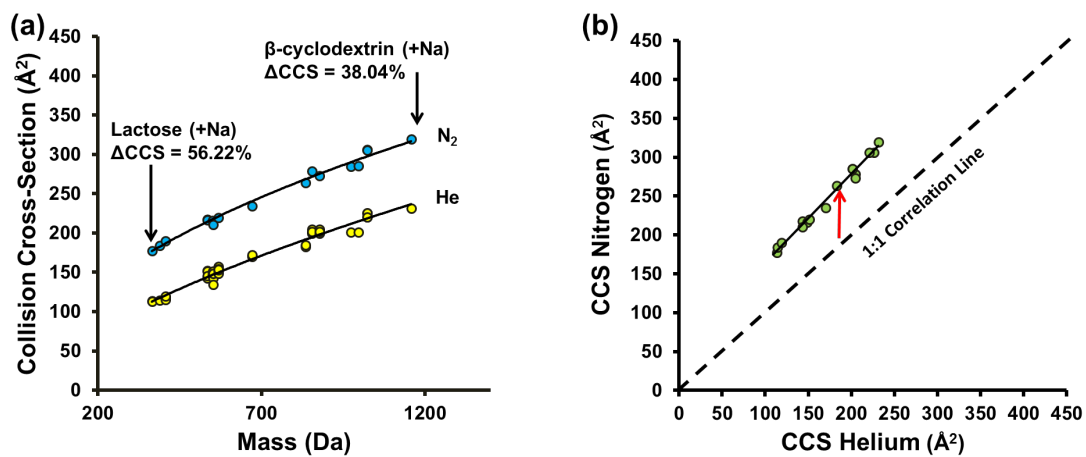
Figure B.1. (a) An IM-MS plot of selected carbohydrate ions measured independently in both helium and nitrogen buffer gases using electrostatic field instruments. There is an average deviation of 45% (±9%) between the helium and nitrogen CCS values for carbohydrates. (b) A comparison plot between CCS measured in helium verses nitrogen. A positive deviation to the central axis is observed.
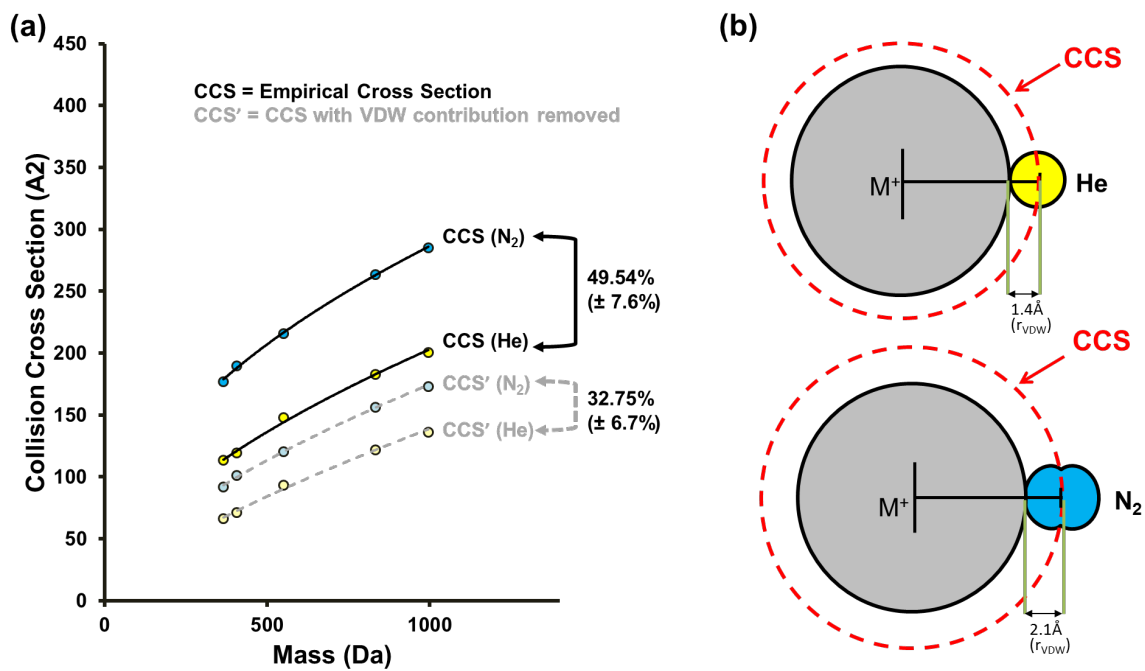
Figure B.2. (a) A 2D IM-MS plot of selected carbohydrate ions across a mass range of 350-1000 Da measured independently in both helium and nitrogen buffer gases where cross sections are calculated by the Mason-Schamp equation. CCS values were corrected for the contribution of the size of the buffer gas using the Van der Waals (VDW) radius resulting in values termed CCS'. (b) A cartoon schematic of fundamental differences of CCS measurements in helium and nitrogen buffer gases.[4] The theoretical CCS illustrated describes the contribution of helium and nitrogen buffer gases based on the VDW radius alone.

Challenges of CCS Measurements from TWIM-MS

Due to the varying electric field applied to the mobility region in TWIM-MS, the Mason-Schamp equation cannot be solved to determine the CCS value from traveling wave data. To mitigate this challenge, several groups have utilized mobility calibration methods.[1,5] Calibration methods commonly convert drift times measured in nitrogen using known CCS values of standards measured in helium. To reduce the error associated with the change in buffer gas, the nitrogen database described above serves as a source for calibrant standards measured in nitrogen. Although both DTIM and TWIM separate based on collisions with a buffer gas, fundamental differences in separation time prevent the use of correction factors.[1] Figure B.3. (a) plots empirical drift times for a series of carbohydrates, where the top series in blue was acquired from an electrostatic field (DTIM) MS instrument and the lower series in green was performed on an electrodynamic (TWIM) MS instrument, both using nitrogen as a buffer gas. The difference in time scale arises mainly from the varied length of the drift cells (78 cm DTIM cell and 25.4 cm TWIM cell). The electrodynamic field data was adjusted by a multiplicative factor in Figure B.3. (b) to illustrate that linear scaling does not align the data sets. It can be noted that the trends of the two series differ in that the electrodynamic field produces a more linear series than that of the electrostatic field data. This characteristic is exemplified in Figure B.3. (c-d) where 5 carbohydrate ions were selected across a mass range of approximately 300-1200 Da. While the molecules are separated in the same order (based on size and charge), the distributions differ due to fundamental differences in the mobility field, and further demonstrate both the challenge and the necessity of mobility calibrations for electrodynamic mobility analyses.
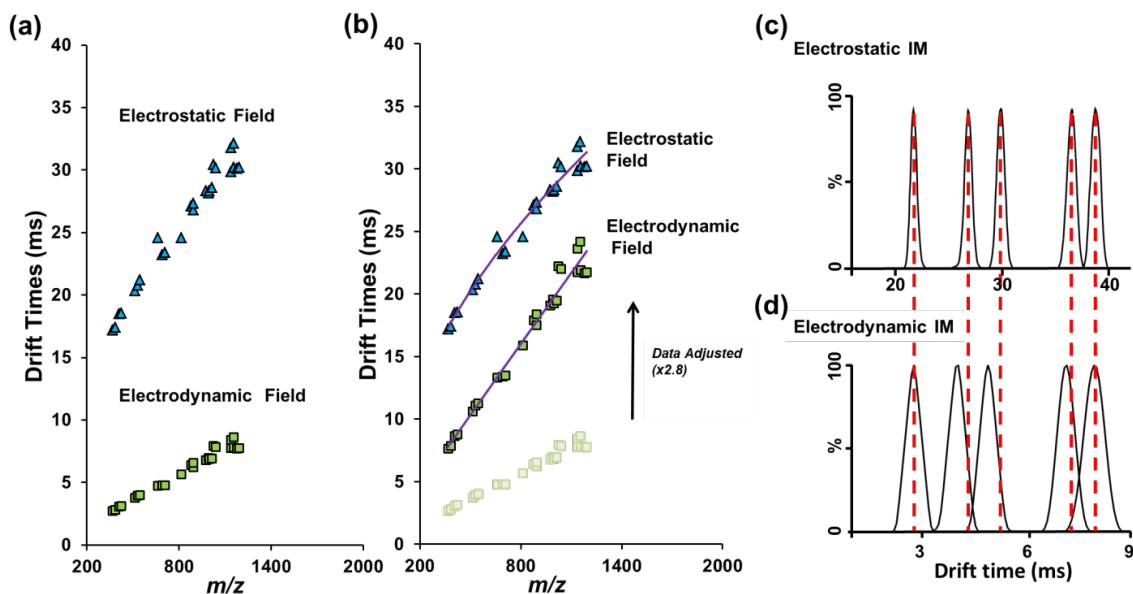
Figure B.3. (a-b) A series of carbohydrates analyzed in both electrostatic and electrodynamic field IM-MS instruments. (a) A plot of the raw drift time data from the two platforms, where the electrostatic field data is represented by blue triangles and the electrodynamic field data by green squares. (b) Plots describing the application of a multiplicative factor of 2.8 to the electrodynamic field drift times to better demonstrate fit shape. In both plots (a) and (b) it can be noted that the electrodynamic field data adopts a more linear fit to the overall trend of the dataset than that of the electrostatic field data. (c-d) Five selected carbohydrate ions across the mass range of approximately 300 to 1200 Da plotted by their drift time chromatograms.

The database summarized in Table B.1 provided a sample set of data for benchmarking a modified calibration method. A series of carbohydrate ions were measured on the TWIM-MS instrument using nitrogen as the buffer gas and the TAA salts as calibrants. Due to differences in solubility, the TAA salt calibrant series is not suitable as an internal calibrant for the carbohydrate mix. Thus, a novel calibration method was developed for this study. TAA salts were intermittently acquired using the G2-S lockspray infusion port. Every 10 seconds, the instrument acquired IM-MS data in a secondary function which was accessed post analysis to measure the drift times of the TAA salts. Alternatively, the TAA salt mixture could be run before or after the sample acquisition. A calibration curve was produced using the drift times of the TAA salts and the CCS values obtained on the DTIM instrument. Table B.1 summarizes CCS values from both electrostatic and electrodynamic IM-MS instruments for 10 selected carbohydrate ions. The series of carbohydrates in Table 2 have an average percent error of 1.2%, which is within the bounds of experimental error.[6] Calibration of the electrodynamic drift time measurements may be further improved by the use of matched (same chemical class) calibrant sets. The CCS values obtained on the electrostatic field instrument provide values for calibration of electrodynamic field instruments for those lacking access to an electrostatic field instrument. Similarly, the peptide and lipid datasets would be well suited for calibration of peptide and lipid based studies, respectively.

References

1.   Bush, M. F.; Campuzano, I. D.; Robinson, C. V. Anal Chem 2012, 84. 7124-30.

2.   Campuzano, I.; Bush, M. F.; Robinson, C., V.; Beaumont, C.; Richardson, K.; Kim, H.; Kim, H. I. Analytical Chemistry 2012, 84.

3.	Mesleh, M. F.; M., H.; Shvartsburg, A. A.; Schatz, G. C.; Jarrold, M. F. The Journal of Physical Chemistry 1996, 100. 16082-16086.

4.	Wyttenbach, T.; Bleiholder, C.; Bowers, M. T. Analytical Chemistry 2013, 85. 2191-2199.

5.	Bush, M. F.; Hall, Z.; Giles, K.; Hoyes, J.; Robinson, C. V.; Ruotolo, B. T. Analytical Chemistry 2010, 82. 9557-9565; Ruotolo, B. T.; Benesch, J. L. P.; Sandercock, A. M.; Hyung, S.-J.; Robinson, C. V. Nature Protocol 2008, 3. 1139-1152; Thalassinos, K.; Grabenauer, M.; Slade, S. E.; Hilton, G. R.; Bowers, M. T.; Scrivens, J. H. Analytical Chemistry 2009, 81. 248-254.

6.	Plasencia, M. D.; Isailovic, D.; Merenbloom, S. I.; Mechref, Y.; Clemmer, D. E. Journal of the American Society for Mass Spectrometry 2008, 19. 1706-1715.

Table B.1. Measured CCS Values for Selected Carbohydrates Compared with Electrodynamic Calibrated CCS Values

		Selected Electrostatic and Electrodynamic CCS Values								
	Lactose (+Na)	HexNAc-Fuc-Hex -H_2O (+H)	Hex_3 (+K)	Hex_4 (+Na)	Lacto-N-Fuco-pentose II (+Na)	HexNAc-Hex_4 (+Na)	HexNAc-Fuc_4-Hex (+Na)	Lacto-N-Difuco-hexaose II (+K)	β-Cyclo-dextrin (+H)	Hex_7 (+K)
Mass [Da]	365.11	512.20	543.13	689.21	876.30	892.27	990.36	1038.33	1135.38	1191.34
CCS (electro-dynamic)[a] [Å²]	173.8 ±0.7 (N=3)	207.0 ±0.4 (N=3)	215.9 ±3.2 (N=2)	233.1 ±0.6 (N=3)	270.8 ±0.7 (N=3)	268.3 ±2.1 (N=2)	281.8 ±0.7 (N=3)	299.1 ±0.2 (N=3)	296.3 ±1.9 (N=3)	296.8 ±0.9 (N=3)
CCS (electro-static)[b] [Å²]	177.4 ±0.8 (N=7)	208.2 ±0.5 (N=16)	216.8 ±0.7 (N=16)	235.3 ±0.5 (N=16)	270.2 ±0.3 (N=7)	268.8 ±1.1 (N=11)	284.1 ±0.7 (N=10)	303.5 ±0.7 (N=14)	301.3 ±0.9 (N=14)	303.4 ±0.5 (N=14)
Percent Error[c] [%]	2.03	0.55	0.39	0.94	0.93	1.04	0.81	1.44	1.65	2.17

[a]Electrodynamic values are derived from calibration with TAA salts using methods from the literature.[20,21] Calibration methods have been adjusted such that agreement between the electrodynamic and electrostatic CCS values is maximized. [b]Electrostatic field CCS values are directly calculated using the Mason-Schamp equation. [c]The percent error is the difference between electrodynamic CCS and the electrostatic CCS as a percentage of the electrostatic CCS.
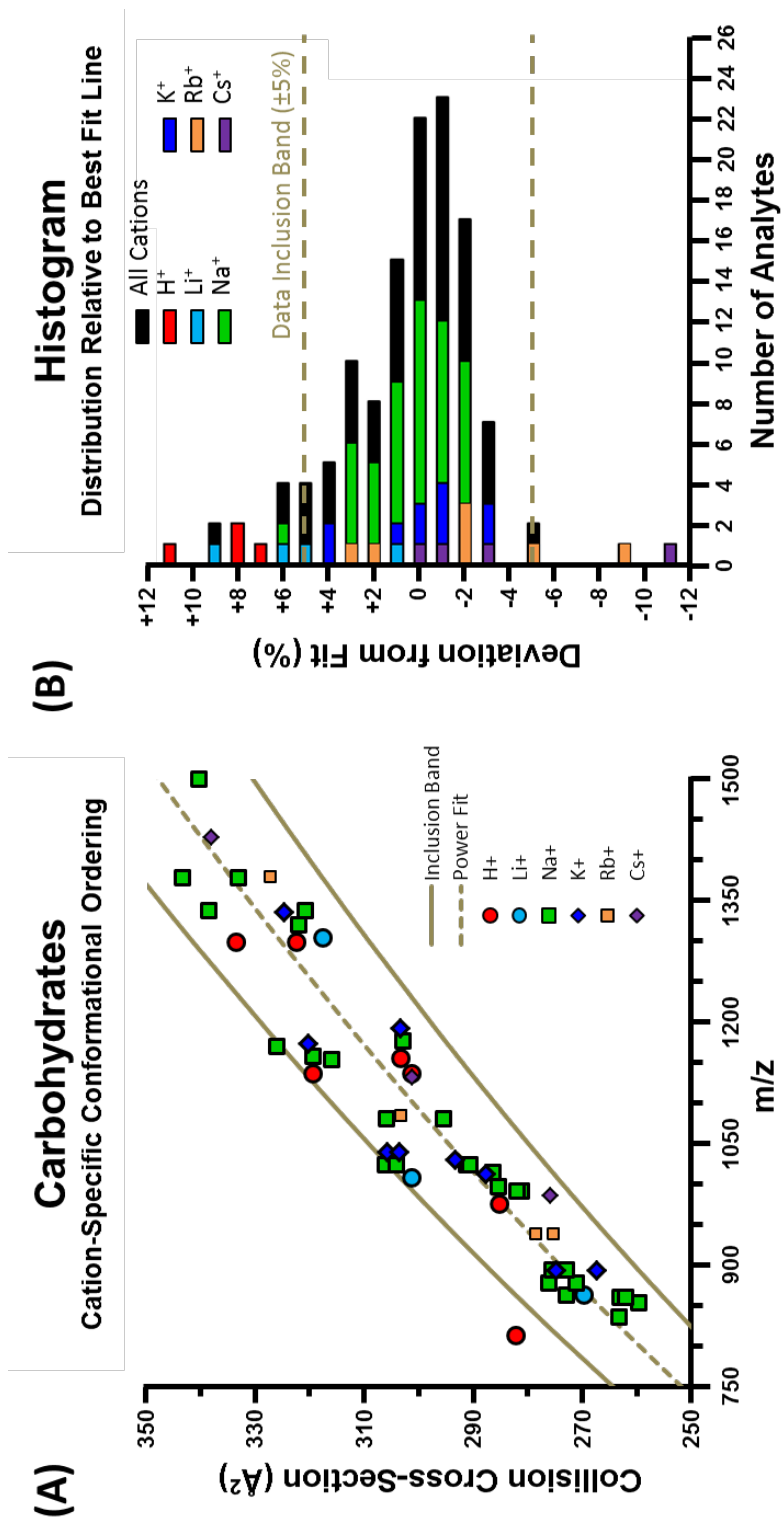
Figure B.4. Cation-Specific Conformational Space Analysis of Carbohydrates
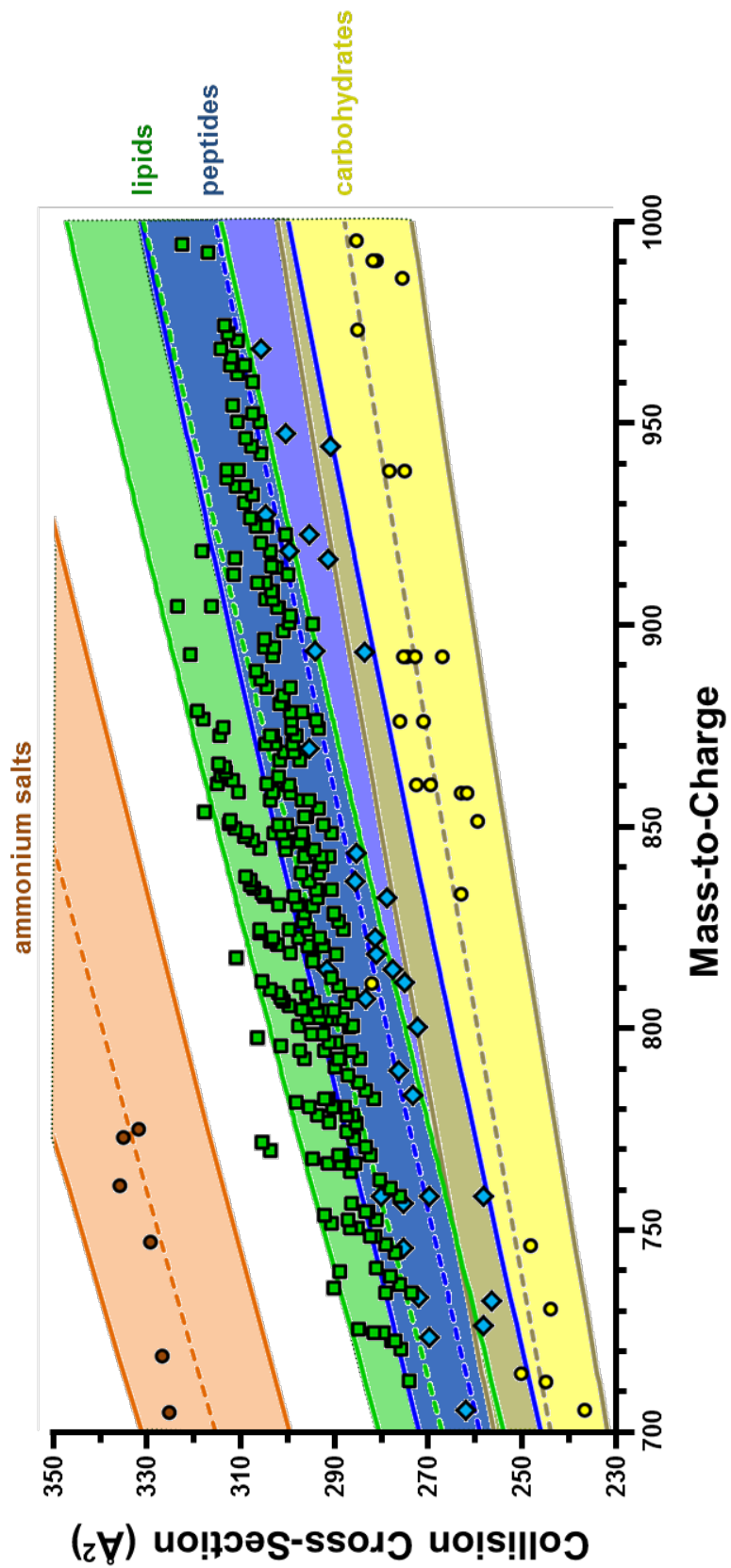
Figure B.5. Class-Specific Mobility-Mass Correlations at Intermediate Mass-to-Charge

Table B.2. – Collision Cross-Section Database of Tetraalkylammonium Salt Cations

Analyte	z	Molecular Formula	Exact m/z	Meas-ured m/z	Mass Accuracy (ppm)	K_0	K_0 σ	CCS	CCS σ	RSD (%)	N	Chemical Class	Analyte Source	Vendor Source
TAA3 - 2H	+	C12H26N	184.21	184.21	-5.0	1.517	0.007	142.8	0.7	0.5%	14	TAA salt	Derivative Signal	
TAA3	+	C12H28N	186.22	186.22	-1.9	1.506	0.010	144.0	0.7	0.5%	23	TAA salt	Analytical Standard	Acros Organics
TAA4 - CH4	+	C15H32N	226.25	226.25	-0.7	1.306	0.005	163.9	0.6	0.3%	16	TAA salt	Derivative Signal	
TAA4 - (CH2) (peak 1)	+	C15H34N	228.27	228.27	-2.7	1.313	0.005	162.9	0.7	0.4%	15	TAA salt	Derivative Signal	
TAA4 - (CH2) (peak 2)	+	C15H34N	228.27	228.27	-2.7	1.326	0.006	161.3	0.7	0.5%	7	TAA salt	Derivative Signal	
TAA4	+	C16H36N	242.28	242.28	-4.8	1.280	0.007	166.6	0.9	0.5%	16	TAA salt	Analytical Standard	Sigma-Aldrich
TAA5 - (CH2)2 - 2H	+	C18H38N	268.30	268.30	1.8	1.166	0.004	181.9	0.6	0.3%	8	TAA salt	Derivative Signal	
TAA5 - (CH2)2	+	C18H40N	270.32	270.32	1.6	1.163	0.005	182.3	0.7	0.4%	16	TAA salt	Derivative Signal	
TAA5 - (CH2)	+	C19H42N	284.33	284.33	-3.2	1.155	0.006	183.2	0.9	0.5%	15	TAA salt	Derivative Signal	
TAA5	+	C20H44N	298.35	298.35	-0.9	1.116	0.003	190.1	1.0	0.5%	28	TAA salt	Analytical Standard	Acros Organics
TAA6 - (CH2)3 - 2H	+	C21H44N	310.34	310.35	4.3	1.046	0.003	201.5	0.7	0.3%	16	TAA salt	Derivative Signal	
TAA6 - (CH2)3	+	C21H46N	312.36	312.36	0.9	1.074	0.004	196.3	0.7	0.4%	16	TAA salt	Derivative Signal	
TAA6 - (CH2)2	+	C22H48N	326.38	326.38	1.7	1.032	0.004	203.7	0.7	0.4%	16	TAA salt	Derivative Signal	
TAA6 - (CH2) - 2H	+	C23H48N	338.37	338.38	-9.3	1.031	0.004	203.8	0.7	0.4%	15	TAA salt	Derivative Signal	
TAA6 - (CH2)	+	C23H50N	340.39	340.40	3.2	1.008	0.002	208.4	0.4	0.2%	16	TAA salt	Derivative Signal	
TAA6 - 2H	+	C24H50N	352.39	352.39	2.3	0.971	0.002	215.4	0.9	0.4%	31	TAA salt	Derivative Signal	
TAA6	+	C24H52N	354.41	354.41	2.1	0.986	0.003	213.5	1.0	0.5%	31	TAA salt	Analytical Standard	Sigma-Aldrich
TAA7 - (CH2)2	+	C26H56N	382.44	382.44	0.8	0.926	0.003	225.8	0.8	0.4%	16	TAA salt	Derivative Signal	
TAA7 - (CH2) (peak 1)	+	C27H58N	396.46	396.45	4.3	0.913	0.004	228.7	1.1	0.5%	15	TAA salt	Derivative Signal	
TAA7 - (CH2) (peak 2)	+	C27H58N	396.46	396.45	4.3	0.910	0.003	229.4	0.9	0.4%	13	TAA salt	Derivative Signal	
TAA7 - 2H	+	C28H58N	408.46	408.46	-1.7	0.898	0.004	232.3	0.8	0.3%	28	TAA salt	Derivative Signal	
TAA7	+	C28H60N	410.47	410.47	-3.3	0.883	0.001	236.4	0.4	0.2%	31	TAA salt	Analytical Standard	Sigma-Aldrich
TAA8 - (CH2)2 - 2H	+	C30H62N	436.49	436.49	-5.3	0.852	0.002	244.4	0.6	0.3%	31	TAA salt	Derivative Signal	
TAA8 - (CH2)2 (peak 1)	+	C30H64N	438.50	438.50	0.8	0.874	0.002	238.3	0.5	0.2%	16	TAA salt	Derivative Signal	
TAA8 - (CH2)2 (peak 2)	+	C30H64N	438.50	438.50	0.8	0.855	0.002	243.6	0.7	0.3%	16	TAA salt	Derivative Signal	

TAA8 - (CH2)	+	C31H66N	452.52	452.52	-2.4	0.827	0.004	251.6	1.2	0.5%	16	16	TAA salt	Derivative Signal	
TAA8 - 2H	+	C32H66N	464.52	464.52	-0.4	0.818	0.003	254.3	0.9	0.4%	16	16	TAA salt	Derivative Signal	
TAA8	+	C32H68N	466.54	466.54	1.4	0.808	0.001	256.6	0.7	0.3%	31	31	TAA salt	Analytical Standard	Acros Organics
TAA10 - (CH2)7	+	C33H70N	480.55	480.55	-3.9	0.791	0.003	262.5	1.1	0.4%	16	16	TAA salt	Derivative Signal	
TAA10 - (CH2)6	+	C34H72N	494.57	494.57	1.7	0.779	0.002	266.6	0.6	0.2%	31	31	TAA salt	Derivative Signal	
TAA10 - (CH2)5	+	C35H74N	508.58	508.58	1.6	0.769	0.002	269.9	0.7	0.3%	31	31	TAA salt	Derivative Signal	
TAA10 - (CH2)4 - 2H	+	C36H74N	520.58	520.58	-0.6	0.781	0.003	265.4	0.9	0.3%	16	16	TAA salt	Derivative Signal	
TAA10 - (CH2)4 (peak 1)	+	C36H76N	522.60	522.60	-0.7	0.793	0.003	260.7	1.2	0.5%	31	31	TAA salt	Derivative Signal	
TAA10 - (CH2)4 (peak 2)	+	C36H76N	522.60	522.60	-0.7	0.754	0.003	275.5	1.0	0.4%	31	31	TAA salt	Derivative Signal	
TAA10 - (CH2)2	+	C38H80N	550.63	550.63	-0.1	0.729	0.002	284.7	0.9	0.3%	28	28	TAA salt	Derivative Signal	
TAA10 - (CH2)	+	C39H82N	564.64	564.64	-2.5	0.711	0.002	290.8	0.6	0.2%	28	28	TAA salt	Derivative Signal	
TAA10	+	C40H84N	578.66	578.66	-8.2	0.702	0.001	293.5	0.7	0.2%	28	28	TAA salt	Analytical Standard	Sigma-Aldrich
TAA12 - (CH2)7	+	C41H86N	592.68	592.66	-2.9	0.697	0.002	296.0	0.8	0.3%	27	27	TAA salt	Derivative Signal	
TAA12 - (CH2)6	+	C42H88N	606.69	606.68	-2.2	0.686	0.003	301.5	1.3	0.4%	28	28	TAA salt	Derivative Signal	
TAA12 - (CH2)4	+	C44H92N	634.72	634.72	-1.0	0.668	0.003	308.6	1.3	0.4%	14	14	TAA salt	Derivative Signal	
TAA12 - (CH2)3	+	C45H94N	648.74	648.74	-1.7	0.649	0.002	317.6	1.2	0.4%	9	9	TAA salt	Derivative Signal	
TAA12 - (CH2)2	+	C46H96N	662.75	662.75	-1.9	0.655	0.002	316.3	1.6	0.5%	22	22	TAA salt	Derivative Signal	
TAA12 - (CH2)	+	C47H98N	676.77	676.77	-0.7	0.641	0.002	320.1	1.5	0.5%	21	21	TAA salt	Derivative Signal	
TAA12	+	C48H100N	690.79	690.79	-3.4	0.644	0.002	319.0	0.9	0.2%	24	24	TAA salt	Analytical Standard	Sigma-Aldrich
TAA16 - (CH2)15	+	C49H102N	704.80	704.80	-1.8	0.627	0.000	325.5	1.6	0.5%	18	18	TAA salt	Derivative Signal	
TAA16 - (CH2)14	+	C50H104N	718.82	718.82	0.1	0.625	0.002	327.2	1.6	0.5%	22	22	TAA salt	Derivative Signal	
TAA16 - (CH2)12	+	C52H108N	746.85	746.85	-1.0	0.624	0.002	329.6	1.0	0.3%	12	12	TAA salt	Derivative Signal	
TAA16 - (CH2)11	+	C53H9N	760.86	760.86	-0.8	0.611	0.003	336.3	1.6	0.5%	9	9	TAA salt	Derivative Signal	
TAA16 - (CH2)10 - 2H	+	C54H9N	772.87	772.86	3.8	0.613	0.002	335.3	1.0	0.3%	11	11	TAA salt	Derivative Signal	
TAA16 - (CH2)10	+	C54H112N	774.88	774.88	-0.2	0.619	0.001	332.1	0.4	0.1%	12	12	TAA salt	Derivative Signal	
TAA16 - (CH2)2	+	C62H128N	887.01	887.00	5.2	0.562	0.002	364.6	1.3	0.4%	9	9	TAA salt	Derivative Signal	
TAA16 - (CH2)	+	C63H11N	901.03	901.02	11.5	0.584	0.002	350.9	1.3	0.4%	8	8	TAA salt	Derivative Signal	
TAA16	+	C64H132N	915.04	915.04	-0.9	0.569	0.004	360.3	0.9	0.2%	25	25	TAA salt	Analytical Standard	Sigma-Aldrich

TAA18 - (CH2)7	+	C65H11N	929.05	929.04	-11.4	0.577	0.003	355.1	1.8	0.5%	10	TAA salt	Derivative Signal	
TAA18 - (CH2)6	+	C66H136N	943.07	943.07	-0.6	0.554	0.002	369.7	1.4	0.4%	10	TAA salt	Derivative Signal	
TAA18 - (CH2)4	+	C68H140N	971.10	971.09	-3.8	0.578	0.002	354.5	1.4	0.4%	6	TAA salt	Derivative Signal	
TAA18 - (CH2)2	+	C70H144N	999.13	999.12	-6.6	0.540	0.002	379.2	1.2	0.3%	6	TAA salt	Derivative Signal	
TAA18	+	C72H148N	1027.16	1027.16	-2.0	0.538	0.002	379.0	1.7	0.3%	6	TAA salt	Analytical Standard	Alfa Aesar
TAA (1064)	+	C75H149N	1064.17	1064.15	-16.0	0.521	0.002	392.7	1.3	0.3%	8	TAA salt	Derivative Signal	
TAA (1120)	+	C79H173N	1120.23	1120.22	-9.9	0.495	0.002	412.8	1.9	0.5%	6	TAA salt	Derivative Signal	
TAA (1232)	+	C87H173N	1232.36	1232.34	-10.2	0.476	0.002	428.6	1.9	0.4%	6	TAA salt	Derivative Signal	

Table B.3. Collision Cross-Section Database of Carbohydrates

Analyte	z	Molecular Formula	Exact m/z	Measured m/z	Mass Accuracy (ppm)	K_0	K_0 σ	CCS	CCS σ	RSD (%)	N	Chemical Class	Analyte Source	Vendor Source
Mannitol	+Li	C6H14O6Li	189.10	189.10	0.8	1.497	0.001	144.5	0.1	0.1%	14	Carbohydrate	Analytical Standard	Sigma-Aldrich
Sorbitol	+H	C6H15O6	189.10	189.09	-6.6	1.470	0.004	147.2	0.4	0.3%	8	Carbohydrate	Analytical Standard	Sigma-Aldrich
Mannitol	+Na	C6H14O6Na	205.07	205.07	-3.4	1.531	0.006	140.6	0.5	0.4%	14	Carbohydrate	Analytical Standard	Sigma-Aldrich
Sorbitol (peak 1)	+Na	C6H14O6Na	205.07	205.07	-6.9	1.544	0.004	139.4	0.3	0.2%	8	Carbohydrate	Analytical Standard	Sigma-Aldrich
(Hex)$_2$ - H$_2$O	+Na	C12H20O10Na	347.10	347.09	-1.9	1.220	0.006	172.0	0.8	0.5%	14	Carbohydrate	Derivative Signal	
Lactose	+Li	C12H22O11Li	349.13	349.13	-3.2	1.126	0.003	186.3	0.5	0.3%	7	Carbohydrate	Analytical Standard	Sigma-Aldrich
Lactose/Mannose Mixture	+Na	C12H22O11Na	365.11	365.11	4.2	1.178	0.005	177.8	0.8	0.4%	15	Carbohydrate	Analytical Standard	Sigma-Aldrich
Lactose	+Na	C12H22O11Na	365.11	365.10	-9.3	1.176	0.002	178.1	0.3	0.1%	8	Carbohydrate	Analytical Standard	Sigma-Aldrich
Lactose/Mannose Mixture	+K	C12H22O11K	381.08	381.08	-1.9	1.155	0.005	181.1	0.8	0.5%	16	Carbohydrate	Analytical Standard	Sigma-Aldrich
HexNAc-Hex - H$_2$O	+Na	C14O10N1H23Na	388.12	388.12	-0.2	1.134	0.004	184.3	0.6	0.3%	16	Carbohydrate	Derivative Signal	
HexNAc-Hex	+Na	C14H25NO11Na	406.13	406.14	6.6	1.097	0.003	190.2	0.5	0.3%	16	Carbohydrate	Derivative Signal	
HexNAc-Hex	+K	C14H25NO11K	422.11	422.11	2.0	1.091	0.003	191.1	0.6	0.3%	16	Carbohydrate	Derivative Signal	
Hex-(Fuc)$_2$ - H$_2$O (peak 1)	+H	C18H31O13	455.18	455.18	2.1	1.071	0.005	194.2	0.9	0.5%	13	Carbohydrate	Derivative Signal	
Hex-(Fuc)$_2$ - H$_2$O (peak 2)	+H	C18H31O13	455.18	455.18	2.1	1.053	0.004	197.6	0.8	0.4%	9	Carbohydrate	Derivative Signal	
Maltotriose	+H	C18H33O16	505.18	505.18	-2.7	0.959	0.005	216.3	1.0	0.5%	14	Carbohydrate	Analytical Standard	Sigma-Aldrich
Melezitose	+H	C18H33O16	505.18	505.18	-0.7	1.023	0.005	202.6	1.0	0.5%	10	Carbohydrate	Analytical Standard	Sigma-Aldrich
(Hex)$_3$ - H$_2$O	+Na	C18H31O15	509.15	509.15	-2.0	1.012	0.003	204.9	0.7	0.3%	16	Carbohydrate	Derivative Signal	
Melezitose	+Li	C18H32O17	511.19	511.18	-0.8	1.022	0.001	202.9	0.3	0.1%	14	Carbohydrate	Analytical Standard	Sigma-Aldrich
HexNAc-Fuc-Hex - H$_2$O	+H	C20H34N1O14	512.20	512.20	-2.4	0.996	0.003	208.2	0.5	0.3%	16	Carbohydrate	Derivative Signal	
Melezitose	+Na	C18H32NaO16	527.16	527.16	-1.7	0.974	0.004	212.8	0.8	0.4%	16	Carbohydrate	Analytical Standard	Sigma-Aldrich

Name	Adduct	Formula												
Maltotriose	+Na	C18H32O16Na	527.16	527.16	1.0	1.022	0.001	202.7	0.2	0.1%	14	Carbohydrate	Analytical Standard	Sigma-Aldrich
Raffinose	+Na	C18H32O16Na	527.16	527.15	-12.9	0.983	0.001	210.7	0.2	0.1%	8	Carbohydrate	Analytical Standard	Sigma-Aldrich
HexNAc-Fuc-Hex - H$_2$O	+Na	C20O14NH33Na	534.18	534.17	-11.9	0.969	0.005	213.7	1.1	0.5%	16	Carbohydrate	Derivative Signal	
Maltotriose	+K	C18H32O16K	543.13	543.13	-2.3	0.955	0.003	216.8	0.7	0.3%	16	Carbohydrate	Analytical Standard	Sigma-Aldrich
melezitose	+K	C18H32KO16	543.13	543.13	-0.8	0.933	0.004	221.9	0.9	0.4%	14	Carbohydrate	Analytical Standard	Sigma-Aldrich
Raffinose	+K	C18H32O16K	543.13	543.13	-13.0	0.973	0.002	212.7	0.3	0.2%	8	Carbohydrate	Analytical Standard	Sigma-Aldrich
HexNAc-(Hex)$_2$ - H$_2$O	+Na	C20H33NO15Na	550.17	550.17	-17.4	0.957	0.005	216.3	1.0	0.5%	15	Carbohydrate	Derivative Signal	
HexNAc-Fuc-Hex	+Na	C20O15NH35Na	552.19	552.18	-16.4	0.969	0.005	213.6	1.1	0.5%	13	Carbohydrate	Derivative Signal	
HexNAc-(Hex)$_2$	+Na	C20H35NO16Na	568.19	568.18	-5.5	0.940	0.004	220.0	1.0	0.5%	16	Carbohydrate	Derivative Signal	
Melezitose (peak 1)	+Rb	C18H32O16Rb	589.08	589.08	-3.3	1.012	0.001	204.1	0.2	0.1%	13	Carbohydrate	Analytical Standard	Sigma-Aldrich
Melezitose (peak 2)	+Rb	C18H32O16Rb	589.08	589.08	-3.3	0.943	0.004	219.2	0.9	0.4%	13	Carbohydrate	Analytical Standard	Sigma-Aldrich
Raffinose (peak 1)	+Rb	C18H32O16Rb	589.08	589.09	23.0	0.945	0.004	218.7	0.9	0.4%	7	Carbohydrate	Analytical Standard	Sigma-Aldrich
Raffinose (peak 2)	+Rb	C18H32O16Rb	589.08	589.09	23.0	0.900	0.003	229.7	0.9	0.4%	7	Carbohydrate	Analytical Standard	Sigma-Aldrich
Melezitose	+Cs	C18H32CsO16	637.07	637.07	-4.6	1.002	0.001	205.8	0.2	0.1%	14	Carbohydrate	Analytical Standard	Sigma-Aldrich
(Hex)$_4$ - H$_2$O	+H	C24H41O20	649.22	649.21	-6.6	0.878	0.004	234.7	1.2	0.5%	15	Carbohydrate	Derivative Signal	
HexNAc-(Fuc)$_2$-Hex - H$_2$O	+H	C26O18NH44	658.26	658.25	-3.5	0.827	0.004	249.3	1.1	0.4%	14	Carbohydrate	Derivative Signal	
Maltotetraose	+H	C24H42O21	667.23	667.23	-5.5	0.865	0.004	238.3	1.2	0.5%	14	Carbohydrate	Analytical Standard	Sigma-Aldrich
(Hex)$_4$ - H$_2$O	+Na	C24O20H40Na	671.20	671.20	-3.5	0.877	0.003	234.8	0.8	0.3%	16	Carbohydrate	Derivative Signal	
HexNAc-(Fuc)$_2$-Hex - H$_2$O	+Na	C26O18NH43Na	680.24	680.23	-14.4	0.858	0.004	240.2	1.1	0.5%	16	Carbohydrate	Derivative Signal	
Maltotetraose	+Na	C24H42O21Na	689.21	689.21	-0.2	0.875	0.002	235.3	0.5	0.2%	16	Carbohydrate	Analytical Standard	Sigma-Aldrich
HexNAc-Fuc-(Hex)$_2$ - H$_2$O	+Na	C26O19NH43Na	696.23	696.23	-8.2	0.845	0.004	243.8	1.2	0.5%	16	Carbohydrate	Derivative Signal	
(Hex)$_4$	+K	C24H42O21K	705.19	705.18	-4.2	0.870	0.003	236.6	0.8	0.3%	16	Carbohydrate	Derivative Signal	
HexNAc-(Hex)$_3$ - H$_2$O	+Na	C26H43N1O20Na	712.23	712.22	-4.9	0.840	0.003	244.9	1.0	0.4%	16	Carbohydrate	Derivative Signal	
HexNAc-Fuc-(Hex)$_2$	+Na	C26O20NH45Na	714.24	714.24	-6.7	0.822	0.004	250.3	1.2	0.5%	16	Carbohydrate	Derivative Signal	
HexNAc-(Hex)$_3$	+Na	C26H45N1O21Na	730.24	730.23	-5.2	0.843	0.002	244.0	0.4	0.2%	16	Carbohydrate	Derivative Signal	

Name	Adduct	Formula	Calc. mass	Obs. mass	ppm							Class	Type	Source
HexNAc-(Hex)$_3$	+K	C26H45N1O21K	746.21	746.21	-9.9	0.829	0.004	248.2	1.1	0.5%	16	Carbohydrate	Derivative Signal	
(Hex)$_5$ - H$_2$O	+H	C30O25H51	811.27	811.27	-7.9	0.727	0.002	282.3	0.7	0.3%	14	Carbohydrate	Derivative Signal	
(Hex)$_5$ - H$_2$O	+Na	C30O25H50Na	833.25	833.25	-7.3	0.780	0.002	263.1	0.8	0.3%	16	Carbohydrate	Derivative Signal	
(Hex)$_5$	+Na	C30O26H52Na	851.26	851.26	-4.7	0.791	0.003	259.5	0.8	0.3%	16	Carbohydrate	Derivative Signal	
HexNAc-Fuc-(Hex)$_3$ - H$_2$O (peak 1)	+Na	C32O24NH53Na	858.29	858.28	-3.6	0.780	0.004	263.1	1.3	0.5%	14	Carbohydrate	Derivative Signal	
HexNAc-Fuc-(Hex)$_3$ - H$_2$O (peak 2)	+Na	C32O24NH53Na	858.29	858.28	-3.6	0.783	0.003	262.0	0.9	0.3%	7	Carbohydrate	Derivative Signal	
HexNAc-(Fuc)$_2$-(Hex)$_2$	+Na	C32O24NH55Na	860.30	860.30	-6.0	0.752	0.004	272.8	1.4	0.5%	16	Carbohydrate	Derivative Signal	
Lacto-N-Fucopentaose I	+Li	C32O25NH55Li	860.32	860.32	-3.6	0.761	0.002	269.6	0.6	0.2%	14	Carbohydrate	Analytical Standard	Dextra Laboratories
Lacto-N-Fucopentaose II	+Na	C32O25NH55Na	876.30	876.29	-12.1	0.756	0.001	271.1	0.3	0.1%	8	Carbohydrate	Analytical Standard	Dextra Laboratories
Lacto-N-Fucopentaose I	+Na	C32O25NH55Na	876.30	876.29	-3.4	0.743	0.001	276.1	0.4	0.1%	13	Carbohydrate	Analytical Standard	Dextra Laboratories
Lacto-N-Fucopentaose II	+K	C32O25NH55K	892.27	892.26	-15.6	0.767	0.002	267.2	0.7	0.3%	8	Carbohydrate	Analytical Standard	Dextra Laboratories
Lacto-N-Fucopentaose I	+K	C32O25NH55K	892.27	892.27	-3.5	0.746	0.001	274.7	0.5	0.2%	14	Carbohydrate	Analytical Standard	Dextra Laboratories
HexNAc-(Hex)$_4$ (peak 1)	+Na	C32O26NH55Na	892.29	892.27	-27.3	0.751	0.004	272.9	1.3	0.5%	16	Carbohydrate	Derivative Signal	
HexNAc-(Hex)$_4$ (peak 2)	+Na	C32O26NH55Na	892.29	892.27	-27.3	0.744	0.002	275.5	0.9	0.3%	16	Carbohydrate	Derivative Signal	
Lacto-N-Fucopentaose II	+Rb	C32O25NH55Rb	938.22	938.21	-11.2	0.736	0.003	278.4	1.0	0.4%	7	Carbohydrate	Analytical Standard	Dextra Laboratories
Lacto-N-Fucopentaose I	+Rb	C32O25NH55Rb	938.22	938.21	-4.5	0.744	0.002	275.2	0.8	0.3%	13	Carbohydrate	Analytical Standard	Dextra Laboratories
Alpha-Cyclodextrin	+H	C36O30H61	973.32	973.32	-3.0	0.718	0.002	285.2	0.8	0.3%	14	Carbohydrate	Analytical Standard	Sigma-Aldrich
Lacto-N-Fucopentaose I	+Cs	C32O25NH55Cs	986.21	986.21	-2.4	0.743	0.003	275.6	0.9	0.3%	14	Carbohydrate	Analytical Standard	Dextra Laboratories
HexNAc-(Fuc)$_4$-Hex (peak 1)	+Na	C38O27NH65Na	990.36	990.35	-17.3	0.728	0.002	281.2	0.7	0.2%	14	Carbohydrate	Derivative Signal	
HexNAc-(Fuc)$_4$-Hex (peak 2)	+Na	C38O27NH65Na	990.36	990.35	-17.3	0.726	0.001	282.1	0.5	0.2%	6	Carbohydrate	Derivative Signal	
Alpha-Cyclodextrin	+Na	C36O30H60Na	995.31	995.31	1.3	0.717	0.001	285.5	0.4	0.1%	14	Carbohydrate	Analytical Standard	Sigma-Aldrich
Lacto-N-Difucohexaose I	+Li	C38H65NO29Li	1006.38	1006.38	-3.4	0.679	0.001	301.4	0.3	0.1%	14	Carbohydrate	Analytical Standard	Dextra Laboratories
Alpha-Cyclodextrin	+K	C36O30H60K	1011.28	1011.28	-3.3	0.711	0.001	287.7	0.6	0.2%	14	Carbohydrate	Analytical Standard	Sigma-Aldrich
Maltohexaose	+Na	C36O31H62Na	1013.32	1013.31	-3.7	0.714	0.002	286.4	0.7	0.2%	14	Carbohydrate	Analytical Standard	Sigma-Aldrich

Name	Adduct	Formula												Source
Lacto-N-Difucohexaose II (peak 1)	+Na	C38H65NO29Na	1022.35	1022.34	-11.9	0.703	0.003	291.2	1.4	0.5%	8	Carbohydrate	Analytical Standard	Dextra Laboratories
Lacto-N-Difucohexaose II (peak 2)	+Na	C38H65NO29Na	1022.35	1022.34	-11.9	0.668	0.001	306.3	0.6	0.2%	8	Carbohydrate	Analytical Standard	Dextra Laboratories
Lacto-N-Difucohexaose I (peak 1)	+Na	C38H65NO29Na	1022.35	1022.35	-2.8	0.704	0.003	290.6	1.3	0.5%	14	Carbohydrate	Analytical Standard	Dextra Laboratories
Lacto-N-Difucohexaose I (peak 2)	+Na	C38H65NO29Na	1022.35	1022.35	-2.8	0.673	0.001	304.2	0.5	0.2%	14	Carbohydrate	Analytical Standard	Dextra Laboratories
Maltohexaose	+K	C36O31H62K	1029.29	1029.29	-4.1	0.698	0.002	293.3	0.6	0.2%	14	Carbohydrate	Analytical Standard	Sigma-Aldrich
Lacto-N-Difucohexaose II	+K	C38H65NO29K	1038.33	1038.31	-13.9	0.669	0.002	305.8	0.8	0.3%	8	Carbohydrate	Analytical Standard	Dextra Laboratories
Lacto-N-Difucohexaose I	+K	C38H65NO29K	1038.33	1038.33	-2.8	0.674	0.001	303.5	0.4	0.1%	14	Carbohydrate	Analytical Standard	Dextra Laboratories
(HexNAc)$_2$-(Hex)$_3$-Fuc (peak 2)	+Na	C40H68N2O30Na	1079.38	1079.37	-3.4	0.692	0.003	295.5	1.4	0.5%	12	Carbohydrate	Derivative Signal	
(HexNAc)$_2$-(Hex)$_3$-Fuc (peak 1)	+Na	C40H68N2O30Na	1079.38	1079.37	-3.4	0.668	0.003	306.0	1.5	0.5%	10	Carbohydrate	Derivative Signal	
Lacto-N-Difucohexaose I	+Rb	C38H65NO29Rb	1084.28	1084.27	-4.4	0.674	0.002	303.2	0.7	0.2%	14	Carbohydrate	Analytical Standard	Dextra Laboratories
Lacto-N-Difucohexaose I	+Cs	C38H65NO29Cs	1132.27	1132.27	-3.5	0.679	0.002	301.2	0.7	0.2%	14	Carbohydrate	Analytical Standard	Dextra Laboratories
Beta-Cyclodextrin (peak 1)	+H	C42O35H71	1135.38	1135.37	-3.9	0.678	0.002	301.3	0.9	0.3%	14	Carbohydrate	Analytical Standard	Sigma-Aldrich
Beta-Cyclodextrin (peak 2)	+H	C42O35H71	1135.38	1135.37	-3.9	0.639	0.002	319.6	1.2	0.4%	12	Carbohydrate	Analytical Standard	Sigma-Aldrich
HexNAc-(Fuc)$_4$-(Hex)$_2$	+Na	C44O32NH75Na	1152.42	1152.40	-15.8	0.646	0.002	316.1	0.9	0.3%	12	Carbohydrate	Derivative Signal	
Maltoheptaose	+H	C42O36H73	1153.39	1153.39	0.1	0.674	0.002	303.3	0.7	0.2%	14	Carbohydrate	Analytical Standard	Sigma-Aldrich
Beta-Cyclodextrin	+Na	C42O35H70Na	1157.36	1157.36	-1.9	0.639	0.000	319.7	0.7	0.2%	11	Carbohydrate	Analytical Standard	Sigma-Aldrich
HexNAc-(Fuc)$_3$-(Hex)$_3$	+Na	C44O33NH75Na	1168.41	1168.41	-3.6	0.626	0.003	326.3	1.5	0.4%	11	Carbohydrate	Derivative Signal	
Beta-Cyclodextrin	+K	C42O35H70K	1173.33	1173.33	1.2	0.638	0.001	320.3	0.5	0.2%	12	Carbohydrate	Analytical Standard	Sigma-Aldrich
Maltoheptaose	+Na	C42O36H72Na	1175.37	1175.37	-0.9	0.674	0.001	303.1	0.5	0.2%	14	Carbohydrate	Analytical Standard	Sigma-Aldrich
Maltoheptaose	+K	C42O36H72K	1191.34	1191.34	-3.6	0.673	0.001	303.4	0.5	0.2%	14	Carbohydrate	Analytical Standard	Sigma-Aldrich
(Hex)$_8$ - H$_2$O	+H	C48H81O40	1297.43	1297.42	-4.5	0.611	0.001	333.8	0.8	0.2%	12	Carbohydrate	Derivative Signal	
Gamma-Cyclodextrin	+H	C48H81O40	1297.43	1297.43	1.2	0.633	0.001	322.6	0.7	0.2%	12	Carbohydrate	Analytical Standard	Sigma-Aldrich
Gamma-Cyclodextrin	+Li	C48H80LiO41	1303.44	1303.44	2.0	0.642	0.001	317.7	0.4	0.1%	12	Carbohydrate	Analytical Standard	Sigma-Aldrich

Name	Adduct	Formula	m/z obs	m/z calc	ppm							Class	Type	Source
Gamma-Cyclodextrin	+Na	C48H80NaO42	1319.41	1319.42	2.1	0.633	0.001	322.1	0.5	0.2%	12	Carbohydrate	Analytical Standard	Sigma-Aldrich
Gamma-Cyclodextrin	+K	C48H80KO43	1335.39	1335.39	1.8	0.628	0.001	324.8	0.5	0.2%	12	Carbohydrate	Analytical Standard	Sigma-Aldrich
(Hex)$_8$ (peak 1)	+Na	C48O41H82Na	1337.42	1337.42	-2.0	0.636	0.003	320.9	1.3	0.4%	7	Carbohydrate	Derivative Signal	
(Hex)$_8$ (peak 2)	+Na	C48O41H82Na	1337.42	1337.42	-2.0	0.602	0.001	338.8	0.7	0.2%	10	Carbohydrate	Derivative Signal	
HexNAc-(Hex)$_7$ (peak 1)	+Na	C50H85N1O41Na	1378.45	1378.45	-1.5	0.612	0.003	333.4	1.7	0.5%	11	Carbohydrate	Derivative Signal	
HexNAc-(Hex)$_7$ (peak 2)	+Na	C50H85N1O41Na	1378.45	1378.45	-1.5	0.593	0.001	343.7	0.8	0.2%	10	Carbohydrate	Derivative Signal	
Gamma-Cyclodextrin	+Rb	C48H80O44Rb	1381.33	1381.33	-0.3	0.623	0.001	327.3	0.6	0.2%	12	Carbohydrate	Analytical Standard	Sigma-Aldrich
Gamma-Cyclodextrin	+Cs	C48H80CsO45	1429.33	1429.33	-1.3	0.603	0.001	338.2	0.6	0.2%	10	Carbohydrate	Analytical Standard	Sigma-Aldrich
(Hex)$_9$ - H$_2$O	+H	C54H91O45	1459.48	1459.48	-0.3	0.577	0.002	353.3	1.2	0.4%	10	Carbohydrate	Derivative Signal	
(Hex)$_9$ (peak 1)	+Na	C54H92O46Na	1499.48	1499.48	-0.4	0.598	0.003	340.5	1.6	0.5%	10	Carbohydrate	Derivative Signal	
(Hex)$_9$ (peak 2)	+Na	C54H92O46Na	1499.48	1499.48	-0.4	0.579	0.002	351.9	1.5	0.4%	10	Carbohydrate	Derivative Signal	
HexNAc-(Hex)$_8$	+H	C56H96N1O46	1518.52	1518.52	-3.4	0.586	0.003	347.8	1.5	0.4%	10	Carbohydrate	Derivative Signal	
HexNAc-(Hex)$_8$ (peak 1)	+Na	C56H95N1O46Na	1540.50	1540.50	-0.5	0.575	0.003	354.2	1.7	0.5%	10	Carbohydrate	Derivative Signal	
HexNAc-(Hex)$_8$ (peak 2)	+Na	C56H95N1O46Na	1540.50	1540.50	-0.5	0.579	0.003	351.6	1.5	0.4%	8	Carbohydrate	Derivative Signal	
(Hex)$_{10}$ - H$_2$O	+H	C60H101O50	1621.54	1621.54	0.8	0.531	0.001	383.4	0.9	0.2%	8	Carbohydrate	Derivative Signal	
HexNAc-(Fuc)$_2$-(Hex)$_7$ - H$_2$O	+H	C62H104N1O48	1630.57	1630.58	6.0	0.556	0.001	366.1	0.8	0.2%	10	Carbohydrate	Derivative Signal	
(Hex)$_{10}$ (peak 1)	+H	C60H103O51	1639.55	1639.55	2.2	0.558	0.002	365.1	1.4	0.4%	9	Carbohydrate	Derivative Signal	
(Hex)$_{10}$ (peak 2)	+H	C60H103O51	1639.55	1639.55	2.2	0.522	0.001	390.3	0.8	0.2%	8	Carbohydrate	Derivative Signal	
(Hex)$_{10}$ (peak 1)	+Na	C60H102O51Na	1661.53	1661.53	3.3	0.558	0.002	365.1	1.3	0.4%	10	Carbohydrate	Derivative Signal	
(Hex)$_{10}$ (peak 2)	+Na	C60H102O51Na	1661.53	1661.53	3.3	0.545	0.002	373.8	1.1	0.3%	8	Carbohydrate	Derivative Signal	
(Hex)$_{11}$ - H$_2$O	+H	C66H111O55	1783.59	1783.60	8.0	0.537	0.002	379.1	1.5	0.4%	6	Carbohydrate	Derivative Signal	
(Hex)$_{11}$	+Li	C66H112O56Li	1807.61	1807.59	-11.4	0.546	0.002	372.4	1.1	0.3%	8	Carbohydrate	Derivative Signal	
(Hex)$_{11}$	+Na	C66H112O56Na	1823.58	1823.60	8.9	0.529	0.002	384.6	1.4	0.4%	8	Carbohydrate	Derivative Signal	
(Hex)$_{11}$ (peak 1)	+K	C66H112O56K	1839.56	1839.53	-12.9	0.554	0.002	367.4	1.6	0.4%	7	Carbohydrate	Derivative Signal	
(Hex)$_{11}$ (peak 2)	+K	C66H112O56K	1839.56	1839.53	-12.9	0.550	0.002	369.7	1.4	0.4%	8	Carbohydrate	Derivative Signal	
(Hex)$_{11}$ (peak 1)	+Rb	C66H112O56Rb	1885.50	1885.48	-13.8	0.556	0.002	365.7	1.3	0.4%	8	Carbohydrate	Derivative Signal	
(Hex)$_{11}$ (peak 2)	+Rb	C66H112O56Rb	1885.50	1885.48	-13.8	0.546	0.002	372.5	1.5	0.4%	6	Carbohydrate	Derivative Signal	

(Hex)$_{12}$ - H$_2$O (peak 1)	+H	C72H121O60	1945.64	1945.65	6.5	0.508	0.001	400.3	0.6	0.1%	8	Carbohydrate	Derivative Signal
(Hex)$_{12}$ - H$_2$O (peak 2)	+H	C72H121O60	1945.64	1945.65	6.5	0.481	0.001	422.9	1.3	0.3%	6	Carbohydrate	Derivative Signal
(Hex)$_{12}$ - H$_2$O (peak 1)	+Na	C72H120O60Na	1967.62	1967.63	5.4	0.520	0.001	390.6	0.9	0.2%	8	Carbohydrate	Derivative Signal
(Hex)$_{12}$ - H$_2$O (peak 2)	+Na	C72H120O60Na	1967.62	1967.63	5.4	0.496	0.002	410.0	1.4	0.4%	6	Carbohydrate	Derivative Signal
(Hex)$_{13}$ (peak 1)	+Na	C78H132O66Na	2147.69	2147.72	13.6	0.504	0.001	402.7	1.0	0.2%	6	Carbohydrate	Derivative Signal
(Hex)$_{13}$ (peak 2)	+Na	C78H132O66Na	2147.69	2147.72	13.6	0.494	0.001	411.6	1.1	0.3%	6	Carbohydrate	Derivative Signal

175

Table B.4. Collision Cross-Section Database of Peptides

Analyte	z	Molecular Formula	Exact m/z	Measured m/z	Mass Accuracy (ppm)	K_0	K_0 σ	CCS	CCS σ	RSD (%)	N	Chemical Class	Analyte Source	Vendor Source	Source Protein
DGDK	+H	C16H28N5O9	434.19	434.19	12.9	1.064	0.004	195.8	0.7	0.3%	7	Peptide	Analytical Standard	Waters	ENOLASE_YST
YVR	+H	C20H33N6O5	437.25	437.25	-1.8	1.006	0.002	207.0	0.4	0.2%	8	Peptide	Analytical Standard	Waters	ADH_YST
DVCK	+H	C18H34N5O7S	464.22	464.22	-2.2	1.016	0.004	204.7	0.7	0.4%	7	Peptide	Analytical Standard	Waters	ALBUMIN_BOV
WIR	+H	C23H36N7O4	474.28	474.27	-17.3	0.964	0.003	215.4	0.7	0.3%	8	Peptide	Analytical Standard	Waters	PHOSPH_RAB
GVFR	+H	C22H36N7O5	478.28	478.28	-1.0	0.967	0.001	214.8	0.3	0.1%	7	Peptide	Analytical Standard	Waters	ENOLASE_YST
SDGRG	+H	C17H31N8O9	491.22	491.22	-1.4	1.015	0.003	204.6	0.5	0.3%	11	Peptide	Analytical Standard	Sigma-Aldrich	SYNTHETIC
GRGDS	+H	C17H31N8O9	491.22	491.22	-1.4	1.008	0.001	205.9	0.2	0.1%	14	Peptide	Analytical Standard	Sigma-Aldrich	SYNTHETIC
FGER	+H	C22H34N7O7	508.25	508.24	-13.2	0.955	0.002	217.1	0.4	0.2%	8	Peptide	Analytical Standard	Waters	ENOLASE_YST
VYAR	+H	C23H38N7O6	508.29	508.29	-0.8	0.912	0.001	227.2	0.3	0.1%	7	Peptide	Analytical Standard	Waters	PHOSPH_RAB
SDGRG	+Na	C17H30N8O9Na	513.20	513.20	-4.5	1.018	0.002	203.5	0.5	0.2%	11	Peptide	Analytical Standard	Sigma-Aldrich	SYNTHETIC
GRGDS	+Na	C17H30N8O9Na	513.20	513.20	-4.5	0.996	0.002	208.2	0.3	0.2%	14	Peptide	Analytical Standard	Sigma-Aldrich	SYNTHETIC
ADLAK	+H	C22H41N6O8	517.30	517.30	5.2	0.908	0.004	228.3	1.1	0.5%	7	Peptide	Analytical Standard	Waters	ALBUMIN_BOV
QENK	+H	C20H36N7O9	518.26	518.26	-1.0	0.946	0.003	219.0	0.6	0.3%	6	Peptide	Analytical Standard	Waters	PHOSPH_RAB
MVIR	+H	C22H44N7O5S	518.31	518.31	0.0	0.906	0.001	228.7	0.3	0.1%	7	Peptide	Analytical Standard	Waters	PHOSPH_RAB
WMGK	+H	C24H37N6O5S	521.25	521.26	8.1	0.941	0.002	220.1	0.5	0.2%	7	Peptide	Analytical Standard	Waters	ENOLASE_YST
SDGRG	+K	C17H30N8O9K	529.18	529.17	5.2	1.009	0.004	205.4	0.8	0.4%	10	Peptide	Analytical Standard	Sigma-Aldrich	SYNTHETIC
GRGDS	+K	C17H30N8O9K	529.18	529.18	5.2	0.984	0.001	210.4	0.2	0.1%	14	Peptide	Analytical Standard	Sigma-Aldrich	SYNTHETIC
FWGK	+H	C28H37N6O5	537.28	537.28	-5.4	0.896	0.003	231.0	0.8	0.3%	7	Peptide	Analytical Standard	Waters	ALBUMIN_BOV

Peptide	Adduct	Formula													Protein
VASLR	+H	C23H45N8O7	545.34	545.34	-0.9	0.890	0.001	232.5	0.3	0.1%	7	Peptide	Analytical Standard	Waters	ALBUMIN_BOV
QENK	+H	C25H41N8O6	549.31	549.31	-1.3	0.889	0.001	232.8	0.3	0.1%	7	Peptide	Analytical Standard	Waters	PHOSPH_RAB
NFNR	+H	C23H36N9O7	550.27	550.27	-1.1	0.920	0.002	225.0	0.6	0.3%	7	Peptide	Analytical Standard	Waters	PHOSPH_RAB
LEYK	+H	C26H42N5O8	552.30	552.30	-1.6	0.863	0.003	239.6	0.9	0.4%	7	Peptide	Analytical Standard	Waters	ADH_YST
FQNK	+Na	C24H38N7O7Na	559.27	559.27	-2.1	0.848	0.005	243.9	1.4	0.6%	5	Peptide	Analytical Standard	Waters	PHOSPH_RAB
FQNK	+Na	C23H44N7O8Na	569.31	569.31	-2.5	0.945	0.002	218.9	0.6	0.3%	7	Peptide	Analytical Standard	Waters	ENOLASE_YST
EWTR	+H	C26H39N8O8	591.29	591.29	-3.2	0.885	0.001	233.4	0.4	0.2%	7	Peptide	Analytical Standard	Waters	PHOSPH_RAB
AMGYR	+H	C25H41N8O7S	597.28	597.28	-2.0	0.843	0.001	245.0	0.3	0.1%	7	Peptide	Analytical Standard	Waters	ADH_YST
QISVR	+H	C25H48N9O8	602.36	602.36	-3.2	0.855	0.001	241.4	0.3	0.1%	7	Peptide	Analytical Standard	Waters	PHOSPH_RAB
LWSAK	+H	C29H46N7O7	604.34	604.35	-1.8	0.865	0.001	238.6	0.3	0.1%	7	Peptide	Analytical Standard	Waters	PHOSPH_RAB
AFDEK	+H	C27H41N6O10	609.29	609.29	-1.1	0.867	0.001	238.3	0.3	0.1%	7	Peptide	Analytical Standard	Waters	ALBUMIN_BOV
FSSDR	+H	C25H39N8O10	611.28	611.28	-2.9	0.870	0.001	237.3	0.3	0.1%	7	Peptide	Analytical Standard	Waters	PHOSPH_RAB
FVVPR (peak 1)	+H	C30H49N8O6	617.37	617.38	-3.6	0.810	0.002	254.7	0.7	0.3%	7	Peptide	Analytical Standard	Waters	PHOSPH_RAB
FVVPR (peak2)	+H	C30H49N8O6	617.37	617.38	-3.6	0.828	0.001	249.3	0.4	0.1%	7	Peptide	Analytical Standard	Waters	PHOSPH_RAB
GQIVGR	+H	C26H49N10O8	629.37	629.37	-2.1	0.840	0.001	245.5	0.3	0.1%	7	Peptide	Analytical Standard	Waters	ADH_YST
VSLAEK	+H	C28H52N7O10	646.38	646.38	-2.6	0.828	0.001	249.0	0.3	0.1%	7	Peptide	Analytical Standard	Waters	PHOSPH_RAB
IETMR or CASIQK	+H	C26H49N8O9S	649.33	649.33	-3.4	0.815	0.001	252.8	0.4	0.2%	7	Peptide	Analytical Standard	Waters	ALBUMIN_BOV
AAGHDGK	+H	C26H43N10O10	655.32	655.32	1.1	0.828	0.002	249.0	0.5	0.2%	7	Peptide	Analytical Standard	Waters	ENOLASE_YST
NVATPR	+H	C27H49N10O9	657.37	657.37	-3.8	0.811	0.001	254.0	0.3	0.1%	7	Peptide	Analytical Standard	Waters	PHOSPH_RAB
ANIDVK	+H	C28H51N8O10	659.37	659.37	-3.2	0.831	0.001	248.1	0.4	0.2%	7	Peptide	Analytical Standard	Waters	ENOLASE_YST
VSALYK (peak 1)	+H	C32H54N7O9	680.40	680.40	-2.1	0.787	0.001	261.8	0.3	0.1%	7	Peptide	Analytical Standard	Waters	PHOSPH_RAB
VSALYK (peak 2)	+H	C32H54N7O9	680.40	680.40	-2.1	0.811	0.001	254.0	0.4	0.2%	7	Peptide	Analytical Standard	Waters	PHOSPH_RAB

Peptide	Charge	Formula	m/z obs	m/z calc	ppm							Type	Standard	Vendor	Protein
IHEYK	+H	C32H49N8O9	689.36	689.37	10.6	0.797	0.001	258.5	0.2	0.1%	7	Peptide	Analytical Standard	Waters	PHOSPH_RAB
NIATSGK	+H	C28H52N9O11	690.38	690.38	-3.3	0.801	0.001	257.2	0.3	0.1%	8	Peptide	Analytical Standard	Waters	PHOSPH_RAB
EELFR	+H	C31H49N8O10	693.36	693.35	-2.6	0.810	0.001	254.1	0.3	0.1%	8	Peptide	Analytical Standard	Waters	ADH_YST
DHLVGR	+H	C29H50N11O9	696.38	696.38	-5.2	0.826	0.002	249.4	0.6	0.2%	8	Peptide	Analytical Standard	Waters	PHOSPH_RAB
TVMIGGK	+H	C30H57N8O9S	705.40	705.40	-1.0	0.785	0.001	262.2	0.4	0.2%	7	Peptide	Analytical Standard	Waters	PHOSPH_RAB
GVLHAVK	+H	C33H59N10O8	723.45	723.45	-1.9	0.762	0.001	269.9	0.4	0.2%	7	Peptide	Analytical Standard	Waters	ENOLASE_YST
SVYDSR	+H	C30H48N9O12	726.34	726.34	-2.1	0.796	0.002	258.4	0.6	0.2%	7	Peptide	Analytical Standard	Waters	ENOLASE_YST
VEDVDR	+H	C29H50N9O13	732.35	732.35	-4.1	0.801	0.001	256.6	0.5	0.2%	8	Peptide	Analytical Standard	Waters	PHOSPH_RAB
NVPLYK	+H	C35H57N8O9	733.42	733.42	-5.5	0.756	0.001	272.2	0.4	0.1%	7	Peptide	Analytical Standard	Waters	ENOLASE_YST
QPDLFK	+H	C33H61N8O11	745.45	745.44	-1.9	0.746	0.001	275.5	0.3	0.1%	7	Peptide	Analytical Standard	Waters	ENOLASE_YST
LNQLLR	+H	C33H62N11O9	756.47	756.47	-2.1	0.746	0.001	275.6	0.4	0.1%	7	Peptide	Analytical Standard	Waters	ENOLASE_YST
TNGITPR (peak 1)	+H	C31H56N11O11	758.42	758.41	-1.8	0.733	0.001	280.4	0.3	0.1%	7	Peptide	Analytical Standard	Waters	PHOSPH_RAB
TNGITPR (peak 2)	+H	C31H56N11O11	758.42	758.41	-1.8	0.762	0.001	269.8	0.5	0.2%	7	Peptide	Analytical Standard	Waters	PHOSPH_RAB
TNGITPR (peak 3)	+H	C31H56N11O11	758.42	758.41	-1.8	0.795	0.001	258.4	0.4	0.1%	7	Peptide	Analytical Standard	Waters	PHOSPH_RAB
HLADLSK	+H	C34H59N10O11	783.44	783.43	-4.6	0.752	0.001	273.3	0.5	0.2%	6	Peptide	Analytical Standard	Waters	ENOLASE_YST
LVTDLTK	+H	C35H65N8O12	789.47	789.47	-2.5	0.743	0.001	276.6	0.5	0.2%	7	Peptide	Analytical Standard	Waters	ALBUMIN_BOV
YDLDFK	+H	C38H54N7O12	800.38	800.38	-3.6	0.754	0.001	272.4	0.5	0.2%	7	Peptide	Analytical Standard	Waters	ENOLASE_YST
TFAEALR	+H	C36H59N10O11	807.44	807.43	-1.6	0.724	0.001	283.5	0.5	0.2%	7	Peptide	Analytical Standard	Waters	ENOLASE_YST
YVVDTSK	+H	C36H59N8O13	811.42	811.42	-1.5	0.746	0.001	275.2	0.3	0.1%	7	Peptide	Analytical Standard	Waters	ADH_YST
AADALLLK or DIVGAVLK	+H	C37H68N9O11	814.50	814.50	-0.4	0.704	0.001	291.8	0.4	0.1%	7	Peptide	Analytical Standard	Waters	ENOLASE_YST or ADH_YST
AADALLLK or DIVGAVLK	+H	C37H68N9O11	814.50	814.50	-0.4	0.739	0.001	277.8	0.3	0.1%	7	Peptide	Analytical Standard	Waters	ENOLASE_YST or ADH_YST
ATEEQLK	+H	C34H60N9O14	818.43	818.42	-2.3	0.730	0.001	281.3	0.5	0.2%	7	Peptide	Analytical Standard	Waters	ALBUMIN_BOV

Peptide	Charge	Formula	m/z (calc)	m/z (obs)	ppm							Type		Vendor	Protein
TIAQYAR	+H	C36H60N11O11	822.45	822.45	-2.1	0.729	0.001	281.6	0.5	0.2%	7	Peptide	Analytical Standard	Waters	PHOSPH_RAB
AWEVTVK	+H	C39H62N9O11	832.46	832.45	-4.2	0.736	0.000	279.0	0.7	0.2%	7	Peptide	Analytical Standard	Waters	PHOSPH_RAB
IGDYAGIK	+H	C38H62N9O12	836.45	836.45	-0.6	0.718	0.001	285.9	0.3	0.1%	6	Peptide	Analytical Standard	Waters	ADH_YST
VLVDLER	+H	C37H67N10O12	843.49	843.49	-1.1	0.718	0.001	285.7	0.4	0.1%	7	Peptide	Analytical Standard	Waters	PHOSPH_RAB
FAAYLER	+H	C41H61N10O11	869.45	869.45	-1.4	0.694	0.001	295.5	0.4	0.1%	7	Peptide	Analytical Standard	Waters	PHOSPH_RAB
YGNPWEK	+H	C42H57N10O12	893.42	893.41	-4.1	0.722	0.001	283.8	0.6	0.2%	7	Peptide	Analytical Standard	Waters	PHOSPH_RAB
DIPVPKPK	+H	C42H73N10O11	893.55	893.54	-2.4	0.697	0.002	294.2	0.7	0.2%	7	Peptide	Analytical Standard	Waters	ADH_YST
NLAENISR	+H	C37H66N13O14	916.48	916.48	-2.1	0.703	0.001	291.7	0.6	0.2%	7	Peptide	Analytical Standard	Waters	PHOSPH_RAB
APNDFNLK	+H	C41H64N11O13	918.47	918.46	-4.5	0.683	0.001	300.0	0.6	0.2%	7	Peptide	Analytical Standard	Waters	PHOSPH_RAB
AEFVEVTK	+H	C42H68N9O14	922.49	922.49	-2.8	0.693	0.001	295.7	0.5	0.2%	7	Peptide	Analytical Standard	Waters	ALBUMIN_BOV
YLYEIAR	+H	C44H67N10O12	927.49	927.49	-1.7	0.672	0.001	305.0	0.5	0.2%	7	Peptide	Analytical Standard	Waters	ALBUMIN_BOV
VLGIDGGEGK	+H	C40H70N11O15	944.50	944.50	-3.2	0.703	0.000	291.2	0.2	0.1%	7	Peptide	Analytical Standard	Waters	ADH_YST
NNVVNTMR	+H	C37H67N14O13S	947.47	947.47	1.1	0.681	0.001	300.7	0.6	0.2%	8	Peptide	Analytical Standard	Waters	PHOSPH_RAB
EALDFFAR	+H	C45H66N11O13	968.48	968.48	-0.7	0.669	0.001	305.9	0.4	0.1%	7	Peptide	Analytical Standard	Waters	ADH_YST
LVVSTQTALA	+H	C44H80N11O15	1002.58	1002.58	0.3	0.649	0.001	315.6	0.3	0.1%	6	Peptide	Analytical Standard	Waters	ALBUMIN_BOV
ANELLINVK	+H	C45H81N12O14	1013.60	1013.60	-1.0	0.626	0.001	326.8	0.3	0.1%	6	Peptide	Analytical Standard	Waters	ADH_YST
VIFLENYR	+H	C50H77N12O13	1053.57	1053.57	-0.7	0.643	0.001	318.3	0.4	0.1%	7	Peptide	Analytical Standard	Waters	PHOSPH_RAB
EIWGVEPSR	+H	C48H74N13O15	1072.54	1072.54	-3.4	0.639	0.001	320.2	0.6	0.2%	7	Peptide	Analytical Standard	Waters	PHOSPH_RAB
VAAAFPGDVDR (peak1)	+H	C49H77N14O16	1117.56	1117.56	-0.2	0.626	0.001	326.7	0.5	0.2%	5	Peptide	Analytical Standard	Waters	PHOSPH_RAB
VAAAFPGDVDR (peak 2)	+H	C49H77N14O16	1117.56	1117.56	-0.2	0.630	0.001	324.3	0.4	0.1%	6	Peptide	Analytical Standard	Waters	PHOSPH_RAB
GVIFYESHGK	+H	C53H78N13O15	1136.57	1136.57	-0.3	0.614	0.001	332.9	0.5	0.2%	5	Peptide	Analytical Standard	Waters	ADH_YST
IGSEVYHNLK	+H	C52H83N14O16	1159.61	1159.61	-2.1	0.586	0.001	348.4	0.7	0.2%	5	Peptide	Analytical Standard	Waters	ENOLASE_YST

LVNELTEFAK	+H	C53H87N12O17	1163.63	1163.63	0.0	0.593	0.000	344.4	0.2	0.1%	5	Peptide	Analytical Standard	Waters	ALBUMIN_BOV
SISIVGSYVGNR	+H	C54H91N16O18	1251.67	1251.67	1.0	0.585	0.001	349.1	0.8	0.2%	6	Peptide	Analytical Standard	Waters	ADH_YST
VFADYEEYVK	+H	C60H84N11O19	1262.59	1262.59	-3.0	0.557	0.002	366.4	1.2	0.3%	6	Peptide	Analytical Standard	Waters	PHOSPH_RAB
VNQIGTLSESIK	+H	C55H98N15O20	1288.71	1288.71	0.5	0.569	0.001	358.7	0.5	0.1%	5	Peptide	Analytical Standard	Waters	ENOLASE_YST
SIGGEVFIDFTK	+H	C61H94N13O19	1312.68	1312.68	-0.4	0.534	0.001	382.3	0.9	0.2%	5	Peptide	Analytical Standard	Waters	ADH_YST
TVMENFVAFVDK	+H	C64H99N14O19S	1399.69	1399.69	-0.1	0.522	0.003	390.2	1.9	0.5%	5	Peptide	Analytical Standard	Waters	ALBUMIN_BOV
AVDDFLISLDGTANK	+H	C69H112N17O25	1578.80	1578.80	1.2	0.474	0.001	429.7	0.7	0.2%	6	Peptide	Analytical Standard	Waters	ENOLASE_YST
TAGIQIVADDLTVTNPK	+H	C76H131N20O27	1755.95	1755.95	-0.1	0.452	0.000	450.6	0.5	0.1%	4	Peptide	Analytical Standard	Waters	ENOLASE_YST

Table B.5. Collision Cross-Section Database of Lipids

Analyte	z	Molecular Formula	Exact m/z	Measured m/z	Mass Accuracy (ppm)	K_0	K_0 σ	CCS	CCS σ	RSD (%)	N	Chemical Class	Analyte Source	Vendor Source
GlcCer 34:01	+Na	C40H77NO8Na	722.55	722.55	-7.3	0.742	0.002	277.3	0.8	0.3%	15	Lipid	Analytical Standard	Avanti Polar Lipids
GlcCer 34:00	+Na	C40H79NO8Na	724.57	724.56	-8.2	0.730	0.002	281.7	0.7	0.2%	14	Lipid	Analytical Standard	Avanti Polar Lipids
GlcCer 36:02	+Na	C42H79NO8Na	748.57	748.56	-7.2	0.727	0.002	282.6	0.6	0.2%	14	Lipid	Analytical Standard	Avanti Polar Lipids
GlcCer 36:01	+Na	C42H81NO8Na	750.59	750.58	-2.1	0.717	0.001	286.7	0.4	0.1%	14	Lipid	Analytical Standard	Avanti Polar Lipids
GlcCer 37:01	+Na	C43H83NO8Na	764.60	764.59	-12.0	0.717	0.002	286.8	0.9	0.3%	14	Lipid	Analytical Standard	Avanti Polar Lipids
GlcCer 36:01 h	+Na	C42H81NO9Na	766.58	766.58	-4.3	0.705	0.001	291.5	0.4	0.1%	14	Lipid	Analytical Standard	Avanti Polar Lipids
GlcCer 38:02	+Na	C44H83NO8Na	776.60	776.60	-7.7	0.705	0.002	291.4	1.0	0.3%	14	Lipid	Analytical Standard	Avanti Polar Lipids
GlcCer 38:01	+Na	C44H85NO8Na	778.62	778.61	-4.6	0.699	0.001	293.8	0.4	0.1%	14	Lipid	Analytical Standard	Avanti Polar Lipids
GlcCer 38:00	+Na	C44H87NO8Na	780.63	780.63	-7.7	0.695	0.001	295.6	0.5	0.2%	14	Lipid	Analytical Standard	Avanti Polar Lipids
GlcCer 38:02 h	+Na	C44H83NO9Na	792.60	792.59	-8.5	0.692	0.002	296.6	0.8	0.3%	14	Lipid	Analytical Standard	Avanti Polar Lipids
GlcCer 38:01 h	+Na	C44H85NO9Na	794.61	794.61	-3.9	0.690	0.001	297.7	0.5	0.2%	14	Lipid	Analytical Standard	Avanti Polar Lipids
GlcCer 40:03	+Na	C46H85NO7Na	802.62	802.61	-6.8	0.694	0.003	295.8	1.3	0.4%	14	Lipid	Analytical Standard	Avanti Polar Lipids
GlcCer 40:02	+Na	C46H87NO8Na	804.63	804.63	-4.1	0.691	0.002	297.1	0.6	0.2%	14	Lipid	Analytical Standard	Avanti Polar Lipids
GlcCer 40:01	+Na	C46H89NO8Na	806.65	806.65	-3.4	0.682	0.001	301.1	0.5	0.2%	14	Lipid	Analytical Standard	Avanti Polar Lipids
GlcCer 40:00	+Na	C46H91NO8Na	808.66	808.66	-7.4	0.679	0.001	302.3	0.5	0.2%	14	Lipid	Analytical Standard	Avanti Polar Lipids
GlcCer 41:02	+Na	C47H89NO8Na	818.65	818.64	-5.7	0.685	0.001	299.6	0.6	0.2%	14	Lipid	Analytical Standard	Avanti Polar Lipids
GlcCer 41:01	+Na	C47H91NO8Na	820.66	820.65	-13.2	0.679	0.001	302.5	0.5	0.2%	14	Lipid	Analytical Standard	Avanti Polar Lipids
GlcCer 40:01 h	+Na	C46H89NO9Na	822.64	822.64	1.0	0.677	0.001	303.4	0.4	0.1%	14	Lipid	Analytical Standard	Avanti Polar Lipids
GlcCer 40:00 h	+Na	C46H91NO9Na	824.66	824.65	-6.0	0.671	0.001	306.1	0.6	0.2%	14	Lipid	Analytical Standard	Avanti Polar Lipids
GlcCer 42:03	+Na	C48H89NO8Na	830.65	830.64	-5.1	0.679	0.001	302.3	0.4	0.1%	14	Lipid	Analytical Standard	Avanti Polar Lipids
GlcCer 42:02	+Na	C48H91NO9Na	832.66	832.67	3.1	0.672	0.001	305.2	0.5	0.1%	14	Lipid	Analytical Standard	Avanti Polar Lipids
GlcCer 42:01	+Na	C48H93NO10Na	834.68	834.68	-1.5	0.667	0.001	307.5	0.4	0.1%	14	Lipid	Analytical Standard	Avanti Polar Lipids
GlcCer 42:00	+Na	C48H95NO8Na	836.70	836.68	-18.3	0.666	0.001	308.2	0.5	0.2%	14	Lipid	Analytical Standard	Avanti Polar Lipids
GlcCer 43:03	+Na	C49H91NO8Na	844.66	844.65	-19.3	0.670	0.002	306.1	0.7	0.2%	14	Lipid	Analytical Standard	Avanti Polar Lipids

Name	Adduct	Formula												
GlcCer 43:02	+Na	C49H93NO9Na	846.68	846.67	-8.1	0.667	0.002	307.8	1.0	0.3%	14	Lipid	Analytical Standard	Avanti Polar Lipids
GlcCer 42:02 h	+Na	C48H91NO9Na	848.66	848.66	4.3	0.664	0.001	309.0	0.4	0.1%	14	Lipid	Analytical Standard	Avanti Polar Lipids
GlcCer 42:01 h	+Na	C48H93NO9Na	850.67	850.68	0.4	0.656	0.001	312.7	0.4	0.1%	12	Lipid	Analytical Standard	Avanti Polar Lipids
GlcCer 44:03	+Na	C50H93NO8Na	858.68	858.67	-6.3	0.660	0.001	310.7	0.7	0.2%	12	Lipid	Analytical Standard	Avanti Polar Lipids
GlcCer 44:02	+Na	C50H95NO9Na	860.70	860.69	-4.2	0.651	0.001	315.3	0.4	0.1%	12	Lipid	Analytical Standard	Avanti Polar Lipids
GlcCer 43:02 h	+Na	C49H93NO9Na	862.67	862.69	12.0	0.652	0.001	314.6	0.4	0.1%	12	Lipid	Analytical Standard	Avanti Polar Lipids
GlcCer 43:01 h	+Na	C49H95NO9Na	864.69	864.68	-10.7	0.654	0.001	313.7	0.4	0.1%	12	Lipid	Analytical Standard	Avanti Polar Lipids
GlcCer 44:04 h	+Na	C50H91NO9Na	872.66	872.65	-7.8	0.652	0.001	314.7	0.4	0.1%	12	Lipid	Analytical Standard	Avanti Polar Lipids
GlcCer 44:03 h	+Na	C50H93NO9Na	874.67	874.67	-5.3	0.653	0.001	314.0	0.6	0.2%	12	Lipid	Analytical Standard	Avanti Polar Lipids
GlcCer 44:02 h	+Na	C50H95NO9Na	876.69	876.69	-2.3	0.644	0.001	318.4	0.4	0.1%	12	Lipid	Analytical Standard	Avanti Polar Lipids
GlcCer 44:01 h	+Na	C50H97NO9Na	878.71	878.70	-8.2	0.642	0.001	319.5	0.4	0.1%	12	Lipid	Analytical Standard	Avanti Polar Lipids
GlcCer 44:02 h	+K	C50H95NO9K	892.66	892.68	19.0	0.639	0.001	321.1	0.7	0.2%	12	Lipid	Analytical Standard	Avanti Polar Lipids
GlcCer 47:09	+K	C53H87NO8K	904.61	904.60	-3.1	0.648	0.001	316.4	0.6	0.2%	12	Lipid	Analytical Standard	Avanti Polar Lipids
GlcCer 46:02 h	+Na	C52H99NO9Na	904.72	904.72	-7.1	0.633	0.001	323.8	0.6	0.2%	12	Lipid	Analytical Standard	Avanti Polar Lipids
GlcCer 47:10 h	+K	C53H85NO9K	918.59	918.59	6.5	0.643	0.001	318.6	0.5	0.2%	12	Lipid	Analytical Standard	Avanti Polar Lipids
PC 31:02	+K	C39H74NO8PK	754.48	754.48	6.2	0.725	0.002	283.6	0.8	0.3%	8	Lipid	Analytical Standard	Avanti Polar Lipids
PC 31:01	+K	C39H76NO8PK	756.49	756.50	3.4	0.718	0.002	286.5	0.7	0.2%	8	Lipid	Analytical Standard	Avanti Polar Lipids
PC 32:03	+K	C40H74NO8PK	766.48	766.49	11.1	0.711	0.001	288.9	0.6	0.2%	8	Lipid	Analytical Standard	Avanti Polar Lipids
PC 32:02	+K	C40H76NO8PK	768.49	768.50	5.2	0.711	0.001	289.2	0.5	0.2%	8	Lipid	Analytical Standard	Avanti Polar Lipids
PC 33:04	+K	C41H74NO8PK	778.48	778.48	4.6	0.715	0.002	287.5	0.7	0.3%	10	Lipid	Analytical Standard	Avanti Polar Lipids
PC 33:03	+K	C41H76NO8PK	780.49	780.50	10.5	0.708	0.001	290.1	0.5	0.2%	8	Lipid	Analytical Standard	Avanti Polar Lipids
PC 33:02	+K	C41H78NO8PK	782.51	782.52	11.1	0.705	0.001	291.5	0.6	0.2%	9	Lipid	Analytical Standard	Avanti Polar Lipids
PC 34:04	+K	C42H76NO8PK	792.49	792.50	2.7	0.711	0.002	289.0	1.0	0.3%	10	Lipid	Analytical Standard	Avanti Polar Lipids
PC 34:03	+K	C42H78NO8PK	794.51	794.51	5.1	0.702	0.002	292.4	0.8	0.3%	10	Lipid	Analytical Standard	Avanti Polar Lipids
PC 34:02	+K	C42H80NO8PK	796.53	796.53	2.6	0.705	0.001	291.3	0.6	0.2%	8	Lipid	Analytical Standard	Avanti Polar Lipids
PC 36:07	+Na	C44H74NO8PNa	798.50	798.51	8.6	0.702	0.002	292.5	0.7	0.2%	9	Lipid	Analytical Standard	Avanti Polar Lipids
PC 35:06	+K	C43H74NO8PK	802.48	802.48	2.9	0.704	0.002	291.8	1.0	0.3%	10	Lipid	Analytical Standard	Avanti Polar Lipids
PC 35:05	+K	C43H76NO8PK	804.49	804.50	4.3	0.699	0.001	293.8	0.6	0.2%	9	Lipid	Analytical Standard	Avanti Polar Lipids

PC 35:04	+K	C43H78NO8PK	806.51	806.51	2.5	0.697	0.002	294.5	0.7	0.2%	10	Lipid	Analytical Standard	Avanti Polar Lipids
PC 35:03	+K	C43H80NO8PK	808.53	808.53	5.8	0.693	0.001	296.1	0.6	0.2%	10	Lipid	Analytical Standard	Avanti Polar Lipids
PC 35:02	+K	C43H82NO8PK	810.54	810.54	4.0	0.690	0.001	297.7	0.6	0.2%	10	Lipid	Analytical Standard	Avanti Polar Lipids
PC 38:10	+Na	C46H72NO8PNa	820.49	820.50	17.1	0.694	0.001	295.9	0.6	0.2%	9	Lipid	Analytical Standard	Avanti Polar Lipids
PC 38:09	+Na	C46H74NO8PNa	822.50	822.51	3.8	0.689	0.001	297.8	0.6	0.2%	10	Lipid	Analytical Standard	Avanti Polar Lipids
PC 38:08	+Na	C46H76NO8PNa	824.52	824.52	0.1	0.684	0.002	299.9	0.7	0.2%	10	Lipid	Analytical Standard	Avanti Polar Lipids
PC 37:07	+K	C45H76NO8PK	828.49	828.50	2.3	0.692	0.001	296.6	0.6	0.2%	10	Lipid	Analytical Standard	Avanti Polar Lipids
PC 37:06	+K	C45H78NO8PK	830.51	830.51	0.7	0.688	0.001	298.2	0.5	0.2%	10	Lipid	Analytical Standard	Avanti Polar Lipids
PC 37:05	+K	C45H80NO8PK	832.53	832.53	2.2	0.686	0.001	299.0	0.6	0.2%	8	Lipid	Analytical Standard	Avanti Polar Lipids
PC 40:15	+Na	C48H66NO8PNa	838.44	838.45	7.2	0.699	0.002	293.5	1.0	0.3%	9	Lipid	Analytical Standard	Avanti Polar Lipids
PC 40:14	+Na	C48H68NO8PNa	840.46	840.46	2.4	0.700	0.001	293.3	0.6	0.2%	8	Lipid	Analytical Standard	Avanti Polar Lipids
PC 40:13	+Na	C48H70NO8PNa	842.47	842.47	-2.3	0.692	0.002	296.6	0.8	0.3%	8	Lipid	Analytical Standard	Avanti Polar Lipids
PC 40:12	+Na	C48H72NO8PNa	844.49	844.49	0.4	0.683	0.001	300.6	0.6	0.2%	8	Lipid	Analytical Standard	Avanti Polar Lipids
PC 40:11	+Na	C48H74NO8PNa	846.50	846.50	-0.4	0.682	0.002	300.7	0.7	0.2%	9	Lipid	Analytical Standard	Avanti Polar Lipids
PC 40:10	+Na	C48H76NO8PNa	848.52	848.52	-1.8	0.680	0.001	301.5	0.5	0.2%	8	Lipid	Analytical Standard	Avanti Polar Lipids
PC 40:10	+Na	C48H78NO8PNa	850.54	850.53	-6.3	0.679	0.002	302.2	0.7	0.2%	10	Lipid	Analytical Standard	Avanti Polar Lipids
PC 39:07	+K	C47H80NO8PK	856.53	856.53	-0.4	0.675	0.002	303.8	0.7	0.2%	10	Lipid	Analytical Standard	Avanti Polar Lipids
PC 39:06	+K	C47H82NO8PK	858.54	858.54	-1.4	0.676	0.001	303.4	0.7	0.2%	9	Lipid	Analytical Standard	Avanti Polar Lipids
PC 39:05	+K	C47H84NO8PK	860.56	860.55	-4.7	0.673	0.002	304.7	0.7	0.2%	9	Lipid	Analytical Standard	Avanti Polar Lipids
PC 42:15	+Na	C50H70NO8PNa	866.47	866.47	1.0	0.679	0.003	301.9	1.1	0.4%	10	Lipid	Analytical Standard	Avanti Polar Lipids
PC 42:14	+Na	C50H72NO8PNa	868.49	868.49	-1.4	0.686	0.002	299.0	0.7	0.2%	10	Lipid	Analytical Standard	Avanti Polar Lipids
PC 42:13	+Na	C50H74NO8PNa	870.50	870.50	-5.2	0.673	0.002	304.9	0.7	0.2%	9	Lipid	Analytical Standard	Avanti Polar Lipids
PC 42:12	+Na	C50H76NO8PNa	872.52	872.52	-4.5	0.675	0.002	303.9	0.7	0.2%	9	Lipid	Analytical Standard	Avanti Polar Lipids
PC 43:17	+K	C51H68NO8PK	892.43	892.44	9.5	0.675	0.001	303.5	0.5	0.2%	8	Lipid	Analytical Standard	Avanti Polar Lipids
PC 43:16	+K	C51H70NO8PK	894.45	894.44	-5.8	0.674	0.002	304.1	0.7	0.2%	10	Lipid	Analytical Standard	Avanti Polar Lipids
PE O-18:03/0:00	+Na	C23H42NO7PNa	498.26	498.26	-3.3	0.941	0.003	220.5	0.6	0.3%	11	Lipid	Analytical Standard	Avanti Polar Lipids
PE O-20:05	+Na	C25H42NO7PNa	522.26	522.26	-3.3	0.956	0.004	216.8	0.9	0.4%	11	Lipid	Analytical Standard	Avanti Polar Lipids
PE O-20:04	+Na	C25H44NO7PNa	524.28	524.27	-3.6	0.913	0.002	226.9	0.5	0.2%	11	Lipid	Analytical Standard	Avanti Polar Lipids

PE O-20:03	+Na	C25H46NO7PNa	526.29	526.29	-3.9	0.906	0.002	228.7	0.6	0.3%	11	Lipid	Analytical Standard	Avanti Polar Lipids
PE O-22:07	+Na	C27H42NO7PNa	546.26	546.26	-2.8	0.938	0.007	220.6	1.7	0.8%	11	Lipid	Analytical Standard	Avanti Polar Lipids
PE O-22:06	+Na	C27H44NO7PNa	548.28	548.27	-7.5	0.907	0.003	228.1	0.7	0.3%	8	Lipid	Analytical Standard	Avanti Polar Lipids
PE 21:03	+K	C26H46NO8PK	570.26	570.26	-2.6	0.908	0.003	227.8	0.7	0.3%	8	Lipid	Analytical Standard	Avanti Polar Lipids
PE 21:02	+K	C26H48NO8PK	572.28	572.27	-4.1	0.902	0.001	229.3	0.3	0.2%	8	Lipid	Analytical Standard	Avanti Polar Lipids
PE O-26:05	+K	C31H54NO7PK	622.33	622.31	-25.5	0.851	0.002	242.4	0.4	0.2%	8	Lipid	Analytical Standard	Avanti Polar Lipids
PE 26:06	+K	C31H50NO8PK	634.29	634.27	-35.3	0.854	0.003	241.7	1.0	0.4%	8	Lipid	Analytical Standard	Avanti Polar Lipids
PE 26:05	+K	C31H52NO8PK	636.31	636.29	-33.4	0.850	0.003	242.6	0.8	0.3%	8	Lipid	Analytical Standard	Avanti Polar Lipids
PE 26:04	+K	C31H54NO8PK	638.32	638.30	-39.6	0.841	0.003	245.4	1.0	0.4%	8	Lipid	Analytical Standard	Avanti Polar Lipids
PE 28:07	+K	C33H52NO8PK	660.31	660.29	-32.8	0.843	0.003	244.4	0.8	0.3%	8	Lipid	Analytical Standard	Avanti Polar Lipids
PE 28:06	+K	C33H54NO8PK	662.32	662.30	-32.8	0.829	0.002	248.7	0.7	0.3%	8	Lipid	Analytical Standard	Avanti Polar Lipids
PE 28:05	+K	C33H56NO8PK	664.34	664.32	-31.4	0.821	0.002	250.9	0.5	0.2%	8	Lipid	Analytical Standard	Avanti Polar Lipids
PE O-31:06	+K	C36H62NO7PK	690.39	690.37	-27.2	0.799	0.002	257.8	0.5	0.2%	13	Lipid	Analytical Standard	Avanti Polar Lipids
PE 32:01	+Na	C37H72NO8PNa	712.49	712.49	-2.1	0.751	0.002	274.1	0.7	0.3%	8	Lipid	Analytical Standard	Avanti Polar Lipids
PE O-34:04	+Na	C39H72NO7PNa	720.49	720.49	-7.1	0.746	0.002	275.9	0.7	0.2%	11	Lipid	Analytical Standard	Avanti Polar Lipids
PE O-34:03	+Na	C39H74NO7PNa	722.51	722.51	-3.1	0.740	0.003	278.0	0.9	0.3%	12	Lipid	Analytical Standard	Avanti Polar Lipids
PE O-34:02	+Na	C39H76NO7PNa	724.53	724.52	-6.9	0.735	0.002	279.7	0.8	0.3%	12	Lipid	Analytical Standard	Avanti Polar Lipids
PE 34:04	+Na	C39H70NO8PNa	734.47	734.47	-5.6	0.752	0.003	273.6	1.2	0.5%	8	Lipid	Analytical Standard	Avanti Polar Lipids
PE O-O-36:04	+Na	C41H78NO6PNa	734.55	734.55	0.7	0.736	0.003	279.3	1.2	0.4%	8	Lipid	Analytical Standard	Avanti Polar Lipids
PE 34:03	+Na	C39H72NO8PNa	736.49	736.49	-0.8	0.745	0.003	276.1	1.0	0.4%	10	Lipid	Analytical Standard	Avanti Polar Lipids
PE 34:02	+Na	C39H74NO8PNa	738.51	738.50	2.1	0.739	0.001	278.3	0.6	0.2%	11	Lipid	Analytical Standard	Avanti Polar Lipids
PE 34:01	+Na	C39H76NO8PNa	740.52	740.52	0.9	0.731	0.002	281.3	0.6	0.2%	11	Lipid	Analytical Standard	Avanti Polar Lipids
PE 33:00	+K	C38H76NO8PK	744.49	744.49	-5.3	0.742	0.003	277.2	1.2	0.4%	11	Lipid	Analytical Standard	Avanti Polar Lipids
PE O-36:05	+Na	C41H74NO7PNa	746.51	746.51	-4.9	0.736	0.002	279.2	0.7	0.3%	11	Lipid	Analytical Standard	Avanti Polar Lipids
PE O-36:04	+Na	C41H76NO7PNa	748.53	748.52	-4.4	0.730	0.002	281.6	0.6	0.2%	11	Lipid	Analytical Standard	Avanti Polar Lipids
PE O-36:03	+Na	C41H78NO7PNa	750.54	750.54	-1.5	0.720	0.003	285.4	1.1	0.4%	11	Lipid	Analytical Standard	Avanti Polar Lipids
PE 35:02	+Na	C40H76NO8PNa	752.52	752.52	-2.1	0.731	0.001	281.3	0.3	0.1%	8	Lipid	Analytical Standard	Avanti Polar Lipids
PE O-36:02	+Na	C41H80NO7PNa	752.56	752.55	-6.2	0.716	0.001	287.3	0.6	0.2%	12	Lipid	Analytical Standard	Avanti Polar Lipids

Name	Adduct	Formula												
PE 35:01	+Na	C40H78NO8PNa	754.54	754.54	5.4	0.727	0.001	282.9	0.6	0.2%	11	Lipid	Analytical Standard	Avanti Polar Lipids
PE 36:06	+Na	C41H70NO8PNa	758.47	758.47	-3.2	0.744	0.001	276.3	0.5	0.2%	11	Lipid	Analytical Standard	Avanti Polar Lipids
PE 36:05	+Na	C41H72NO8PNa	760.49	760.49	-1.8	0.739	0.001	278.2	0.5	0.2%	11	Lipid	Analytical Standard	Avanti Polar Lipids
PE 36:04	+Na	C41H74NO8PNa	762.50	762.51	0.3	0.732	0.001	280.6	0.5	0.2%	11	Lipid	Analytical Standard	Avanti Polar Lipids
PE 36:02	+Na	C41H78NO8PNa	766.54	766.54	1.5	0.719	0.001	285.7	0.4	0.2%	11	Lipid	Analytical Standard	Avanti Polar Lipids
PE 35:02	+K	C40H76NO8PK	768.49	768.49	-2.3	0.728	0.002	282.5	0.7	0.2%	12	Lipid	Analytical Standard	Avanti Polar Lipids
PE 36:01	+Na	C41H80NO8PNa	768.55	768.55	-0.8	0.712	0.001	288.5	0.6	0.2%	11	Lipid	Analytical Standard	Avanti Polar Lipids
PE 35:01	+K	C40H78NO8PK	770.51	770.51	-0.2	0.725	0.001	283.6	0.6	0.2%	10	Lipid	Analytical Standard	Avanti Polar Lipids
PE 35:00	+K	C40H80NO8PK	772.53	772.53	-0.6	0.718	0.002	286.2	0.7	0.2%	11	Lipid	Analytical Standard	Avanti Polar Lipids
PE O-38:05	+Na	C43H78NO7PNa	774.54	774.54	-3.4	0.714	0.001	287.7	0.3	0.1%	11	Lipid	Analytical Standard	Avanti Polar Lipids
PE O-O-38:05	+K	C43H80NO6PK	776.54	776.53	-4.6	0.720	0.003	285.6	1.0	0.4%	10	Lipid	Analytical Standard	Avanti Polar Lipids
PE 37:03	+Na	C42H78NO8PNa	778.54	778.54	-1.3	0.718	0.002	286.2	0.7	0.2%	12	Lipid	Analytical Standard	Avanti Polar Lipids
PE 37:02	+Na	C42H80NO8PNa	780.55	780.55	-1.3	0.713	0.001	288.2	0.4	0.2%	12	Lipid	Analytical Standard	Avanti Polar Lipids
PE 38:08	+Na	C43H70NO8PNa	782.47	782.46	-11.8	0.729	0.002	281.9	0.7	0.2%	13	Lipid	Analytical Standard	Avanti Polar Lipids
PE 37:01	+Na	C42H82NO8PNa	782.57	782.56	-3.5	0.703	0.002	292.2	0.9	0.3%	12	Lipid	Analytical Standard	Avanti Polar Lipids
PE 38:07	+Na	C43H72NO8PNa	784.49	784.49	-0.9	0.724	0.001	283.7	0.5	0.2%	11	Lipid	Analytical Standard	Avanti Polar Lipids
PE 38:06	+Na	C43H74NO8PNa	786.50	786.50	-0.7	0.721	0.001	285.0	0.5	0.2%	11	Lipid	Analytical Standard	Avanti Polar Lipids
PE 38:05	+Na	C43H76NO8PNa	788.52	788.52	0.3	0.715	0.001	287.2	0.5	0.2%	11	Lipid	Analytical Standard	Avanti Polar Lipids
PE 38:04	+Na	C43H78NO8PNa	790.54	790.54	1.5	0.708	0.001	290.0	0.5	0.2%	12	Lipid	Analytical Standard	Avanti Polar Lipids
PE 37:04	+K	C42H76NO8PK	792.49	792.49	-5.7	0.721	0.002	284.7	0.7	0.2%	11	Lipid	Analytical Standard	Avanti Polar Lipids
PE 38:03	+Na	C43H80NO8PNa	792.55	792.54	-9.7	0.710	0.002	289.3	0.7	0.2%	11	Lipid	Analytical Standard	Avanti Polar Lipids
PE 37:03	+K	C42H78NO8PK	794.51	794.51	-2.6	0.717	0.001	286.5	0.4	0.2%	11	Lipid	Analytical Standard	Avanti Polar Lipids
PE 37:02	+K	C42H80NO8PK	796.53	796.52	-4.8	0.709	0.001	289.8	0.6	0.2%	11	Lipid	Analytical Standard	Avanti Polar Lipids
PE 37:01	+K	C42H82NO8PK	798.54	798.54	-3.0	0.696	0.001	295.0	0.5	0.2%	11	Lipid	Analytical Standard	Avanti Polar Lipids
PE 38:07	+K	C43H72NO8PK	800.46	800.48	19.7	0.716	0.001	287.0	0.5	0.2%	11	Lipid	Analytical Standard	Avanti Polar Lipids
PE 39:06	+Na	C44H76NO8PNa	800.52	800.52	1.1	0.717	0.002	286.4	0.7	0.3%	11	Lipid	Analytical Standard	Avanti Polar Lipids
PE 37:00	+K	C42H84NO8PK	800.56	800.56	1.3	0.690	0.001	297.8	0.5	0.2%	10	Lipid	Analytical Standard	Avanti Polar Lipids
PE 38:06	+K	C43H74NO8PK	802.48	802.48	-0.2	0.711	0.001	288.7	0.5	0.2%	12	Lipid	Analytical Standard	Avanti Polar Lipids

PE O-39:06	+K	C44H78NO7PK	802.52	802.52	5.8	0.706	0.001	290.9	0.5	0.2%	12	Lipid	Analytical Standard	Avanti Polar Lipids
PE O-O-40:06	+K	C45H82NO6PK	802.55	802.55	0.7	0.700	0.000	293.3	0.7	0.2%	11	Lipid	Analytical Standard	Avanti Polar Lipids
PE 39:04	+Na	C44H80NO8PNa	804.55	804.55	1.1	0.701	0.002	292.8	0.8	0.3%	11	Lipid	Analytical Standard	Avanti Polar Lipids
PE 40:09	+Na	C45H72NO8PNa	808.49	808.49	-1.6	0.717	0.001	286.6	0.5	0.2%	10	Lipid	Analytical Standard	Avanti Polar Lipids
PE 40:08	+Na	C45H74NO8PNa	810.50	810.50	-2.3	0.710	0.001	289.2	0.3	0.1%	10	Lipid	Analytical Standard	Avanti Polar Lipids
PE 40:07	+Na	C45H76NO8PNa	812.52	812.52	0.5	0.706	0.001	290.8	0.6	0.2%	11	Lipid	Analytical Standard	Avanti Polar Lipids
PE 40:05	+Na	C45H80NO8PNa	816.55	816.55	-1.8	0.696	0.002	294.8	0.7	0.2%	11	Lipid	Analytical Standard	Avanti Polar Lipids
PE O-O-42:11	+K	C47H74NO6PK	818.49	818.50	11.2	0.708	0.002	289.8	0.9	0.3%	12	Lipid	Analytical Standard	Avanti Polar Lipids
PE O-O-42:10	+K	C47H76NO6PK	820.50	820.51	11.7	0.702	0.001	292.6	0.6	0.2%	11	Lipid	Analytical Standard	Avanti Polar Lipids
PE 39:03	+K	C44H82NO8PK	822.54	822.54	-6.9	0.700	0.002	293.4	0.8	0.3%	11	Lipid	Analytical Standard	Avanti Polar Lipids
PE O-O-44:14	+Na	C49H72NO6PNa	824.50	824.48	-18.2	0.712	0.002	288.2	1.0	0.3%	11	Lipid	Analytical Standard	Avanti Polar Lipids
PE 39:02	+K	C44H84NO8PK	824.56	824.55	-10.2	0.694	0.001	295.9	0.6	0.2%	11	Lipid	Analytical Standard	Avanti Polar Lipids
PE O-O-44:13	+Na	C49H74NO6PNa	826.52	826.50	-21.0	0.709	0.001	289.4	0.6	0.2%	10	Lipid	Analytical Standard	Avanti Polar Lipids
PE O-O-42:08	+K	C47H82NO6PK	826.55	826.56	10.1	0.691	0.002	297.0	0.7	0.2%	11	Lipid	Analytical Standard	Avanti Polar Lipids
PE O-O-44:12	+Na	C49H76NO6PNa	828.53	828.51	-20.8	0.707	0.002	290.4	0.8	0.3%	11	Lipid	Analytical Standard	Avanti Polar Lipids
PE 40:06	+K	C45H78NO8PK	830.51	830.53	20.0	0.696	0.002	294.7	0.8	0.3%	11	Lipid	Analytical Standard	Avanti Polar Lipids
PE 42:10	+Na	C47H74NO8PNa	834.50	834.50	-5.1	0.705	0.002	291.0	0.7	0.2%	12	Lipid	Analytical Standard	Avanti Polar Lipids
PE 42:09	+Na	C47H76NO8PNa	836.52	836.52	-2.9	0.694	0.001	295.6	0.4	0.1%	12	Lipid	Analytical Standard	Avanti Polar Lipids
PE 42:08	+Na	C47H78NO8PNa	838.54	838.53	-3.8	0.690	0.001	297.3	0.5	0.2%	11	Lipid	Analytical Standard	Avanti Polar Lipids
PE O-O-44:14	+K	C49H74NO6PK	842.49	842.49	6.9	0.704	0.002	291.4	0.7	0.3%	11	Lipid	Analytical Standard	Avanti Polar Lipids
PE O-O-44:13	+K	C49H76NO6PK	844.50	844.51	4.4	0.696	0.001	294.7	0.6	0.2%	12	Lipid	Analytical Standard	Avanti Polar Lipids
PE O-O-44:12	+K	C49H78NO6PK	846.52	846.52	3.5	0.691	0.001	297.0	0.6	0.2%	12	Lipid	Analytical Standard	Avanti Polar Lipids
PE 42:10	+K	C47H72NO8PK	848.46	848.48	20.9	0.705	0.001	290.8	0.5	0.2%	11	Lipid	Analytical Standard	Avanti Polar Lipids
PE O-O-44:11	+K	C49H80NO6PK	848.54	848.53	-2.9	0.691	0.002	297.1	0.9	0.3%	11	Lipid	Analytical Standard	Avanti Polar Lipids
PE O-O-46:15	+Na	C51H74NO6PNa	850.52	850.50	-19.2	0.701	0.002	292.7	0.7	0.2%	11	Lipid	Analytical Standard	Avanti Polar Lipids
PE 42:08	+K	C47H76NO8PK	852.49	852.51	18.7	0.693	0.002	296.1	0.8	0.3%	11	Lipid	Analytical Standard	Avanti Polar Lipids
PE O-O-45:14	+K	C50H76NO6PK	856.50	856.51	4.9	0.690	0.002	297.2	1.0	0.3%	11	Lipid	Analytical Standard	Avanti Polar Lipids
PE 44:12	+Na	C49H74NO8PNa	858.50	858.51	4.8	0.685	0.002	299.7	1.0	0.3%	8	Lipid	Analytical Standard	Avanti Polar Lipids

PE 44:11	C49H76NO8PNa	+Na	860.52	860.51	-11.5	0.683	0.002	300.3	1.0	0.3%	8	Lipid	Analytical Standard	Avanti Polar Lipids
PE O-O-46:16	C51H74NO6PK	+K	866.49	866.49	6.7	0.689	0.002	297.7	1.1	0.4%	12	Lipid	Analytical Standard	Avanti Polar Lipids
PE O-O-46:15	C51H76NO6PK	+K	868.50	868.51	5.4	0.682	0.002	300.8	0.7	0.2%	11	Lipid	Analytical Standard	Avanti Polar Lipids
PE O-O-46:14	C51H78NO6PK	+K	870.52	870.52	3.0	0.677	0.001	302.9	0.5	0.2%	10	Lipid	Analytical Standard	Avanti Polar Lipids
PE O-45:12	C50H78NO7PK	+K	874.52	874.51	-11.4	0.685	0.002	299.3	1.0	0.3%	7	Lipid	Analytical Standard	Avanti Polar Lipids
PE 44:11	C49H74NO8PK	+K	876.49	876.50	7.6	0.685	0.001	299.3	0.5	0.2%	10	Lipid	Analytical Standard	Avanti Polar Lipids
PE O-47:16	C52H74NO7PNa	+Na	878.51	878.51	0.8	0.684	0.002	299.7	0.9	0.3%	11	Lipid	Analytical Standard	Avanti Polar Lipids
PE O-O-47:16	C52H76NO6PK	+K	880.50	880.51	4.4	0.681	0.002	301.3	0.8	0.3%	11	Lipid	Analytical Standard	Avanti Polar Lipids
PE O-46:14	C51H76NO7PK	+K	884.50	884.51	7.0	0.684	0.003	299.8	1.4	0.5%	8	Lipid	Analytical Standard	Avanti Polar Lipids
PE O-46:13	C51H78NO7PK	+K	886.52	886.52	9.1	0.670	0.002	306.0	1.1	0.4%	8	Lipid	Analytical Standard	Avanti Polar Lipids
PE O-O-48:16	C53H78NO6PK	+K	894.52	894.52	1.1	0.672	0.001	305.1	0.7	0.2%	11	Lipid	Analytical Standard	Avanti Polar Lipids
PE O-47:14	C52H78NO7PK	+K	898.52	898.52	4.9	0.680	0.001	301.2	0.5	0.2%	11	Lipid	Analytical Standard	Avanti Polar Lipids
PE O-47:13	C52H80NO7PK	+K	900.53	900.53	-1.4	0.684	0.003	299.9	1.2	0.4%	11	Lipid	Analytical Standard	Avanti Polar Lipids
PE 46:11	C51H80NO8PK	+K	904.53	904.51	-17.3	0.678	0.002	302.4	0.9	0.3%	8	Lipid	Analytical Standard	Avanti Polar Lipids
PE O-O-49:17	C54H78NO6PK	+K	906.52	906.52	2.5	0.672	0.002	304.9	0.9	0.3%	9	Lipid	Analytical Standard	Avanti Polar Lipids
PE O-48:16	C53H76NO7PK	+K	908.50	908.49	-7.6	0.675	0.002	303.5	0.9	0.3%	9	Lipid	Analytical Standard	Avanti Polar Lipids
PE O-O-49:15	C54H82NO6PK	+K	910.52	910.52	7.0	0.672	0.001	304.9	0.6	0.2%	9	Lipid	Analytical Standard	Avanti Polar Lipids
PE O-49:17	C54H76NO7PK	+K	920.50	920.50	-2.6	0.670	0.002	306.1	1.0	0.3%	8	Lipid	Analytical Standard	Avanti Polar Lipids
PE O-49:16	C54H78NO7PK	+K	922.52	922.52	1.4	0.682	0.002	300.6	1.1	0.4%	9	Lipid	Analytical Standard	Avanti Polar Lipids
PE O-49:15	C54H80NO7PK	+K	924.53	924.53	-6.4	0.673	0.003	304.7	1.2	0.4%	12	Lipid	Analytical Standard	Avanti Polar Lipids
PE O-49:14	C54H82NO7PK	+K	926.55	926.55	-1.6	0.665	0.002	308.1	1.0	0.3%	10	Lipid	Analytical Standard	Avanti Polar Lipids
PE O-50:17	C55H78NO7PK	+K	934.52	934.51	-6.6	0.658	0.002	311.2	1.0	0.3%	9	Lipid	Analytical Standard	Avanti Polar Lipids
PE O-51:16	C56H82NO7PK	+K	950.55	950.54	-9.4	0.659	0.002	311.0	0.7	0.2%	11	Lipid	Analytical Standard	Avanti Polar Lipids
PE (1008.51)	--	--	1008.51	1008.51	--	0.637	0.002	321.2	0.8	0.3%	11	Lipid	Analytical Standard	Avanti Polar Lipids
PE O-O-62:19	C67H100NO6PK	+K	1084.69	1084.69	0.0	0.600	0.001	340.5	0.8	0.2%	10	Lipid	Analytical Standard	Avanti Polar Lipids
PE O-O-62:18	C67H102NO6PK	+K	1086.71	1086.71	0.7	0.598	0.001	341.8	0.7	0.2%	10	Lipid	Analytical Standard	Avanti Polar Lipids
PE O-O-64:19	C69H104NO6PK	+K	1112.72	1112.72	1.0	0.589	0.002	347.3	1.1	0.3%	10	Lipid	Analytical Standard	Avanti Polar Lipids
PE O-O-66:21	C71H104NO6PK	+K	1136.72	1136.73	3.5	0.586	0.001	348.9	0.7	0.2%	10	Lipid	Analytical Standard	Avanti Polar Lipids

Name	Adduct	Formula	m/z	m/z	ppm							Type	Grade	Source
PE Dimer 36:05+36:04	+Na	C82H146N2O16P2Na	1500.00	1500.00	-3.4	0.481	0.001	423.9	0.8	0.2%	10	Lipid	Analytical Standard	Avanti Polar Lipids
PE Dimer 36:04	+Na	C82H148N2O16P2Na	1502.02	1502.02	-1.0	0.477	0.001	426.9	0.8	0.2%	10	Lipid	Analytical Standard	Avanti Polar Lipids
PE Dimer 36:05+38:05	+Na	C84H148N2O16P2Na	1526.02	1526.02	2.7	0.474	0.001	429.9	0.7	0.2%	10	Lipid	Analytical Standard	Avanti Polar Lipids
PE Dimer 36:05+38:04	+Na	C85H154N2O15P2Na	1528.04	1528.04	2.9	0.473	0.001	430.3	0.6	0.1%	10	Lipid	Analytical Standard	Avanti Polar Lipids
PE Dimer 38:06	+Na	C86H148N2O16P2Na	1550.02	1550.03	6.8	0.472	0.001	431.8	0.9	0.2%	10	Lipid	Analytical Standard	Avanti Polar Lipids
PE Dimer 38:06+38:05	+Na	C86H150N2O16P2Na	1552.04	1552.04	4.1	0.470	0.001	433.5	0.6	0.1%	10	Lipid	Analytical Standard	Avanti Polar Lipids
PE Dimer 39:06	+Na	C88H152N2O16P2Na	1578.05	1578.06	3.0	0.460	0.000	443.1	0.3	0.1%	8	Lipid	Analytical Standard	Avanti Polar Lipids
PE Dimer 40:07	+Na	C90H152N2O16P2Na	1602.05	1602.05	1.4	0.460	0.001	442.8	0.8	0.2%	8	Lipid	Analytical Standard	Avanti Polar Lipids
PS O-O-36:03	+Na	C42H80NO8PNa	780.55	780.55	1.4	0.707	0.002	290.6	0.6	0.2%	11	Lipid	Analytical Standard	Avanti Polar Lipids
PS O-O-36:02	+Na	C42H82NO8PNa	782.57	782.57	0.7	0.703	0.002	292.2	0.7	0.3%	10	Lipid	Analytical Standard	Avanti Polar Lipids
PS O-36:05	+Na	C42H72NO10PNa	804.52	804.52	2.6	0.708	0.002	290.2	0.9	0.3%	10	Lipid	Analytical Standard	Avanti Polar Lipids
PS 36:04	+Na	C42H74NO10PNa	806.49	806.50	1.8	0.713	0.003	287.8	1.0	0.4%	13	Lipid	Analytical Standard	Avanti Polar Lipids
PS 37:04	+Na	C43H76NO10PNa	820.51	820.51	3.6	0.696	0.002	295.0	1.0	0.3%	11	Lipid	Analytical Standard	Avanti Polar Lipids
PS 38:07	+Na	C44H72NO10PNa	828.48	828.48	-3.3	0.707	0.001	290.2	0.4	0.1%	11	Lipid	Analytical Standard	Avanti Polar Lipids
PS 38:06	+Na	C44H76NO10PNa	832.51	832.51	1.0	0.698	0.001	294.0	0.6	0.2%	10	Lipid	Analytical Standard	Avanti Polar Lipids
PS 38:05	+Na	C44H78NO10PNa	834.53	834.53	1.2	0.698	0.002	294.2	0.8	0.3%	12	Lipid	Analytical Standard	Avanti Polar Lipids
PS 37:02	+K	C43H80NO10PK	840.52	840.51	-3.6	0.700	0.002	293.0	0.9	0.3%	10	Lipid	Analytical Standard	Avanti Polar Lipids
PS 39:07	+Na	C45H74NO10PNa	842.49	842.50	1.5	0.700	0.002	293.1	1.0	0.3%	11	Lipid	Analytical Standard	Avanti Polar Lipids
PS 39:06	+Na	C45H78NO10PNa	846.53	846.52	-2.0	0.689	0.002	297.7	1.0	0.3%	9	Lipid	Analytical Standard	Avanti Polar Lipids
PS 39:05	+Na	C45H80NO10PNa	848.54	848.54	-0.9	0.677	0.002	303.3	0.9	0.3%	11	Lipid	Analytical Standard	Avanti Polar Lipids
PE 38:04	+K	C44H78NO10PK	850.50	850.50	2.0	0.683	0.002	300.5	1.0	0.3%	11	Lipid	Analytical Standard	Avanti Polar Lipids
PS O-O-41:10	+K	C47H76NO8PK	852.49	852.49	-2.6	0.692	0.002	296.6	0.6	0.2%	7	Lipid	Analytical Standard	Avanti Polar Lipids
PS 40:08	+Na	C46H74NO10PNa	854.49	854.49	-0.7	0.699	0.002	293.6	0.8	0.3%	11	Lipid	Analytical Standard	Avanti Polar Lipids
PS 40:07	+Na	C46H76NO10PNa	856.51	856.51	0.4	0.694	0.001	295.6	0.6	0.2%	10	Lipid	Analytical Standard	Avanti Polar Lipids
PS 40:06	+Na	C46H80NO10PNa	860.54	860.54	-1.9	0.684	0.002	299.9	0.9	0.3%	10	Lipid	Analytical Standard	Avanti Polar Lipids
PS 40:05	+Na	C46H82NO10PNa	862.56	862.56	-1.7	0.679	0.002	302.2	0.8	0.3%	10	Lipid	Analytical Standard	Avanti Polar Lipids
PS 41:07	+Na	C47H78NO10PNa	870.53	870.52	-3.0	0.686	0.002	299.2	0.9	0.3%	11	Lipid	Analytical Standard	Avanti Polar Lipids
PS O-O-44:13	+Na	C50H76NO8PNa	872.52	872.51	-16.7	0.687	0.002	298.4	1.0	0.3%	8	Lipid	Analytical Standard	Avanti Polar Lipids

PS 41:06	+Na	C47H80NO10PNa	872.54	872.54	-4.7	0.676	0.002	303.3	1.1	0.4%	11	Lipid	Analytical Standard	Avanti Polar Lipids
PS 42:12	+Na	C48H70NO10PNa	874.46	874.46	0.5	0.698	0.003	293.7	1.1	0.4%	10	Lipid	Analytical Standard	Avanti Polar Lipids
PS 42:11	+Na	C48H72NO10PNa	876.48	876.48	0.1	0.697	0.002	294.2	0.7	0.2%	10	Lipid	Analytical Standard	Avanti Polar Lipids
PS 42:10	+Na	C48H74NO10PNa	878.49	878.49	-1.3	0.690	0.001	297.1	0.6	0.2%	10	Lipid	Analytical Standard	Avanti Polar Lipids
PS 42:09	+Na	C48H76NO10PNa	880.51	880.51	1.2	0.679	0.002	302.0	0.7	0.2%	10	Lipid	Analytical Standard	Avanti Polar Lipids
PS 42:08	+Na	C48H78NO10PNa	882.53	882.53	-0.7	0.681	0.002	301.3	0.9	0.3%	12	Lipid	Analytical Standard	Avanti Polar Lipids
PS 42:07	+Na	C48H80NO10PNa	884.54	884.54	-0.3	0.673	0.001	304.7	0.6	0.2%	10	Lipid	Analytical Standard	Avanti Polar Lipids
PS 42:05	+Na	C48H84NO10PNa	888.57	888.57	-2.6	0.668	0.001	307.0	0.6	0.2%	10	Lipid	Analytical Standard	Avanti Polar Lipids
PS 43:09	+Na	C49H78NO10PNa	894.52	894.53	-3.3	0.676	0.002	303.2	1.0	0.3%	10	Lipid	Analytical Standard	Avanti Polar Lipids
PS 43:08	+Na	C49H80NO10PNa	896.53	896.54	-9.1	0.672	0.001	305.2	0.6	0.2%	10	Lipid	Analytical Standard	Avanti Polar Lipids
PS 44:13	+Na	C50H72NO10PNa	900.48	900.48	6.0	0.695	0.002	294.9	0.8	0.3%	8	Lipid	Analytical Standard	Avanti Polar Lipids
PS 44:12	+Na	C50H74NO10PNa	902.50	902.49	0.9	0.684	0.001	299.7	0.5	0.2%	10	Lipid	Analytical Standard	Avanti Polar Lipids
PS 44:11	+Na	C50H76NO10PNa	904.51	904.51	-2.2	0.679	0.001	302.1	0.6	0.2%	10	Lipid	Analytical Standard	Avanti Polar Lipids
PS 44:10	+Na	C50H78NO10PNa	906.52	906.53	-1.3	0.675	0.001	303.5	0.6	0.2%	10	Lipid	Analytical Standard	Avanti Polar Lipids
PS 44:09	+Na	C50H80NO10PNa	908.54	908.54	-5.0	0.675	0.002	303.7	0.7	0.2%	10	Lipid	Analytical Standard	Avanti Polar Lipids
PS 44:08	+Na	C50H82NO10PNa	910.56	910.56	3.5	0.668	0.001	306.8	0.5	0.2%	10	Lipid	Analytical Standard	Avanti Polar Lipids
PS 45:15	+K	C49H80NO10PK	912.51	912.52	-9.8	0.683	0.002	300.2	0.9	0.3%	8	Lipid	Analytical Standard	Avanti Polar Lipids
PS 44:07	+Na	C50H84NO10PNa	912.58	912.57	3.7	0.657	0.002	311.8	1.0	0.3%	13	Lipid	Analytical Standard	Avanti Polar Lipids
PS 45:14	+K	C50H70NO10PK	914.47	914.47	-3.1	0.677	0.002	302.6	1.0	0.3%	11	Lipid	Analytical Standard	Avanti Polar Lipids
PS 43:07	+K	C49H82NO10PK	914.53	914.53	-3.4	0.675	0.002	303.6	0.7	0.2%	8	Lipid	Analytical Standard	Avanti Polar Lipids
PS 44:05	+Na	C50H88NO10PNa	916.62	916.60	15.5	0.658	0.002	311.5	0.8	0.3%	10	Lipid	Analytical Standard	Avanti Polar Lipids
PS O-45:12	+K	C51H78NO9PK	918.51	918.51	5.2	0.674	0.001	304.0	0.6	0.2%	10	Lipid	Analytical Standard	Avanti Polar Lipids
PS 44:09	+K	C50H80NO10PK	924.52	924.52	0.3	0.667	0.002	307.0	0.7	0.2%	10	Lipid	Analytical Standard	Avanti Polar Lipids
PS 46:12	+Na	C52H78NO10PNa	930.53	930.53	1.2	0.662	0.002	309.5	0.8	0.3%	10	Lipid	Analytical Standard	Avanti Polar Lipids
PS 46:11	+Na	C52H80NO10PNa	932.54	932.54	3.3	0.666	0.002	307.7	0.8	0.3%	10	Lipid	Analytical Standard	Avanti Polar Lipids
PS 46:10	+Na	C52H82NO10PNa	934.56	934.56	3.9	0.663	0.002	309.2	0.8	0.3%	11	Lipid	Analytical Standard	Avanti Polar Lipids
PS 45:10	+K	C51H80NO10PK	936.52	936.52	0.9	0.654	0.002	313.2	0.9	0.3%	10	Lipid	Analytical Standard	Avanti Polar Lipids
PS 45:09	+K	C51H82NO10PK	938.53	938.53	-2.8	0.659	0.002	310.6	1.1	0.4%	12	Lipid	Analytical Standard	Avanti Polar Lipids

PS 46:08	+Na	C52H86NO10PNa	938.59	938.60	15.1	0.654	0.002	313.2	0.8	0.2%	8	Lipid	Analytical Standard	Avanti Polar Lipids
PS O-47:14	+K	C53H78NO9PK	942.51	942.51	4.7	0.670	0.002	305.9	0.7	0.2%	11	Lipid	Analytical Standard	Avanti Polar Lipids
PS O-47:13	+K	C53H80NO9PK	944.52	944.52	-3.4	0.665	0.002	308.1	1.0	0.3%	12	Lipid	Analytical Standard	Avanti Polar Lipids
PS O-47:12	+K	C53H82NO9PK	946.54	946.53	-10.5	0.662	0.002	309.2	1.0	0.3%	11	Lipid	Analytical Standard	Avanti Polar Lipids
PS 46:10	+K	C52H82NO10PK	950.53	950.52	-12.7	0.669	0.002	306.3	1.0	0.3%	12	Lipid	Analytical Standard	Avanti Polar Lipids
PS 48:15	+Na	C54H76NO10PNa	952.51	952.52	13.5	0.666	0.002	307.8	0.8	0.3%	10	Lipid	Analytical Standard	Avanti Polar Lipids
PS 48:14	+Na	C54H78NO10PNa	954.53	954.53	1.2	0.657	0.002	312.0	0.8	0.3%	10	Lipid	Analytical Standard	Avanti Polar Lipids
PS 49:18	+Na	C55H72NO10PNa	960.48	960.47	-12.7	0.665	0.001	307.7	0.5	0.2%	8	Lipid	Analytical Standard	Avanti Polar Lipids
PS 47:12	+K	C53H80NO10PK	960.52	960.52	0.6	0.665	0.002	307.8	0.8	0.3%	11	Lipid	Analytical Standard	Avanti Polar Lipids
PS 47:11	+K	C53H82NO10PK	962.53	962.53	-5.7	0.659	0.000	311.0	0.2	0.1%	9	Lipid	Analytical Standard	Avanti Polar Lipids
PS 49:16	+Na	C55H76NO10PNa	964.51	964.50	-6.8	0.661	0.001	309.6	0.7	0.2%	7	Lipid	Analytical Standard	Avanti Polar Lipids
PS O-50:16	+Na	C56H80NO9PNa	964.55	964.54	-4.6	0.655	0.001	312.4	0.6	0.2%	11	Lipid	Analytical Standard	Avanti Polar Lipids
PS 49:15	+Na	C55H78NO10PNa	966.53	966.52	-3.4	0.656	0.000	312.3	1.2	0.4%	12	Lipid	Analytical Standard	Avanti Polar Lipids
PS 49:14	+Na	C55H80NO10PNa	968.54	968.54	-0.2	0.651	0.002	314.6	0.8	0.3%	10	Lipid	Analytical Standard	Avanti Polar Lipids
PS 48:14	+K	C54H78NO10PK	970.50	970.50	2.6	0.658	0.001	311.0	0.6	0.2%	10	Lipid	Analytical Standard	Avanti Polar Lipids
PS 48:13	+K	C54H80NO10PK	972.52	972.52	2.4	0.654	0.002	313.0	0.9	0.3%	10	Lipid	Analytical Standard	Avanti Polar Lipids
PS 48:12	+K	C54H82NO10PK	974.53	974.53	0.9	0.653	0.002	313.6	0.9	0.3%	10	Lipid	Analytical Standard	Avanti Polar Lipids
PS 51:16	+Na	C57H80NO10PNa	992.54	992.54	-1.0	0.645	0.002	317.3	0.8	0.3%	10	Lipid	Analytical Standard	Avanti Polar Lipids
PS 51:15	+Na	C57H82NO10PNa	994.56	994.56	-2.4	0.634	0.001	322.8	0.8	0.2%	10	Lipid	Analytical Standard	Avanti Polar Lipids
PS 52:19	+Na	C58H76NO10PNa	1000.51	1000.51	2.7	0.646	0.002	316.7	0.9	0.3%	10	Lipid	Analytical Standard	Avanti Polar Lipids
PS 52:18	+Na	C58H78NO10PNa	1002.53	1002.53	3.6	0.641	0.001	319.1	0.7	0.2%	10	Lipid	Analytical Standard	Avanti Polar Lipids
PS 52:17	+Na	C58H80NO10PNa	1004.54	1004.54	1.8	0.637	0.001	321.4	0.6	0.2%	10	Lipid	Analytical Standard	Avanti Polar Lipids
PS 52:16	+Na	C58H82NO10PNa	1006.56	1006.57	9.3	0.635	0.001	322.2	0.4	0.1%	7	Lipid	Analytical Standard	Avanti Polar Lipids
PS O-51:10	+K	C56H90NO10PK	1006.63	1006.63	3.6	0.635	0.002	322.4	0.8	0.3%	9	Lipid	Analytical Standard	Avanti Polar Lipids
PS 51:13	+K	C57H86NO10PK	1014.56	1014.55	-15.8	0.626	0.002	326.8	1.0	0.3%	8	Lipid	Analytical Standard	Avanti Polar Lipids
PS 51:12	+K	C57H88NO10PK	1016.58	1016.56	-18.3	0.637	0.001	321.1	0.5	0.2%	8	Lipid	Analytical Standard	Avanti Polar Lipids
PS 53:17	+Na	C57H90NO10PK	1018.56	1018.56	-1.9	0.633	0.001	323.3	0.5	0.2%	7	Lipid	Analytical Standard	Avanti Polar Lipids
PS 55:18	+Na	C61H84NO10PNa	1044.57	1044.57	-0.3	0.621	0.002	329.3	0.9	0.3%	7	Lipid	Analytical Standard	Avanti Polar Lipids

SM 34:01	+Na	C39H79N2O6PNa	725.56	725.56	-2.6	0.722	0.001	285.1	0.4	0.1%	10	Lipid	Analytical Standard	Avanti Polar Lipids
SM O-36:03	+Na	C41H81N2O5PNa	735.57	735.58	-5.5	0.708	0.001	290.4	0.6	0.2%	11	Lipid	Analytical Standard	Avanti Polar Lipids
SM 35:01	+Na	C40H81N2O6PNa	739.57	739.57	-4.1	0.711	0.002	289.1	0.8	0.3%	11	Lipid	Analytical Standard	Avanti Polar Lipids
SM 36:02	+Na	C41H81N2O6PNa	751.57	751.57	-0.5	0.707	0.001	290.9	0.2	0.1%	11	Lipid	Analytical Standard	Avanti Polar Lipids
SM 36:01	+Na	C41H83N2O6PNa	753.59	753.59	3.4	0.703	0.001	292.4	0.2	0.1%	11	Lipid	Analytical Standard	Avanti Polar Lipids
SM 37:01	+Na	C42H85N2O6PNa	767.60	767.60	-3.5	0.697	0.001	294.8	0.6	0.2%	11	Lipid	Analytical Standard	Avanti Polar Lipids
SM O-38:00	+Na	C43H91N2O5PNa	769.66	769.66	-1.6	0.676	0.002	303.9	1.0	0.3%	11	Lipid	Analytical Standard	Avanti Polar Lipids
SM 771.07	--	--	771.67	771.67	-5.0	0.672	0.002	305.6	0.9	0.3%	10	Lipid	Analytical Standard	Avanti Polar Lipids
SM 38:01	+Na	C43H87N2O6PNa	781.62	781.62	-1.2	0.688	0.001	298.5	0.4	0.1%	10	Lipid	Analytical Standard	Avanti Polar Lipids
SM 39:01	+Na	C44H89N2O6PNa	795.63	795.64	-3.6	0.681	0.002	301.6	0.7	0.2%	11	Lipid	Analytical Standard	Avanti Polar Lipids
SM O-40:00	+Na	C45H95N2O5PNa	797.69	797.69	-0.6	0.670	0.002	306.7	0.7	0.2%	9	Lipid	Analytical Standard	Avanti Polar Lipids
SM 40:03	+Na	C45H87N2O6PNa	805.62	805.62	-0.5	0.685	0.002	299.9	0.9	0.3%	11	Lipid	Analytical Standard	Avanti Polar Lipids
SM 40:02	+Na	C45H89N2O6PNa	807.63	807.64	-1.7	0.681	0.001	301.7	0.3	0.1%	11	Lipid	Analytical Standard	Avanti Polar Lipids
SM 40:01	+Na	C45H91N2O6PNa	809.65	809.65	-2.7	0.676	0.001	303.9	0.5	0.2%	11	Lipid	Analytical Standard	Avanti Polar Lipids
SM 40:00	+Na	C45H93N2O5PK	811.66	811.67	-5.7	0.672	0.001	305.7	0.5	0.1%	10	Lipid	Analytical Standard	Avanti Polar Lipids
SM O-42:04	+Na	C47H91N2O5PNa	817.65	817.66	-3.5	0.659	0.001	311.3	0.5	0.2%	9	Lipid	Analytical Standard	Avanti Polar Lipids
SM 41:02	+Na	C46H91N2O6PNa	821.65	821.65	-2.2	0.675	0.001	303.9	0.5	0.2%	11	Lipid	Analytical Standard	Avanti Polar Lipids
SM 41:01	+Na	C46H93N2O6PNa	823.66	823.67	-3.4	0.670	0.001	306.3	0.3	0.1%	9	Lipid	Analytical Standard	Avanti Polar Lipids
SM 42:03	+Na	C47H91N2O6PNa	833.65	833.65	-2.2	0.672	0.001	305.6	0.4	0.1%	11	Lipid	Analytical Standard	Avanti Polar Lipids
SM 42:02	+Na	C47H93N2O6PNa	835.67	835.67	3.2	0.666	0.001	308.2	0.2	0.1%	10	Lipid	Analytical Standard	Avanti Polar Lipids
SM 42:01	+Na	C47H95N2O6PNa	837.68	837.68	-3.4	0.663	0.001	309.3	0.3	0.1%	9	Lipid	Analytical Standard	Avanti Polar Lipids
SM 43:03	+Na	C48H93N2O6PNa	847.66	847.67	-5.0	0.663	0.001	309.6	0.3	0.1%	10	Lipid	Analytical Standard	Avanti Polar Lipids
SM 43:02	+Na	C48H95N2O6PNa	849.68	849.68	-2.6	0.659	0.001	311.5	0.3	0.1%	8	Lipid	Analytical Standard	Avanti Polar Lipids
SM 43:01	+Na	C48H97N2O6PNa	851.69	851.70	-12.6	0.657	0.001	312.5	0.4	0.1%	9	Lipid	Analytical Standard	Avanti Polar Lipids
SM O-43:01	+K	C48H99N2O5PK	853.68	853.69	-15.7	0.645	0.001	318.0	0.7	0.2%	11	Lipid	Analytical Standard	Avanti Polar Lipids
SM 44:03	+Na	C49H95N2O6PNa	861.68	861.68	-4.4	0.657	0.001	312.0	0.5	0.2%	8	Lipid	Analytical Standard	Avanti Polar Lipids
SM 44:02	+Na	C49H97N2O6PNa	863.70	863.70	-2.2	0.654	0.001	313.5	0.4	0.1%	10	Lipid	Analytical Standard	Avanti Polar Lipids
SM 44:01	+Na	C49H99N2O6PNa	865.71	865.71	-7.2	0.651	0.001	315.1	0.3	0.1%	9	Lipid	Analytical Standard	Avanti Polar Lipids

SM dimer 35:01	+Na	C80H162N4O12P2Na	1456.16	1456.17	6.6	0.459	0.001	444.2	0.8	0.2%	4	Lipid	Analytical Standard	Avanti Polar Lipids
SM dimer 36:01+36:02	+Na	C82H164N4O12P2Na	1482.17	1482.18	5.3	0.457	0.000	445.6	0.3	0.1%	4	Lipid	Analytical Standard	Avanti Polar Lipids
SM dimer 36:01	+Na	C82H166N4O12P2Na	1484.19	1484.20	9.3	0.465	0.000	438.1	0.1	0.0%	4	Lipid	Analytical Standard	Avanti Polar Lipids
SM dimer 37:01	+Na	C84H170N4O12P2Na	1512.22	1512.23	8.2	0.458	0.000	444.8	0.3	0.1%	4	Lipid	Analytical Standard	Avanti Polar Lipids
SM dimer 38:01+38:02	+Na	C86H172N4O12P2Na	1538.23	1538.25	8.5	0.469	0.000	433.9	0.3	0.1%	4	Lipid	Analytical Standard	Avanti Polar Lipids
SM dimer 38:01	+Na	C86H174N4O12P2Na	1540.25	1540.26	8.3	0.464	0.000	439.4	0.1	0.0%	4	Lipid	Analytical Standard	Avanti Polar Lipids
SM dimer 38:01+39:02	+Na	C87H174N4O12P2Na	1552.25	1552.26	9.4	0.441	0.001	461.7	0.8	0.2%	4	Lipid	Analytical Standard	Avanti Polar Lipids
SM dimer 38:01+39:01	+Na	C87H176N4O12P2Na	1554.27	1554.28	7.9	0.452	0.000	450.2	0.3	0.1%	4	Lipid	Analytical Standard	Avanti Polar Lipids
SM dimer 39:02	+Na	C88H174N4O12P2Na	1564.25	1564.27	13.2	0.464	0.001	438.5	0.6	0.1%	4	Lipid	Analytical Standard	Avanti Polar Lipids
SM dimer 39:01 + 39:02	+Na	C88H176N4O12P2Na	1566.27	1566.28	10.2	0.451	0.000	451.5	0.2	0.1%	4	Lipid	Analytical Standard	Avanti Polar Lipids

Table B.6. CCS Values Measured in Both Helium and Nitrogen Drift Gas.

Analyte		Exact m/z	Nitrogen CCS (This Work) [Å²]	Helium CCS (Literature) [Å²]	Difference in CCS [Å²]	Absolute Difference [%]	Literature Reference for Helium CCS Values
Quaternary Ammonium Salts (N=8)							
Tetramethylammonium	TAA1	74.1	107.4*	48.5	58.9	76%	1
Tetraethylammonium	TAA2	130.3	123.3	65.9	57.4	61%	1
Tetrapropylammonium	TAA3	186.4	144.1	88.9	55.2	47%	1
Tetrabutylammonium	TAA4	242.5	166.6	111.2	55.4	40%	1
Tetrapentylammonium	TAA5	298.6	190.1	133.5	56.6	35%	1
Tetrahexylammonium	TAA6	354.7	213.5	154.9	58.6	32%	1
Tetraheptylammonium	TAA7	410.8	236.4	174.5	61.9	30%	1
Tetraoctylammonium	TAA8	466.5	256.6	194.3	62.3	28%	1
Carbohydrates (N=24)							
Lactose + Na		342.30	178.1	121.1	57.0	38%	2
Maltotetraose + Na		689.21	235.3	159.0	76.3	39%	2
Lacto-N-fucopentaose I + Li		860.32	269.6	203.1	66.5	28%	2
Lacto-N-fucopentaose I + Na		876.30	276.1	204.4	71.7	30%	2
Lacto-N-fucopentaose II + Na		876.30	271.1	201.3	69.8	30%	2
Lacto-N-fucopentaose I + K		892.27	274.7	205.0	69.7	29%	2
Lacto-N-fucopentaose II + K		892.27	267.2	202.6	64.6	28%	2
Lacto-N-fucopentaose I + Rb		938.22	275.2	198.4	76.8	32%	2
Lacto-N-fucopentaose II + Rb		938.22	278.4	197.5	80.9	34%	2
Lacto-N-fucopentaose I + Cs		986.21	275.6	204.0	71.6	30%	2
α-cyclodextrin + Na		995.31	285.5	200.7	84.8	35%	2
Lacto-N-difucohexaose I + Li		1006.38	301.4	225.9	75.5	29%	6
Maltohexaose + Na		1013.32	286.4	206.0	80.4	33%	2
Lacto-N-difucohexaose I + Na		1022.35	290.6	225.6	65.0	25%	2
Lacto-N-difucohexaose I + Na		1022.35	304.2	225.6	78.6	30%	2

193

Lacto-N-difucohexaose II + Na	1022.35	291.2	220.6	70.6	28%	2
Lacto-N-difucohexaose II + Na	1022.35	306.3	220.6	85.7	33%	2
Lacto-N-difucohexaose I + K	1038.33	303.5	229.8	73.8	28%	6
Lacto-N-difucohexaose II + K	1038.33	305.8	225.3	80.5	30%	6
Lacto-N-difucohexaose I + Rb	1084.28	303.2	230.0	73.2	27%	6
Lacto-N-difucohexaose I + Cs	1132.27	301.2	232.3	68.9	26%	6
β-cyclodextrin + Na	1157.36	319.7	231.4	88.3	32%	2
Maltoheptaose + Na	1175.37	303.1	236.4	66.7	25%	6
Maltoheptaose + K	1191.34	303.4	236.7	66.7	25%	6
Tryptic Peptides (N=38)						
YVR + H	437.3	207.0	140.2	66.8	38%	3
GVFR + H	478.3	214.8	146.8	68.1	38%	3
SDGRG + H	491.2	204.6	130.0	74.6	45%	4
GRGDS + H	491.2	205.9	132.0	73.9	44%	4
VYAR + H	508.3	217.1	157.1	60.1	32%	3
ADLAK + H	517.3	228.3	159.3	69.0	36%	3
WMGK + H	521.3	220.1	152.9	67.2	36%	3
FWGK + H	537.3	231.0	160.5	70.5	36%	3
VASLR + H	545.3	232.5	163.7	68.8	35%	3
AFDEK + H	609.3	238.3	168.4	69.9	34%	3
GQIVGR + H	629.4	245.5	173.6	71.9	34%	3
IETMR + H	649.3	252.8	181.3	71.5	33%	3
AAGHDGK + H	655.3	249.0	170.2	78.8	38%	3
ANIDVK + H	659.4	248.1	176.8	71.3	34%	3
GVLHAVK + H	723.5	269.9	199.2	70.7	30%	3
SVVDSR + H	726.3	258.4	184.2	74.3	34%	3
NVPLYK + H	733.4	272.2	195.3	76.9	33%	3
IATAIEK + H	745.4	275.5	202.9	72.6	30%	3

LNQLLR + H	756.5	275.6	205.0	70.6	29%	3
HLADLSK + H	783.4	273.3	201.8	71.6	30%	3
LVTDLTK + H	789.5	276.6	205.8	70.8	29%	3
YDLDFK + H	800.4	272.4	201.0	71.4	30%	3
TFAEALR + H	807.4	283.5	210.0	73.5	30%	3
AADALLLK + H	814.5	291.8	223.9	68.0	26%	3
DIVGAVLK + H	814.5	277.8	206.1	71.7	30%	3
ATEEQLK + H	818.4	281.3	206.4	74.9	31%	3
IGDYAGIK + H	836.5	285.9	210.4	75.5	30%	3
DIPVPKPK + H	893.5	294.2	219.2	75.0	29%	3
AEFVEVTK + H	922.5	295.7	223.4	72.3	28%	3
YLYEIAR + H	927.5	305.0	228.0	76.9	29%	3
EALDFFAR + H	968.5	305.9	231.1	74.9	28%	3
LVVSTQTALA + H	1002.6	315.6	239.3	76.3	28%	3
ANELLINVK + H	1013.6	326.8	249.7	77.1	27%	3
GVIFYESHGK + H	1136.6	332.9	254.9	78.0	27%	3
IGSEVYHNLK + H	1159.6	348.4	269.7	78.7	25%	3
LVNELTEFAK + H	1163.6	344.4	267.5	76.9	25%	3
SISIVGSYVGNR + H	1251.7	349.1	267.8	81.3	26%	3
VNQIGTLSESIK + H	1288.7	358.7	278.8	80.0	25%	3
Lipids (N=49)						
PE 34:02 + Na	738.5	278.3	213.5	64.8	26%	2
PE 34:01 + Na	740.5	281.3	214.7	66.6	27%	2
SM (36:01) + Na	753.6	292.4	221.3	71.1	28%	2
PC 32:01 + Na†	754.5	283.6	217.6	66.0	26%	5
PC 32:00 + Na	756.6	286.5	217.4	69.1	27%	5
PE 36:04 + Na	762.5	280.6	214.4	66.2	27%	2
PE 36:02 + Na	766.5	285.7	220.9	64.8	26%	2

PE 35:02 + K^{+}	768.6	282.5	221.7	60.8	24%	2
SM O-(38:00) + Na^{+}	769.6	303.9	222.7	81.2	31%	2
PC 34:02 + Na	780.6	290.1	218.9	71.2	28%	2
SM (38:01) + Na	781.6	298.5	231.3	67.2	25%	2
PC 34:01 + Na	782.6	291.5	221.7	69.8	27%	2
PE 38:05 + Na	788.5	287.2	220.6	66.6	26%	2
PE 38:04 + Na	790.5	290.0	228.1	61.9	24%	2
SM O-(40:00) + Na^{+}	797.6	306.7	227.9	78.8	29%	5
PC 34:01 + K	798.5	292.5	222.0	70.5	27%	5
PC 36:04 + Na	804.6	293.8	221.3	72.5	28%	5
PC 36:03 + Na^{+}	806.6	294.5	220.6	73.9	29%	5
GlcCer 40:01 + Na	806.6	301.1	232.9	68.2	26%	2
PC 36:02 + Na	808.6	296.1	226.7	69.4	27%	2
GlcCer 40:00 + Na^{+}	808.6	302.3	236.6	65.7	24%	2
SM (40:01) + Na^{+}	809.7	303.9	225.4	78.5	30%	5
PC 36:01 + Na	810.6	297.7	228.1	69.6	26%	2
GlcCer 41:01 + Na^{+}	820.6	302.5	236.2	66.3	25%	2
PC 36:03 + K	822.5	297.8	222.9	74.9	29%	5
GlcCer 40:01 h + Na	822.6	303.4	234.6	68.8	26%	2
PC 36:02 + K	824.6	299.9	226.2	73.7	28%	2
GlcCer 40:00 h + Na^{+}	824.6	306.1	237.9	68.2	25%	2
PC 38:05 + Na	830.6	298.2	222.2	76.0	29%	2
PC 38:04 + Na	832.6	299.0	228.5	70.5	27%	2
GlcCer 42:02 + Na	832.7	305.2	238.8	66.4	24%	2
PS 38:05 + Na^{+}	834.5	294.2	225.5	68.7	26%	2
GlcCer 42:01 + Na	834.7	307.5	239.3	68.2	25%	2
SM (42:02) + Na	835.7	308.2	239.4	68.8	25%	2
GlcCer 42:00 + Na^{+}	836.7	308.2	240.2	68.0	25%	2

Lipid						
SM (42:01) + Na	837.7	309.3	239.3	70.0	26%	2
PS 37:02 + K†	840.6	293.0	222.6	70.4	27%	2
PC 38:06 + K	844.5	300.6	224.6	76.0	29%	5
GlcCer 43:02 + Na†	846.6	307.8	238.8	69.0	25%	2
PC 38:04 + K	848.6	301.5	230.0	71.5	27%	5
GlcCer 42:02 h + Na	848.7	309.0	240.3	68.7	25%	2
GlcCer 42:01 h + Na†	850.6	312.7	242.8	69.9	25%	5
SM O-(43:01) + K†	853.7	318.0	241.2	76.8	27%	5
GlcCer 44:02 + Na	860.7	315.3	245.9	69.4	25%	5
GlcCer 43:02 h + Na†	862.7	314.6	244.3	70.3	25%	5
GlcCer 43:01 h + Na†	864.6	313.7	245.2	68.5	25%	2
GlcCer 44:02 h + Na	876.7	318.4	246.7	71.7	25%	5
PS 42:09 + Na	880.5	302.0	238.0	64.0	24%	2
PS 42:08 + Na	882.5	301.3	230.8	70.5	26%	2

* TAA1 nitrogen CCS value obtained from Reference 1.

† Denotes lipid identifications which are different than originally reported in literature, due to the higher mass accuracy measurements obtained in this study.

References:
1. I. Campuzano, M.F. Bush, C.V. Robinson, C. Beaumont, K. Richardson, H. Kim, H.I. Kim, *Analytical Chemistry* **2012**, *84*(2), 1026-33.
2. L.S. Fenn, M. Kliman, A. Mahsut, S. Zhao, J.A. McLean, *Analytical and Bioanalytical Chemistry* **2009**, *394*, 235-244.
3. S.J. Valentine, A.E. Counterman, D.E. Clemmer, *Journal of the American Society for Mass Spectrometry* **1999**, *10*, 1188-1211.
4. M.F. Bush, Z. Hall, K. Giles, J. Hoyes, C.V. Robinson, B.T. Ruotolo, *Analytical Chemistry* **2010**, *82*(22), 9557-9565.
5. W.B. Ridenour, M. Kliman, J.A. McLean, R.M. Caprioli, *Analytical Chemistry* **2010**, *82*(5), 1881-1889.
6. Unpublished values measured in helium on a uniform field IM-MS instrument (Vanderbilt drift tube). For instrumentation details, see: S. Sundarapandian, J.C. May, J.A. McLean, *Analytical Chemistry* **2010**, *82*, 3247-3254.

B.1.4. Carbohydrate Nomenclature:

1.   Hexose assignments in the database are based on exact mass measurement. The
      exact type of hexose is uncertain

2.   All pentose identifications are assigned as fucose in the database as this is the
      only pentose present in the samples

3.   N-acetylated hexosamine are labeled such that the exact type of hexose is
      uncertain.

B.1.5. Carbohydrate abbreviations not previously listed:

Lacto-N-fucopentaose I   Fucα1-2Galβ1-3GlcNAcβ1-3Galβ1-4Glc

Lacto-N-fucopentaose II   Galβ1-3[Fucα1-4]GlcNAcβ1-3Galβ1-4Glc

Lacto-N-difucohexaose I   Fucα1-2Galβ1-3[Fucα1-4]GlcNAcβ1-
3Galβ1-4Glc

Lacto-N-difucohexaose II   Galβ1-3[Fucα1-4]GlcNAcβ1-3Galβ1-
4[Fucα1-3]Glc

α-cyclodextrin   Cyclomaltohexaose

β-cyclodextrin   Cyclomaltoheptaose

B.1.6. Lipid Nomenclature:

Glycerophospholipids:

    Ex. PC x:y

    PC, PE, PS = abbreviated names for phosphatidylcholine, phosphatidylethanolamine, phosphatidylserine respectively

        x = total number of carbons in fatty acid chains

        y = total number of double bonds in fatty acid chains

Sphingolipids:

    Ex. SM x:y

    SM, GlcCer = abbreviated names for sphingomyelin and cerebroside respectively

        x = total number of carbons in the amide linked fatty acid of the ceramide plus eighteen carbons from the sphingosine backbone

        y = total number of double bonds, one trans double bond in the sphingosine backbone plus the number of double bonds in the amide linked fatty acid of the ceramide

Hydroxylation on Cerebrosides:

    Ex. GlcCer x:y h

        h = denotes hydroxylation on the number two carbon (from the carbonyl) of the amide linked fatty acid

Alkyl Ether Linkage

    Ex. PS O-x:y

        x = total number of carbons in fatty acid chains

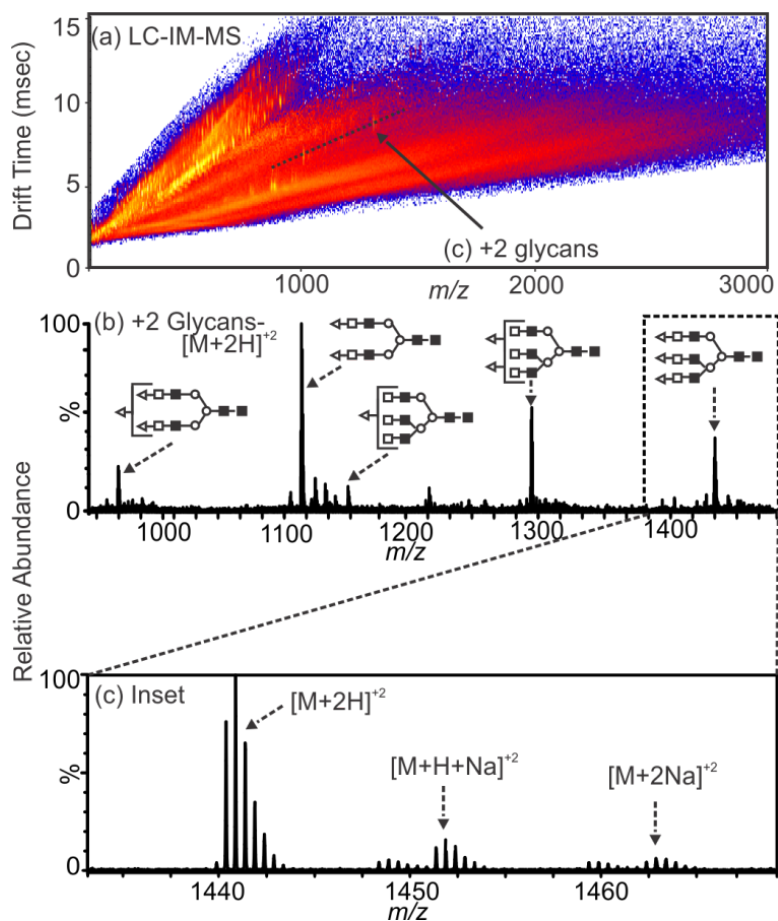   y = total number of double bonds in fatty acid chains

        O = alkyl ether substituent

   O-O = alkyl ether substituent occurs on both chains

SUPPLEMENTARY MATERIALS FOR CHAPTER III

C.1. Supplemental Materials for a Simple LC Glycan Separation

Figure C.1. Charge Adduct Distribution for Bovine Fetuin Released Glycans (a) A 2D IM-MS plot of glycans released from bovine fetuin after treatment with PNGaseF as discussed in the manuscript. Free non-derivatized glycans are separated by the method described above. Doubly charged glycans are annotated as (b). (b) A mobility selected mass spectrum of doubly charged free glycans from fetuin. A glycan segment of the mass spectrum was selected and magnified in the inset noted as (c). (c) A mass spectrum depicting the presence of both proton adducted and sodium adducted glycan species. As noted in the manuscript, the protonated species is more prominent than that of the sodium adducted species.
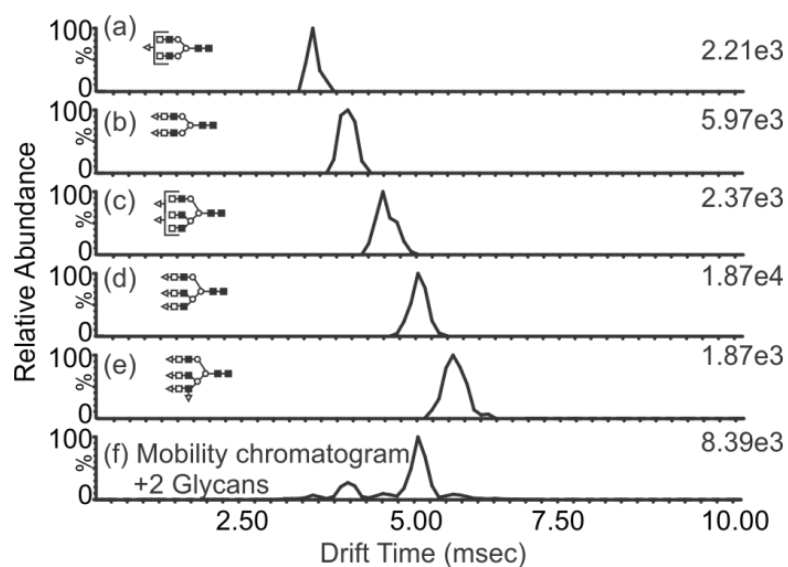
Figure C.2. Mobility Separation of N-Linked Glycans Cleaved from Bovine Fetuin. A series of drift time chromatograms for five of the glycans released from bovine fetuin. (a)- (e) Mobility chromatograms specific to the mass of the glycan depicted to the left of the peak. Relative abundances are noted to the right of the mobility peak. Some peaks do not fit a Gaussian profile, indicating the potential for multiple isomers. Further mobility and fragmentation studies to distinguish these overlapping isomeric peaks contributing to the mobility chromatogram are beyond the scope of this manuscript. (f) A total mobility chromatogram summed from the region annotated as the region of glycans in the 2D IM-MS plot in Figure C.1. above.
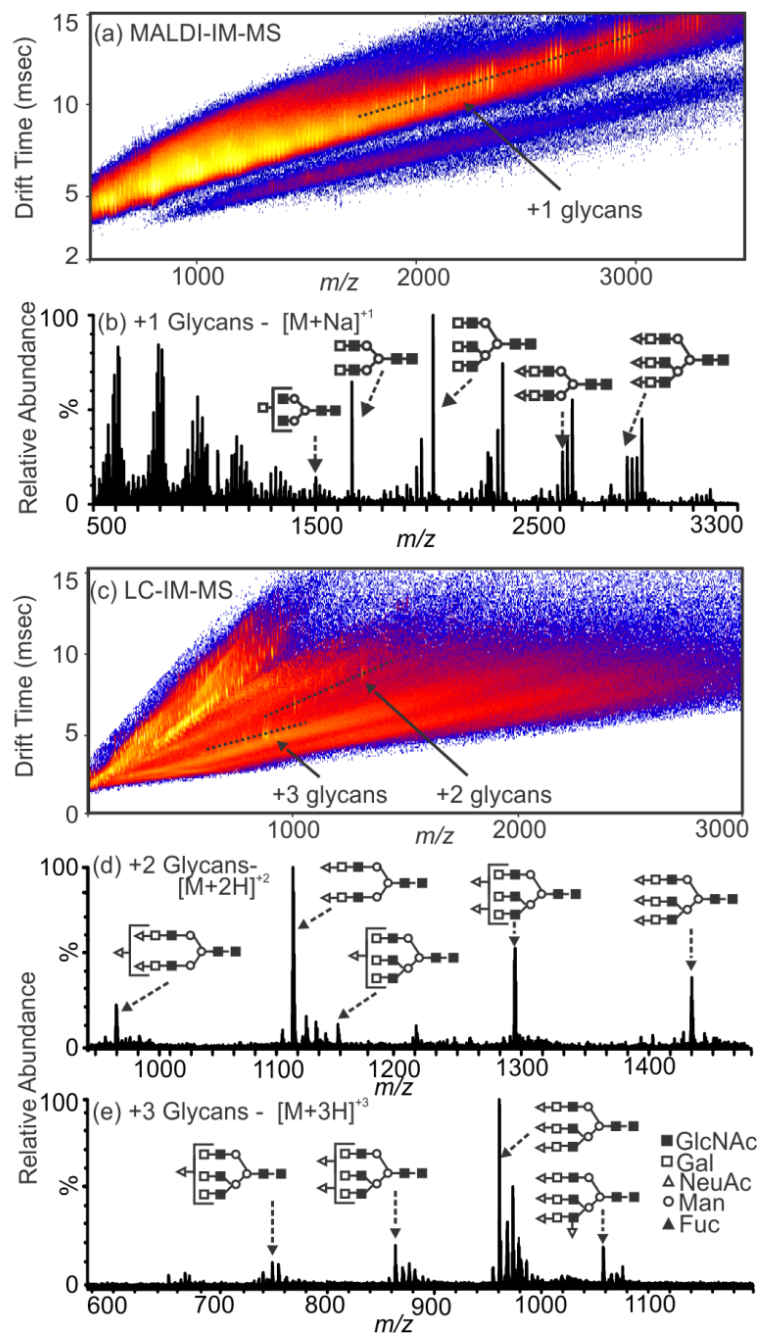
Figure C.3. Experiments in this study utilize Scheme 3 for the separation and analysis of carbohydrates from the model glycoprotein, bovine fetuin. MALDI-IM-MS serves as additional confirmation of LC-ESI-IM-MS results. (a) A 2-D MALDI-IM-MS plot of conformation space for the analysis of fetuin carbohydrates. Selected regions for singly charged glycans represent the extracted mass spectrum (b). (b) Mass spectrum of free N-linked glycans from fetuin. (c) A 2D LC-ESI-IM-MS plot of conformation space for the analysis of fetuin carbohydrates with annotated regions representing the mass spectra, (d) and (e), of the doubly- and triply-charged glycans, respectively.

C.1.1. Comments on Mobility Separation of N-linked Glycans Cleaved from Bovine Fetuin

It should be noted that analysis of carbohydrate by MALDI results in primarily singly charged glycans, $[M+Na]^+$, whereas LC-ESI-IM-MS preferentially creates doubly- and triply- protonated ions, $[M+2H]^{+2}$ and $[M+3H]^{+3}$ respectively. In LC-ESI-IM-MS, the sodiated glycan ions are presents as minor ionization products. The protocol for most MALDI-MS studies of glycans involves doping the sample-matrix solution with trace levels of salt to promote ionization. This gives rise to the sodiated glycans observed in Figure C.3. (b). The LC-IM-MS analysis of fetuin glycans compares favourably (in terms of both the appearance of representative ion signals and their corresponding signal-to-noise) to that of the previous MALDI-IM-MS experiments. This is demonstrated in the spectra in Figure C.3. (d) and (e), which show well-resolved doubly and triply-charged glycan signals.
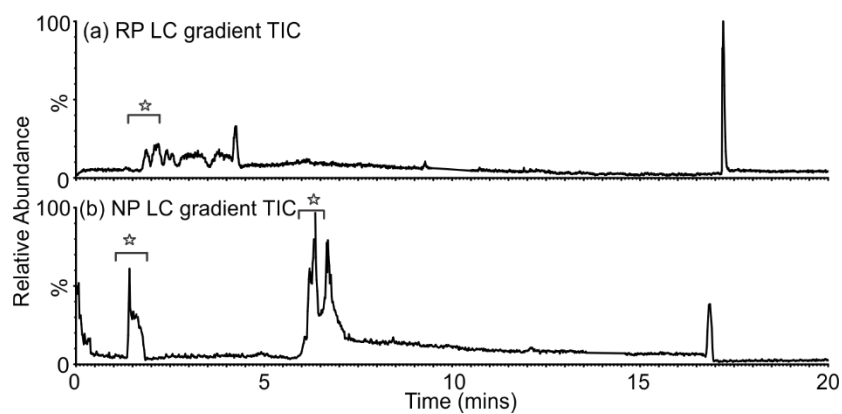
Figure C.4. LC TIC Chromatogram of a Mixture of Maltoses. Liquid chromatography total ion chromatograms of a series of maltose standards (M3-M7). C.4. (a) is an LC chromatogram for the reversed phase gradient annotated with a star for the region of sugars. C.4. (b) illustrates an LC chromatogram using the proposed method of a normal phase gradient and annotates the regions which contain maltose sugars with stars.

APPENDIX D

SUPPLEMENTARY MATERIALS FOR CHAPTER IV

D. 1. Supplemental Materials for Small Molecule Methodology for Experimental and Theoretical Analyses

D.1.1. Theoretical Collision Cross Section Calculations Methods

In order to generate theoretical ranges for large sets of metabolites, a computational approach is needed that can perform this task in a time efficient manner. Current metabolomics databases contain thousands of metabolites, which, regardless of the size of the chemical compounds, is a daunting task for an extensive conformational sampling study. Many conformational sampling techniques utilize molecular dynamics (MD) methods which rely on force fields to describe molecular classes. The various classes of molecular compounds that are represented in the metabolome make it difficult, if not impossible, to find one force field that would accurately describe every metabolite. These challenges suggest that the protocol utilizing distance geometry methods developed in the previous chapter should prove useful in this study. Distance geometry, which samples conformational space based solely on interatomic distances within the molecule, does not rely on a force field to sample conformational space and is a very time efficient computational technique.

Starting structures for all 50 metabolites were obtained from PubChem. These neutral structures initially underwent a geometry optimization at the Hartree Fock level of

theory with a 6-31G* basis set in the Gaussian 09 software.[1] These structures were used to generate the cation coordinating structures for the remainder of the calculation. Each of the neutral structures was also protonated based on pKa values and known protonation sites found in the literature.[2] These protonated structures also underwent a geometry optimization at the Hartree Fock level of theory with a 6-31G* basis set. The structures of the 50 metabolites with their site of protonation identified can be found in the supporting information (Figures D.7-D.12). The geometry optimization not only provides a good starting structure, but it also provides the electrostatic potential needed for partial charge derivation for introducing cations and later energy minimization steps. After the initial geometry optimization, both the protonated and neutral structures underwent a distance geometry calculation with DGEOM95[3] to generate all possible three-dimensional conformations of the metabolite. The distance restraints utilized in this program are described elsewhere in the literature,[4] but a brief description will be provided below. This program provides an RMSD cutoff to reject generated conformations that are too similar to other generated conformations. The set of metabolites spans a mass range of 90 – 828 Da and the number of rotatable bonds ranges from 0 – 25. This suggests that different RMSD cutoffs may be needed across this range. Values of 0.5, 0.75, and 1.00 RMSD were used for mass ranges of 90-199 Da, 200-399 Da, and 400-828 Da, respectfully. These values were determined based on conformational sampling capabilities and their effects on resulting CCS ranges. This data can be found in the supporting information (D.13).

Once the conformations were generated from distance geometry, a sodium cation was added to each of the neutral metabolites with the xLeap software found in

AMBER14[5]. The cation is placed with the neutral molecule according to the electrostatic potential grid. The cationized metabolites, as well as the protonated metabolites, then underwent a short energy minimization with the sander module in AMBER to generate low energy conformations.[6] A theoretical CCS value was then determined for each conformer, or for a subset of conformers (depending on the size of data set), using either MOBCAL[7-9] or PSA[10-13]. Details on the subsets of conformers used for this calculation can be found elsewhere in the appendix (Table D.14.).

D.1.2. Analysis of a Representative set of Small Molecules

The experimental CCS of 10 of these metabolites is overlaid with the theoretical CCS range in Figure 3. The blue circles indicate agreement between experiment and theory where red circles indicate disagreement between the two. Helium results are shown in Figures 3A and 3B and nitrogen results in Figures 3C and 3D. The results are further split into groups of small mass metabolites (Figures 3A and 3C) and large mass metabolites (Figures D.1.A and D.1.D) for viewing clarity. For the small mass metabolites, we see poor agreement for fucose [H+] and kynurenate [H+] for both helium and nitrogen. Both of these metabolites are small (165.08 and 190.05) and reflect the disagreement observed with the smaller metabolites (caffeine and atenolol) mentioned previously. This suggests that there might be a lower end cutoff for utilizing the theoretical ranges to support and guide experimental CCS measurements. Melatonin, cocaine, and ondansetron are the remaining three metabolites shown in Figures 3A and 3C. For Melatonin and cocaine we see good agreement with both helium and nitrogen whereas for ondansetron we only see agreement with helium. This is similar to results for

the larger metabolites in Figures 3B and 3D where we see good agreement for colchicine, raffinose, glutathione oxidized and maltopentose in helium and nitrogen, but for folate we only see agreement in helium. Disagreement of folate and ondansetron in nitrogen only suggest and error on the theoretical CCS calculations.

For the metabolites that do agree, they tend to fall toward the lower end of the theoretical ranges. This observation is due to the fact that all possible three-dimensional conformations are generated with the distance geometry approach producing larger theoretical CCS values than observed experimentally. The addition of the cation, and to some degree the proton, causes the metabolites to form more densely packed conformations which correspond to smaller CCS values.

For the metabolites that do not agree determining the source of error depends on whether the experimental value fell above or below the theoretical range and if we see disagreement in both gases. If the experimental CCS value falls below the theoretical range, there is likely error associated with the theoretical calculation. It is also likely that if we see agreement in helium, but not nitrogen then the error is likely resulting from the theoretical CCS calculation. While nitrogen is becoming more popular for experimental CCS measurements, the theoretical CCS calculations are better suited for comparison with helium CCS measurements. New and improved techniques, such as PSA, are being developed with capabilities to obtain theoretical nitrogen CCS values, but this work is still preliminary at this time.

If the experimental CCS value falls above the theoretical range, there is likely error associated with the experimental measurement. Experimental errors either stem from false peak identifications, poor resolution or failure in assumptions for the kinetic

theory of gases. The kinetic theory of gases, on which CCS calculations are based, assumes completely elastic interactions between the drift gas and the molecular ion. For the smaller metabolites, the polarizability effect of nitrogen is stronger. This corresponds to more inelastic interaction that results in longer drift times and larger CCS values. This trend is observed when the experimental CCS values falling above the theoretical CCS ranges for the smallest metabolite values. Experimental values could also be incorrect due to the false identification of peaks in the IM-MS experiment. Endogenous and exogenous noise in the low mass region of the spectra makes feature selection and identification a challenge for these compounds. Deviations between the theoretical and experimental CCS values will be discussed in further detail in the following section.

D.1.3. Incongruences Between Theoretical Ranges and Experimental Values

At this point it is important to mention possible sources of error for both experimental CCS measurements and theoretical CCS calculations. These sources of error likely contribute to disagreement between the two CCS values and are summarized in Table 2 below. First, the experimental errors will be discussed. Although instrument capabilities are constantly improving, poor mobility resolution for the mass range of the metabolite samples could result in misidentified metabolite ions. Faint sample peaks or endogenous sample noise can make identification difficult for certain species. The remaining sources of error that will be discussed for experimental CCS measurements concern the ion-neutral interaction between the metabolite ion and the neutral drift gas molecules. The Mason-Schamp equation assumes elastic interactions between the ion and netural buffer gas. Previous work has shown that this assumption holds for

209

measurements made in helium, which is a small (4 Da), monoatomic atom. The assumption no longer holds for the larger (28 Da) diatomic nitrogen gas molecule.[13,14] The inelastic interaction between the gas phase ion and nitrogen drift gas results from momentum transfer during the collision, which corresponds to a longer drift time and thus larger CCS values.[15] This momentum transfer will have a greater effect on these small metabolite ions and therefore altering their experimental CCS values to differ from a purely structural measurement. In addition to their size difference, helium and nitrogen have considerably different polarizability values, 0.205Å^3 and 1.641Å^3 respectively.[9] While it has been suggested that polarizability of different drift gases does not effect CCS measurements for larger gas phase ions, it may play a role for the smaller metabolites examined in this work.

There are also sources of error for the theoretical CCS calculations. Distance geometry arguably samples all possible conformations space making it difficult to claim that certain experimentally observed conformations may not have been generated. Achieving appropriate coordination of the cation is more difficult with distance geometry methods and therefore the modeling could fail to generate the observed experimental structures. The remaining sources of error result from the theoretical CCS calculations methods. Both the projection superposition approximation (PSA) and the trajectory method (TM) were used in this work to calculate theoretical CCS values. The PSA calculation starts with the projection approximation, which calculates the area of two-dimensional projected images of the molecule. The calculation then uses a shape factor, which is a measure of the concavity of the molecular surface of the ion, to adjust the projection approximation CCS value.

In order to obtain nitrogen CCS values a set of "preliminary parameters" are used. It is speculated that these parameters are based on previous measurements and theory. The authors of PSA admit that there is room for improvement in these parameters and thus this could contribute to error in these calculated CCS values. This approximation approach only considered the structure of the ion and therefore does not directly incorporate ion-netural interactions that are know to have an influence on CCS for drift gases other than helium. With the exception of the twelve metabolites that do not contain the appropriate ratio of carbon, oxygen, and nitrogen, the PSA method was used to determine theoretical CCS values. The TM is a more rigorous approach to determining theoretical CCS values and was used for the twelve remaining metabolites. It integrates under scattering angles to obtain the rotationally averaged surface area or CCS of the ion. This approach incorporates Lennard-Jones potentials in an attempt to accurately describe the ion-netural interaction. Although this is a theoretically rigorous approach, it can fail to accurately generate CCS values that agree with experimental CCS values. This is most likely due to the method not completely accounting for the polarizability and momemtum transfer that both effect the CCS measurement. Modifications to the original calculation attempt to more accurately model nitrogen as a diatomic atom[17] but for small molecules where polarizability and momentum transfer play a larger role in CCS determination there is still a deviation between experiment and theory.

In order to obtain a clearer picture of ion-neutral interactions in the gas phase, a MD simulation could be performed that would mimic the environment of a drift tube used in an IM experiment. This would allow for the actual interactions between the sample ion and the neutral buffer gas to be observed under the pressure and temperature

conditions that occur experimentally. While this approach would provide very helpful insight into the ion-neutral interactions that influence CCS measurements, it is outside the scope of the present work.

D.1.4. Concluding Remarks on Theoretical Modeling of CCS Values

Ten of the metabolites in the initial data set were not compared to theoretical CCS values due to their preference to form negative ions. Future work will aim to generate theoretical conformations for the negative ions as well as for larger sets of metabolites. Distance geometry should prove useful for the negative ions because the challenge of an additional proton or cation will no longer be a concern.

These theoretical CCS ranges will benefit future generation of CCS values as they provide a benchmark for the experimental measurement. Once the deviations between the theoretical ranges and experimental values are fully understood, corrected databases of theoretical CCS ranges can be constructed. These databases will then offer an additional feature for identifying metabolites in future metabolomics studies.

D. 1.5. References

1.   Frisch, M. J.; Trucks, G. W.; Schlegel, H. B.; Scuseria, G. E.; Robb, M. A.; Cheeseman, J. R.; Scalmani, G.; Barone, V.; Mennucci, B.; Petersson, G. A. Gaussian 09, Revision A. 02, Gaussian. Inc., Wallingford, CT 2009, 2 (3), 4.

2.   Tang, C. L.; Alexov, E.; Pyle, A. M.; Honig, B. Calculation of pK a s in RNA: On the structural origins and functional roles of protonated nucleotides. Journal of Molecular Biology 2007, 366 (5), 1475-1496.

3.   Blaney, J. M.; Crippen, G. M.; Dearing, A.; Dixon, S.; Spellmeyer, D. C. DGEOM95, Chiron Corporation, 1984-1995.

4.   Case, D. A.; Babin, V.; Berryman, J.; Betz, R. M.; Cai, Q.; Cerutti, D. S.; Cheatham Iii, T. E.; Darden, T. A.; Duke, R. E.; Gohlke, H. Amber 142014.

5.	Wang, J.; Wolf, R. M.; Caldwell, J. W.; Kollman, P. A.; Case, D. A. Development and testing of a general amber force field. Journal of Computational Chemistry 2004, 25 (9), 1157-1174.

6.	von Helden, G.; Hsu, M. T.; Gotts, N.; Bowers, M. T. Carbon cluster cations with up to 84 atoms: structures, formation mechanism, and reactivity. The Journal of Physical Chemistry 1993, 97 (31), 8182-8192.

7.	Mesleh, M. F.; Hunter, J. M.; Shvartsburg, A. A.; Schatz, G. C.; Jarrold, M. F. Structural information from ion mobility measurements: effects of the long-range potential. The Journal of Physical Chemistry 1996, 100 (40), 16082-16086.

8.	Campuzano, I.; Bush, M. F.; Robinson, C. V.; Beaumont, C.; Richardson, K.; Kim, H.; Kim, H. I. Structural characterization of drug-like compounds by ion mobility mass spectrometry: comparison of theoretical and experimentally derived nitrogen collision cross sections. Analytical Chemistry 2011, 84 (2), 1026-1033.

9.	Bleiholder, C.; Wyttenbach, T.; Bowers, M. T. A novel projection approximation algorithm for the fast and accurate computation of molecular collision cross sections (I). Method. International Journal of Mass Spectrometry 2011, 308 (1), 1-10.

10.	Bleiholder, C.; Contreras, S.; Do, T. D.; Bowers, M. T. A novel projection approximation algorithm for the fast and accurate computation of molecular collision cross sections (II). Model parameterization and definition of empirical shape factors for proteins. International Journal of Mass Spectrometry 2013, 345, 89-96.

11.	Anderson, S. E.; Bleiholder, C.; Brocker, E. R.; Stang, P. J.; Bowers, M. T. A novel projection approximation algorithm for the fast and accurate computation of molecular collision cross sections (III): Application to supramolecular coordination-driven assemblies with complex shapes. International Journal of Mass Spectrometry 2012, 330-332, 78-84.

12.	Bleiholder, C.; Contreras, S.; Bowers, M. T. A novel projection approximation algorithm for the fast and accurate computation of molecular collision cross sections (IV). Application to polypeptides. International Journal of Mass Spectrometry 2013, 354, 275-280.

13.	Beegle, L. W.; Kanik, I.; Matz, L.; Hill Jr., H. H. Effects of Drift-Gas Polarizability on Glycine Peptides in Ion Mobility Spectrometry. International Journal of Mass Spectrometry, 2002, 216, 257-268.

14.	Hill Jr., H. H.; Hill, C. H., Asbury, G. R.; Wu, C.; Matz, L. M.; Ichiye, T. Charge Location on Gas Phase Peptides. International Journal of Mass Spectrometry, 2002, 219, 23-27.

15.   Larriba-Andaluz, C.; Fernandex-Garcia, J.; Ewing, M. A.; Hogan Jr., C. J.; Clemmer, D. E. Gas Molecule Scattering and Ion Mobility Measurements for Organic Macro-ions in He versus N_2 Environments. Physical Chemistry Chemical Physics, 2015.
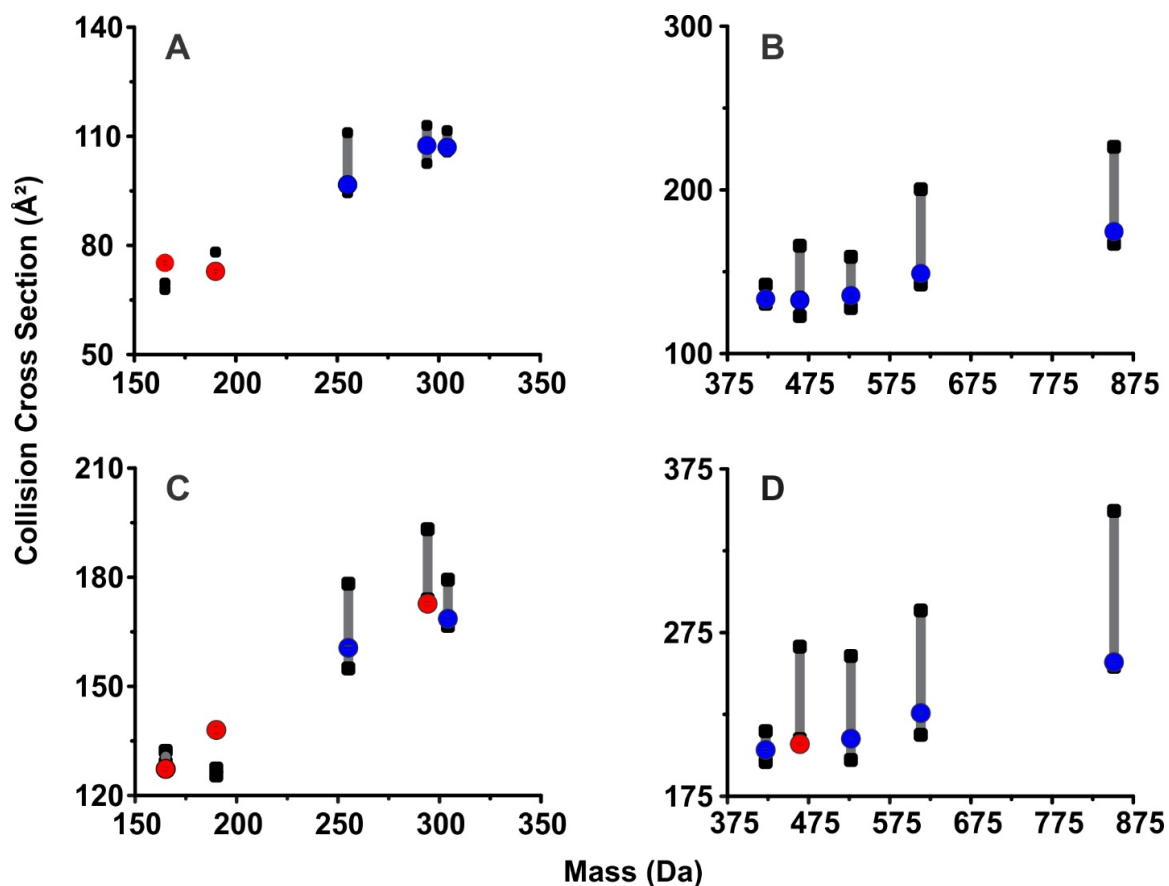
Figure D.1. The experimental CCS values (blue and red circles) for the DTIM instrument are compared with the theoretical CCS ranges (grey bars with black end points) in these plots. The *m/z* values are plotted on the x-axis and the CCS values are plotted on the y-axis. Results for helium are shown in A) for a selected group of low mass metabolites and in B) for a selected group of high mass metabolites. Results for nitrogen are shown in C) for a selected group of low mass metabolites and in D) for a selected group of high mass metabolites. Blue circles indicate agreement between experiment and theory where red circles indicate disagreement between the two.

Potential Sources for Error in CCS Calculations	
Experiment	Theory
• Poor resolution	• Cation sampling
• Poor senesitive for small ions	• Approximation based calculations
• Ion and drift gas interaction	• Scattering angle calculations

Table D.1. Potential sources of error for both experimental and theoretical

Table D.2. The metabolites examined in this study are listed in the table below with their *m/z* values.

Metabolite (Abbreviation)	*m/z* (M+H)⁺[M+Na]⁺	Metabolite (Abbreviation)	*m/z* (M+H)⁺[M+Na]⁺
Lactic Acid (LA)	(91.04) [113.02]	Biotin (BIO)	(245.10) [267.08]
Choline (CHO)	104.11 [M⁻]⁺	2'deoxyadenosine (2DE)	(252.11) [274.09]
Nicotinic Acid (NIC)	(124.04) [146.02]	Thiamine (THI)	265.11 [M⁻]⁺
5-Fluorouracil (5FL)	(131.03) [153.01]	Adenosine (ADO)	(268.10) [290.09]
Leucine (LEU)	(132.10) [154.08]	Guanosine (GUA)	(284.10) [306.08]
Amphetamine (APH)	(136.11) [158.09]	Ondansetron (OND)	(294.16) [316.14]
Salicylic Acid (SAL)	(139.04) [161.02]	Cocaine (COC)	(304.15) [326.14]
Fucose (FUC)	(165.08) [187.06]	Glutathione (GTA)	(308.09) [330.07]
Quinolinic Acid (QUN)	(168.03) [190.01]	NANA (NAN)	(310.11) [332.10]
Uric Acid (URC)	(169.04) [191.02]	CMP (CMP)	(324.06) [346.04]
Glucose (GLU)	(181.07) [203.05]	UMP (UMP)	(325.04) [347.03]
Mannose (MAN)	(181.07) [203.05]	Sucrose (SUC)	(343.12) [365.11]
Tyrosine (TYR)	(182.08) [204.06]	Melibiose (MEB)	(343.12) [365.11]
Sorbitol (SOR)	(183.09) [205.07]	AMP (AMP)	(348.07) [370.05]
Kynurenate (KYN)	(190.05) [212.03]	LacNAc (LAC)	(370.13) [392.12]
Citric Acid (CIT)	(193.03) [215.02]	Colchicine (COL)	(400.18) [422.16]
MDMA (MDM)	(194.12) [216.10]	ADP (ADP)	(428.04) [450.02]
Caffeine (CAF)	(195.09) [217.07]	Folate (FOL)	(442.15) [464.13]
ADMA (ADM)	(203.15) [225.13]	Glycodeoxycholate (GLY)	(450.32) [472.30]
Pantothenic Acid (PAN)	(220.12) [242.10]	Verapamil (VER)	(455.29) [477.27]
GlcNAc (GLC)	(222.10) [244.08]	Raffinose (RAF)	(505.18) [527.16]
GalNAc (GAL)	(222.10) [244.08]	Glutathione Oxidized (GOX)	(613.16) [635.14]
Melatonin (MLT)	(233.13) [255.11]	Stachyose (STA)	(667.23) [689.21]
Thymidine (THY)	(243.10) [265.08]	Acetyl coenzyme A (ACA)	(810.13) [832.11]
Cytidine (CYT)	(244.09) [266.07]	Maltopentose (MLP)	(829.28) [851.26]

Table D.3. Feature descriptors for small molecules in nitrogen drift gas

Compound	Ion	Mass (Da)	Measured Mass (Da)	Mass ACC (ppm)	CCS (Å^2)	SD CCS (Å^2)	RSD	N	Theoretical CCS Range (Å^2)
N-ethylaniline	H+	122.10	122.10	-12.54	66.4	0.3	0.4%	12	-
Amphetamine	H+	136.11	136.11	19.24	60.8	0.8	1.3%	12	69.6-71.7
Leucine	Na+	154.08	154.10	-74.64	71.6	0.4	0.6%	20	70.3-87.6
Fucose	H+	165.08	165.09	-80.60	75.2	0.4	0.5%	14	67.8-69.6
Quinolinic Acid	H+	168.03	168.03	11.79	67.9	0.6	0.9%	20	68.9-69.5
Benzophenone	H+	183.08	183.08	17.95	80.9	0.4	0.5%	6	-
Fucose	Na+	187.06	187.06	-9.94	77.7	0.5	0.6%	14	73.3-75.9
Quinolinic Acid	Na+	190.01	190.01	9.62	74.3	0.4	0.5%	14	75.3-75.5
Kynurate	H+	190.05	190.05	-9.39	72.9	0.4	0.6%	14	77.3-80.7
MDMA	H+	194.12	194.11	23.17	83.2	0.5	0.6%	14	82.5-87.2
Caffeine	H+	195.09	195.08	17.41	76.2	0.4	0.5%	14	78.9-78.9
Glucose	Na+	203.05	203.06	-15.00	85.1	0.6	0.7%	14	73.9-81.3
Mannose	Na+	203.05	203.05	-4.65	74.7	0.5	0.7%	14	73.2-81.0
Sorbitol	Na+	205.07	205.07	5.39	78.9	0.4	0.5%	21	74.7-88.2
Kynurate	Na+	212.03	212.03	-3.01	83.8	0.5	0.6%	14	87.2-87.2
MDMA	Na+	216.10	216.10	15.93	86.2	0.4	0.5%	14	84.9-93.8
Caffeine	Na+	217.07	217.07	-12.71	83.5	0.4	0.5%	14	86.6-86.6
Pantothenic Acid	H+	220.12	220.11	28.58	85.7	0.4	0.5%	14	83.0-94.1
Melatonin	H+	233.13	233.12	31.30	93.0	0.6	0.6%	14	91.4-102.5
Pantothenic Acid	Na+	242.10	242.09	31.13	86.7	0.6	0.7%	14	86.6-103.2
GalNAc	Na+	244.08	244.08	3.29	84.1	0.5	0.6%	14	85.5-104.7
Cytidine	H+	244.09	244.08	46.05	84.1	0.4	0.5%	7	87.0-92.3
biotin	H+	245.10	245.08	83.57	86.6	0.5	0.6%	14	85.9-100.4
2'-deoxyadenosine	H+	252.11	252.11	8.17	88.8	0.6	0.7%	14	89.4-96.8
Melatonin	Na+	255.11	255.10	37.01	96.7	0.6	0.6%	14	94.4-111.0
Propranolol	H+	260.17	260.17	-0.60	100.1	0.5	0.5%	12	94.6-111.8
Thymidine	Na+	265.08	265.07	30.32	94.6	0.5	0.6%	20	93.1-104.6
Thiamine (vit B)	M	265.11	265.11	18.49	99.8	0.7	0.7%	21	97.5-107.3
Cytidine	Na+	266.08	266.06	45.05	91.9	0.5	0.6%	7	90.7-98.4
Atenolol	H+	267.17	267.17	0.22	95.4	0.5	0.5%	12	97.0-117.6
Adeonsine	H+	268.10	268.10	7.36	89.8	0.5	0.6%	14	92.3-98.7
Metroprolol	H+	268.19	268.19	0.22	109.4	0.6	0.5%	13	99.1-122.8
2'-Deoxyadenosine	Na+	274.09	274.09	13.88	94.0	0.5	0.6%	14	93.5-104.4
Imipramine	H+	281.20	281.20	3.07	102.6	0.5	0.5%	12	101.7-113.1
Adeonsine	Na+	290.09	290.08	12.13	94.1	0.6	0.6%	14	95.3-105.2
Atropine	H+	290.18	290.17	4.51	106.3	0.7	0.7%	12	99.9-113.4
Ondansetron	H+	294.16	294.13	87.47	107.5	0.7	0.6%	14	102.5-113.0
Cocaine	H+	304.15	304.13	94.61	107.0	0.6	0.6%	14	105.7-111.5
NANA	H+	310.11	310.08	93.84	100.5	0.5	0.5%	7	97.9-1077
Quinine	H+	325.19	325.19	9.51	113.0	0.6	0.5%	12	110.7-120.0
UMP	Na	347.03	347.02	23.73	99.3	0.6	0.6%	14	96.7-117.7

AMP	H+	348.07	348.06	19.56	102.0	0.6	0.6%	14	99.0-116.5
Sucrose	Na+	365.11	365.08	65.67	104.0	0.6	0.6%	7	104-123.2
Melibiose	Na+	365.11	365.10	22.12	106.6	0.6	0.6%	14	102.8-124.3
AMP	Na+	370.05	370.04	22.57	107.2	0.6	0.6%	14	101.0-124.2
Colchicine	H+	400.18	400.17	25.25	130.4	0.9	0.7%	14	126.5-137.2
LacNAc	Na+	406.13	406.12	26.16	117.5	0.7	0.6%	14	111.0-135.7
Colchicine	Na+	422.16	422.15	28.07	133.4	0.9	0.7%	14	130.4-142.0
Folate	H+	442.15	442.13	41.39	123.6	0.8	0.7%	21	120.1-156.0
Verapamil	H+	455.29	455.28	29.80	141.8	0.9	0.7%	14	135.0-171.8
Folate	Na+	464.13	464.11	42.11	132.6	0.8	0.6%	7	122.9-165.9
Verapamil	Na+	477.27	477.26	33.34	145.3	1.0	0.7%	14	136.8-178.7
Raffinose	Na+	527.16	527.14	37.74	135.5	0.8	0.6%	14	127.8-158.1
Glutathione Oxidized	H+	613.16	613.14	39.27	148.9	1.0	0.7%	14	142.1-200.4
Glutathione Oxidized	Na+	635.14	635.11	42.39	149.7	1.0	0.7%	14	145.2-204.7
Stachyose	Na+	689.21	689.18	43.84	155.9	1.2	0.8%	14	149.6-190.2
Maltopentose	H+	829.28	829.24	49.79	174.9	1.5	0.8%	14	167.2-222.7
Maltopentose	Na+	851.26	851.22	52.56	174.5	1.4	0.8%	14	167.07-226.9

Table D.4. Feature descriptors for small molecules in nitrogen drift gas

| Compound	Ion	Mass (Da)	Measured Mass (Da)	Mass ACC (ppm)	CCS (Å²)	SD CCS (Å²)	RSD	N	Theoretical CCS Range (Å²)
fucose	H+	165.08	165.07	-53.3	127.3	0.55	0.4%	16	128.9-132.3
kynurenate	H+	190.05	190.05	-13.8	138.0	0.96	0.7%	16	125.5-127.4
caffeine	H+	195.09	195.09	-15.4	151.6	0.77	0.5%	15	140.1-141.0
mannose	Na+	203.05	203.05	-13.1	150.2	0.77	0.5%	16	130.5-151.8
sorbitol	Na+	205.07	205.07	-17.6	152.9	1.00	0.7%	16	133.5-159.6
kynurenate	Na+	212.03	212.03	-17.3	155.4	1.11	0.7%	16	137.5-139.9
pantothenic acid	Na+	242.10	242.10	-19.2	154.4	0.56	0.4%	16	133.2-154.3
GlcNAc	Na+	244.08	244.08	-11.9	164.2	0.73	0.4%	16	127.4-138.8
Melatonin	Na+	255.11	255.11	-17.4	160.6	0.57	0.4%	16	154.9-178.2
propranolol	H+	260.17	260.16	-8.3	162.2	0.41	0.3%	16	-
thymidine	Na+	265.08	265.08	-16.7	167.9	1.06	0.6%	16	143.1-158.9
biotin	Na+	267.08	267.07	-17.0	167.1	1.64	1.0%	16	116.7-164.5
atenolol	H+	267.17	267.17	-7.0	156.5	0.40	0.3%	16	-
adenosine (peak 1)	H+	268.10	268.10	-17.4	153.2	1.93	1.3%	16	159.2-169.3
adenosine (peak 2)	H+	268.10	268.10	-16.7	162.7	1.08	0.7%	16	159.2-169.3
metroprol	H+	268.19	268.19	-9.2	171.5	0.58	0.3%	16	-
imipramine	H+	281.20	281.20	-15.9	165.4	0.45	0.3%	16	-
Adenosine	Na+	290.09	290.08	-14.6	171.8	0.56	0.3%	8	161.9-175.9
atropine	H+	290.18	290.18	1.4	175.5	2.10	1.2%	16	-
ondansetron	H+	294.16	294.16	-6.2	172.7	0.52	0.3%	16	173.9-193.2
cocaine	H+	304.15	304.15	-16.7	168.6	0.55	0.3%	16	166.6-179.3
quinine	H+	325.19	325.19	-7.1	179.8	0.69	0.4%	16	-
NANA	Na+	332.10	332.09	-17.0	168.7	0.52	0.3%	16	143.1-167.5
chloroamphenicol	Na+	345.00	345.00	-11.9	180.6	0.75	0.4%	16	-
UMP	Na+	347.03	347.02	-14.8	178.9	0.85	0.5%	15	146.6-182.5
melibiose	Na+	365.11	365.10	-11.2	178.5	0.63	0.4%	16	166.7-209.3
Sucrose	Na+	365.11	365.10	-16.6	173.4	0.50	0.3%	16	170.1-211.0
AMP	Na+	370.05	370.05	-10.7	180.8	4.32	2.4%	16	167.0-203.8
AMP	K+	386.03	386.26	592.0	199.1	0.55	0.3%	16	-
colchicine	H+	400.18	400.17	-9.3	196.3	0.58	0.3%	16	189.8-206.2
LacNAc	Na+	406.13	406.13	-10.7	187.5	0.52	0.3%	16	157.4-190.0
colchicine	Na+	422.16	422.15	-10.5	203.3	0.90	0.4%	16	195.9-214.8
colchicine	K+	438.13	438.13	-10.2	201.6	0.62	0.3%	16	-
verapamil H	H+	455.29	455.29	-6.1	209.3	0.60	0.3%	16	207.6-262.0
folate	Na+	464.13	464.12	-10.7	206.9	0.68	0.3%	16	209.9-266.4
verapamil	Na+	477.27	477.27	-10.5	217.3	1.00	0.5%	16	210.3-273.1
raffinose	Na+	527.16	527.15	-9.7	210.2	0.64	0.3%	16	197.2-260.7
gluthatione oxidized	H+	613.16	613.15	-9.1	225.8	0.70	0.3%	16	212.5-288.5
stachyose	Na+	689.21	689.21	-9.2	235.5	0.73	0.3%	16	227.5-288.9
maltopentaose	Na+	851.26	851.26	-8.9	256.9	0.87	0.3%	16	254.1-349.3

Table D.5. Timetable of solvent composition for the nanopump during chip based LC runs in support of single field CCS measurements.

	Time (min)	A (H$_2$O w/0.1%F.A.)	B (ACN w/0.1% F.A.)	Flow (µL/min)
	0	98%	2%	0.3
1	5.00	68%	32%	0.3
2	8.50	20%	80%	0.3
3	9.50	20%	90%	0.3
4	9.51	98%	3%	0.3
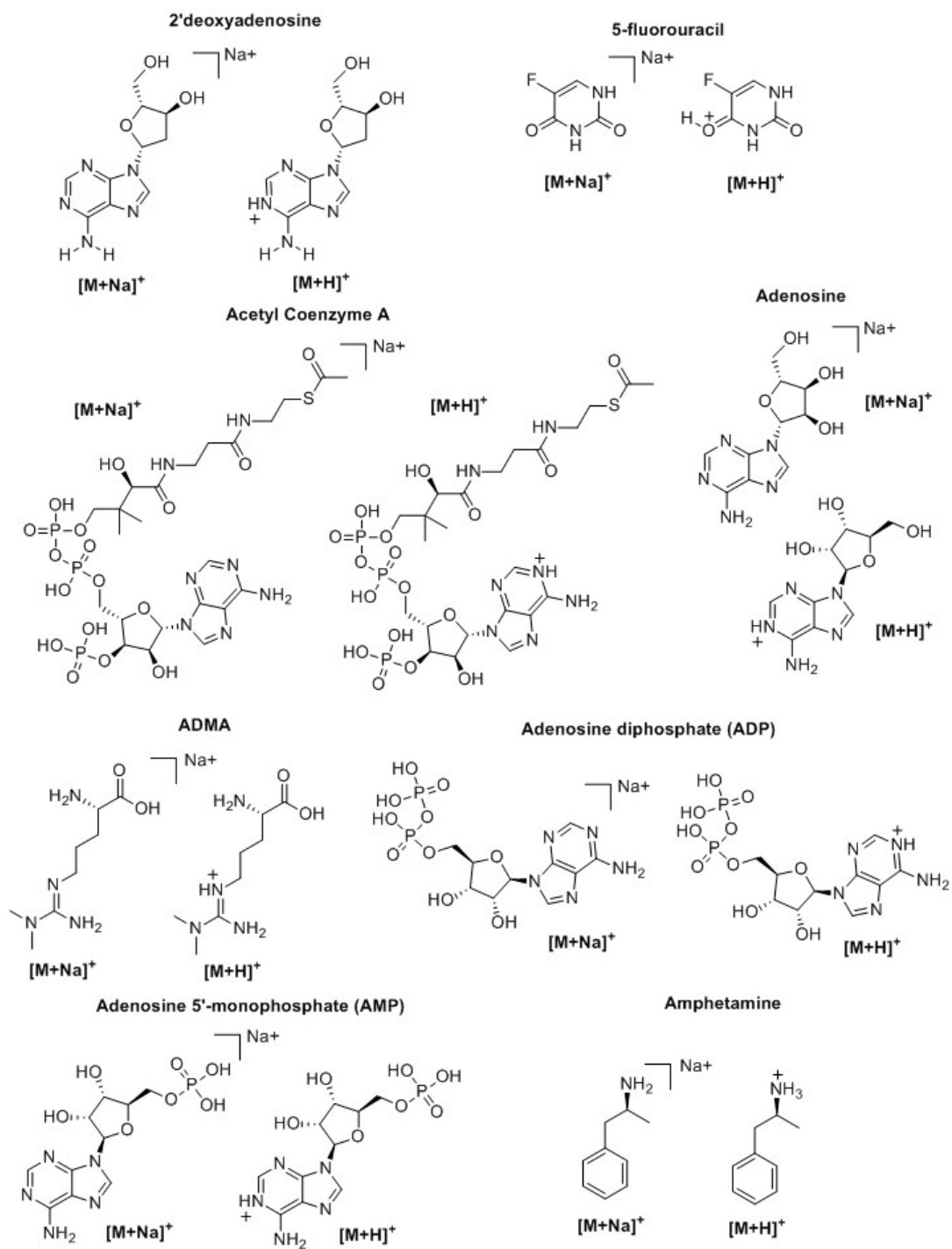
Figure D.2. Structures of the metabolites examined in the study. The cation coordinating species as well as the attached protonated species are shown.
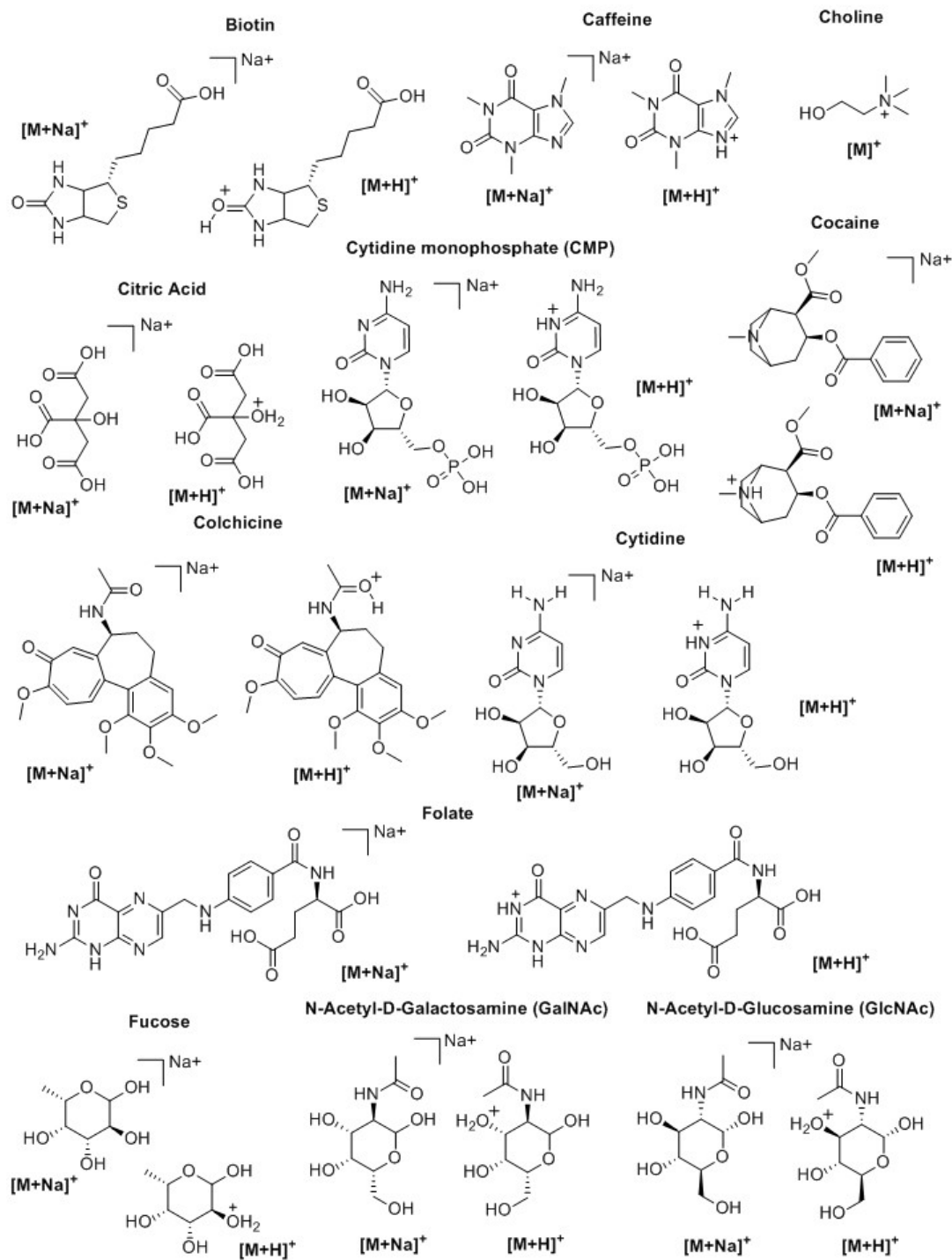
Figure D.3. Structures of the metabolites examined in the study. The cation coordinating species as well as the attached protonated species are shown.
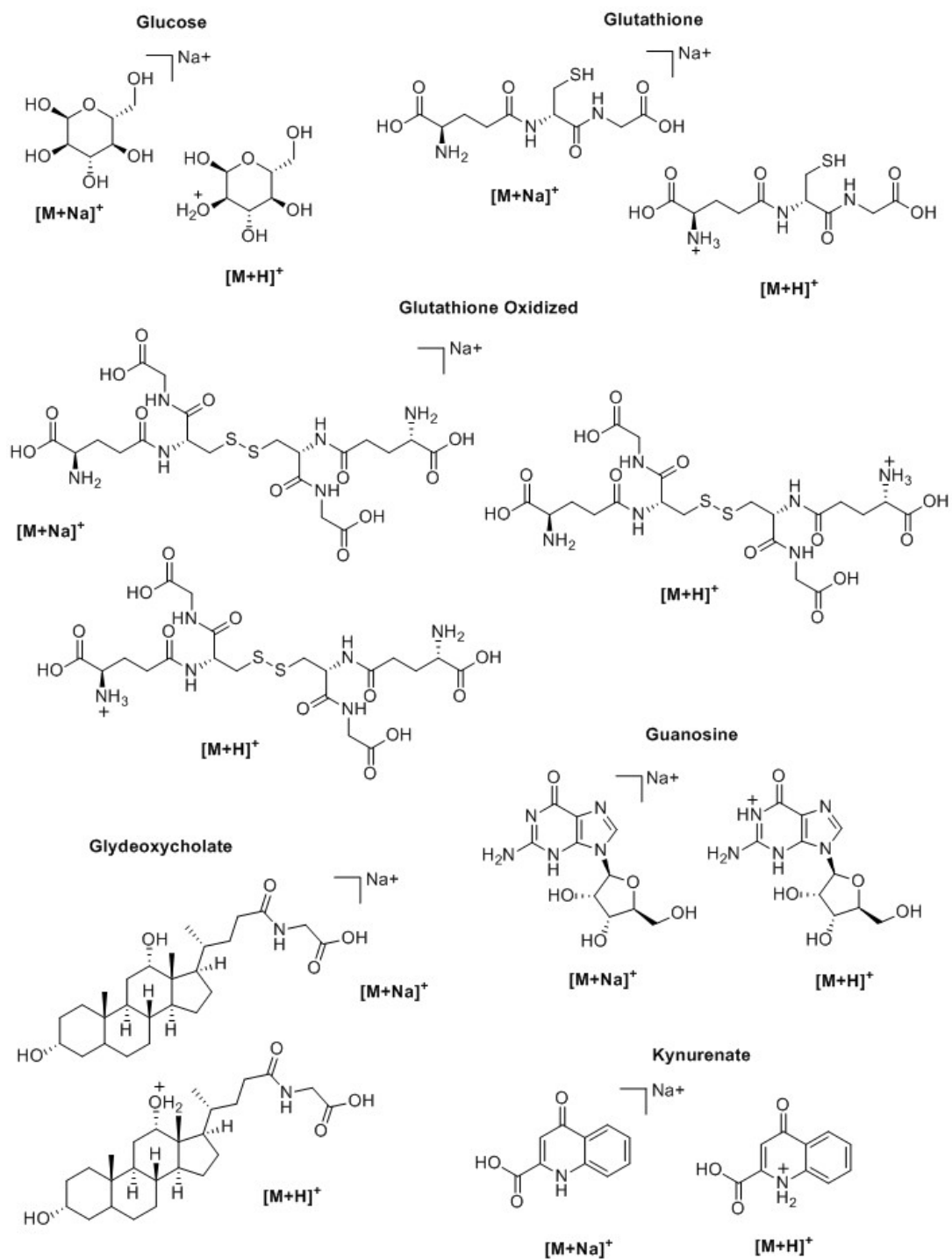
Figure D.4. Structures of the metabolites examined in the study. The cation coordinating species as well as the attached protonated species are shown.
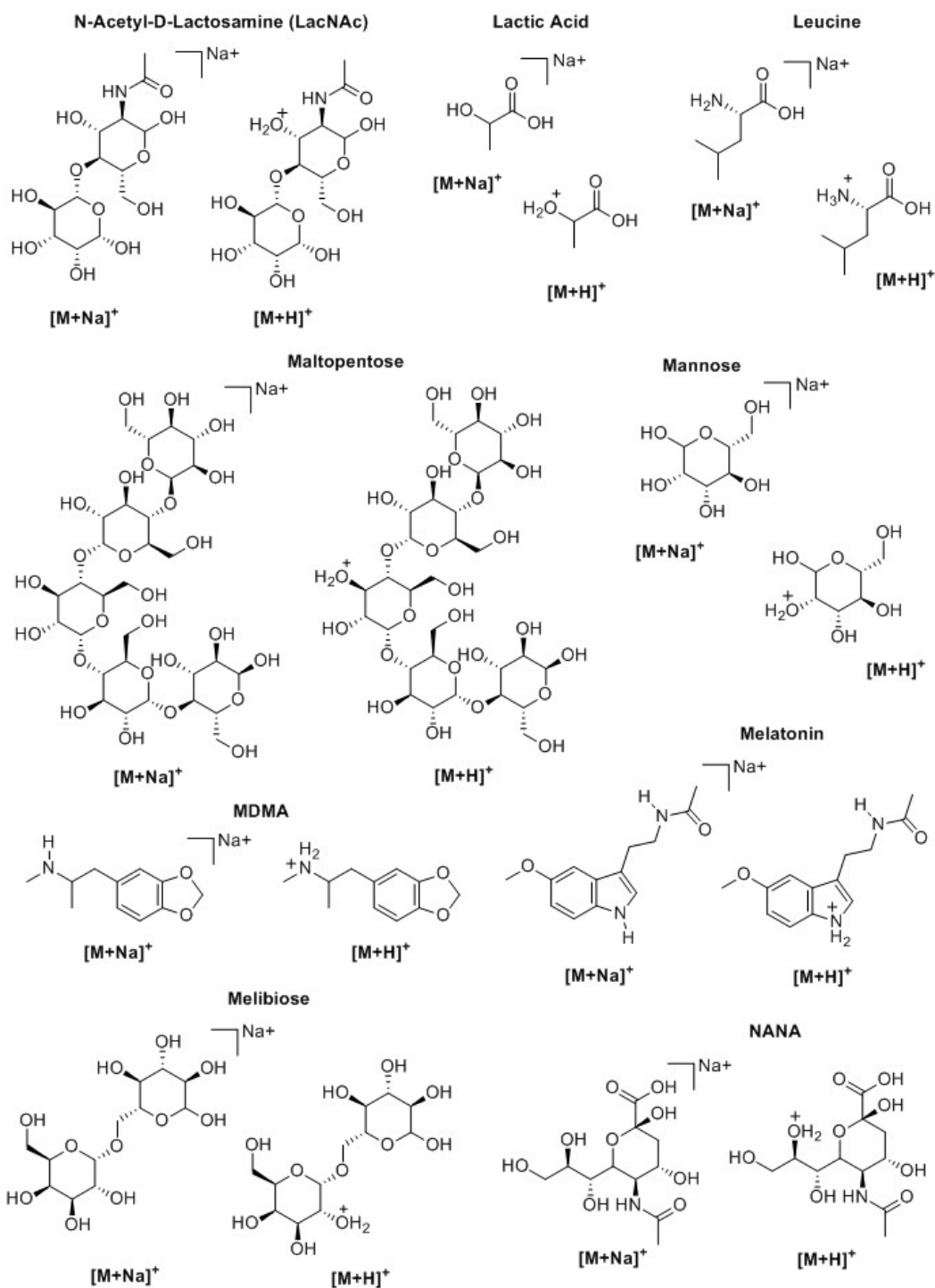
Figure D5. Structures of the metabolites examined in the study. The cation coordinating species as well as the attached protonated species are shown.
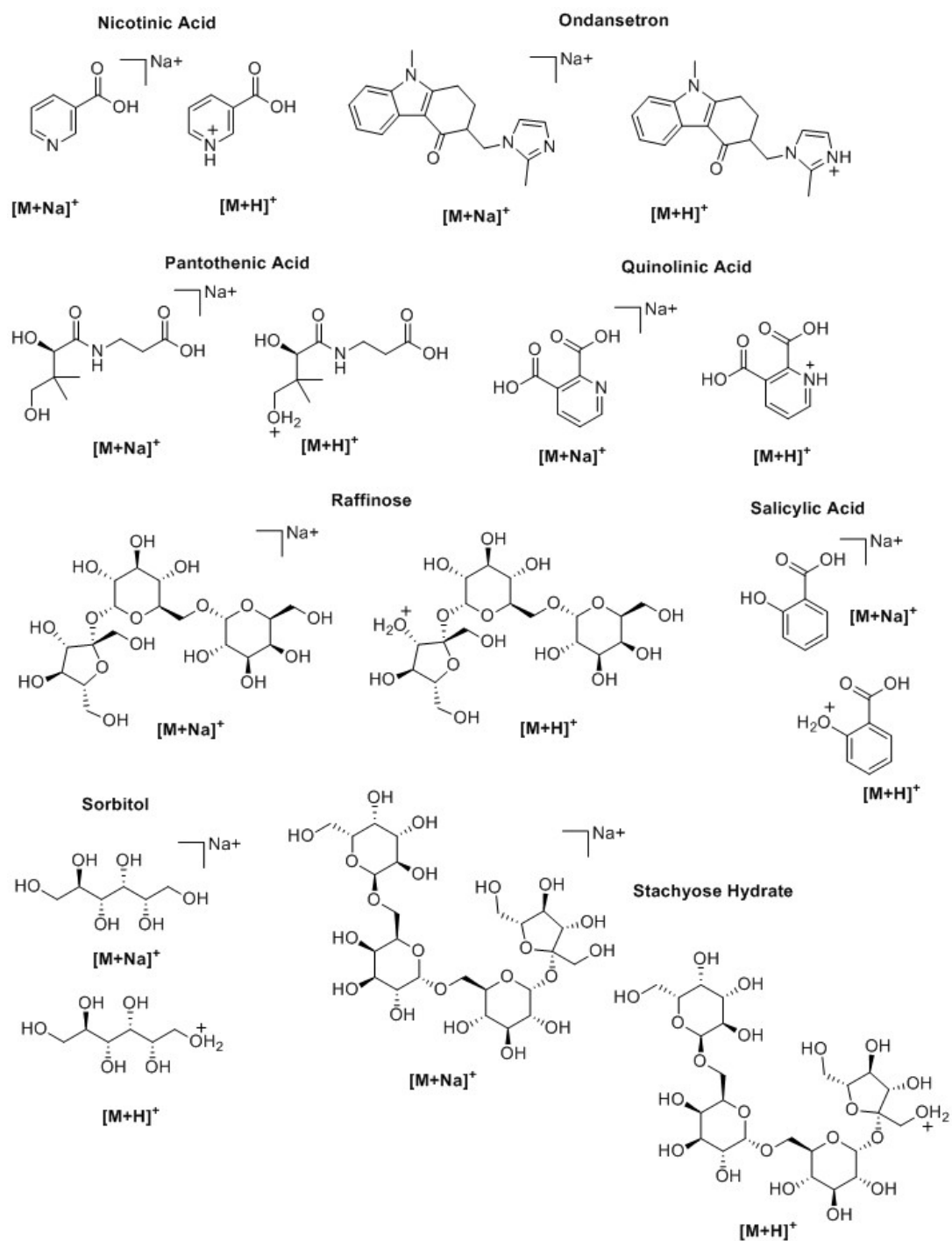
Figure D.6. Structures of the metabolites examined in the study. The cation coordinating species as well as the attached protonated species are shown.
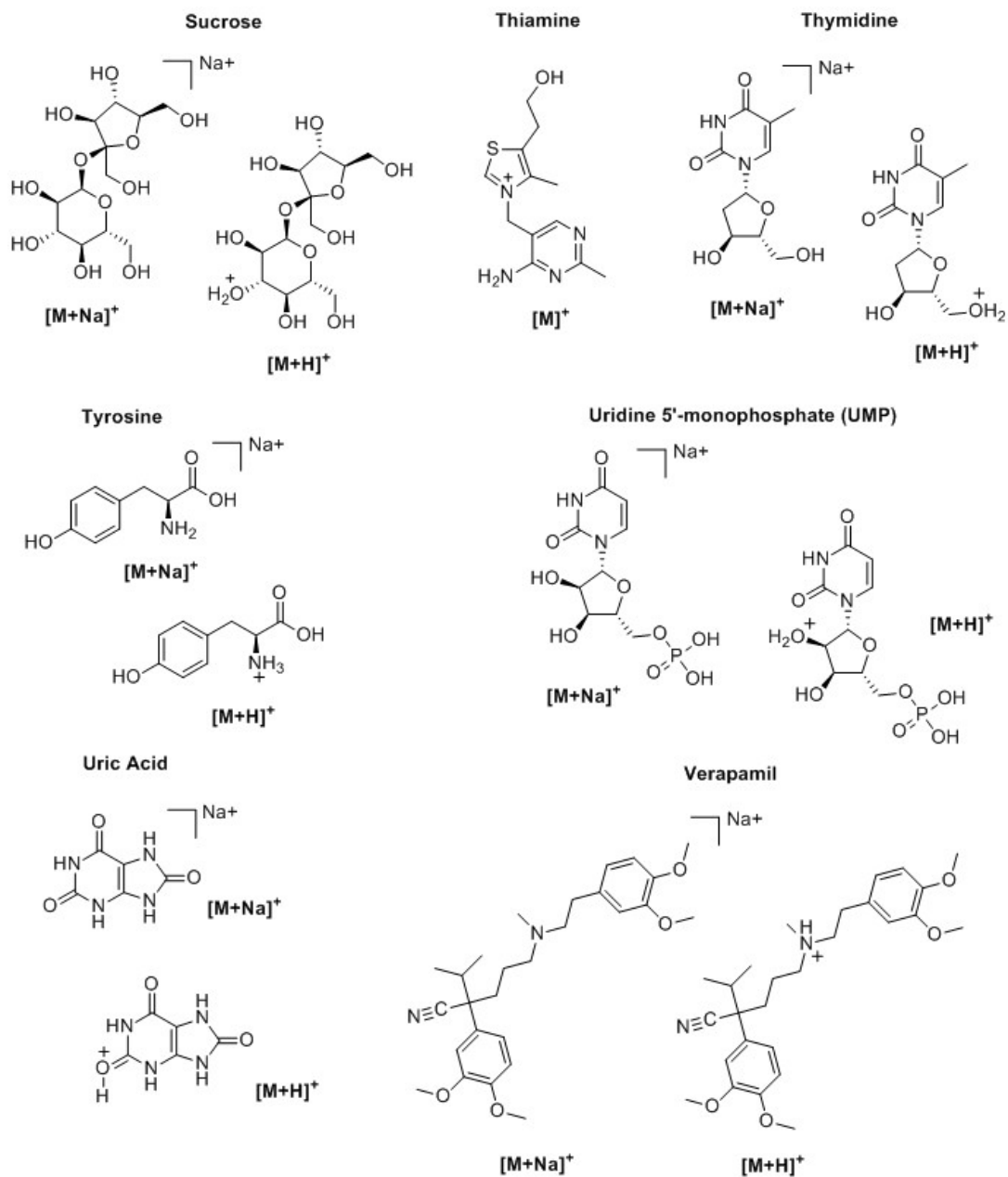
Figure D.7. Structures of the metabolites examined in the study. The cation coordinating species as well as the attached protonated species are shown.
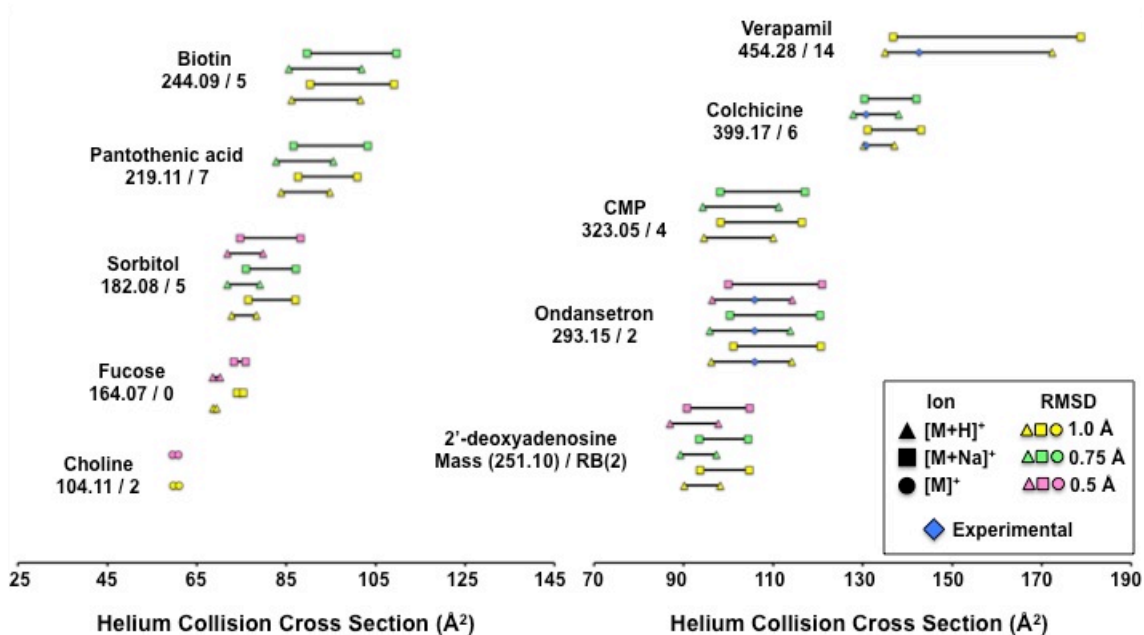
Figure D.8. Determination of RMSD cutoff for distance geometry calculations is based on the data in this plot. The CCS is on the x-axis and the theoretical ranges are plotted for these 10 metabolites for different RMSD cutoff values used in the distance geometry calculation to determine how this affects the conformational space sampled. The yellow indicates a cutoff of 1.0 Å, the green a cutoff of 0.75 Å, and the pink a cutoff of 0.5 Å. The different shapes represent different gas phase ions. Based on the results above, a 0.5 Å cutoff was used for metabolites with a molecular weight less than 200 Da, a 0.75 Å cutoff was used for metabolites with a molecular weight less between 200 and 400 Da, and a 1.0 Å cutoff was used for metabolites with a molecular weight more than 400 Da.

Table D.6. Initial Parameterization and Theoretical CCS Calculations for Selected metabolites are displayed below. The initial parameterization includes a geometry optimization and an electrostatic potential grid calculation.

Molecule	*CPU Time*
Initial Parameterization (m/z, method)	
Lactic acid [M] (90.03, HF)	4 min 54 sec
Biotin [M] (244.09, HF)	2 hours 22 min 47 sec
Maltopentose [M] (828.27, HF)	1 day 3 hours 43 min 31 sec
Amphetamine [M] (135.10, HF)	14 min 26 sec
Amphetamine [M+H]$^+$ (136.11, PM6)	42 sec
Verapamil [M] (454.28, HF)	15 hours 24 min 56 sec
Verapamil [M+H]$^+$ (455.29, PM6)	30 min 34 sec
Theoretical CCS Calculation (m/z, method, number of structures)	
Colchicine [M+Na]$^+$ (422.16, PA, 30)	1 min. 44 sec.
Colchicine [M+Na]$^+$ (422.16, PSA, 30)	21 min. 39 sec.
Fucose [M+Na]$^+$ (187.06, TM, 2)	~ 1 day
Raffinose [M+Na]$^+$ (527.16, TM, 2)	~ 4 days
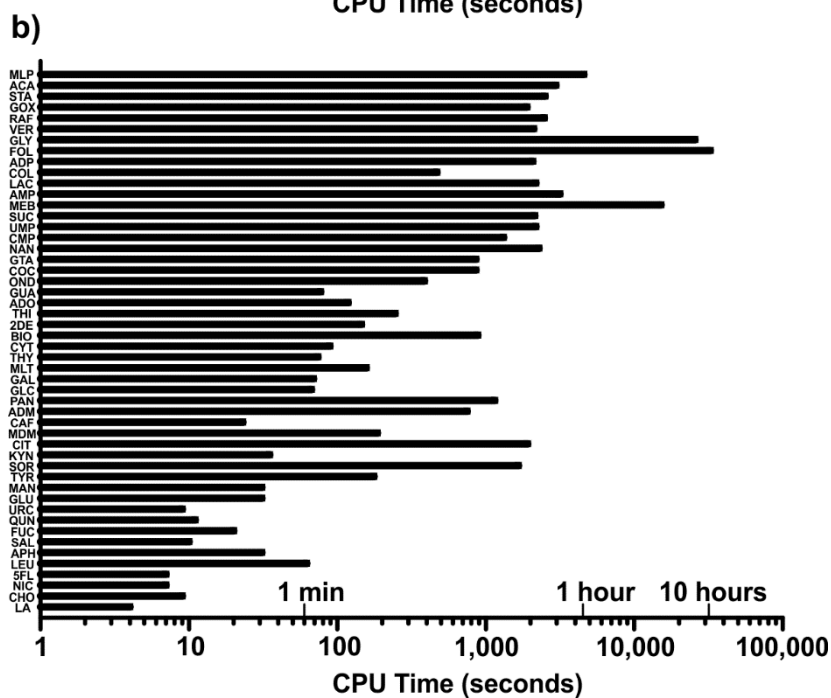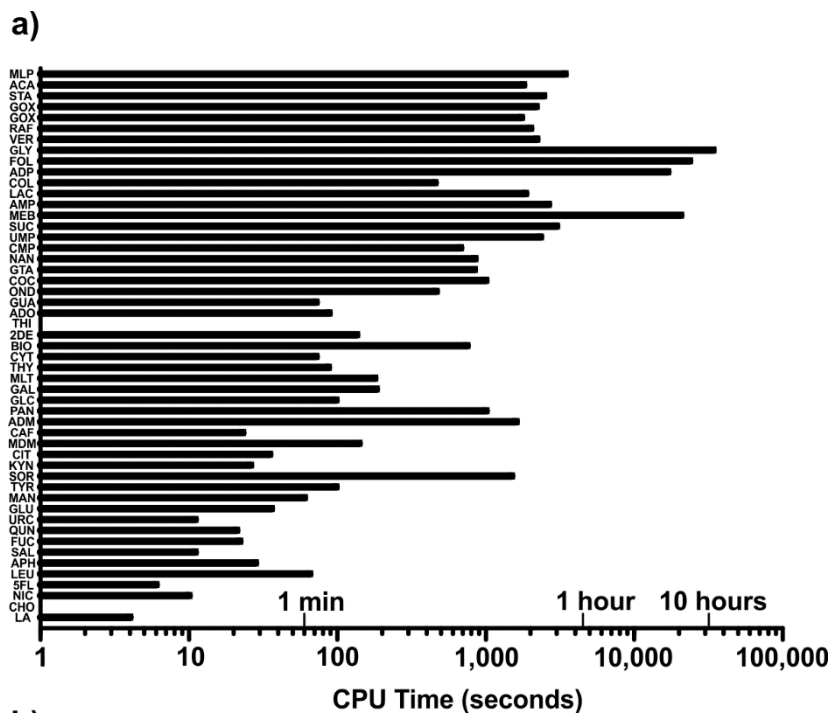
Figure D.9. The CPU time required for sampling the conformational space with the distance geometry protocol is shown in these plots for the a) protonated species and b) sodiated species. The CPU time is presented on the x-axis in log scale and the metabolites are listed on the y-axis. The $[M]^+$ species are shown with the sodiated data.
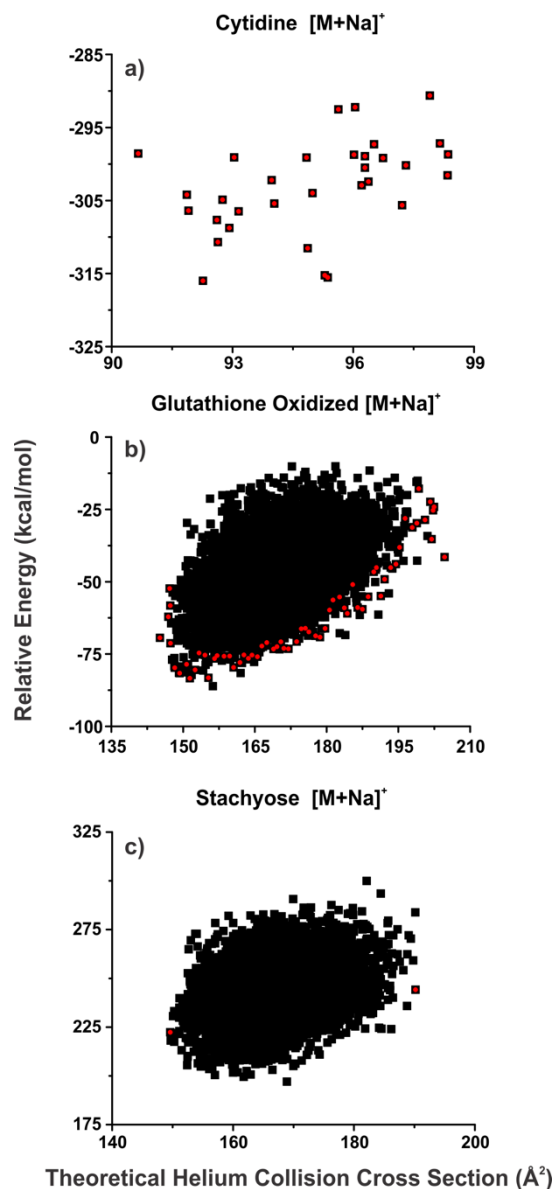
Figure D.10 Sample theoretical conformational space plots to show which conformations were selected for nitrogen CCS calculations. The data is shown for helium, and the conformations that were used for nitrogen are shown in red. For metabolites where 100 or less conformations were generated with distance geometry they were all submitted to PSA N_2 calculations as shown in a) for cytidine. When more than 100 conformations were generated with distance geometry as shown in b) for glutathione oxidized low energy conformations than span the CCS range were selected for the PSA N_2 calculations. For molecules that do not contain the appropriate ratio of carbon, oxygen and nitrogen atoms as is the case for stachyose as shown in c) the trajectory method in MOBCAL must be used to get nitrogen CCS value. This calculation is very computationally expensive and only the smallest and largest CCS conformations are used to the MOBCAL N_2 calculation.

APPENDIX E

CURRICULUM VITAE

Nichole M. Lareau, Ph.D.

Vanderbilt University Department of Chemistry
7330 Stevenson Center, Station B 35-1822
Nashville, TN 37235
Lab: (615) 343-4563
nichole.m.lareau@vanderbilt.edu
nichole.lareau@gmail.com

EDUCATION

Vanderbilt University   Nashville, TN
Ph.D. in Chemistry   May 2016

Dissertation: Development of Ion Mobility and Mass Spectrometry Strategies in Support
            of Integrated Omics and Systems Biology
Advisor: Dr. John A. McLean

The College of New Jersey   Ewing, NJ
Bachelor of Science in Chemistry, ACS Certified   May 2011
Advisor: Dr. Lynn Bradley

RESEARCH EXPERIENCE

Graduate Research Assistant   Aug 2011-May 2016
Vanderbilt University, Nashville, TN
Advisor: Dr. John A. McLean
Development and application of separation technologies for simultaneous analysis of
glycomics, proteomics and metabolomics by ion mobility-mass spectrometry for
systems biology applications.

Independent Undergraduate Research   Aug 2009-May 2011
The College of New Jersey, Ewing, NJ
Advisor: Dr. Lynn Bradley

Designed a modified Birch reduction to be implemented in an undergraduate organic chemistry laboratory course utilized silica embedded sodium metal catalysts.

National Science Foundation-REU   May 2010-Aug 2010
Vanderbilt University, Chemical Biology Interface NSF-REU, Nashville, TN
Advisor: Dr. John A. McLean
Conducted integrated 'omics' research utilizing ion mobility-mass spectrometry to study both the conformation space of natural products and the detection limits of caustic contaminants in infant formula

Trace Explosives Detection Junior Chemist   May 2009-Aug 2009
Department of Homeland Security, Atlantic City, NJ
Advisor: Dr. Stefan Lewok
Assisted in the design of electrical, hardware, and software integration of an IMS with MS for explosive detection

PUBLICATIONS

8. **Nichole M. Lareau**[*], Sarah M. Stow[*], Terry P. Lybrand, and John A. McLean, " Ion Mobility-Mass Spectrometry Strategies in Support of Small Molecule Analysis: Considerations for Chip-based LC and the Development of Small Molecule Structural Prediction," In Preparation for *Nature Molecular Phenomics*, 2016. ([*]Co-first authors)

7. **Nichole M. Lareau**, and John A. McLean, "Multimodal Fragmentation Enhanced by Ion Mobility for Glycoproteomics," In Preparation for *Analytical Chemistry*, 2016.

6. A. J. Farrand, K. P. Haley, **N. M. Lareau**, S. Heilbronner, J. A. McLean, T. Foster, E. P. Skaar, An Iron-regulated Autolysin Remodels the Cell Wall to Facilitate Heme Acquisition in *Staphylococcus lugdunensis*. *Infection and Immunity*, **2015**, *83*, 3578-3589.

5. **N. M. Lareau**, J. C. May, J. A. McLean, Non-derivatized Glycan Analysis by Reverse Phase Liquid Chromatography and Ion Mobility-Mass Spectrometry, *Analyst*, **2015**, *140*, 3335-3338.

4. N. G. Hendricks, **N. M. Lareau**, J. A. McLean, R. R. Julian, Bond Specific Dissociation following Excitation Energy Transfer for Distance Constraint Determination in the Gas Phase, *J.A.C.S.*, **2014**, *136*, 13363-13370.

3. J. C. May, C. R. Goodwin, **N. M. Lareau**, K. L. Leaptrot, C. B. Morris, R. T. Kurulugama, A. Mordehai, C. Klein, W. Barry, E. Darland, G. Overney, K. Imatani, G. C. Stafford, J. C. Fjeldsted, J. A. McLean, Conformational Ordering of Biomolecules in the Gas Phase: Nitrogen Collision Cross Sections Measured on a

Prototype High Resolution Drift Tube Ion Mobility-Mass Spectrometer, *Anal. Chem.*, **2014**, *86*, 2107-2116.

2. H. Abourahma, L. Bradley, **N. M. Lareau**, M. Reesbeck, Modified Birch Reduction for the Introductory Undergraduate Organic Laboratory, *J. Chem. Ed,* **2014**, *91,* 443-445.

1. S. M. Stow, **N. M. Lareau,** K. M. Hines, C. R. McNees, C. R. Goodwin, B. O. Bachmann, and J. A. McLean, "Structural Separations for Secondary Metabolite Characterization by Ion Mobility-Mass Spectrometry: Fundamental Theory to Emerging Applications," *Natural Products Analysis: Instrumentation, Methods, and Applications*, Haylicek, V., Spizek, J., Ed., Wiley-Blackwell: New York, **2013.**

PRESENTATIONS

26. **N. M. Lareau**, S. M. Stow, J. C. May, J. A. McLean, *Development of Ion Mobility and Mass Spectrometry Strategies in Support of Integrated Omics and Systems Biology*, Vanderbilt Institute of Chemical Biology Symposium, Nashville, TN, Aug 2015, **ORAL** (VICB Prize)

25. **N. M. Lareau**, J. C. May, J. A. McLean, *Ion Mobility-Mass Spectrometry Based Structural Separations of Biological Classes*, Chemical Biological Interface Career Development Conference, Nashville, TN, August 2015 **POSTER**.

24. **N. M. Lareau**, S. M. Stow, J. C. May, E. Darland, R. T. Kurulugama, E. E. Rennie, J. C. Fjeldsted, J. A. McLean, *Mining Secondary Metabolites by HPLC Chip Cube and Ion Mobility-Mass Spectrometry*, 63rd ASMS Conference on Mass Spectrometry and Allied Topics, St. Louis, MO, May 2015 **POSTER**.

23. **N. M. Lareau**, J. A. McLean, *Ion Mobility-Mass Spectrometry (IM-MS) in Support of Complementary Fragmentation Techniques for Glycoprotein Characterization*, 66th Southeastern Regional Meeting of the American Chemical Society, Nashville, TN, Oct 2014 **ORAL**.

22. **N. M. Lareau**, J. C. May, J. A. McLean, *Ion Mobility-Mass Spectrometry Separations of Carbohydrates and Fundamental Considerations of Drift Gases and Metal Adduction,* ASMS Asilomar Advances in Glycomics and Glycoproteomics: Methods and Applications, Asilomar, CA, Oct 2014 **ORAL** (selected for a Poster Highlight Talk).

21. **N. M. Lareau**, J. A. McLean, *Enhancing Glycoprotein Characterization with Ion Mobility-Mass Spectrometry* Techniques, Vanderbilt Institute of Chemical Biology 2014 Student Symposium, Aug 2014 **POSTER**.

20. **N. M. Lareau**, J. C. May, J. A. McLean, *Combined Electron Transfer Dissociation-Ion Mobility-Collision Induced Dissociation-Mass Spectrometry (ETD-IM-CID-MS) Techniques for the Characterization of Proteins, Glycans and Glycoproteins,* 62nd Annual ASMS Conference on Mass Spectrometry and Allied Topics, Baltimore, MD, June 2014 **POSTER**.

19. J. C. May, K. L. Leaptrot, **N. M. Lareau**, R. T. Kurulugama, G. C. Stafford, A. Mordehai, J. C. Fjeldsted, J. A. McLean, *Understanding Global Ion Mobility Separation Differences of Biomolecules in Alternative Drift Gases*, 62nd Annual ASMS Conference on Mass Spectrometry and Allied Topics, Baltimore, MD, June 2014 **POSTER**.

18. N. Hendricks, **N. M. Lareau**, J. A. McLean, R. R. Julian, *Action-EET Based Dissociation of Disulfide Bonds with Tryptophan as a Donor in the Gas Phase*, 62nd Annual ASMS Conference on Mass Spectrometry and Allied Topics, Baltimore, MD, June 2014 **ORAL**.

17. **N. M. Lareau**, J. C. May, J. A. McLean, *Structural Separations of Biological Classes by Ion Mobility-Mass Spectrometry Techniques,* Chemical Biological Interface Career Development Conference, Madison, WI, June 2014 **POSTER**.

16. R. M. Reyes, **N. M. Lareau**, J. C. May, J. A. McLean, *Enhancing Biomolecular Class Separation in Complex Sample Analysis Using Ion Mobility Mass Spectrometry (IM-MS)*, 65th SERMACS Meeting, Atlanta, GA, Nov 2013. **POSTER**.

15. J. G. Forsythe, C. R. Goodwin, J. C. May, K. M. Hines, **N. M. Lareau**, J. A. McLean, *Advances in Comprehensive Metabolomic Strategies Using Structural mass Spectrometry*, 65th SERMACS Meeting, Atlanta, GA, Nov 2013. **ORAL**.

14. **N. M. Lareau**, J. C. May, J. A. McLean, *Structural Analysis of Carbohydrates in the Gas Phase Using Ion Mobility-Mass Spectrometry (IM-MS)*, Vanderbilt Institute of Chemical Biology Symposium, Nashville, TN, Aug 2013 **POSTER**.

13. **N. M. Lareau**, J. C. May, J. A. McLean, *A Carbohydrate Collision Cross Section (CCS) Database for Glycomics by Ion Mobility- Mass Spectrometry (IM-MS),* Gordon Research Conference: Biological Molecules in the Gas Phase & in Solution, Holderness, NH July 2013 **POSTER**.

12. **N. M. Lareau**, C. R. Goodwin, J. C. May, R. Kurulugama, E. Darland, B. O. Bachmann, J. A. McLean, *The Characterization of Bacterial Metabolites by Atmospheric Solids Analysis Probe-Ion Mobility-Mass Spectrometry (ASAP-IM-MS) Methodologies,* 61st Annual ASMS Conference on Mass Spectrometry and Allied Topics, Minneapolis, MN, June 2013 **POSTER**.

11. **N. M. Lareau**, C. R. Goodwin, J. C. May, B. O. Bachmann, J. A. McLean, *The Prioritization of Bacterial Metabolites by Ion Mobility-Mass Spectrometry (IM-MS)Methodologies*, 10th Anniversary of the Vanderbilt Institute of Chemical Biology Research Symposium, Nashville, TN, March, 2013. **POSTER**.

10. **N. M. Lareau**, C. R. Goodwin, B. O. Bachmann, J. A. McLean, *Structural Mass Spectrometry Techniques for the Rapid Characterization of Bacterial Metabolites,* Aegis Sciences Corporation-Vanderbilt University Department of Chemistry Research Symposium, Nashville, TN, Dec 2012 **ORAL**.

9. **N. M. Lareau**, L. S. Fenn, C. R. Goodwin, J. C. May, J. A. McLean, *Native Glycan Analysis by Structural Ultra Performance liquid Chromatography- Ion Mobility- Mass Spectrometry (UPLC-IM-MS),* Vanderbilt Institute of Chemical Biology Symposium, Nashville, TN, Aug 2012 **POSTER**.

8. **N. M. Lareau**, L. S. Fenn, C. R. Goodwin, J. C. May, D. R. Marshall, J. A. McLean, *Ion Mobility-Mass Spectrometry Methodology for the Characterization of N-Linked Carbohydrate and Carbohydrate-Conjugate Isomers,* 60th Annual ASMS Conference on Mass Spectrometry and Allied Topics, Vancouver, BC, Canada, May 2012 **POSTER**.

7. **N. M. Lareau**, L. S. Fenn, C. R. Goodwin, J. C. May, B. O. Bachmann, J. A. McLean, *Characterization of Carbohydrates and Carbohydrate Natural Products by LC- Ion Mobility-Mass Spectrometry,* ASMS Sanibel Conference on Mass Spectrometry Technologies for Structural Biology, St. Petersburg, FL, Jan. 2012 **POSTER**.

6. **N. M. Lareau**, L. S. Fenn, C. R. Goodwin, B. O. Bachmann, J. A. McLean, *Exploring Conformation Space for Natural Product Discovery,* American Chemical Society National Conference, Anaheim, CA, March 2011 **POSTER**.

5. **N. M. Lareau**, L. S. Fenn, C. R. Goodwin, B. O. Bachmann, J. A. McLean, *Exploring Conformation Space for Natural Product Discovery,* The Pittsburg Conference on Analytical Chemistry and Applied Spectroscopy, Atlanta, GA, March 2011 **POSTER**.

4. **N. M. Lareau**, L. S. Fenn, C. R. Goodwin, B. O. Bachmann, J. A. McLean, *Exploring Conformation Space for Natural Product Discovery*, The Vanderbilt Summer Academy Research Symposium, Nashville, TN, Aug 2011 **POSTER**.

3. C. R. Goodwin, L. S. Fenn, R. McNees, **N. M. Lareau,** B. O. Bachmann, J. A. McLean*, Ion Mobility-Mass Spectrometry Driven Natural Product Discovery*, 4th Annual q-bio Conference on Cellular Information Processing, Santa Fe, NM. August 2010 **POSTER**.

2. **N. M. Lareau**, M. Reesbeck, H. Abourahma, L. Bradley, *The Reduction of Naphthalene using Na-SG(1) in the Undergraduate Organic Laboratory*, The College of New Jersey Fall Research Poster Session, Ewing, NJ, December, 2010 **POSTER**.

1. **N. M. Lareau**, M. Reesbeck, H. Abourahma, L. Bradley, *Towards the Design of a Birch Reduction for the Undergraduate Organic Chemistry Laboratory*, The College of New Jersey Spring Research Poster Session, Ewing, NJ, May 2010 **POSTER**.

FELLOWSHIPS, HONORS, & AWARDS

Richard N. Armstrong Prize in Chemical Biology   Aug 2015
Vanderbilt University

ASMS Student Travel Award   Oct 2014, May 2014, Jan 2012
American Society for Mass Spectrometry

Chemical Biology Interface Training (T32GM065086)   July 2012-June 2014
Vanderbilt University

Vanderbilt Institute of Chemical Biology Poster Award   Aug 2013
Vanderbilt University

NSF-Graduate Research Fellowship Program-Honorable Mention   March 2013
National Science Foundation

Vanderbilt Institute of Chemical Biology Fellowship   May 2011-May 2012
Vanderbilt University

Hercules Fellowship   May 2011-May 2012
Vanderbilt University

Triiota Women's Honors Society   April 2011
The College of New Jersey

NSF Travel Chemistry Leadership Award Recipient   March 2011
National Science Foundation

TEACHING AND LEADERSHIP EXPERIENCE

Teaching Assistant for General Chemistry, *Vanderbilt University*   June-Dec 2015

2015 CBI Career Conference Organizing Committee, *Student Rep.* Aug 2015
Vanderbilt Chemical Biology Association of Students, *Gen. Member* Aug 2011-Present
President Aug 2013-Aug 2014
V. President Aug 2012-Aug 2013
General Chemistry Tutor August 2014-May 2015
Lab Safety & Biosafety Representative, *Vanderbilt* Dec 2011-May 2014
Research Mentor to 3 NSF REU-Students, *Vanderbilt* May-Aug 2012, 2013
Volunteer Tutor, *Vanderbilt School of Math & Science* Aug 2011-Aug 2012

PROFESSIONAL MEMBERSHIP

American Society of Mass Spectrometry
American Society of Chemistry